Targeting the Chemokine Signalling Pathway Using Tick Saliva Peptides



Yara Hamid Alenazi

Worcester College

University of Oxford

This thesis is submitted for the degree of

Doctor of Philosophy

Cardiovascular Medicine

Michaelmas Term 2018

Abstract

Chemokines are signalling proteins that function to recruit immune cells from the innate and adaptive immune response. Chemokines are classified based on the position of their cysteine residues at the N-terminus as CC, CXC, CX_3C or XC (C-cysteine, X-amino acid). Increased expression of chemokines is one of the key findings in a range of inflammatory diseases. Chemokines operate in a network, where multiple chemokines bind a single receptor, and vice versa, and multiple chemokine receptors are expressed on immune and inflammatory cells. While chemokines are validated therapeutic targets, targeting a single chemokine or receptor has failed as a therapeutic approach in inflammatory disease.

Ticks, blood-feeding parasites, feed on their hosts for several days to weeks without eliciting their hosts immune response. Ticks achieve this through secreting numerous anti-inflammatory peptides into their hosts, during feeding. Evasins are proteins identified from tick saliva that bind and neutralize multiple chemokines and are thought to reduce inflammation at the site of the tick bite. Systemic administration of evasins effectively reduce inflammation in a range of preclinical models of inflammatory disease, suggesting that they could be used as therapeutics for such diseases. Limitations of published evasins include lack of binding to important chemokines (e.g. CCL2, CCL13, CXCL10), and inability of a single evasin to target both CC and CXC chemokines. Therefore, this thesis aimed to expand the chemokine-binding repertoire of identified evasins and hypothesised that other tick species would have novel evasins that are also capable of modulating chemokine activity.

Using bioinformatic analysis of eight tick species from the *Amblyomma*, *Rhipicephalus* and *Ixodes* genera, 352 evasin-like sequences were identified, and constructed into a yeast surface display library. This library was screened using fluorescently labelled CC and CXC chemokines to identify individual clones that bound. 16 novel evasins were identified, including P1156 and P1243. P1156 binds six ELR+ CXC chemokines with high affinity and neutralises CXC chemokine function. P1243 evasin binds 21 CC chemokines with high affinity and neutralises CC chemokine function.

Typically, both CC and CXC chemokines are expressed in inflammatory disease. To develop agents that can target both chemokine classes, genetically engineered ‘two-warhead’ evasins were created and were shown to be capable of simultaneously binding CC and CXC chemokines and neutralising their function, *in vitro*. Thus, the two-warhead evasin provides a concept of achieving precision targeting of disease-relevant CC and CXC chemokine subsets, as a single agent.

Acknowledgments

Firstly, I would like to express my sincerest gratitude to Professor Shoumo Bhattacharya for giving me the opportunity to be part of his wonderful team, as well as his continuous guidance, patience and support throughout my time as his student. I would also like express my special thanks to Dr Akane Kawamura, my second supervisor, for her continued direction and advice. Moreover, I am most grateful to my funding body, the Saudi Arabian Cultural Bureau, for the opportunity to pursue my higher education in one of the greatest institutions in the world.

I must also express my gratitude to the members of the Bhattacharya laboratory, for their continuous support, encouragement and their valuable and constructive advice during our Friday meetings. With a special thanks owed to Graham and Kamayani, Graham is always the voice of reason, and his input over the years has been crucial to this project. To Kamayani, I am grateful for her friendship and advice over the years, especially in the early years of my DPhil. Also, to James, my fellow DPhil, thank you for those unwinding tea breaks and listening to my useless monologues. I'm glad we finally made it!

Finally, my deepest appreciation goes to my family. I am very fortunate to have a loving and supporting family who are always a phone call away. I am thankful to my mother for showing me what a powerful woman can be. My mother is an inspirational woman, who embraces hardships and perseveres through them, showing the true strength of women. I am also grateful for my intelligent father, whom has taught me determination, perseverance and the power of education. My parents have each sacrificed greatly for their children's success, and I am forever in their debt. To my brothers, Weal and Hasham, I am very grateful for your witty and frank conversations, thank you for keeping me grounded over the years. I am also grateful to my sisters, my best friends, Jenna and Ala. Jenna is everything I wanted to be growing up, witty, confident and determined. I am so proud of everything our sunshine is and cannot wait to see what her future holds for her. Finally, to Ala, my life-coach. She is the powerhouse of the family, constantly encouraging confidence and ambition in everyone she meets. Everyone needs an Ala in their lives. Ala, I am so happy and grateful to have you in my life, you're my inspiration and my motivator, so thank you.

Publications leading to this research

- Alenazi Y, Singh K, Davies G, Eaton JRO, Elders P, Kawamura A, et al. Genetically engineered two-warhead evasins provide a method to achieve precision targeting of disease-relevant chemokine subsets. Sci Rep. 82018.

- Eaton JRO, Alenazi Y, Singh K, Davies G, Geis-Asteggiante L, Kessler B, et al. The N-terminal domain of a tick evasin is critical for chemokine binding and neutralization and confers specific binding activity to other evasins. J Biol Chem. 2018;293(16):6134-46.

- Singh K, Davies G, Alenazi Y, Eaton JRO, Kawamura A, Bhattacharya S. Yeast surface display identifies a family of evasins from ticks with novel polyvalent CC chemokine-binding activities. Sci Rep. 2017;7(1):4267.

Table of Contents

ABSTRACT **3**

ACKNOWLEDGMENTS **4**

PUBLICATIONS LEADING TO THIS RESEARCH **5**

TABLE OF CONTENTS **6**

LIST OF FIGURES **11**

LIST OF TABLES **14**

NOMENCLATURE **15**

CHAPTER 1. INTRODUCTION **17**

1.1. INFLAMMATION **17**

1.1.1. NEUTROPHILS 18

1.1.2. MONOCYTES 20

1.1.3. MACROPHAGES 21

1.2. INFLAMMATION IN DISEASE **22**

1.2.1. ATHEROSCLEROSIS 24

1.2.2. MYOCARDIAL INFARCTION 25

1.3. CHEMOKINES **28**

1.3.1. CHEMOKINE CLASSIFICATION 28

1.3.1.1. CC chemokines *29*

1.3.1.2. CXC chemokines *31*

1.3.1.3. CX_3C chemokines *33*

1.3.1.4. XC chemokines *33*

1.3.2. CHEMOKINE FUNCTION 34

1.3.2.1. Homeostatic chemokines *34*

1.3.2.2. Inflammatory chemokines *34*

1.3.3. CHEMOKINE STRUCTURE 35

1.4. CHEMOKINE RECEPTORS 36

1.4.1. CHEMOKINE RECEPTOR STRUCTURE 36
1.4.2. CHEMOKINE SIGNALLING PATHWAY 37
1.4.3. GAG BINDING 39
1.4.4. ATYPICAL RECEPTORS 39
1.4.5. CHEMOKINE NETWORK 39

1.5. THE ROLE OF CHEMOKINES IN DISEASE 40

1.5.1. GENETIC STUDIES 42
1.5.2. CHEMOKINE EXPRESSION IN DISEASE 43
1.5.3. ANIMAL MODEL STUDIES 43

1.6. TARGETING CHEMOKINES 44

1.6.1. HELMINTH-DERIVED CHEMOKINE BINDING PROTEINS 45
1.6.2. VIRUS-DERIVED CHEMOKINE BINDING PROTEINS 46
1.6.3. TICK-DERIVED CHEMOKINE BINDING PROTEINS 47

1.7. EVASINS 48

1.7.1. CC CHEMOKINE BINDING EVASINS 48
1.7.2. CXC CHEMOKINE BINDING EVASINS 49
1.7.3. EVASIN STRUCTURE 49
1.7.4. EVASINS *IN VIVO* 50

CHAPTER 2. MATERIALS & METHODS 53

2.1. MATERIALS 53

2.1.1. BUFFERS 53
2.1.2. MEDIA 55
2.1.3. CELL LINES 56
2.1.4. PLASMIDS 56
2.1.4.1. Yeast surface display plasmids 56
2.1.4.2. Protein expression plasmids 57

2.2. METHODS 58

2.2.1. BIOINFORMATIC IDENTIFICATION OF NOVEL EVASINS 58
2.2.2. YEAST SURFACE DISPLAY (YSD) 59
2.2.2.1. Transformation of evasin library into YSD vectors 59

2.2.2.2. YSD fluorescent activated cell sorting (FACS) *59*
2.2.2.3. Colony PCR and plasmid rescuing *60*
2.2.2.4. Chemokine binding assay in yeast cells *62*
2.2.3. PROTEIN PRODUCTION AND PURIFICATION 62
2.2.4. PROTEIN SEQUENCE ANALYSIS 63
2.2.5. PROTEIN DEGLYCOSYLATION 64
2.2.6. TANDEM (MS/MS) MASS SPECTRONOMY AND N-TERMINAL SEQUENCING 64
2.2.7. BIO-LAYER INTERFEROMETRY (BLI) 65
2.2.7.1. BLI chemokine cross-binding assay *65*
2.2.7.2. BLI chemokine binding affinity assay *66*
2.2.7.3. BLI dual-chemokine binding assay *67*
2.2.8. CELL MIGRATION ASSAYS 67
2.2.8.1. CC chemokine induced cell migration *68*
2.2.8.2. CXC chemokine induced cell migration *68*
2.2.9. ISOLATING GRANULOCYTES FROM HUMAN WHOLE BLOOD AND BUFFY COAT 69
2.2.10. CELL SURFACE LABELLING 69
2.2.11. RESTRICTION ENZYME DIGEST 70

CHAPTER 3. IDENTIFYING PUTATIVE EVASINS USING YEAST SURFACE DISPLAY 71

3.1. INTRODUCTION 71

3.1.1. INFLAMMATION AND CHEMOKINES 71
3.1.2. CHEMOKINE TARGETED THERAPY 72

3.2. RESULTS 74

3.2.1. BIOINFORMATIC IDENTIFICATION OF 352 PUTATIVE EVASINS 74
3.2.2. CLONING OF EVASIN LIBRARY INTO YEAST SURFACE DISPLAY (YSD) VECTORS 75
3.2.3. CHEMOKINE SCREENING USING FACS YIELDS PUTATIVE EVASINS 76
3.2.3.1. CCL8 FACS screening *77*
3.2.3.2. CCL15 FACS screening *80*
3.2.3.3. CCL17 FACS screening *80*
3.2.3.4. CCL19 FACS screening *83*
3.2.3.5. CCL20 FACS screening *83*
3.2.3.6. CXCL8 FACS screening *86*
3.2.3.7. CXCL12 FACS screening *86*

3.3. DISCUSSION 91

CHAPTER 4. CHARACTERISING THE NOVEL EVASIN P1243 97

4.1. INTRODUCTION 97

4.1.1. CC CHEMOKINES 97

4.1.2. TARGETING CC CHEMOKINES THERAPEUTICALLY 98

4.2. RESULTS 101

4.2.1. SEQUENCE ANALYSIS OF P1243 SHOWS SEQUENCE HOMOLOGY TO EVASINS 1 AND 4 101

4.2.2. P1243 EXPRESSES AS A HIGHLY GLYCOSYLATED PROTEIN 101

4.2.3. ANALYSIS OF THE BIOCHEMICAL PROFILE OF P1243 SHOWS IT IS A SELECTIVE CC CHEMOKINE BINDER 106

4.2.4. P1243 NEUTRALISES CC CHEMOKINES ACTIVITY 110

4.3. DISCUSSION 112

CHAPTER 5. CHARACTERISING THE NOVEL EVASIN P1156 118

5.1. INTRODUCTION 118

5.1.1. CXC CHEMOKINES 118

5.1.2. THE ROLE OF CXC CHEMOKINES IN INFLAMMATORY DISEASE 119

5.2. RESULTS 122

5.2.1. SEQUENCE ANALYSIS OF P1156 122

5.2.2. P1156 EXPRESSES AS A HIGHLY GLYCOSYLATED PROTEIN 122

5.2.3. ANALYSIS OF THE BIOCHEMICAL PROFILE OF P1156 SHOWS IT IS A SELECTIVE CXC CHEMOKINE BINDER 126

5.2.4. P1156 NEUTRALISES CXC CHEMOKINE ACTIVITY *IN VITRO* 129

5. 3. DISCUSSION 132

CHAPTER 6. GENETICALLY ENGINEERING THE TWO-WARHEAD EVASINS 138

6.1. INTRODUCTION 138

6.1.1. CHEMOKINES IN INFLAMMATORY DISEASE 138

6.1.2. EVASINS 139

6.2. RESULTS 140

6.2.1. SEQUENCE ANALYSIS OF TWO-WARHEAD EVASINS 140

6.2.2. GENETICALLY ENGINEERING EVASINS TO CREATE A 'TWO-WARHEAD' FUSION 140

6.2.3. TWO-WARHEAD EVASINS ARE EXPRESSED AS HIGHLY GLYCOSYLATED PROTEINS 145

6.2.4. ANALYSIS OF THE BIOCHEMICAL PROFILE OF TWO-WARHEAD EVASINS SHOW THEY BIND BOTH CC AND CXC CHEMOKINES WITH HIGH AFFINITY 149

6.2.5. TWO-WARHEAD EVASINS SIMULTANEOUSLY BIND CC AND CXC CHEMOKINES 152

6.2.6. TWO-WARHEAD EVASINS NEUTRALISE CC CHEMOKINE ACTIVITY *IN VITRO* 154

6.2.7. TWO-WARHEAD EVASINS NEUTRALISE CXC CHEMOKINE ACTIVITY *IN VITRO* 154

6. 3. DISCUSSION 157

CHAPTER 7. GENERAL DISCUSSION 167

CHAPTER 8. REFERENCES 175

CHAPTER 9. APPENDICES 195

APPENDIX A. **196**

APPENDIX B. **198**

APPENDIX C. **199**

APPENDIX D. **201**

APPENDIX E. **203**

APPENDIX F. **210**

APPENDIX G. **212**

APPENDIX H **214**

List of Figures

FIGURE 1. 1. SCHEMATIC SHOWING CHEMOKINE-INDUCED LEUKOCYTE EXTRAVASATION. 23
FIGURE 1.2. CLASSES OF CHEMOKINES 29
FIGURE 1. 3. SCHEMATIC SHOWING THE THREE-DIMENSIONAL STRUCTURE OF CHEMOKINES 36
FIGURE 1. 4. SCHEMATIC REPRESENTATION OF THE CHEMOKINE G-PROTEIN COUPLED RECEPTOR (GPCR) 38
FIGURE 1. 5. HUMAN CHEMOKINE NETWORK 41
FIGURE 3. 1. SCHEMATIC REPRESENTATION OF YEAST SURFACE DISPLAY EVASIN EXPRESSION PLASMIDS 75
FIGURE 3. 2. SCHEMATIC REPRESENTATION SHOWING THE EVASIN YEAST SURFACE DISPLAY SCREENING AND RE-TESTING PIPELINE 78
FIGURE 3. 3. CCL8 YEAST SURFACE DISPLAY SCREEN 79
FIGURE 3. 4. CCL15 YEAST SURFACE DISPLAY SCREEN. 81
FIGURE 3. 5. CCL17 YEAST SURFACE DISPLAY SCREEN. 82
FIGURE 3. 6. CCL19 YEAST SURFACE DISPLAY SCREEN. 84
FIGURE 3. 7. CCL20 YEAST SURFACE DISPLAY SCREEN. 85
FIGURE 3. 8. CXCL8 YEAST SURFACE DISPLAY SCREEN 87
FIGURE 3. 9. CXCL12 YEAST SURFACE DISPLAY SCREEN 88
FIGURE 4. 1. OVERVIEW OF THE CC CHEMOKINE NETWORK 100
FIGURE 4. 2. CLUSTAL-W SEQUENCE ALIGNMENT OF P1243 WITH PUBLISHED CC CHEMOKINE BINDING EVASINS 102
FIGURE 4. 3. PROTEIN EXPRESSION OF P1243. 104
FIGURE 4. 4. CHARACTERISATION OF THE P1243 PROTEIN SEQUENCE 105
FIGURE 4. 5. BIO-LAYER INTERFEROMETRY (BLI) SENSOGRAMS OF P1243 AGAINST HUMAN CHEMOKINES 109
FIGURE 4. 6. SUMMARY OF THE BIOCHEMICAL PROFILE OF P1243 109
FIGURE 4. 7. NEUTRALISATION PROFILE OF P1243 AGAINST CC CHEMOKINES 111
FIGURE 5. 1. OVERVIEW OF THE CXC CHEMOKINE NETWORK 120

FIGURE 5. 2. GRAPHICAL OVERVIEW OF CLUSTAL-W SEQUENCE ALIGNMENT OF P1156 WITH PUBLISHED CXC CHEMOKINE BINDING EVASIN, EVASIN-3 122
FIGURE 5. 3. ANALYSIS OF PROTEIN EXPRESSION OF HISTIDINE-TAGGED-P1156..... 124
FIGURE 5. 4. CHARACTERISING OF P1156 PROTEIN SEQUENCE..... 125
FIGURE 5. 5. BIO-LAYER INTERFEROMETRY (BLI) SENSOGRAMS OF P1156 AGAINST HUMAN CXC CHEMOKINES 127
FIGURE 5. 6. BINDING AFFINITY PROFILE OF P1156 AGAINST CXC CHEMOKINES..... 128
FIGURE 5. 7. DOSE DEPENDANT MIGRATION OF HUMAN GRANULOCYTES IN RESPONSE TO CXCL1 AND CXCL8. 130
FIGURE 5. 8. ANALYSIS OF THE NEUTRALISATION PROFILE OF P1156 AGAINST CXC CHEMOKINES 131
FIGURE 6. 1. A SCHEMATIC OVERVIEW DISPLAYING THE STRUCTURE OF THE TWO-WARHEAD EVASINS EXPRESSION CONSTRUCTS..... 140
FIGURE 6. 2. SCHEMATIC OVERVIEW OF THE STEPS TAKEN TO CREATE THE TWO-WARHEAD EVASINS 142
FIGURE 6. 3. GEL ELECTROPHORESIS OF THE STEPS TO CREATE THE TWO-WARHEAD EVASIN: P1243:G4S:P1156..... 143
FIGURE 6. 4. GEL ELECTROPHORESIS OF THE STEPS TO CREATE THE TWO-WARHEAD EVASIN: P1156:G4S:P1243..... 144
FIGURE 6. 5. PROTEIN PURIFICATION AND CHARACTERISATION OF THE TWO-WARHEAD EVASINS 146
FIGURE 6. 6. CHARACTERISING THE PEPTIDE SEQUENCE OF THE TWO-WARHEAD EVASIN P1243:G4S:P1156..... 147
FIGURE 6. 7. CHARACTERISING THE PEPTIDE SEQUENCE OF THE TWO-WARHEAD EVASIN P1156:G4S:P1243..... 148
FIGURE 6. 8. BIOCHEMICAL PROFILE SHOWING CC CHEMOKINE BINDING TO SINGLE AND TWO-WARHEAD EVASINS: P1243:G4S:P1156 AND P1156:G4S:P1243..... 150
FIGURE 6. 9. BIOCHEMICAL PROFILE SHOWING CXC CHEMOKINE BINDING TO SINGLE AND TWO-WARHEAD EVASINS: P1243:G4S:P1156 AND P1156:G4S:P1243..... 151
FIGURE 6. 10. POLYVALENT BINDING OF TWO-WARHEAD EVASINS P1243:G4S:P1156 AND P1156:G4S:P1243 TO HUMAN CC AND CXC CHEMOKINES, DETERMINED USING BIO-LAYER INTERFEROMETRY..... 153

FIGURE 6. 11. NEUTRALISATION OF CC CHEMOKINE INDUCED CELL MIGRATION BY TWO-WARHEAD EVASINS 155
FIGURE 6. 12. NEUTRALISATION OF CXC CHEMOKINE INDUCED CELL MIGRATION BY TWO-WARHEAD EVASINS 156

List of Tables

TABLE 1. 2. SUBTYPES OF MONOCYTES 54
TABLE 2. 1. BUFFERS USED IN THIS STUDY, THEIR CONSTITUENTS AND SUPPLIER. 54
TABLE 2. 2. MEDIA USED IN THIS STUDY, ITS CONSTITUENTS AND SUPPLIER. 55
TABLE 2. 3. PCR PROGRAMME 61
TABLE 3. 1. SUMMARY PROFILE OF NOVEL EVASINS 89
TABLE 3. 2. SUMMARY OF IDENTIFIED NOVEL EVASINS AND THEIR SEQUENCE HOMOLOGY TO PUBLISHED EVASINS. 90
TABLE 6. 1. PCR PRIMER SETS FOR THE TWO-WARHEAD EVASIN: P1243:G4S:P1156 .. 143
TABLE 6. 2. PCR PRIMER SETS FOR THE TWO-WARHEAD EVASIN: P1156:G4S:P1243 .. 144

Nomenclature

AMBAM	Amblyomma americanum
BLAST	Basic Local Alignment Search Tool
BLI	Bio-layer interferometry
BSA	Bovine serum albumin
C	Cysteine
CC-CKBP	CC-chemokine binding protein
CCL	C-C motif ligand
CCR	C-C motif receptor
CKBPs	Chemokine binding protein
CXC-CKBP	CXC-chemokine binding protein
CXCL	C-X-C motif ligand
CXCR	C-X-C motif receptor
EC80	80 percent maximal effective concentration
FACS	Fluorescent activated cell sorting
FBS	Foetal bovine serum
FCS	Foetal calf serum
FITC	Fluorescein isothiocyanate
G4S	GGGGS
GAG	Glycosaminoglycans
GPCR	G-protein coupled receptor
HEK293F	Human embryonic kidney 293 cells
His	Histidine
IC_{50}	Half maximal inhibitory concentration
IFN	Interferon
IL	Interleukin
IXORI	Ixodes ricinus
K_d	Binding affinity
kDa	Kilodaltons (molecular weight)
LPS	Lipopolysaccharide
M	Molar

MFI	Mean fluorescence intensity
MI	Myocardial infarction
Ni-NTA	Nickel affinity
NK	Natural killer
nM	Nanomolar
nm	Nanometre
PAMP	Pathogen associated molecular pattern
PBMC	Peripheral blood mononuclear cells
PBS	Phosphate buffered saline
PCR	Polymerase chain reaction
PMN	Polymorphonuclear cells
PsiBLAST	Position-Specific Iterated BLAST
RA	Rheumatoid arthritis
RHISA	Rhipicephalus sanguineus
ROS	Reactive oxidising species
RT	Residence time
SD	Standard deviation
SDS-PAGE	Sodium dodecyl sulfate-polyacrylamide gel electrophoresis
SEC	Size exclusion chromatography
SGE	Salivary gland extract
t1/2	Half-life
TLR	Toll-like receptor
TNF	Tumour necrosis factor
vCKBP	Viral chemokine binding proteins
YSD	Yeast surface display

Chapter 1.

Introduction

1.1. Inflammation

Inflammation, from the latin “inflammare” (to burn), is the living hosts defence against foreign stimuli (3). Inflammation is a dynamic and complex process activated in response to infection, injury or trauma, with the primary aim of rapidly destroying or isolating the activating source, removing damaged tissue and restoration of tissue homeostasis (4). The inflammatory response manifests as two responses, innate or adaptive.

The innate response is the ‘first-defence’ against foreign agents and refers to a rapid and non-specific response, with the principal aim of eliminating the foreign bodies as quickly as possible. Defences attributed to innate immunity include physical barriers (skin and gastrointestinal, respiratory and digestive tracts), humoral components (complement and opsonins), antimicrobial proteins and cellular responses (5). The innate response is activated upon recognition of a range of molecular patterns, called pathogen-associated molecular patterns (PAMPs), displayed on pathogens but considered foreign to mammals. PAMPs include lipopolysaccharides, surface phosphatidylserine and aldehyde-derived proteins and oxidised or glycosylated low-density lipoproteins (5, 6). Circulating immune cells of the innate immune response recognise PAMPs and initiate a pro-inflammatory signal which activates the cellular component of the response. Key cells of the innate response include neutrophils,

monocytes and macrophages, which are discussed in detail below, other cells include dendritic cells, eosinophils, basophils, mast cells and natural killer (NK) cells (5).

The adaptive response, also known as the acquired response, refers to an antigen-specific response. Unlike the innate response, this response is not as rapid, on first exposure, as antigens need to be recognised and processed prior to initiating a response (7). During this process, foreign antigens are presented on antigen-presenting cells, such as macrophages and dendritic cells, which are then recognised by T cells and a targeted response is generated. Typically, the targeted response involves cytotoxic T cells, targeting the antigen-presenting cells, and stimulation of the antibody production by B cells (7).

Moreover, depending on the speed and duration of the response, inflammation can be acute or chronic. Acute inflammation is rapid and primarily involves granulocytes of the innate immune response. Unresolved acute inflammation can often result in chronic inflammation, a prolonged response, lasting several months to years. Chronic inflammation describes unregulated inflammation and ultimately results in a range of inflammatory disorders or conditions, such as rheumatoid arthritis or psoriasis (4).

1.1.1. Neutrophils

Neutrophils are the most abundant granulocytic-type white blood cell found in circulation and the first cells recruited to sites of inflammation, appearing within only hours after initial stimulation of the innate immune response. Furthermore, neutrophils typically display short life-spans, surviving only for a few hours. However, during inflammation, the production of neutrophils rapidly increases, and their lifespans also increase from hours to days (8). Neutrophils are generated in the bone marrow, in a process known as granulopoiesis, from granulocyte monocyte precursor hematopoietic stem cells (HSC), under the control

granulocyte colony stimulating factor (G-CSF) (9). The transcription factors C/EBPα, PU.1, CBF, and c-Myb are predominantly required to achieve neutrophil specification (10). Moreover, as neutrophils exhibit multi-lobed nuclei, they belong to the polymorphonuclear cells family (PMNs), along with basophils and eosinophils. Also, neutrophils, similar to basophils and eosinophils, exhibit granules in their cytoplasm, thus they are also referred to as granulocytes (8, 11). Upon stimulation, neutrophils migrate from the bone marrow to the inflamed site where they recognise pathogenic products and/or host derived damage molecules, either directly, through pattern recognition receptors (PRRs), or indirectly, through opsonised pathogens, marked by Fc or complement receptors (8). Upon interaction, pathogens are eliminated through phagocytosis or through the release of specialised granules (degranulation) (12).

In phagocytosis, pathogens are encased in a vacuole, termed the phagosome, which fuses with neutrophilic granules containing anti-microbial molecules (13). Degranulation involves the release membrane-bound secretory granules, which includes myeloperoxidase (MPO), defensins, cathepsins, lysozymes, and serine proteases (12, 13). Moreover, reactive oxidising species (ROS) are generated, and crucial for destructing the phagosome. The NADPH (nicotinamide adenine dinucleotide phosphate) oxidase complex, enclosed in secondary granules, generates the oxygen free radical, superoxide (O_2^-), which can cause damage to pathogens directly (12, 14). The importance of ROS species in combating pathogens was exemplified in patients with chronic granulomatous disease (CGD), who have a dysfunctional NADPH oxidase complex, and often display chronic infections (15).

Furthermore, neutrophils are also capable of NETosis, a specialised form of cellular death whereby cells release their DNA extracellularly, which assembles into an extracellular structure coated with many anti-microbial peptides, forming neutrophil extracellular traps (NETs) (16). NETs establish an antimicrobial milieu at the inflamed site and ultimately result

in the destruction of invading pathogens (17). Moreover, neutrophils are capable of releasing a range of pro-inflammatory agents, such as cytokines and chemokines, that stimulate the migration of other immune cells into sites of inflammation (8).

1.1.2. Monocytes

Following neutrophil infiltration into the inflamed sites, monocytes are then recruited. Monocytes are mononuclear cells that originate from myeloid progenitors in the bone marrow, under the influence of cytokine macrophage colony stimulating factor (M-CSF), and the transcription factor PU.1 (18). In humans, monocytes represent 10% of white blood cells and primarily function to mediate inflammatory responses against pathogenic infection (19). Monocytes typically have short-lives, ~8-20 hours, and are highly phagocytic in removing dead or pathogenic cells (20). Once recruited into tissues, monocytes differentiate into either dendritic cells or macrophages, this differentiation is dependent on the growth factors present at the inflamed sites, such as pro-inflammatory cytokines or microbial compounds (21).

The directional migration of monocytes to the inflamed sites is mediated through chemokines, integrins and adhesion molecules, which bind to the receptors on the surface of monocytes and induce their migration (20). Decades of research has expanded heavily on the monocyte. Flow cytometric analysis, single cell sequencing techniques and animal models have aided the identification of different subsets of monocytes and their functions. These different subsets are defined based on their cell surface expression markers, as either classical, intermediate and non-classical (20). Table 1.1 summarises the differences in the three subsets of monocytes in humans.

Monocyte function is crucial to the maintenance of health, thus abnormal levels in monocytes results in disease. Monocytopenia describes deficiencies in circulating monocyte levels and typically observed in patients with aplastic anaemia or hairy cell leukaemia (22). On the other

hand, increased levels of monocytes, known as monocytosis, is typically observed in a range of inflammatory diseases, including autoimmune diseases, pulmonary disorders and viral and bacterial infections (23).

Monocyte Subtype	**Circulating levels**	**Cell surface markers**	**Chemokine receptors**	**Function**
Classical	80-90%	$CD14^{hi}$, $CD16^{-}$, $CD64^{+}$, $CD62L^{+}$, $TNFR1^{+}$, $TNFR2^{low}$	$CCR2^{high}$, $CX3CR1^{low}$	Phagocytic, microbial activity, low level production of cytokines
Intermediate	<15%	$CD14^{high}$, $CD16^{+}$, $CD64^{+}$, HLA-DR^{high}, $TNFR1^{high}$, $TNFR2^{+}$	$CCR2^{low}$, $CCR5^{+}$, $CX3CR1^{low}$	Production of TNFα, IL-6, IL-1β
Non-classical	<15%	$CD14^{low}$, $CD16^{high}$, $CD64^{-}$, $TNFR1^{low}$, $TNFR2^{high}$	$CCR2^{low}$, CX_3CR1^{hi}	Anti-inflammatory effect, constitutive production of IL-1 receptor antagonist (IL-1RA)

Table 1. 1. Subtypes of monocytes. CCR2, CC chemokine receptor 2; CX3CR1, CX3C-chemokine receptor 1, TNFR1, tumour necrosis factor receptor 1; TNFR2, tumour necrosis factor receptor 2; HLA-DR, human leukocyte antigen- antigen D related; CCR5, CC chemokine receptor. (19, 21, 24-29)

1.1.3. Macrophages

Macrophages are present in all tissues of the body and are critical for immunesurveillance (7). As mentioned above, macrophages are derived from monocytes that have entered into inflamed tissues following initiation of the immune response. Broadly, macrophages have two primary functions, firstly tissue homeostasis whereby, they are responsible for the clearance of apoptotic and necrotic cellular debris (30). Secondly, macrophages are able to identify and phagocytose foreign antigens and subsequently stimulate the adaptive immune response,

through antigen processing and presentation (30). Upon activation in response to foreign stimuli, macrophages are also able to express inflammatory cytokines which activate signalling pathways, alter genetic expression and stimulate adaptive immunity (30, 31). Furthermore, macrophages can exist in two different states, the classically activated M1 state, which are pro-inflammatory, and the alternative activated M2 state, which promotes tissue repair (32).

1.2. Inflammation in disease

A prolonged or excessive inflammatory response is harmful to the host and can not only result in inflammatory disease, but also propagate the pathogenesis of existing disease. Increasing evidence has shown an influx of immune cells and their mediators into diseased tissue, thus showing the role of inflammation in disease. Examples of such diseases include those affecting the heart, such as myocarditis (33), vasculitis (34), atherosclerosis (34, 35) and myocardial infarction (36), the neurological system, such as Alzheimer's (37), multiple sclerosis (38) and stroke (39), gastrointestinal system, including inflammatory bowel disease (40) and pancreatitis (41), respiratory system, such as lung fibrosis (42) and asthma (43), joints and bones, such as rheumatoid arthritis (44) and osteoarthritis (45), as well as the skin, which includes psoriasis (46) and scleroderma (47). The section below will discuss the cardiovascular diseases: atherosclerosis and myocardial infarction, and the role of immune cells in those diseases.

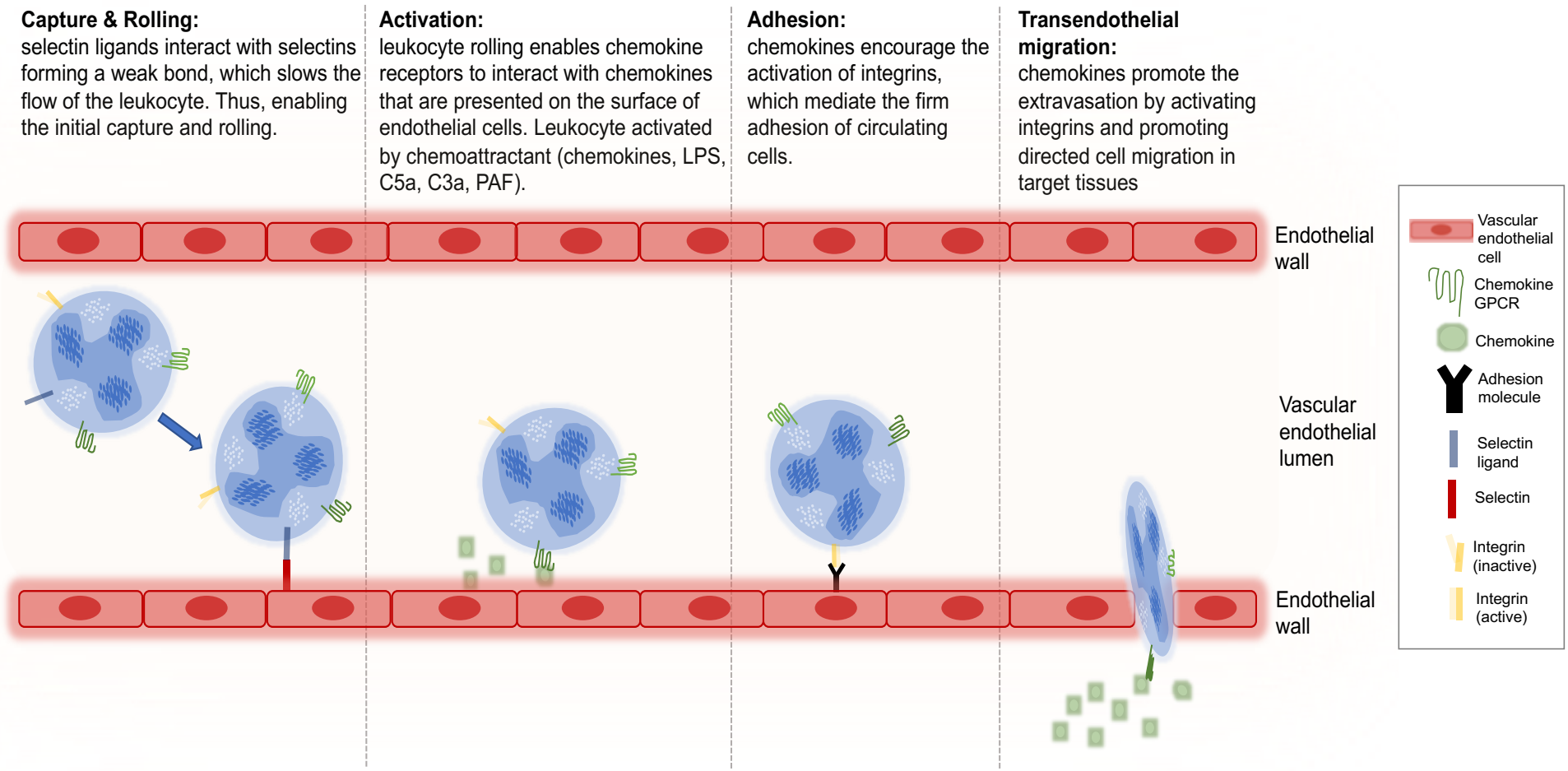


Figure 1. 1. Schematic showing chemokine-induced leukocyte extravasation. Leukocyte extravasation describes the movement of leukocytes from blood circulation into tissues. LPS- lipopolysaccharide, C5a or C3a- complement factors, PF- platelet factor (48, 49).

1.2.1. Atherosclerosis

Atherosclerosis, the leading cause of death worldwide, is a chronic inflammatory disease and the underlying cause of ischemic heart disease and stroke (50). Atherosclerosis is chronic inflammatory disease of the arteries, driven by the accumulation of oxidised low-density lipoproteins (oxLDL) into the arterial wall coupled with progressive recruitment of inflammatory cells (51).

Elevated levels of LDLs result in endothelial dysfunction and formation of free radicals, which increase endothelial permeability of atherogenic lipoproteins. The activation of endothelial cells results in increased expression of adhesion molecules, such as intercellular adhesion molecule (ICAM) and vascular cell adhesion molecule (VCAM-1), and production of chemokines. As a result, this process promotes the adhesion of circulating immune cells and their transmigration cross the endothelium (Figure 1. 1) (52, 53).

During early stages of disease, recruited macrophages can engulf modified LDL's and form cholesterol-laden foam cells, which accumulate to form a fatty streak lesion. Foam cells also release several inflammatory mediators, such as cytokines, chemokines and matrix metalloproteinases (MMPs), which recruit more inflammatory cells and progress pathogenesis (54). Fatty streaks can develop into fibrous plaques in the inner layer of the blood vessel wall, which comprises accumulating smooth muscle cells (SMC), macrophages and lymphocytes. Moreover, plaques can grow as they aggregate cells and protrude into the arterial lumen, resulting in narrowing of blood vessels and in restrictions to blood flow (53).

Additionally, atherosclerotic plaques can enter an advanced state where they calcify, and are prone to degradation by MMPs, thus increasing the vulnerability of the plaque and its destabilisation (55). Rupturing of plaques due to instability results in the release of the plaques thrombogenic contents, promoting activation of platelets and the blood coagulation cascade,

and formation of a thrombus. These events can ultimately result in blood vessel occlusion, further restrictions to blood flow and increased susceptibility to ischemic events, such as myocardial infarction or stroke (56).

Moreover, recently, neutrophils have been implicated in all stages of atherosclerosis (57). *In vivo* models of atherosclerosis have shown macrophages release mediators that recruit neutrophils to the atherosclerotic plaques (58-61). Zernecke *et al*., (59) showed depletion of neutrophils reduced atherogenesis, likely by reducing plaque inflammation. In addition to this, once within the lesion, neutrophils are able to release their granular enzymes (neutrophilic degranulation), such as azurocidin, MPO and defensins, which promote the recruitment of monocytes (62). Neutrophils also release ROS which recruit more neutrophils, oxidises LDL and contributes to plaque vulnerability (63).

Furthermore, *in vivo* studies have shown the formation of atherosclerotic lesions is dependent on the differentiation of monocytes into macrophages. Smith *et al*., (64) have shown M-CSF (macrophage colony-stimulating factor) knockout mice were resistant to developing atherosclerosis. Moreover, de Villiers *et al*., (65) and Rajavashisth *et al*., (66) showed monocyte-deficient apolipoprotein E (ApoE) knockout mice displayed reduced lesion formation, thus highlighting the role of monocytes in atherogenesis.

1.2.2. Myocardial infarction

Myocardial infarction (MI) belongs to the acute coronary syndrome (ACS) family, which comprises a spectrum of pathologic states characterised by reduced blood flow through the coronary arteries. MI describes a sudden pathologic event whereby blood flow to the heart is restricted, resulting in an ischemic cascade and eventually cardiomyocyte death (67). The most

common cause of MI is a ruptured atherosclerotic plaque, which upon rupturing blocks blood flow through the arteries.

The adult human heart has limited capacity for cardiomyocyte renewal thus, following an extensive ischemic event, the hearts self-renewal process is incapable of sufficiently compensating the loss of cardiomyocytes and results in a decrease in cardiac function (68). This large loss in cardiomyocytes results in scar formation, cardiac remodelling, compensatory hypertrophy, and can eventually result in heart failure (69).

Following the ischemic event, immune cells are central to initiating, developing and resolving inflammation. Cardiomyocyte death result in exposure of damage-associated molecular patterns (DAMPs), which are recognised by resident macrophages and circulating monocytes, through their PRRs. Upon recognition, a signalling cascade is initiated producing various chemokines and cytokines, which recruit immune cells to the infarction site and initiate inflammation (67).

Recruited neutrophils are responsible for clearing cellular debris and degrading ECM, which aids myocardial repair. However, neutrophils also produce ROS (70). The production of ROS can further aggravate inflammation through oxidative stress, activation of pro-apoptotic signalling pathways, and stimulating the production of MMPs. Oxidative stress can cause endothelial dysfunction, up-regulate the expression of adhesion molecules, which increases the permeability of in endothelial cells, and increases the migration of neutrophils (71). Thus, regulating the production of ROS and reducing oxidative stress are mechanisms of reducing cardiac tissue damage and recovering functional cardiac tissue. Moreover, neutrophils release various neutrophilic chemoattractants, such as CXCL1 and CXCL8, further increasing the numbers of neutrophils (8).

Moreover, neutrophilic degranulation, as observed in atherosclerosis, can occur resulting in increased blood vessel permeability and recruitment of proinflammatory monocytes to the inflamed site, which may increase infarct size (70). Furthermore, the neutrophilic recruitment of monocytes post-MI are thought to be detrimental in the long-term, as Dutta *et al*., (72) showed increased recruitment of monocytes following MI accelerated atherosclerosis in mice. Patient studies conducted by Goldstein *et al*., (73) and Milonas *et al*., (74) observed similar clinical findings, whereby an increase in cardiovascular events were observed in patients surviving a MI.

The role of immune cells in propagating the pathogenesis of inflammatory diseases has validated them as target for therapy in those diseases. The movement of immune cells into inflammatory sites is inevitable and challenging to control, however, controlling the mediators that recruit them may be achievable (75). As a result, the mediators of inflammation have been examined as therapeutic targets in inflammatory disease (76). For example, the CANTOS trial examined the effects of targeting the inflammatory mediator interleukin-1β in patients with previous myocardial infarction and a high-sensitivity C-reactive protein (CRP). Using a monoclonal antibody, Canakinumab, they showed patients displayed a significant reduction in recurrent cardiovascular events, compared to placebo (77).

One of the key mediators of immune cell recruitment is chemokines, furthermore, increased expression of chemokines is one of the key findings in a range of inflammatory diseases. Therefore they have been examined as targets for therapy in a range of diseases driven by inflammation (78).

1.3. Chemokines

Chemokines, ~ 8-12 kDa, are a family of chemoattractant cytokines that control the migration of leucocytes that mediate both adaptive and innate immunity. During inflammation, chemokines are released from mast cells, macrophages, platelets, lymphocytes and endothelial cells in response to pro-inflammatory cytokines (TNF-α), and bacterial (lipopolysaccharide) and viral products (dsRNA) (79). Furthermore, chemokines mediate various functions during haematopoiesis (80), angiogenesis (81) and organogenesis (82, 83). Thus, chemokines can be categorised functionally as homeostatic and/or inflammatory. Moreover, chemokines are classified structurally into four subgroups, based on the position of their conserved cysteine residues at their N-terminus (84).

1.3.1. Chemokine classification

Chemokines are classified based on the position of their conserved cysteine residues at the N-terminus, as either CC, CXC, XC or CX_3C (C-cysteine and X-amino acid group) (Figure 1. 2). These chemokines are also known as β, α, γ and δ chemokines, respectively (84). Chemokines nomenclature describes their subgroups followed by the ligand (L) number, for example CCL1 describes the chemokine belonging to the CC-motif subgroup, ligand number 1. Furthermore, chemokine receptors are also grouped into four subgroups: CCR, CXCR, XCR and CX_3CR (R-receptor), which interact with either CC-, CXC-, XC- or CX_3C-chemokines, respectively.

Chemokines first appeared 700 million years ago from a common ancestral gene and since then have evolved extensively and rapidly through large gene duplication events and successive selection. Chemokines exist selectively in vertebrates and the majority are encoded within the same chromosomes and clusters (85). Clustered chemokines form certain groups, such as the growth-regulated oncogene (GRO) group on chromosome 4, and perform similar functions indicating they have common evolutionary origins. The CXC GRO group of chemokines,

CXCL1-8, are responsible for the recruitment of neutrophils to sites of inflammation (discussed in more detail below) (2).

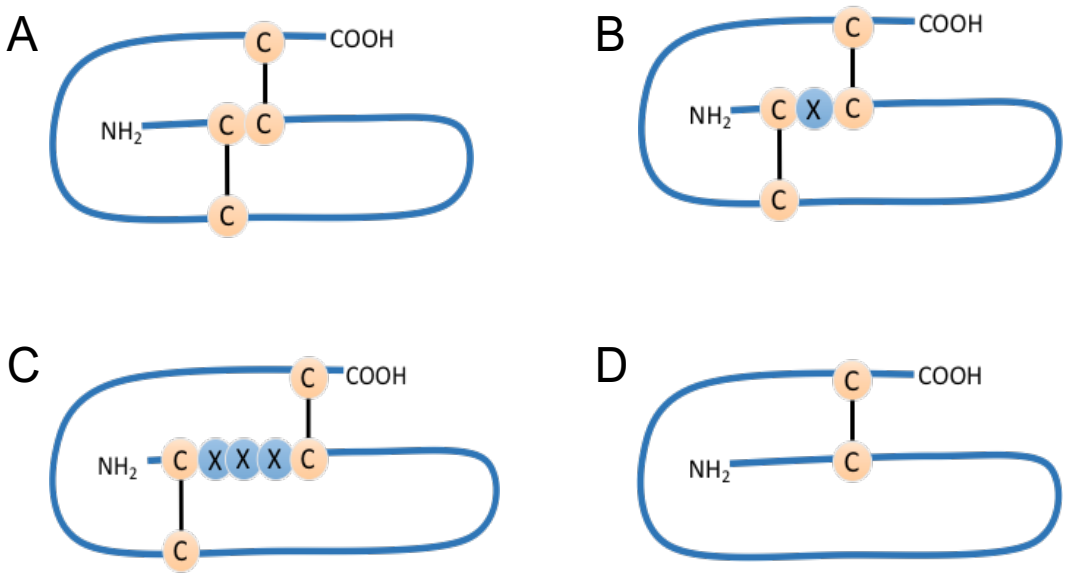


Figure 1.2. Classes of chemokines. Chemokines are divided into four classes based on the position of their cysteine (C) residue at the N-terminus (NH_2). COOH: carboxylic acid, indicating C-terminus. NH_2: amide, indicating N-terminus. Blue lines indicate peptide sequence length and black lines connecting C-groups indicate a disulphide bond. (A) CC chemokines: conserved cysteines are adjacent to each other at the N-terminus. (B) CXC chemokines: conserved cysteines are separate by a single amino acid group. (C) CX_3C chemokines: two conserved cysteine groups are separated by three amino groups. (D) XC chemokines: only has one conserved cysteine at the N-terminus.

1.3.1.1. CC chemokines

CC chemokines describe a group of signalling ligands that structurally possess two, out of their four, conserved cysteines adjacent to each other (Figure 1. 2). This subgroup of chemokines represents the largest of the four chemokine subgroups. Moreover, the majority of the genes encoding the CC chemokines are found clustered together on chromosome 17q11.2 (86). Thus, indicating these chemokines arose through gene duplication and subsequent divergence. Furthermore, these clustered chemokines show

they retain similar functions, recruiting mononuclear cells (86). Within the cluster at chromosome 17, two sub-clusters encoding CC chemokines can be distinguished.

The first cluster shows the MCP (Monocyte Chemoattractant Protein) chemokines: CCL1, CCL2, CCL7, CCL8, CCL11 and CCL13 (86). These closely related chemokines are responsible for the recruitment of monocytes, hence the name, as well as T and NK cells. Moreover, CCL7, CCL8 and CCL13, which signal through CCR2 and CCR3, are also able to recruit eosinophils (84). CCL11, eotaxin-1, is also a potent eosinophil-chemoattractant. The remaining eotaxin family, CCL24 (eotaxin-2) and CCL26 (eotaxin-3), are located in a mini-cluster at chromosome 7 (86). The eotaxin family also recruits the CCR3-expressing mast cells and Th2 cells (84). Interestingly, CCL26 is antagonistic to CCR1, CCR2 and CCR5 (87, 88), suggesting CCL26 has a more modulatory function as opposed to an inflammatory function.

The second sub-cluster on chromosome 17, encodes the CCR1 and CCR5 ligands: CCL5, CCL14, CCL15, CCL16 and CCL23 (89) in a mini-cluster and CCL3, CCL4 and CCL18 in a another mini-cluster (86). Both CCL3 and CCL4 bind CCR5, however CCL3 also binds CCR1 (90, 91).

The remaining chemokines not located in these clusters are found as single units or as part of a mini-cluster. CCL19, CCL21 and CCL27 are located in a mini-cluster on chromosome 9 (86) and all signal to recruit lymphocytes. CCL19 and CCL21 signal through CCR7 (92, 93), whereas CCL27 signals through CCR10 (94). Furthermore, the closely related CCL17 and CCL22 are found on chromosome 16 (86). Both chemokines are expressed highly in the thymus and signal through CCR4 to recruit Th2 type memory T cells into inflamed sites.

Finally, the chemokines CCL20, CCL25 and CCL28 are located as single members on chromosome 2, 19 and 5, respectively. CCL20 is the only ligand to signal through CCR6, similar to β-defensins (antimicrobial peptides) (95). CCL25 is the only ligand to signal through CCR9 to recruit dendritic cells, thymocytes and activated macrophages (86), and CCL28 signals through CCR10, similar to CCL27, and also CCR3. However, unlike CCL27, CCL28 is expressed in mucosal tissues, thus suggests its role in the recruitment of cells into those areas (86).

1.3.1.2. CXC chemokines

Structurally, CXC chemokines have a single variable amino acid separating their N-terminal conserved cysteines (Figure 1. 2) (84). Collectively, the CXC chemokine signalling system, in humans, comprises of fifteen ligands and six receptors and display functions not limited to the immune response. Moreover, the CXC chemokines are likely to be recently evolutionarily developed as the majority appear exclusive to mammals (86). An exception is observed for the homeostatic chemokines CXCL12 and CXCL14, where unambiguous orthologues have been found in fish (96).

Furthermore, similar to CC chemokines, the majority of the CXC chemokines cluster together on chromosome 4 and organised into two sub-clusters. The first sub-cluster contains the CXC GRO genes that encode for CXCL1, CXCL2, CXCL3, CXCL4, CXCL5, CXCL6, CXCL7 and CXCL8 (86). The members of this group, with the exception of CXCL4, all contain the ELR (glutamic-leucine-arginine) motif adjacent to the first conserved cysteine and described as ELR+. Chemokines that lack the ELR motif, such as CXCL4, are described as ELR-. Through the binding of CXCR1 and/or CXCR2, the ELR+ CXC chemokines result in the recruitment of neutrophils. The redundancy observed in this

signalling pathway is likely to provide a method of controlling immune cell migration in a specific manner (97). These chemokines also confer pro-angiogenic effects, promoting the formation of new blood vessels (81). On the other hand, CXCL4, mainly found in platelets, is angiostatic, inhibiting endothelial cell proliferation and formation of new blood vessels (81).

The second sub-cluster in chromosome 4 encodes the ELR- CXC chemokines: CXCL9, CXCL10, CXCL11 (86). These chemokines all signal through CXCR3 and induce the chemotaxis of Th1 cells and NK cells. Moreover, these chemokines are antagonistic for CCR3, which recruits Th2 cells, therefore when these chemokines signal through CXCR3 to recruit Th1 cells, they are also concomitantly antagonising the recruitment of CCR3 expressing Th2 cells (98). Furthermore, similar to CXCL4, these chemokines are also angiostatic (81).

CXCL13 is also found on chromosome 4, although more distant that the aforementioned clusters. CXCL13 is a homeostatic chemokine that signals through CXCR5 to promote the homing of B cells into specific locations in secondary lymphoid organs (99).

Another homeostatic chemokine is CXCL12, encoded by a gene located on chromosome 10 (86). This multi-functional chemokine is ubiquitously expressed in various cells and tissues and signals through CXCR4 to attract lymphocytes (84) and endothelial progenitor cells from bone marrow, which are crucial for angiogenesis (75).

Finally, CXCL14 and CXCL16 are encoded by genes found on chromosomes 5 and 17, respectively (86). CXCL14, similar to CXCL12, is also ubiquitously expressed in tissues and cells. The signalling receptor for this chemokine has not yet been identified, although studies have shown it is chemoattract for monocytes (100) and dendritic cells (101).

CXCL16, on the other hand, shares a similar structure to CX_3CL1 (102) (discussed below) and signals through CXCR6 to recruit T cells and NK T cells (86).

1.3.1.3. CX_3C chemokines

The CX_3C chemokine motif describes three amino acid groups separating the cysteines at the N-terminus (Figure 1.2), and only have one member: CX_3CL1 (Fractalkine). The gene encoding this chemokine is found on chromosome 16, situated between the genes encoding CCL17 and CCL22, although it bears no structural similarities to CC chemokines (86). Moreover, CX_3CL1 can exists in two forms, bound to the membrane (103) and as a soluble entity, and recruits monocytes and T cells through CX_3CR1 signalling (86).

Structurally, CX_3CL1 differs dramatically from other chemokines, with the exception of CXCL16. Structurally, CX_3CL1 and CXCL16 have four distinct domains: a chemokine domain, mucin-like stalk, a transmembrane domain and a cytoplasmic domain (102, 103). The mucin-like stalk, displayed above the chemokine domain, enables interactions with the surface of target cells (103).

1.3.1.4. XC chemokines

XC chemokines are unlike the other three subgroups of chemokines as they do not have a first and third cysteines, thus possessing only a single conserved cysteine at the N-terminus (Figure 1.2) (84). The XC chemokine subgroup is encoded by genes in a mini-cluster on chromosome 1 and comprises of only XCL1 (lymphotactin-α) and XCL2 (lymphotactin-β) (86). Both chemokines are abundantly expressed by CD8+ T cells and signal through XCR1 to recruit T and NK cells (104).

1.3.2. Chemokine function

Functionally, chemokines can be categorised as homeostatic and/or inflammatory. Chemokines functions are finely regulated in the immune system, in which the controlled secretion of specific chemokines, coupled with their spatial and temporal production, ensures measured responses (75).

1.3.2.1. Homeostatic chemokines

Homeostatic chemokines are constitutively expressed in lymphoid tissue and other organs, and responsible for the spatial organisation of chemokines in specific locations. For example, CCL19, CCL20, CCL21 and CXCL12 are actively expressed in secondary lymphoid organs, such as the spleen and lymph nodes, and responsible for the homing of T and B lymphocytes and dendritic cells (105, 106). Moreover, CCL19, CCL21 and CXCL12 are expressed in the vasculature of the blood-brain barrier and responsible for the recruitment of immune cells into the central nervous system for immunesurveillance (107). Moreover, CX_3CL1 is involved in maintaining the survival of neuronal cells and microglia communication (107, 108). Increasing evidence has shown homeostatic chemokines are crucial for preparing the immune cell composition of tissues and organs, so that following foreign insult, immune cells can be rapidly trafficked (4).

1.3.2.2. Inflammatory chemokines

On the other hand, inflammatory chemokines are not constitutively expressed, and only released from circulating cells upon activation, thus, they are also termed ‘inducible’ chemokines. Inflammatory chemokines function to recruit both innate and adaptive immune cells, following injury and infection, to the inflamed sites (75). For example, CXCL1 and CXCL8 are both inflammatory chemokines, chemotactic for neutrophils (109).

Moreover, certain chemokines cannot be exclusively attributed a homeostatic or inflammatory status, as they exhibit both features, these chemokines are termed 'dual-function' chemokines (110). Figure 1. 5 summarises chemokines interaction with their receptors and their functional nature.

1.3.3. Chemokine structure

The majority of chemokines exhibit a similar structural arrangement and highly conserved tertiary structure (111). Crucial to the tertiary structure are the four conserved cysteines, two of these cysteines are located close to the N-terminus, one is located centrally, and the forth is located closer to the C-terminus (Figure 1. 2). Moreover, the structural arrangement of chemokines cysteines shows the first and third cysteines are linked, and the second and fourth cysteines are also linked through disulphide bonds (Figure 1. 2, Figure 1. 3) (84).

More specifically, a highly flexible N-terminus, an N-loop (following the first two cysteines), a helix (3_{10} helix), three-stranded anti-parallel β-sheet and a C-terminal α-helix, comprise the general structure of chemokines (Figure 1. 3) (111). The strands and helices found in the chemokine structure are linked by a series of loops termed 30S, 40S and 50S, in which the numbers reflect the residue number of the mature protein (84). The chemokines three-stranded β-sheet is connected by 30S and 40S loops (Figure 1. 3) (111). The N-terminus of a chemokine, which contains the N-loop, is responsible for forming the interactions between the chemokine and their receptors, and subsequent receptor activation (112).

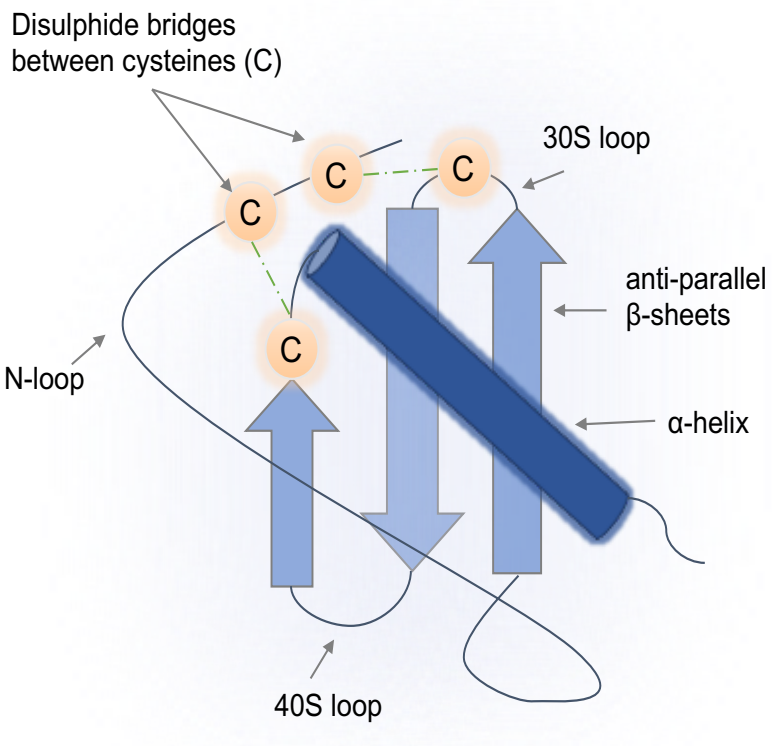


Figure 1. 3. Schematic showing the three-dimensional structure of chemokines. Chemokines typically exhibit a flexible N-terminus, with an N-loop, three anti-parallel β-sheets, connected by 30S and 40S loops, and a C-terminal α-helix. Generally, chemokine have four conserved cysteines, two of which are found at the N-terminus. The first and third cysteines, and the second and fourth cysteines, are connected by disulphide bridges. Schematic shown here is based on structure reviewed in (113).

1.4. Chemokine receptors

1.4.1. Chemokine receptor structure

Chemokines interactions with their receptors, expressed on the surface of immune cells, ensures mobilisation of target cells from the bone marrow and their extravasation from circulation into target tissues (Figure 1. 1) (48). Chemokine-receptor signalling is transduced through seven transmembrane G-protein coupled receptors (GPCR), embedded in the lipid bilayer of the target cell (110). Chemokine receptor GPCR's exhibit the same canonical

topology, comprising of an unstructured extracellular N-terminus, three extracellular loops, three intracellular loops and an intracellular C-terminus (114). Furthermore, chemokine receptors exhibit the conserved motif: aspartic acid-arginine-tyrosine (DRY) at the third cytoplasmic transmembrane domain, which is proven critical to signalling (115, 116) (Figure 1. 4). The chemokine transduction pathway has several downstream effects, including chemotaxis, cellular adhesion, proliferation and controlling genetic expression (117, 118).

1.4.2. Chemokine signalling pathway

The structural regions that show ligand binding and receptor activation, of a number of chemokines and their receptors, has been defined. It has been postulated chemokines bind to their receptors through a two-site model, defined by chemokine recognition sites 1 (CRS1) and 2 (CRS2). CRS1 designates the chemokine globular core (N-loop/40S loop groves) interacting with the extracellular N-terminus of the receptor. CRS2 designates the interaction of the chemokines N-terminus to the receptors extracellular transmembrane helical domain. Thus, chemokine binding to the CRS2 pocket results in stabilisation of the receptors structure and permits the intracellular interaction of the receptor to the heterotrimeric G proteins, α, β and γ subunits (Figure 1. 4).

Upon chemokine binding, and receptor activation, the GPCR binds the G-protein subunits (α, β and γ) and acts as a guanine nucleotide exchange factors (GEFs), whereby guanosine diphosphate (GDP) is exchanged for guanosine triphosphate (GTP). Subsequently, the GTP-bound Gα-subunit dissociates from the αβγ heterodimeric subunit to propagate downstream signalling pathways. When GPCRs are inactive, GDP is bound to the Gα-subunit (119). Mammalian Gα proteins are comprised of four subgroups: $G\alpha_s$, $G\alpha_{i/o}$, $G\alpha_{q/11}$, $G\alpha_{12/13}$ (117, 119, 120). The majority of chemokine signalling is mainly mediated through the $G\alpha_i$ proteins (121).

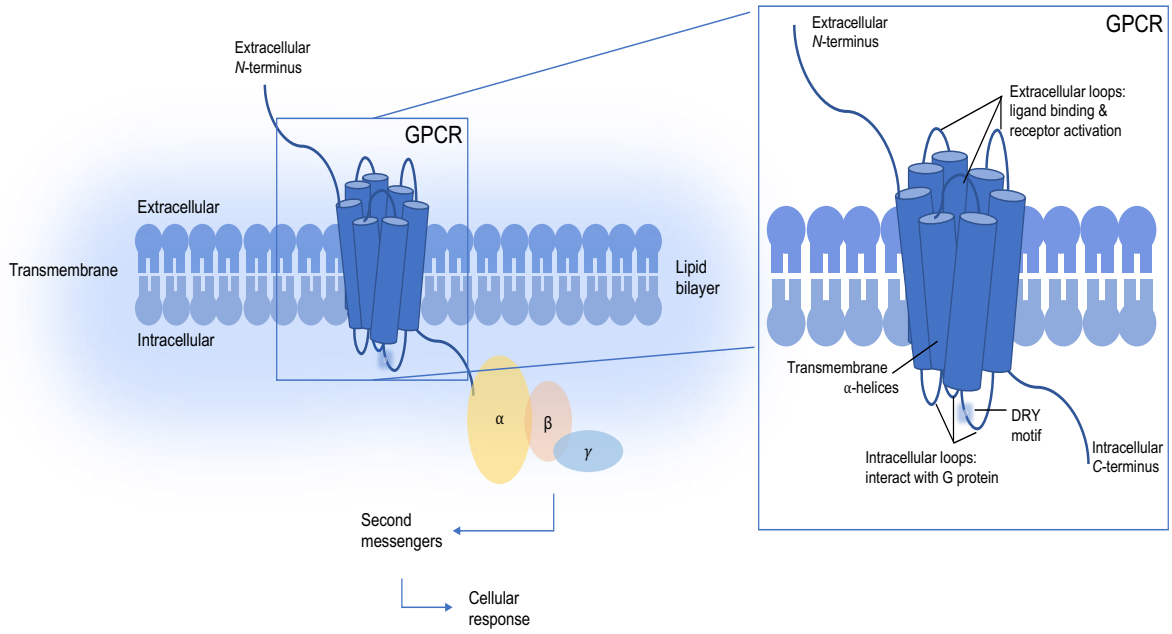


Figure 1. 4. Schematic representation of the chemokine G-protein coupled receptor (GPCR). Chemokines GPCRs comprise of unstructured extracellular N-terminus, seven transmembrane domains (embedded in the lipid bilayer of the target cell) and an intracellular C-terminus. The extracellular loops linking the extracellular domains are important for ligand binding and receptor activation. The DRY (aspartic acid-arginine-tyrosine) domain is located at the third (cytoplasmic) transmembrane domain and proven to be proven critical to signalling. Upon chemokine binding, the receptor is activated and binds the G-protein subunits (α, β and γ). G-protein subunits then propagate downstream signalling pathways (110).

1.4.3. GAG binding

Following production, chemokines are secreted from cells and able to bind to glycosaminoglycans (GAGs), found on the surface of cells or in the extracellular matrix. This binding immobilises chemokines and encourages the formation of a chemokine gradient (48). Thus, this gradient promotes the directional migration of leukocytes from circulation to sites of injury, or infection, via chemokine signalling through GPCRs (122). In some cases, chemokines bind to receptors and GAGs using different domains, although in some instances these domains can overlap (123, 124).

1.4.4. Atypical receptors

Chemokine receptors that lack the DRY motif, such as D6, bind chemokines, however they do not promote a signalling response, acting as scavenger receptors or decoys, and termed atypical receptors (115). Humans have three chemokine receptors that lack the DRY motif: D6, Duffy Antigen Receptor for Chemokines (DARC) and Chemokine Receptor Like-1 (CCRL1) (125). These scavenging receptors are thought to control chemokine levels *in vivo* (115, 126).

1.4.5. Chemokine network

Despite the chemokine network being broadly variable, it has also proven to be highly robust, as a result of redundancy and binding promiscuity of chemokines and their receptors (127). To-date, 20 chemokine receptors have been identified, this coupled with the knowledge over 50 chemokines have been identified, highlights the redundancy of chemokine signalling (84). Redundancy is typically employed by biochemical pathways to ensure the pathways output is insensitive to changes (128, 129). Indeed, multiple chemokines are able to bind a single

receptor, receptors bind multiple chemokines and immune cells express multiple chemokine receptors (2) (Figure 1. 5).

The redundancy in the chemokine network is observed by chemokines action on their target cells, as no single chemokine is exclusively active against a single leucocyte population. For example, the MCP chemokines (CCL1, CCL2, CCL7, CCL8, CCL11 and CCL13 (86)) all interact through the CCR2 chemokine receptor go recruit monocytes (2). Moreover, polyspeirism is displayed in the chemokine network, this describes the redundant expression of numerous chemokines, upon stimulation, by a single cell type (127). Polyspeirism is displayed most dramatically by the mononuclear phagocytes (monocytes, macrophage and dendritic cells), which upon stimulation by bacterial products (such as LPS), release CX_3CL1 as well as numerous CC and CXC chemokines (126, 130).

1.5. The role of chemokines in disease

Increased expression of chemokines is one of the key findings in a range of inflammatory diseases. Evidence highlighting the significance of chemokines, and validating their potential as therapeutic targets in inflammatory disease, has been supported by their upregulated expression in diseased tissue, coupled with a range of genetic and animal model studies (131). Moreover, chemokines themselves pose a potentially deleterious consequences as a feed-forward loop exists, whereby immune cells, recruited by chemokines into the inflamed site, secrete chemokines that drive the recruitment of even more immune cells into the inflamed site (84).

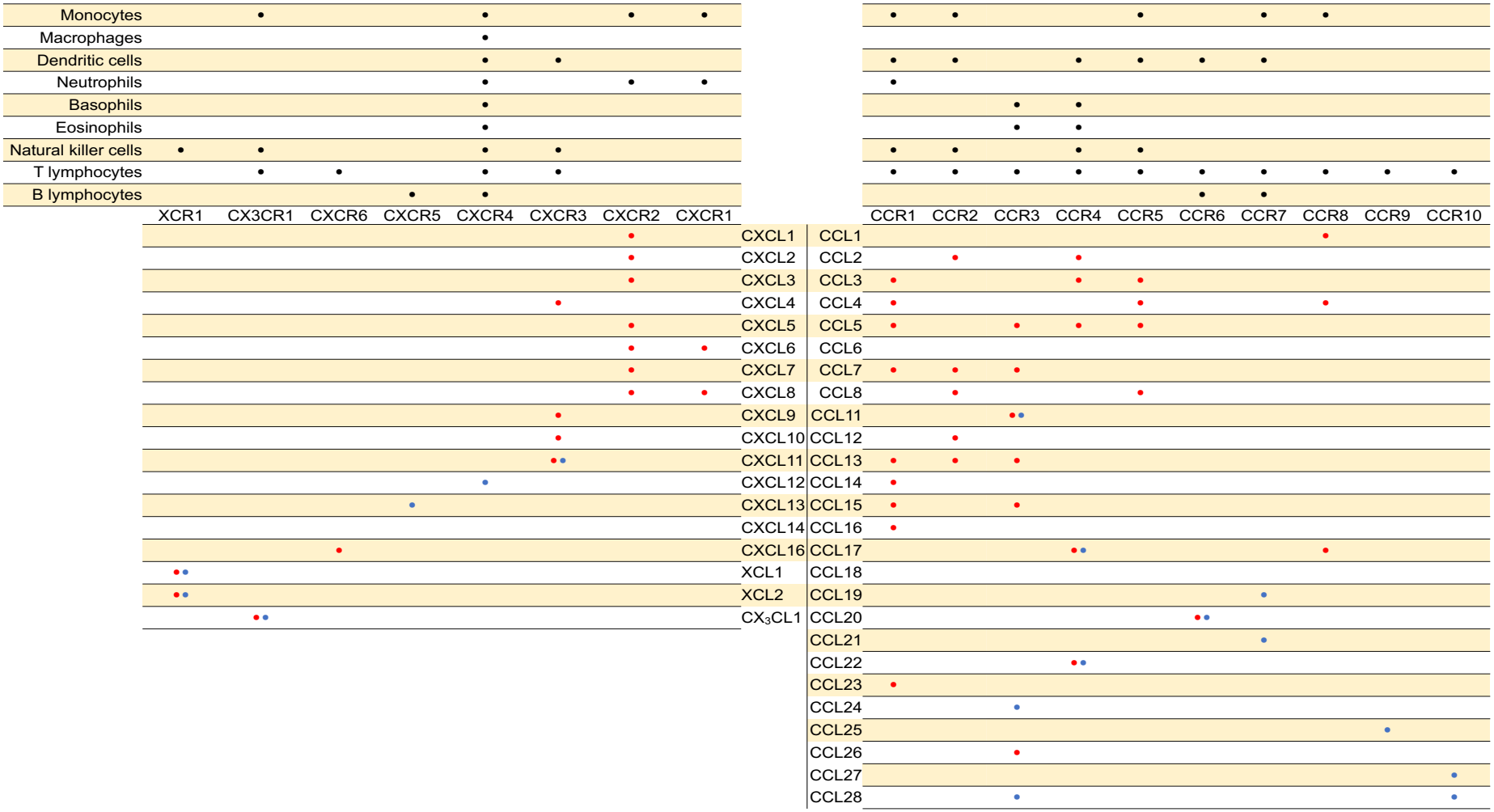


Figure 1. 5. Human chemokine network. Individual chemokines can bind multiple receptors, a single receptor can bind multiple chemokines and immune cells express multiple receptors. Black circles indicate receptor interactions with chemokines, red circles indicate inflammatory function and blue circles indicate homeostatic function. Some chemokine exhibit both inflammatory and homeostatic functions, this is indicated by red and blue circles. CCL18 and CXCL14 are both homeostatic chemokines, their signalling receptors have not been identified (1, 2)

1.5.1. Genetic studies

Epidemiological studies identified numerous genetic polymorphisms in the genes encoding chemokines, or their receptors, and their association with disease. A genetic polymorphism in the gene encoding the CCL2 promoter, whereby guanine (G) is substituted for an adenine (A) at position -2518, results in upregulated transcription of the CCL2 gene. A significant number of patients with coronary artery disease (CAD), who were referred for coronary bypass surgery, displayed homozygous for this variant (132). Moreover, this polymorphism was shown to be an independent predictor of occult ischemia in healthy, but high-risk, populations (133). Furthermore, through ultrasonography, HIV-infected individuals exhibiting this polymorphism were associated with a five-fold increased risk of developing atherosclerosis (134).

In addition to this, Bai *et al*., (135) showed a high frequency of patients with chronic obstructive pulmonary disease (COPD) displayed polymorphisms in both the CCL2 (-2518 A/G) and CCR2 (190G/A) genes, thus suggesting these polymorphisms as new risk factors for COPD. Simeoni *et al.* (136) reported the 403A polymorphism in the CCL5 gene was associated with developing coronary atherosclerosis, independent of conventional risk factors and biomarkers, and Boger *et al.* (137) reported this polymorphism, in patients with type 2 diabetes mellitus and end stage renal disease, is associated with all-cause mortality.

Furthermore, a substitution of threonine (T) for alanine (A), at amino acid 23 (A23T), in the CCL11 gene (CCL11-23T) is associated with increased risk of developing allergic inflammatory disorders, such as asthma (138). In addition to this, Zee *et al*., (139) showed that the CCL11-23T allele increased the incidence risk of myocardial infarction, and changes to other risk factors, such as body mass index (BMI) and medical history, did not affect the significance of the results.

1.5.2. Chemokine expression in disease

Moreover, numerous studies over the years have examined chemokines potential as biomarkers in various inflammatory diseases, where they may serve as predictors of a pathological state or condition (140). In atherosclerosis, a number chemokines have been found to be highly expressed in atherosclerotic plaques, including CCL1 (141), CCL2, CCL3, CCL8, CCL13 (142), CCL5, CCL11 (143), CCL17 (144), CCL18, CCL19 (145), CCL20 (146), CCL25, CXCL8 (34), CXCL9, CXCL10 (147), CXCL12 (35), CXCL16 (148) and CX_3CL1 (149). Moreover, increased levels of CCL2, CCL5 and CXCL8 in plasma and/or serum have been reported in patients with Takayasu arteritis (inflammation of the arterial walls) (150).

Damås *et al*., (151) showed the levels of CXCL1, CXCL5 and CXCL8 progressively increased, in combination with increases with the New York Heart Association functional class, in patients with congestive heart failure.

In addition to this, increased levels of the chemokines CCL2, CCL3, CCL4, CCL5, CCL8, CXCL8 and CXCL10 have been reported in stroke, Alzheimer's disease, Creutzfeldt Jakob and traumatic brain injury (152-154), and collections of joint synovial fluid and tissue biopsies from arthritis patients showed the expression of a range of chemokines including CCL1, CCL3, CCL5, CXCL8 and CXCL10 (155).

1.5.3. Animal model studies

With increasing data associating chemokines with disease, several studies examined these findings *in vivo*. Kukielka *et al*., (156) showed, in a canine model, increasing and persistent levels of CXCL8 were observed following myocardial ischemia/reperfusion, which contributed to myocardial injury through neutrophil recruitment. Ono *et al*., (157) showed increasing levels of CCL2 were observed following myocardial ischemia/reperfusion, and its

neutralisation (24-hours after reperfusion) significantly reduced the size of the infarct. Moreover, quantitative histological analysis of CCR2 knockout Apoe-/- mice aorta lesions showed reduced macrophage infiltration in the vessel wall and inhibition of plaque formation (158). Moreover, Gu *et al*., (159) showed CCL2 knockout LDL-/- mice displayed an 83% reduction in atherosclerotic lesion formation.

Additionally, several studies have shown the use of monoclonal antibodies to target CXCL8 reduced neutrophil infiltration and subsequent prevention of tissue injury in animal models of acute inflammation LPS-induced dermatitis, LPS/IL-1-induced arthritis, acute immune complex-type glomerulonephritis (160, 161), lung reperfusion injury (160, 162) and endotoxin-induced pleurisy (163).

Collectively, these studies show the importance of chemokines in disease and their validation as targets, for therapy, in diseases driven by inflammation. Subsequently a range of agents targeting chemokines have been developed.

1.6. Targeting chemokines

Pharmaceutical intervention targeting the chemokine network has largely focused on generating small molecule inhibitors of chemokine receptors. This is largely due to the success of GPCR (7TM receptor) inhibitors (164). Indeed, several chemokine receptor antagonists have been developed over the years that have reached the market, such as Maraviroc (Pfizer), which inhibits CCR5, and Plerixafor (Anormed), which inhibits CXCR4 (165). In addition to this, clinical trials are currently ongoing for antibodies targeting CCL2, CCL5, CXCL10, CCR2, CCR4, CCR5 and CXCR4 (166).

However, a large number of studies targeting the chemokine network, in inflammatory disease, have failed at the clinical trials stage, mainly due to lack of efficacy (167). Indeed, increasing clinical studies have shown the chemokine network is relatively insensitive to intervention that targets single components (nodes) of the network (167). For example, in rheumatoid arthritis, ABN912, a monoclonal antibody targeting CCL2 (168), and MLN3897, a small molecule targeting CCR1 (169), both failed during the early clinical stages due to lack of efficacy and no clinical improvement. Moreover, Berlex Biosciences developed BX-471, a CCR1 antagonist, for multiple sclerosis patients, which failed at Phase II trials due to a lack in efficacy (170). The lack of success in these studies may be due to the robustness of the chemokine network, as chemokines can bind multiple receptors and a single receptor can bind multiple chemokines (171). Thus, neutralising a single chemokine, or single node in the network, does not ensure neutralisation of signalling pathway (Figure 1. 5).

On the other hand, studies into numerous parasitic and viral species, which target living systems, have identified they exhibit a range of immunomodulatory agents capable of aiding immune-evasion, such as chemokine binding proteins (CKBPs). Increasing studies have identified CKBPs, present in nature, are likely to have more of an impact on targeting the chemokine network as, crucially, they are able to target multiple chemokines. CKBPs have been reported in helminths (172), viruses (173), and ticks (174, 175).

1.6.1. Helminth-derived chemokine binding proteins

Helminths are multicellular parasitic worms that inhabit both humans and animals and infect almost one-third of the global population (176). The global prevalence of this parasite highlights the parasites ability to successfully modulate the hosts immune response, and has been examined in numerous studies (177).

For example, anti-chemokine activity was reported in the parasite *Schistosoma mansoni (S.mansoni*), which infects humans resulting in schistosomiasis (178). Smith *et al*., (172) identified, through cross-linking assays and chemokine labelling, the CKBP: *S.mansoni* CKBP (smCKBP) from the *S.mansoni*'s egg secretions. Moreover, smCKBP was also found in two other schistosomular species: *S. haematobiumand* and *S. japonicum* (172). This CKBP was not found in other life stages of the parasite, remains the only identified helminth-CKBP and is entirely unique in its genetic coding, showing no sequence homology to the identified CKBP's or mammalian proteins. Additionally, characterisation of this CKBP shows its binds CCL2, CCL3, CCL5, CXCL8 and CX_3CL1, and neutralises chemokine-mediated cellular activity (172).

1.6.2. Virus-derived chemokine binding proteins

Viruses are replicating infectious agents that need to actively evade the hosts immune system to avoid elimination (179). Thus, a common strategy for immune-evasion, employed by the poxviruses and herpesviruses, is to encode homologues to cytokines, chemokines and their receptors (180). Another strategy to overcome the chemokine network is the expression of viral CKBP (vCKBPs), which share no sequence homology to hosts chemokines or their receptors (173). Moreover, little to no sequence homology exists between the amino acid sequences of different viruses vCKBPs (181), although crystal structures show similar structural patterns, likely a result of parallel evolutions (182).

Numerous studies have identified and characterised a series of vCKBPs that exhibit binding to multiple chemokines (180). For example, the M3 protein, encoded by murine gammaherpesvirus 68 (MHV-68), and Glycoprotein G (gG), from alphaherpesviruses, both neutralise chemokine activity through binding to multiple chemokines directly, *in vitro* and *in*

vivo (183, 184). Moreover, studies by Pyo *et al*., (185) and Martin *et al*., (186) showed the expression of M3 *in vivo* prevented disease in models of femoral arterial injury and in autoimmune diabetes, respectively.

However, vCKBPs tend to exhibit an unrestrained approach to binding chemokines, with the exception of a few, they largely show binding to multiple chemokines from multiple classes (180). For example, the poxvirus CKBP M-T7 binds not only chemokine from multiple classes but also IFN-γ (187). Similarly, M3, expressed by gammaherpesvirus murine herpesvirus 68 (MHV-68), also binds chemokines from all four classes (188). Such modes of action can potentially become harmful as not all chemokines are inflammatory, and many are required for homeostatic or reparative functions, even in disease (75). Therefore, the use of vCKBP's as therapeutics may result in off-target effects.

1.6.3. Tick-derived chemokine binding proteins

Similar to viruses, hard ticks (Ixodidae) require immuno-evasive qualities to enable them to feed on their hosts for prolonged periods of time, several days to weeks, without eliciting their hosts immune response (189). To achieve this, ticks inject during feeding more than 3000 different peptides from their saliva into their hosts which, in redundant levels, display anti-analgesic, anti-clotting, vasodilatory, anti-inflammatory and immunomodulatory components (190).

Anti-chemokine activity was first reported in ticks by Hajnická *et al*., demonstrating the saliva gland extracts (SGE) of a number of Ixodid tick species exhibited anti-CXCL8 activity (191). Subsequent studies performed by Frauenschuh *et al*., (192) and Deruaz *et al*., (193) generated a cDNA library from the salivary glands of the *Rhipicephalus sanguineus* tick and screened for chemokine binders. These studies yielded four CKBP's termed Evasins 1, 2, 3 and 4, although

no known ligand has been identified for Evasin 2 (192). Evasins are capable of binding to multiple chemokines, Evasin 1 and 4 bind selectively to CC chemokines, whereas Evasin 3 binds only CXC chemokines (192, 193). Furthermore, searches of the mammalian genome for sequences sharing homology to evasins yielded no results (174), thus showing evasins are exclusively tick-derived.

1.7. Evasins

1.7.1. CC chemokine binding evasins

Evasin 1 and 4 share sequence homology and both exhibit CC chemokine binding selectivity (192, 193). Evasin 1 is a highly selective CKBP, showing binding to only CCL3, CCL4 and CCL18. Whereas, Evasin 4 displays a far larger binding profile compared to Evasin 1, binding to at least 18 CC chemokines (194). Moreover, evasin homologs have been found in other tick species, including *Amblyomma maculatum* (195) and *Amblyomma americanum* (196). Further studies by Vancova *et al*., (197) showed SGE from the *Rhipicephalus appendiculatus* tick exhibited activity against CCL2, CCL3, CCL5, CCL11 and CXCL8.

Most recently, studies by Singh *et al*., (175) and Hayward et al., (198) identified and characterised a large array of novel evasins. Singh *et al*., (175) describe identifying 16 novel CC chemokine binding evasins, identified through bioinformatics. Hayward *et al*., (198) also described their novel evasins were identified through bioinformatic evasin homology searches, spanning the *Amblyomma*, *Rhipicephalus* and *Ixodes* genera. Collectively, the CKBP's identified from these two studies targeted only CC chemokines.

1.7.2. CXC chemokine binding evasins

The only CXC CKBP identified to-date is Evasin 3. Evasin 3 shares no sequence homology to Evasin 1 and 4 and exhibits binding to a specific subset of CXC chemokines, the ELR+ CXC chemokines: CXCL1, CXCL2, CXCL3, CXCL5, CXCL6 and CXCL8 (192, 193). Moreover, studies by Vancova *et al*. (199) described Evasin 3-like activity, anti-CXCL1/CXCL8, in *Amblyomma variegatum, Rhipicephalus appendiculatus, and Dermacentor reticulatus* tick species (199). These findings show targeting CXC chemokines to be a common feature of the Ixodid tick species and highlights the importance of targeting neutrophils when suppressing inflammation (8, 109).

1.7.3. Evasin structure

Evasins are relatively small proteins, in comparison to vCKBPs, with molecular masses ranging from 7–11 kDa in size. Structurally, evasins can be divided into two classes based on the number of cysteines (Cys) they exhibit, moreover these finding also correlate with those evasins functions. The first class of CKBPs typically contain eight conserved Cys residues, also called '8-Cys' tick CKBPs. These evasins include the CC-CKBPs Evasin 1, Evasin 4 (192, 193), P991 (175) and others (198). The second evasin class of possess six conserved Cys residues, also called '6-Cys' tick CKBPs, and include the CXC-CKBP Evasin 3 (192, 193).

Moreover, through the use of X-ray crystallography, the complex of Evasin 1 and human CCL3 has been solved, revealing the N- and C-termini of Evasin 1 interact with the N-terminus and N-loop of CCL3 (200, 201). Additionally, the peptide sequence of Evasin 4 shows it shares the same disulfide bridge pattern as Evasin 1, suggesting it shares a similar three-dimensional fold (201). Furthermore, i*n silico* and mutagenesis assays suggest Evasin 4 also targets the N-

terminus of CCL3 (201). On the other hand, Evasin 3 displays a novel structural fold to Evasin 1 and 4 (201), and its complex with a CXC chemokine has yet to be determined.

1.7.4. Evasins *in vivo*

The effects of the published evasins *in vivo* has been examined in numerous preclinical models. Russo *et al*., (202) showed Evasin 1 displayed both preventative and therapeutic effects in a model of bleomycin-induced lung fibrosis. Following bleomycin challenge, an influx in leukocyte numbers was observed, accompanied by increased expression of CCL2, CCL3, CCL5, TNFα, TGF-β and pulmonary fibrosis. The administration of Evasin 1 proved preventative, on the day of bleomycin administration. Moreover, eight days following bleomycin administration, Evasin 1 proved therapeutic, where a decrease in the levels of leucocytes into the lungs was observed, accompanied by a reduction in the levels of TNFα and TGF-β, and attenuation of pulmonary fibrosis.

Moreover, Deruaz *et al*., (193) showed Evasin 1 reduced inflammation in a preclinical model of psoriasis, which is dependent on the induction of numerous CC chemokines (203). Additionally, Evasin 1 was examined in a graft versus host disease (GVHD) model in a study by Castor *et al*., (204). GVHD is characterised by influx of T cells, which are driven by CCL3 (205). Castor *et al*., (204) showed Evasin 1 reduced migration of T cells (CD4+ and CD8+) and levels of IFN-γ and CCL5 in the small intestine. This was also accompanied by a reduction in the histopathological score at the small intestine, and a reduction in liver damage was also observed through reduction in inflammatory infiltrates and levels of IFN-γ.

A study by Braunersreuther *et al*., (206) examined the effects of Evasin 3 and 4 in a murine model of myocardial injury. Following coronary occlusion, mice were injected with either Evasin 3 or 4. All mice injected with evasin showed a reduction in post-infarction leucocyte

infiltration, ROS release and levels of CCL2 and CXCL1. Moreover, a reduction in infarct size was also observed, compared to controls. However, no improvements were observed in cardiac function, cardiac remodelling and scar formation, although, Evasin 4 did show improvements in mice survival following the ischemic event.

In addition to this, Copin *et al*., (207), examined Evasin 3 in murine models of carotid atherosclerosis (CA) and ischemic stroke (IS), which typically display elevated levels of the chemokines CXCL1 and CXCL2. In the CA model, Evasin 3 reduced the levels of neutrophils and metalloproteinase-9 present within the atherosclerotic plaques, thus reducing plaque vulnerability. Moreover, Evasin 3 reduced the levels of neutrophils infiltrating the brain in the IS model, however, this failed to improve post-stroke outcomes.

Furthermore, Montecucco *et al*., (208) also examined the effects of Evasin 3 and Evasin 4 in disease models of pancreatitis, which are often accompanied by injures to the lungs. Evasin 3 attenuated neutrophil-infiltration, ROS production and apoptosis in the lungs. Evasin 3, also, reduced the levels of neutrophil and macrophage apoptosis and necrosis in the pancreas. However, Evasin 4 only reduced the macrophage levels in the pancreas. Additionally, the effects of Evasin 3 were examined in a murine model of antigen-induced arthritis (AIA), which is primarily driven by neutrophils, and resulted in a significant reduction in the symptoms of disease (174).

Collectively, these studies have shown chemokines involvement in numerous inflammation-driven diseases. Moreover, the systemic administration of evasins effectively reduces inflammation in a range of preclinical models of inflammatory disease, suggesting that they could be used as therapeutics for such diseases. However, the limitations of the evasins, published thus far, include evasins which do not bind to significant chemokines, such as CCL2, CCL13, CXCL10 and inability of a single evasin to target both CC and CXC chemokines.

Therefore, this thesis aimed to expand the chemokine-binding repertoire of identified evasins and hypothesised that other tick species would have novel evasins that are also capable of modulating chemokine activity.

Chapter 2.

Materials & Methods

2.1. Materials

2.1.1. Buffers

Buffer	Constituents	Supplier
His-binding buffer	20mM NaPO4, 500mM NaCl, pH 7.4	Sigma-Aldrich
His-wash buffer	20mM NaPO4, 1M NaCl, 20mM imidazole, pH 7.4	Sigma-Aldrich
His-elution buffer	20mM NaPO4, 500mM NaCl, 500mM imidazole, pH 7.4	Sigma-Aldrich
His-regeneration buffer	1M NaCl + 0.2M EDTA (pH 8.0)	Sigma-Aldrich
Nickel(II) chloride hexahydrate ($NiCl_2$)	10mM $NiCl_2$	Sigma-Aldrich
Glycine	10mM Glycine	Sigma-Aldrich
Size exclusion buffer	Phosphate buffered saline (PBS) + 150 mM sodium chloride, pH 7.4	Gibco, Sigma-Aldrich

SEC wash buffer	1M NaOH	Sigma
Deglycosylation buffer	40mM HEPES, 300mM NaCl and 1mM TCEP	Sigma-Aldrich
FACS wash buffer	0.01% PBS + 0.01% Bovine serum albumin (BSA)	Sigma-Aldrich
MACS RBC lysis buffer (10x)	-	MACS Miltenyi Biotec
HetaSep™ 6% Hetastarch solution	Hetastarch (6% w/v), Sodium chloride, Sodium lactate (anhydrous), Dextrose (hydrous), Calcium chloride dihydrate, Potassium chloride, Magnesium chloride hexahydrate, other ingredients	STEMCELL Technologies
MACS buffer	PBS containing 0.5% BSA and 2 mM EDTA	Sigma-Aldrich
PBST	Phosphate Buffered Saline (PBS) with 0.05% Tween-20	Sigma-Aldrich
TAE buffer	2 M Tris Acetate, 100 mM Na_2EDTA	Sigma-Aldrich
Running buffer	NuPAGE™ MES SDS Running Buffer (20X)	Invitrogen™, Thermo Fisher Scientific
Transfer buffer	NuPAGE™ Transfer Buffer (20X)	Invitrogen™, Thermo Fisher Scientific
Octet buffer	10 mM Na2HPO4, 1.8 mM KH2PO4, 2.7 mM KCl, 500 mM NaCl, 0.1% BSA, 0.002% TWEEN-20, pH 7.4	Sigma-Aldrich

Table 2. 1. Buffers used in this study, their constituents and supplier. Sigma-Aldrich (Gillingham, UK); Invitrogen (Paisley, UK); ThermoFisherScienctific (Loughborough, UK); GE Healthcare (Buckinghamshire, UK); Gibco (distributed by ThermoFisherScienctific (Loughborough, UK); Miltenyi Biotec Ltd (Surrey, UK).

2.1.2. Media

Media	Constituents	Supplier
YPAD (2x)	1L: 20 g Bacto-yeast extract, 40 g Bacto-peptone, 80 mg Adenine Sulfate, 20g Glucose	Sigma-Aldrich, BD
SD-CAA	1L: 6.7 g Yeast Nitrogen Base (YNB) with Ammonium Sulfate, 5 g Casamino Acids, 7.4 g Citric Acid Monohydrate, 10.4 g Sodium Citrate, 10 g Glucose, pH 4.5	MP Biomedicals, Sigma-Aldrich, BD
SG-CAA	1L: 6.7 g Yeast Nitrogen Base (YNB) with Ammonium Sulfate, 5 g Casamino Acids, 5.4 g Na2HPO4 (Sodium Phosphate Dibasic), 8.6 g NaH2PO4 (Sodium Phosphate Monobasic), 2 g Glucose, 18 g Galactose, pH 4.5	MP Biomedicals, Sigma-Aldrich, BD
SOB	0.5% (w/v) yeast extract, 2% (w/v) tryptone, 10 mM NaCl, 2.5 mM KCl, 20 mM MgSO4	Sigma-Aldrich, BD
SOC	SOB +1% of 2M glucose	Sigma-Aldrich, BD
CSM (-Trpysin)	1L: 6.7 g Yeast Nitrogen Base (YNB) with Ammonium Sulfate, 1.92 g Trp Dropout, 10 g Glucose	MP Biomedicals, Sigma-Aldrich
THP-1 cell media	RMPI-1640, 10% heat inactivated Fetal Calf Serum (FCS), 4 mM L-Glutamine	Sigma-Aldrich
HEK293F cell media	FreeStyle™ 293 Expression Medium	Thermo Fisher Scientific
Cell migration media	RMPI-1640, 0.5% heat inactivated Fetal Calf Serum (FCS), 4 mM L-Glutamine	Sigma-Aldrich

Table 2. 2. Media used in this study, its constituents and supplier. Sigma-Aldrich (Gillingham, UK); ThermoFisherScienctific (Loughborough, UK); BD (Wokingham, UK); MP Biochemicals (California, UK).

2.1.3. Cell lines

THP-1 cells were purchased from Sigma. THP-1 cells were maintained at a density of 0.2 × 10^6 cells per a mL in RMPI-1640 +10% heat inactivated Fetal Calf Serum (FCS) + 4 mM L-Glutamine.

HEK293F cells were a gift from Nicola Burgess-Brown (University of Oxford). HEK293F cells were propagated as suspension cultures maintained at a density of 0.5 × 10^6 cells per a mL in FreeStyle™293F media (ThermoFisherScientific).

All cell lines were maintained in a 37°C, 5% CO_2 humidified chamber. Mycoplasma contamination was routinely tested using a MycoAlert™ kit (LONZA) and DAPI staining.

2.1.4. Plasmids

2.1.4.1. Yeast surface display plasmids

Yeast expression plasmid and plasmid libraries were developed as a toolkit for use in GoldenGate cloning. Plasmids were constructed from constituent idempotent parts that included a promoter, signal peptide, cDNA, surface display tags, epitope tags, terminator, replication origins, antibiotic and/or auxotrophic selection markers.

Parts were generated using PCR or gene synthesis (GeneWiz) and cloned into plasmids. Overhangs in evasin parts were designed so that they were compatible with either N- or C-terminal surface display tags. To enable library construction, plasmids were assembled using the single pot GoldenGate/GoldenBraid cloning method and modified to include a negative selection *ccdb* gene cassette (Invitrogen) to improve cloning efficiency.

All yeast plasmids contained a GAL1 promoter, synthetic AMYG_RHIOR signal peptide, 2-micron replication origin and ADH1 terminator, and TRP auxotrophic marker. Yeast surface

display tags were either AGA2_YEAST (from pCTCon2) or SAG1_YEAST (residues 332-650) and were separated from the cDNA using a linker encoding (GGGGS)x3. Three configurations of yeast plasmid containing evasin library were created with either N-terminal AGA2_YEAST, C-terminal AGA2_YEAST, and C-terminal SAG1_YEAST surface display tags. These vectors are referred to as D1211, D1212, and D1213, respectively. Plasmids were designed and constructed by Professor Shoumo Bhattacharya (Radcliffe Department of Medicine, University of Oxford).

2.1.4.2. Protein expression plasmids

Protein expression vectors for P1243, P1243:G4S:P1156 and P1156:G4S:P1243 were constructed in pHLSec plasmids (gift from Radu Aricescu) (209). Protein plasmids were constructed using PCR and infusion cloning (Clontech), following manufacturer's guidelines. All protein expression plasmids contained a C-terminal G4S linker and strep II-8xHis protein purification tag (GGGGGSGGGGSGGASAWSHPQFEKLEHHHHHHHH (210)) and N-terminal ETG sequence from plasmid pHLSec.

P1156 protein expression vector was constructed using idempotent parts using the Bhattacharya laboratory's adaptation of the GoldenGate/GoldenBraid cloning method. Parts included the CAGGS promoter (GeneBank Sequence AB281497), IgK signal peptide (211), StrepII:His tag (GGASAWSHPQFEKLEHHHHHHHH, pQE-Trisystem, Qiagen), and bovine growth hormone terminator (pcDNA3, Invitrogen). Following cleavage of signal peptide, the sequence at the N-terminus is DGG, predicted by SignalP 3.0 (212). Plasmids were designed by Professor Shoumo Bhattacharya (Radcliffe Department of Medicine, University of Oxford).

2.2. Methods

2.2.1. Bioinformatic identification of novel evasins

To identify novel evasin sequences, and build the evasin library, the sequences of evasin 1, 3 and 4 were PsiBLAST against the NCBI tick transcriptome shotgun assembly database (http://blast.ncbi.nlm.nih.gov/). BLAST (Basic Local Alignment Search Tool) is a bioinformatic tool that allows the comparison of amino acids, in protein sequences, or nucleotides, in DNA sequences, to sequences in a library or database. PsiBLAST (Position specific iteration BLAST) is a more sensitive BLAST search that gives each identified sequence a similarity score (position specific score) and allows identification of more evolutionary distant, but similar, sequences (213).

The sequences underwent three iterations or BLAST searches. Mature peptide sequences were identified using SignalP 3.0 server (212). Only sequences having an e-value $<1 \times 10^{-5}$, possess a signal peptide defined by the SignalP 3.0 server, and having a mature peptide less than 200 amino acids long were selected. Selected evasin sequences were imported into Filemaker Pro to create an evasin library database. Once the database was completed each evasin Sequence was given a unique ID number. Mature peptides were then synthesised (Genewiz). Bioinformatic search for novel evasins was conducted by Professor Shoumo Bhattacharya.

Evasin sequences identified belonged to the following tick species: AMBAM - *Amblyomma americanum*, AMBMA – *Amblyomma maculatum*, AMBTR – *Amblyomma triste*, AMBPA, *Amblyomma parvum*, RHISA – *Rhipicephalus sanguineus*, RHIPU- *Rhipicephalus pulchellus*, AMBCA- *Amblyomma cajennense*, and IXORI-*Ixodes ricinus*.

2.2.2. Yeast surface display (YSD)

2.2.2.1. Transformation of evasin library into YSD vectors

Evasin sequences identified through bioinformatic searches were synthesized (Genewiz), then pooled together and transformed into the three YSD vectors (described in Section 2.1.4.1). Device size and inserts were confirmed by digesting with the restriction enzyme: BsmBI (New England Biolabs, NEB). Empty vectors, YSD vectors with the same tags but without the evasin pool, were created and served as controls.

Vectors were then transformed into *saccharomyces cerevisiae* (EBY100 yeast, Invitrogen) using the TRAFO® yeast transformation technique: one yeast colony was inoculated overnight at 30^{o}C, with agitation, in 10 mL of YPAD media (Table 2.2). The next day 2.5 $\times$ 10^8 cells were resuspended in 50 mL of YPAD media and incubated for 4 hours at 30^{o}C, with agitation. Cells were then harvested, by centrifugation, and resuspended in 1 mL of MilliQ H_2O. For each sample transformation, 100 µL of resuspended cells were used. The following was added to each sample: 240 µL of Polyethylene glycol (PEG 3500 50% w/v), 36 µL of Lithium Acetate (1M), 50 µL of boiled Salmon-Sperm carrier DNA (Sigma-Aldrich) and 0.1-1 µg of DNA (diluted in MilliQ H_2O). Samples were then incubated at 42^{o}C for 40 minutes before plating on CSM (-trypsin) plates and incubated for three days at 30^{o}C.

2.2.2.2. YSD fluorescent activated cell sorting (FACS)

To label yeast cells for FACS, EBY100 yeast (transformed with evasin library (D1211, D1212 and D1213)) were galactose-induced. For induction, yeast cells containing different libraries were first cultured in glucose-rich media overnight (SD-CAA) at 37^{o}C, then

incubated again in SD-CAA for five hours and then in a galactose-rich media (SG-CAA) overnight, at 37°C.

For labelling, 5×10^5 galactose-induced cells were labelled with 0.5 μg of biotinylated chemokine (Almac) and Streptavidin-AF647 (Invitrogen) and incubated on ice, in the dark, for 30 minutes. Cells were then washed and resuspended in 0.01% PBS + 0.01% Bovine serum albumin (BSA). Positive samples were then sorted on the Beckman Coulter Legacy MoFlo MLS High Speed Sorter with the aid of Mr. Andrew Worth (Nuffield Department of Medicine, University of Oxford). Following FACS, positive clones were then plated on large CSM (-trypsin) plates and incubated for three days, at 30°C. After incubation, yeast plates were pooled, and sorted for a second time.

2.2.2.3. Colony PCR and plasmid rescuing

Following second FACS, 24 positive yeast clones were picked, and plasmids extracted using the Zymoprep Yeast Plasmid Miniprep II (ZymoResearch). Colony PCR was then performed to amplify DNA.

For colony polymerase chain reaction (PCR), the following primers were used: Gal Forward primer (5'-CTGCATAACCACTTTAAC, 10 ρM/μl) and a mix of 1211 (5'-GCTTCTCTTACAGATCTTCTTCGCTAATCAGTTTCTGTTC, 10 ρM/μL) and 1212 reverse primer (5'- CTCCACCAGAGCCTCCTCCACC, 10 ρM/μl) (Sigma-Aldrich). PCR programme shown in Table 2 .3. Following PCR, samples were resolved on a 2% Agarose gel. Amplified sequences were used for sequencing.

Step	Temperature (°C)	Time (minutes)
1 (initial denaturation)	94	5
2 (denaturation)	94	1
3 (annealing)	60	1
4 (extension)	72	1
5	Cycle steps 2-4, 30 times	
6 (final extension)	72	10

Table 2. 3. PCR programme. PCR programme for colony PCR and amplifying sequences for generating two-warhead evasins (Chapter 6).

Initially all 24 clones were sequenced using 94-well plate sequencing (Source BioScience) and then retested for chemokine binding using flow cytometry. This method proved inefficient and costly as many of the clones failed to retest when rescued, therefore a 24 clone-binding assay (Section 2.2.2.4) was established and incorporated before selecting clones for sequencing and rescuing.

Following DNA isolation, plasmids were then transformed into DH5α *Escherichia coli* (E. Coli) cells by electroporation (set voltage 2.1, 100 ohms, 20 μF, Biorad). Cells were then recovered with SOC buffer (Table 2.1) and plated on LB-kanamycin (10 μg/mL) plates. E. coli DNA extraction and purification was performed using Qiagen Plasmid Miniprep Kit (Qiagen). For re-testing, extracted DNA was transformed back into EBY100 yeast using the TRAFO® yeast transformation protocol, as described in Section 2.2.2.1.

2.2.2.4. Chemokine binding assay in yeast cells

For the pre-rescue binding assay or 24 clone binding assay: one yeast colony was picked and resuspended in SD-CAA in a 96-well plate and incubated at 30°C, with agitation, for 5 hours. Cells were then harvested by centrifugation, resuspended in SG-CAA and incubated, with agitation, at room temperature overnight. The following day, 1.25 x 10^5 cells were labelled with 0.125 μg of biotinylated chemokine (Almac) and Streptavidin-AF647 (Invitrogen), and incubated on ice, in the dark, for 30 minutes. Cells were then washed, resuspended in 0.01% PBS + 0.01% BSA and analysed on the Attune Nxt Flow Cytometer (Invitrogen).

For re-testing, a single colony was first cultured in SD-CAA overnight at 37°C, then incubated again in SD-CAA for five hours and then in a galactose-rich media (SG-CAA) overnight, at 37°C. Cells were then counted, and 0.5 x 10^6 yeast cells were labelled, following the same protocol described above.

2.2.3. Protein production and purification

Proteins were produced using HEK293F cells. Cells were transiently transfected with endotoxin-free DNA, generated using Qiagen Endotoxin-free Maxi-kit, and using the transfection reagent: polyethylenimine (Sigma). Cells were cultured in Freestyle™293 expression medium (Thermofisher), following transfection, at 37C, 8% CO_2 with agitation for four-five days. Each 500 mL flask, at time of transfection, contained 150 x 10^6 cells in 150 mL of media (1 x 10^6 cells/mL), 150 μg of DNA, 0.3 mg of PEI.

Proteins were purified in two steps: first, proteins from filtered supernatants were purified by gravity flow through Nickel charged IMAC Sepharose 6 Fast Flow resin (GE Healthcare). Column was first equilibrated with His-binding buffer (20 mM NaPO4, 500 mM NaCl, pH 7.4), filtered supernatant was then added, followed by a wash with the His-wash buffer (20 mM NaPO4, 1 M NaCl, 20 mM imidazole, pH 7.4) and eluted in His-elution buffer (20 mM NaPO4, 500 mM NaCl, 500 mM imidazole, pH 7.4). His-purified elutions were pooled and concentrated using Amicon Ultra-15 Centrifugal Filter Unit with Ultracel-3-membrane (Millipore).

Secondly, concentrated his-purified elution was purified by size exclusion chromatography (SEC) on an AKTA Start or AKTAFPLC system using HiLoad 16/600 Superdex 75 (GE Healthcare), in SEC buffer (PBS + 150mM NaCl). Fractions showing an absorption at 280 nm were analysed by electrophoresis on a 12% SDS-PAGE gel and stained with colloidal Coomassie. All elutions with protein of interest were pooled and concentrated using the Amicon Ultra-15 Centrifugal Filter Unit with Ultracel-3-membrane (Millipore). Protein concentration was then determined using Pierce™ BCA Protein Assay Kit (ThermoScientific). For storage, proteins were aliquoted into micro-tubes and snap-frozen in liquid nitrogen and stored at -80^{o}C.

2.2.4. Protein sequence analysis

To construct chemokine protein sequence alignments and generate a sequence-similarity based phylogenetic tree, Clustal-W in Megalign Pro (DNAStar version 12.3.1, DNAStar Inc.) was used. Alignments were exported to Figtree (version 1.4.2, http://tree.bio.ed.ac.uk/software/figtree/) to generate phylogenetic tree. To predict glycosylation sites the NetNGlyc1.0 (http://www.cbs.dtu.dk/services/NetNGlyc/) and

NetOGlyc4.0 (http://www.cbs.dtu.dk/services/NetOGlyc/) was used. Molecular weights and isoelectric point (pI) was calculated using ExPASy (http://web.expasy.org/compute_pi/).

2.2.5. Protein deglycosylation

To produce de-glycosylated proteins, P1243, P1156 and the two-warhead evasins (P1243:G4S:P1156 and P1156:G4S:P1243) were prepared as described previously (Section 2.2.3), however Kifunensine (Sigma), at a final concentration of 7.5 µg/mL, was added to cells following addition of transfection mixture and incubated with cells for four-five days.

Proteins were purified (as previously described in Section 2.2.3) and diluted 1:1 with 40 mM HEPES, 300 mM NaCl and 1 mM TCEP, and then treated with PNGaseF (NEB) and EndoF1 (gift from Professor Christian Siebold, NDM, University of Oxford) at a ratio of 1:1000 and incubated overnight at 37 °C. De-glycosylated protein was then purified again by SEC.

2.2.6. Tandem (MS/MS) Mass Spectronomy and N-terminal sequencing

Tandem (MS/MS) mass spectrometry was performed on deglycosylated P1243, P1156 and the two-warheads evasins (P1243:G4S:P1156 and P1156:G4S:P1243) (Section 2.2.5). Mass spectrometry and analysis was performed with the aid of Dr Rod Chalk (Burgess-Brown laboratory, SGC, University of Oxford), using methods described here (214). For analysis, a custom database, containing the sequences of the evasins, was generated in MASCOT. All obtained peptides were then searched against the custom sequences.

For P1243 and the two-warhead evasins (P1243:G4S:P1156 and P1156:G4S:P1243), no coverage of the N-terminus could be obtained from MS/MS. Therefore, N-terminal sequencing of the proteins was performed by Alta Bioscience (Redditch, UK).

2.2.7. Bio-layer interferometry (BLI)

Bio-layer interferometry (BLI) was performed on the OctetRed® System (ForteBio) at 30ºC (manufacturers recommendations) using the Ni-NTA dip and read biosensors (ForteBio). Assays were performed using 384-well plates and the octet buffer (10 mM Na_2HPO_4, 1.8 mM KH2PO4, 2.7 mM KCl, 500 mM NaCl, 0.1% BSA, 0.002% TWEEN-20, pH 7.4). All proteins and chemokines were diluted using the octet buffer.

Purified evasins were immobilised on the Ni-NTA sensors using 1 μm of evasin in assay buffer for 500 seconds, followed by a washing step in buffer for 60 seconds, sensor was then exposed to chemokine in assay buffer to record an association phase for 600 seconds, followed by a dissociation phase for 600 seconds, in which the sensor was exposed to assay buffer. Finally, the sensor was exposed to Glycine (10nM, pH1.7) for 5 seconds and assay buffer for 5 seconds, three times, followed by 10 seconds in 10 mM $NiCl_2$, to strip the bound protein and regenerate the sensor, respectively.

To account for baseline drift, sensor with bound evasin was placed in wells with assay buffer alone and subtracted from final data. Data was processed using ForteBio Data Analysis 9 software (ForteBio).

2.2.7.1. BLI chemokine cross-binding assay

For cross-binding assays of P1243 and P1156, 300 nM of chemokine was used. For the two-warhead evasins, 100 nM of chemokine was used in order to eliminate low-affinity binders. The following chemokines were omitted as they bound to the sensor non-specifically: CCL25, CCL26 and CXCL16. The following chemokines were not assayed as they were not available from Peprotech: CCL17, CXCL4L1 and XCL2. The same protocol was used for human and mouse chemokines (Peprotech).

2.2.7.2. BLI chemokine binding affinity assay

To determine binding affinities, similar protocol to above was used. Titration experiments to determine binding affinity were performed only once. After washing the evasin loaded sensor the sensors were dipped into a chemokine serial dilution that ranged from 600 nM to 0.4 nM for 600 seconds to determine the association phase followed by the dissociation step. A non-chemokine binding protein, reference protein, was used to account for non-specific binding to the sensor, sequence:

DGGQRNAICRLPPDEGICRASIPRFYFNPAEGKCSFFIYGGCEGNENNFETIEECEKT CGEPERPSDFEGADFETGCAPKPQRGFCKGFLDHWFFNVTSGECEAFLYSGCGGN DNNYESKEECEIACKLTGGASAWSHPQFEKLEHHHHHHHH.

For analysis, a double-subtraction was performed where by any binding to the reference sensor, and the baseline drift, was subtracted from final data. Previous data determined by the Bhattacharya group showed this reference protein does not bind human or mouse chemokines. Data was processed using ForteBio Data Analysis 9 software.

Association (k_{on}), dissociation (k_{off}), and affinity (K_d) constants were determined by using the 1:1 binding-model, and global fitting, followed by 'R_{max} unlinked by sensor' to allow independent fitting of R_{max} (maximal signal response upon saturating binding of the partner to the immobilized protein). Only curve fits showing $R^2>0.9$ were included, all those that did not were excluded as fit could not be determined. To determine dissociation half-life (minutes) the following calculation was used: $0.693/ (k_{off} \times 60)$ from the off-rate (k_{off}, s^{-1}) obtained from biolayer interferometry analysis. The same protocol was used for human and mouse chemokines (Peprotech).

2.2.7.3. BLI dual-chemokine binding assay

To examine the dual-binding function of the two-warhead evasins. P1243:G4S:P1156, P1156:G4S:P1243, P991:G4S:P1156 and P1156:G4S:P991, the dual-chemokine binding assay was performed. Purified evasins were immobilised on the Ni-NTA sensors, as described above, however the programme on the Octet changes to incorporate and second association phase.: evasins are dipped into wells containing chemokine in the first association phase (600 seconds), followed by dipping into a second well, containing a different chemokine, for the second association phase (600 seconds), followed by the dissociation phase (600 seconds) and sensor regeneration.

2.2.8. Cell migration assays

All migration assays were performed using the Corning HTS Transwell-96-well tissue culture systems (5 μm or 3 μm pore size). All assays were performed as, both, technical and biological triplicates (n=3). All assays were performed in the cell migration media: RPMI-1640 + L-glu (4mM) + 0.5% heat-treated FBS. Chemoattractant (human chemokines, Peprotech), 150 μL, was placed in the lower chamber of the 96-well plate and 50 μL of cells, at an optimised density, were placed in the upper chamber. For IC_{50} experiments, evasin was incubated with chemoattractant for 30 minutes, at 37^{o}C, prior to adding to the lower chambers of the plate. Assay plate was then incubated at 37^{o}C for an optimised period of time. After incubation, plate was then agitated at 850 r.p.m. for 10 minutes before transfer to U-bottomed 96-well plate for counting on the ATTUNE Nxt Flow Cytometer (Thermo Fisher Scientific) using a forward-scatter (FSC) and side-scatter (SSC) dot plots.

EC_{50} and EC_{80} values were analysed using an agonist response curve with 4 parameters and IC_{50} values were analysed using an inhibitor response curve with 4 parameters on GraphPad

Prism. The mean IC_{50} for three biological triplicates was then calculated. All statistical analysis was conducted using GraphPad Prism.

2.2.8.1. CC chemokine induced cell migration

For the CC chemokine chemotaxis assay, the monocytic cell line THP-1 was used. Migration assay was performed as discussed above, 3 x 10^5 cells were placed in top chamber of the 96-well plate (5μm pore size, Corning) and chemoattractant in the lower chamber. Assay was incubated for 4 hours before counting migrated cells on the ATTUNE Nxt Flow Cytometer (Thermo Fisher Scientific). EC_{50} and EC_{80} for chemokines (Peprotech, 0.006-300 nM doses) were determined previously by the Bhattacharya laboratory as three technical and biological triplicates (n=3) (175).

2.2.8.2. CXC chemokine induced cell migration

For the CXC chemokine chemotaxis assay, human granulocytes were used. Human granulocytes were collected from either fresh whole blood or buffy coat (Section 2.2.9). Migration assay was performed as discussed above, 2 x 10^5 granulocytes were placed in upper chamber and chemoattractant in lower chamber. Plate was incubated for 1 hour at 37^{o}C, before counting cells on ATTUNE Nxt Flow Cytometer (Thermo Fisher Scientific).

The EC_{50} and EC_{80} of granulocytes in response to CXCL1 or CXCL8 (Peprotech, 0-100 nM doses) was determined on each day of experiment, for each batch of blood, as a technical triplicate.

2.2.9. Isolating granulocytes from human whole blood and buffy coat

Fresh whole blood was collected, in EDTA-coated tubes (~16 mL), from healthy individuals each day of experiment. Buffy coat (~48 mL) was obtained from National Health Service (NHS) Blood and Transfusion service. Buffy coats were obtained 24-hours following donation and handled according to the University of Oxford guidelines.

To collect granulocytes, red blood cells, from either whole blood or buffy coat, were first depleted using HetaSep™ (StemCell Technologies), following the manufacturer's instructions. Nucleated cells were then washed in MACS buffer and remaining red blood cells lysed using MACS Red Lysis Buffer (MACS, Miltenyi Biotech). Cells were then harvested through centrifugation and washed again with MACS buffer before counting on the ATTUNE Nxt Flow Cytometer (Thermo Fisher Scientific) using FSC and SSC dot plot (Appendix C, Figure C1).

All experiments performed on human blood samples were done according to the University of Oxford guidelines. The studies conducted using human whole blood did not require institutional ethical approval as the human tissue was being used solely as a reagent to assay evasin activity. Verbal consent was taken from each participant and no samples were stored. Formal review of the process was obtained from the University of Oxford Medical Sciences Interdivisional Research Ethics Committee (MS IDREC). All experiments performed on buffy coat samples were done according to the University of Oxford guidelines (Study Title: Assays for the development of anti-inflammatory therapeutics, Ethics reference: 18/YH/0144).

2.2.10. Cell surface labelling

For cell surface expression of CXCR2, cells were labelled with either anti-CXCR2-FITC (CD182, IgG1, Biolegend) or anti-CXCR2-PE (CD182, IgG1, Miltenyi), alongside their isotype controls: FITC-mouse IgG1 κ (Biolegend) or PE-REA control (Miltenyi), respectively.

For CCR3 labelling, cells were labelled with either anti-CCR3-PE (CD193, Biolegend) or anti-CCR3-PE (CD193, Miltenyi), alongside their isotype controls: Mouse IgG2b, κ (Biolegend) or PE-REA control (Miltenyi), respectively.

Following isolation (Section 2.2.9), 1 x 10^6 cells were labelled with either anti-CXCR2, anti-CCR3 or isotype controls (following manufactures instructions). After labelling, cells were washed twice in PBS+0.1% BSA and fluorescence analysed on the ATTUNE Nxt Flow Cytometer (Thermo Fisher Scientific).

2.2.11. Restriction enzyme digest

Restriction enzymes (RE) were obtained from New England Biolabs (UK). For RE digestion, 150 ng of DNA was added to RE enzyme mixture, containing enzyme and enzyme buffer (following manufacturer's instructions) and incubated at 37^{o}C for 1 hour. Digested DNA was then resolved on 1-2% agarose gel containing 1 X TAE buffer and ethidium bromide. A DNA ladder, 50 base-pairs or 1 kilo-base-pair (Bioline) was loaded onto gel to allow comparison of the products to known band sizes. The gel was run at 110V in 1 X TAE buffer and visualised using BioRad ChemiDoc MP system.

Chapter 3.

Identifying Putative Evasins Using Yeast Surface Display

3.1. Introduction

3.1.1. Inflammation and chemokines

Chemokines, chemoattractant cytokines, function to recruit inflammatory cells to sites of inflammation through signalling mediated by GPCRs (84). Inflammatory diseases are characterised by the influx of immune cells, many of which drive the pathogenesis of inflammatory disease (75). In disease, the movement of immune cells into inflammatory sites is inevitable and difficult to control, however, controlling the mediators that recruit them, such as chemokines, may be achievable (78).

However, targeting chemokines is challenging as chemokines, together with their receptors, form a complex robust network (2), chemokines bind multiple receptors, receptors interact with multiple chemokines and immune cells express multiple chemokine receptors (215). To complicate things further, chemokines are able to behave synergistically with other chemokines, and receptors, to create an amplified response (216). Additionally, in a disease

setting, a feed-forward loop exists whereby immune cells at sites of inflammation secrete chemokines that recruit more inflammatory cells (217).

3.1.2. Chemokine targeted therapy

Pharmacological intervention, targeting the chemokine network, has been successful for non-inflammatory diseases, such as the drugs targeting CXCR4 and CCR5 used to treat HIV (218). However, anti-chemokine therapeutics designed to target inflammatory diseases have been largely unsuccessful. Generally, therapeutics targeting the chemokine network have largely failed to pass clinical trials due to lack of efficacy (171). For example, the monovalent agents MLN3897, which targeted CCR1 in rheumatoid arthritis (169), failed to show any efficacy, most likely a result of robustness of the chemokine network.

Interestingly, evolutionary advancements may have succeeded where pharmacological intervention may have not. Ticks, blood-feeding parasites, feed on their hosts for several days to weeks without eliciting their hosts immune response. They do this by injecting, during the bite, approximately 3000 peptides into their hosts (219). This observation was furthered by studies that showed ticks have anti-chemokine activity in their saliva (191-193). From these studies, three different CKBPs, termed evasins, were identified and classified. Evasins 1 and 4 bind selectively to CC chemokines and Evasin 3 binds selectively to CXC chemokines (191-193). These CKBPs are advantageous to those monovalent agents as they target multiple nodes (chemokines) in the chemokine network (174).

Therefore, evasins have also been therapeutically investigated in a range of clinical disease models where their systemic administration proved therapeutically beneficial in models of lung inflammation and fibrosis (202), psoriasis (193), graft versus host disease and myocardial infarction injury (206), antigen-induced arthritis (174), plaque vulnerability in ischemic stroke (207) and acute pancreatitis (208).

The evasins characterised to date have all been identified from the brown dog tick, *Rhipicephalus sanguineus* (193). Over 900 ticks have been identified (220), and are able to feed on several hosts including mammals, reptiles, birds and amphibians (189). To feed on such a vast number of species and avoid detection, ticks would need to have developed a large array of chemokine binding proteins in order to combat the complex nature of their hosts immune systems. Ticks could therefore be housing an arsenal of immunosuppressive agents that can be administered therapeutically in a range of inflammatory diseases.

Considering the aforementioned studies, this chapter hypothesised that other tick species have identified their own array of chemokine binding proteins, which can be therapeutically useful. Therefore, the aim of this chapter is to identify novel chemokine binding proteins from tick species.

3.2. Results

3.2.1. Bioinformatic identification of 352 putative evasins

Novel evasin sequences were identified by BLAST (Basic Local Alignment Search Tool) searching the published sequences of Evasin 1, 3 and 4, against the NCBI tick transcriptome shotgun assembly, using the PsiBLAST programme on the NCBI server. The BLAST search parameters were set to a restricted e-value cut-off of <1E-5 to ensure evasins with less sequence similarity to the published Evasins 1, 3 and 4 could be identified. To widen the search for more evasins with conserved sequences, three iterations, or BLAST searches, were conducted. All evasins with conserved sequence similarities to Evasins 1, 3 and 4 were then imported into a customized FileMaker spreadsheet to form the evasin database. Upon collating the novel putative evasins, they were each given a unique ID, which was denoted with 'PX', in which X is a unique number given to each evasin. Henceforth, each evasin will be referred to by its unique 'PX' ID.

The bioinformatic search for putative evasins identified 352 likely candidates from the following tick species: *Amblyomma americanum* (AMBAM), *Amblyomma maculatum* (AMBMA), *Amblyomma triste* (AMBTR), *Amblyomma parvum* (AMBPA), *Rhipicephalus sanguineus* (RHISA), *Rhipicephalus pulchellus* (RHIPU), *Amblyomma cajennense* (AMBCA) and *Ixodes ricinus* (IXORI). Of the identified putative evasins, 233 candidates displayed more conserved sequence-homology to Evasins 1 and 4, whereas 119 candidates showed more sequence-homology to Evasin 3.

3.2.2. Cloning of evasin library into yeast surface display (YSD) vectors

In order to further investigate putative evasin, all identified sequences were synthesised, pooled into a cDNA evasin library and cloned into yeast surface display vectors. Briefly, novel yeast expression vectors were designed for YSD (175) which allowed the GoldeGate/GoldenBraid (221) in-frame cloning of cDNA fused with either N- or C-terminal yeast cell wall anchorage tags. These tags are either AGA2 and the N- or C- terminus or SAG1 at the C-terminus. The yeast surface display plasmids also contain an antibody epitope tag, either MYC, FLAG or HA (denoted in Figure 3. 1). All plasmids are also under the control of a galactose-inducible promoter (GAL1), which permits galactose-induced conditional expression (Figure 3. 1).

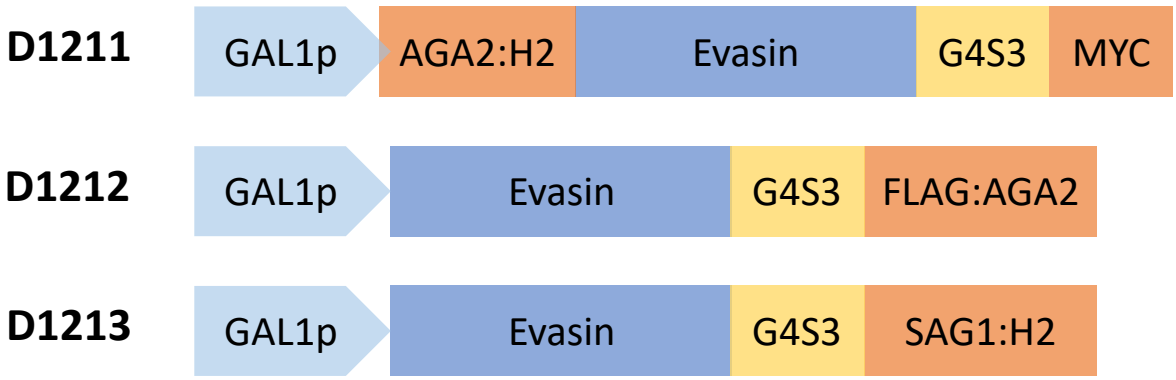


Figure 3. 1. Schematic representation of yeast surface display evasin expression plasmids. All evasin expression plasmids are under the control of a galactose promoter (GAL1p). Evasin expression plasmids differ based on the cell surface tags, either AGA2 at the N- (D1211) or C-terminus (D1212) or SAG1 at the C-terminus (D1212). The plasmids epitope-tags are also shown and are either MYC, FLAG or HA. Evasins are fused to surface tags with a Gly_4Ser_3 (G4S3) linker, as indicated.

3.2.3. Chemokine screening using FACS yields putative evasins

In order to screen the evasin library for chemokine binders, Fluorescent Activated Cell Sorting (FACS) was used (Figure 3. 2). For FACS, yeast cells containing the evasin cDNA library (Figure 3. 1) were first galactose-induced individually, then pooled together and labelled with biotinylated human CC or CXC chemokines and streptavidin-conjugated-AlexaFluor (AF) 647. Next, all yeast cells bound to chemokine were sorted as they expressed the labelled fluorophore, this was done by selecting cells that fall within the 'gate'. FACS gates were refined using negative control sample cells (same pool of yeast cells labelled with streptavidin-AF647 alone). All sorted yeast cells, recovered from the first FACS sort, were re-cultured and sorted for a second time to further enrich the positive population of yeast cells. Following the second sorting, recovered cells were spread on large yeast media plates at a low density to enable isolation of single yeast colonies. The putative evasin libraries were screened for binders against CCL8, CCL15, CCL17, CCL19, CCL20, CXCL8 and CXCL12.

Following screening, initially, 24 single colonies were picked from each yeast plate and yeast cells were then lysed, DNA extracted, amplified by PCR and sequenced to identify the evasin ID. This was then followed by re-testing to confirm binding.

However, sequencing the putative evasins prior to re-testing proved to be a time-consuming and costly process, as a number of samples failed at the re-testing stage. Therefore, a fluorescent binding assay was established to confirm the binding of the FACS-sorted yeast cells prior to DNA sequencing. For this binding assay (24-clone binding assay), the 24 picked colonies were galactose-induced, to enable the expression of the evasin on the surface of the yeast cell, labelled with a biotinylated chemokine and streptavidin-AF647 and fluorescence, indicating binding, examined using flow cytometry.

A selection process was established whereby clones showing mean fluorescence intensity (MFI) of more than three-fold higher than their negative control (same yeast cells labelled with streptavidin-AF64 alone) were isolated for Sanger sequencing and re-testing (Figure 3. 2).

For re-testing, a single colony of yeast was picked, galactose-induced and labelled with the chemokine it bound to during screening. Yeast cells labelled with biotinylated chemokine and streptavidin-AF64 where compared to their control, which was an empty vector, with the same cell surface tags, labelled with biotinylated chemokine and streptavidin-AF64. Schematic representing the YSD screening and re-testing pipeline is shown in Figure 3. 2.

3.2.3.1. CCL8 FACS screening

CCL8 FACS sorting showed 1.7% of the pooled library yeast cells bound to CCL8, upon enrichment, 66.4% of the yeast cells bound to CCL8 (Figure 3. 3. A). The 24 clone assay showed all 24 picked clones having MFI more than three-fold higher than the control. Sanger sequencing identified the following putative evasins: P672 (from the vector D1212), P974 (from the vector D1212), P983 (from the vector D1212), P991 (from the vector D1212), P1180 (from the vector D1212) and P1182 (from the vector D1212).

All identified putative evasins were re-transformed into yeast and labelled with biotinylated CCL8 and streptavidin-AF647 for re-testing. Flow cytometry analysis confirmed all identified putative evasins bound CCL8 (Figure 3. 3. B, Table 3. 1).

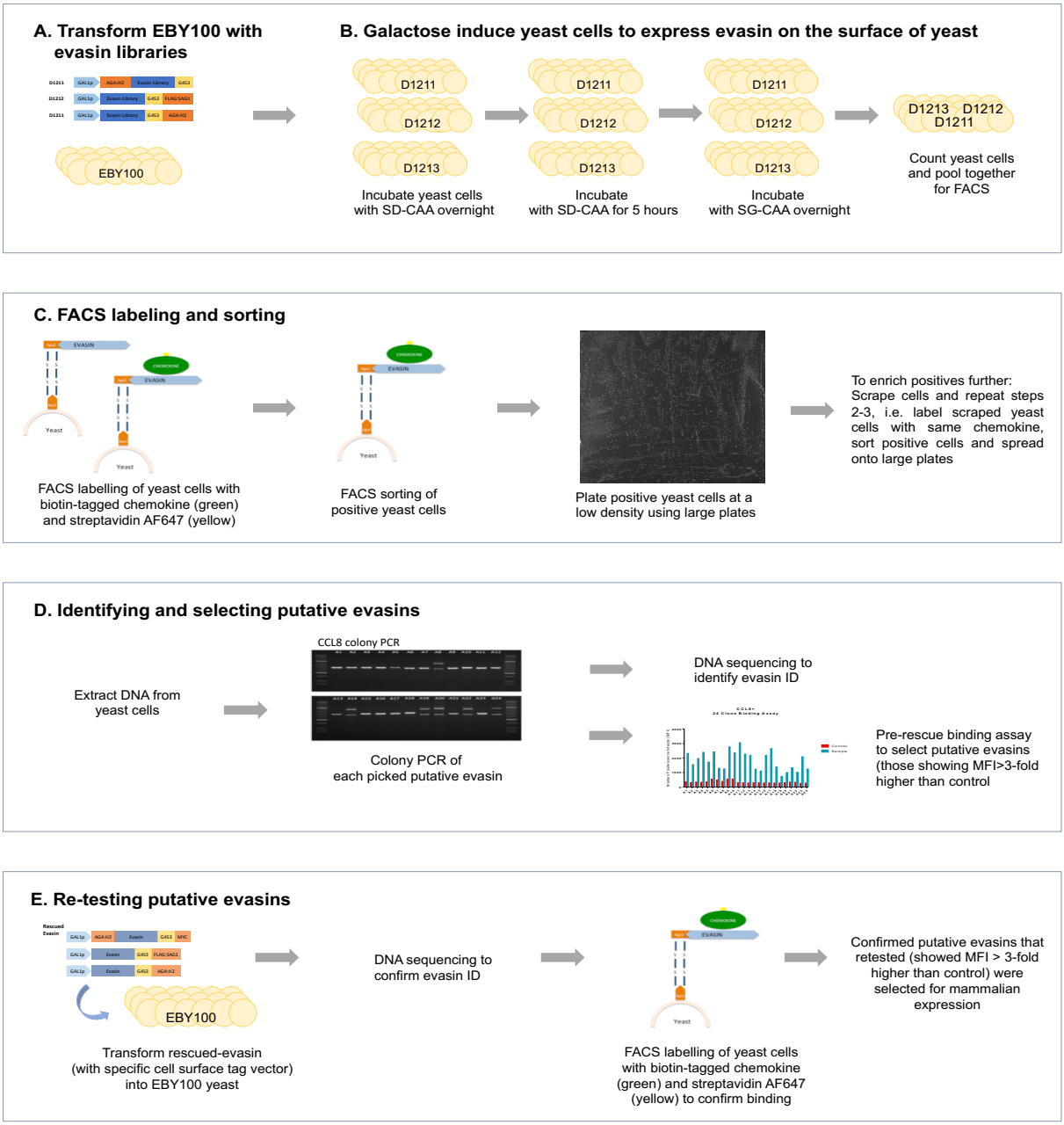


Figure 3. 2. Schematic representation showing the evasin yeast surface display screening and re-testing pipeline. (A) Evasin libraries are first transformed into EBY100 yeast. (B) Yeast cells containing evasin libraries are galactose-induced and pooled together. (C) Pooled yeast cells containing evasin libraries are labelled with biotinylated chemokine (green) and streptavidin AF647 (yellow). All cells binding to chemokine are then sorted, re-cultured and sorted for a second time to further enrich positives. (D) Yeast cells containing evasin clones are isolated and DNA extracted, amplified using colony PCR and labelled in the fluorescence binding assay. All those showing mean fluorescence intensity (MFI) 3-fold higher than their control (cells labelled with streptavidin AF-647 alone) are selected for sequencing to identify evasin ID. (E) Re-testing: each identified evasin is then transformed back into yeast surface display vectors, sequenced to confirm evasin ID and re-labelled with chemokine to confirm binding (three biological repeats).

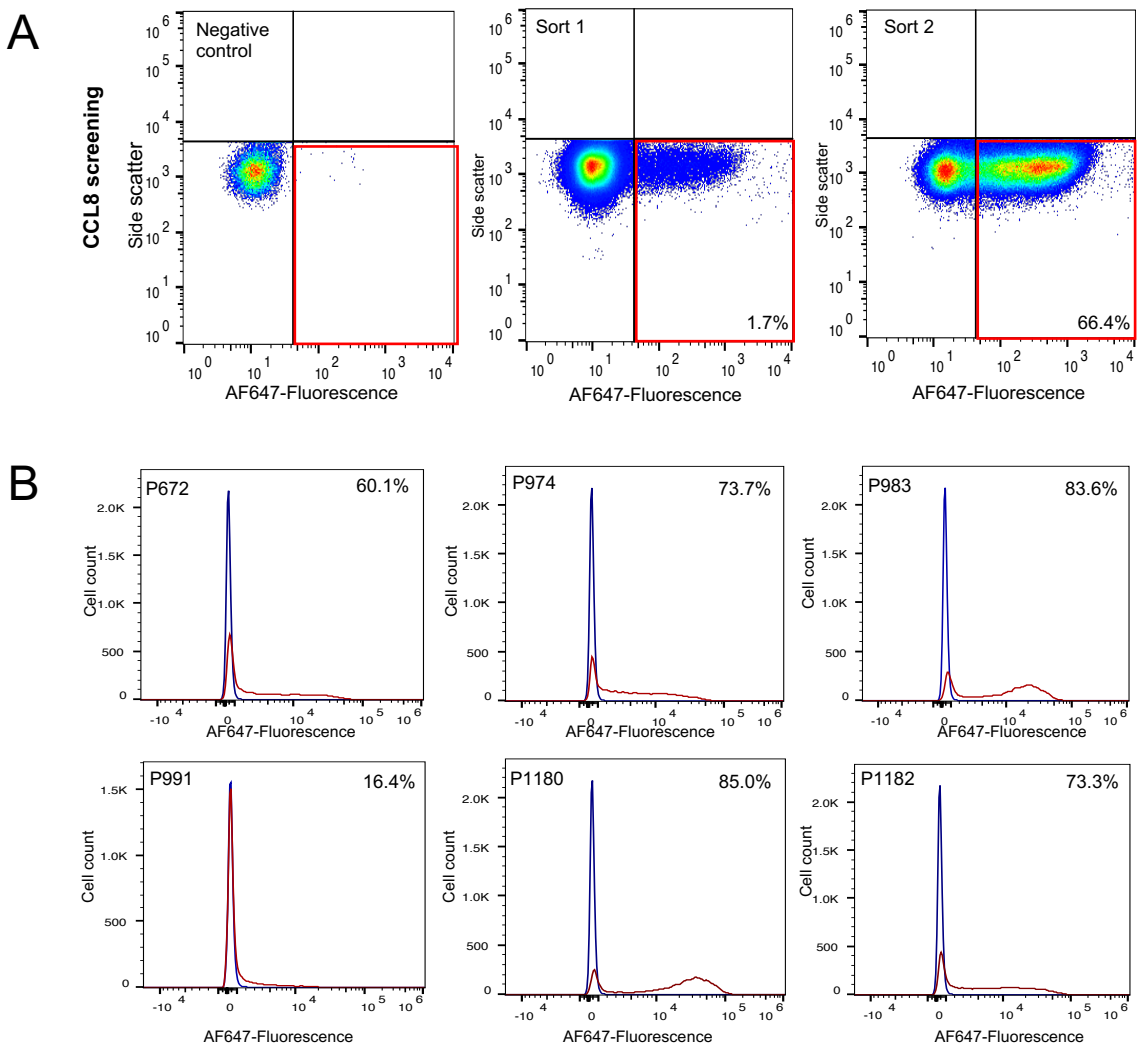


Figure 3. 3. CCL8 yeast surface display screen. (A) Fluorescent profiles of evasin YSD library against human CCL8. Yeast cells were labelled with streptavidin-AF647 alone (negative control, left panel), and with biotinylated CCL8 and streptavidin-AF647 (middle and right panel). Sorting gate was established based on the negative control (red box). All positive cells were sorted (middle panel), re-grown as a pool and sorted again (right panel) to enrich chemokine binding yeast. After the second sort, positive clones were plated at a low-density to allow isolation of single clones. The y-axis shows cell count and x-axis shows the fluorescent intensity on a log-scale. The proportion of cells in the sorting gate are shown as a percentage. (B) Representative fluorescent profiles confirming the binding of the positive clones (red) identified from the above screen to biotinylated CCL8 and streptavidin-AF647. The fluorescent profile of the negative control, empty vector with the same surface display tag, is shown in blue. The y-axis shows cell count and x-axis shows the fluorescent intensity on a log-scale. Positive cells exceeding that of the control are shown as a percentage.

3.2.3.2. CCL15 FACS screening

CCL15 FACS sorting showed 3.5% of the pooled library yeast cells bound to CCL15, upon enrichment, 14.6% of cells showed binding to CCL15 (Figure 3. 4. A). All 24 picked clones were sequenced and identified as P1243, from the vector D1212. A further six more clones were picked and sequenced and were also identified as P1243. Subsequently, P1243 DNA was transformed back into the yeast surface display vector D1212 and labelled with biotinylated CCL15 and streptavidin-AF647 for re-testing. Flow cytometry analysis confirmed P1243 does bind to CCL15 (Figure 3. 4. B, Table 3. 1).

3.2.3.3. CCL17 FACS screening

CCL17 FACS sorting showed 2.8% of the pooled library yeast cells bound to CCL17, upon enrichment, 11.5% of yeast cells bound to CCL17 (Figure 3. 5. A). The 24-clone assay showed 17 out of the 24 picked clones having an MFI more than three-fold higher than their control (empty vector labelled with the same chemokine). Sanger sequencing identified the following putative evasins: P974 (from the vector D1212), P991 (from the vector D1212), P1030 (from the vector D1211) and P1243 (from the vector D1212). Following the transformation of the aforementioned putative evasins into their respective YSD vectors, they were then labelled with biotinylated CCL17 and streptavidin-AF64 for re-testing. Flow cytometry analysis confirmed all identified putative Evasins bound CCL17 (Figure 3. 5. B, Table 3. 1).

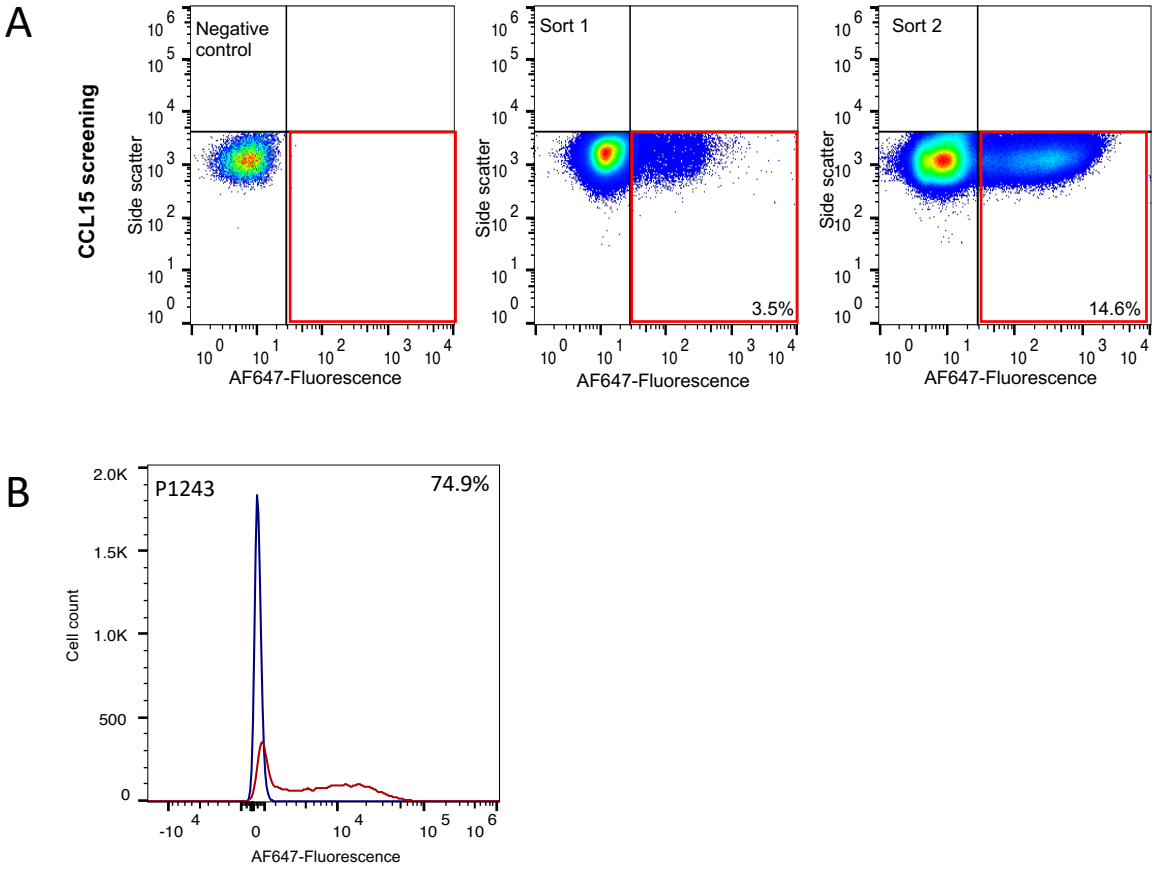


Figure 3. 4. CCL15 yeast surface display screen. (A) Fluorescent profiles of evasin yeast surface display library against human CCL15. Yeast cells were labelled with streptavidin-AF647 alone (negative control, left panel), and with biotinylated CCL15 and streptavidin-AF647 (middle and right panel). Sorting gate was established based on the negative control (red box). All positive cells were sorted (middle panel), re-grown as a pool and sorted again (right panel) to enrich chemokine binding yeast. After the second sort, positive clones were plated at a low-density to allow isolation of single clones. The y-axis shows cell count and x-axis shows the fluorescent intensity on a log-scale. The proportion of cells in the sorting gate are shown as a percentage. (B) Representative fluorescent profile confirming the binding of P1243 (red) identified from the above screen to biotinylated CCL15 and streptavidin-AF647. The fluorescent profile of the negative control, empty vector with the same surface display tag, is shown in blue. The y-axis shows cell count and x-axis shows the fluorescent intensity on a log-scale. Positive cells exceeding that of the control are shown as a percentage.

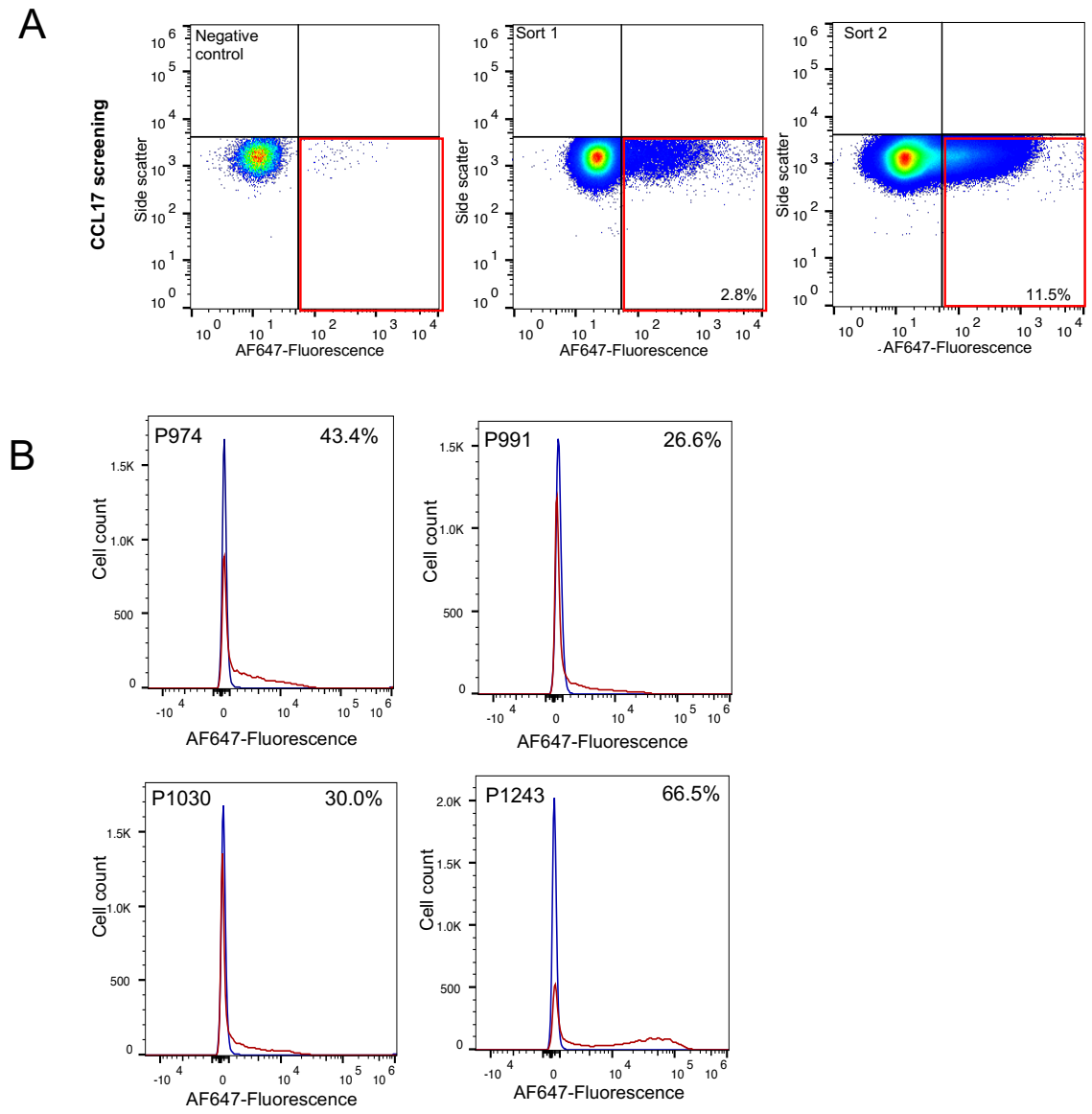


Figure 3. 5. CCL17 yeast surface display screen. (A) Fluorescent profiles of evasin yeast surface display library against human CCL17. Yeast cells were labelled with streptavidin-AF647 alone (negative control, left panel), and with biotinylated CCL17 and streptavidin-AF647 (middle and right panel). Sorting gate was established based on the negative control (red box). All positive cells were sorted (middle panel), re-grown as a pool and sorted again (right panel) to enrich chemokine binding yeast. After the second sort, positive clones were plated at a low-density to allow isolation of single clones. The y-axis shows cell count and x-axis shows the fluorescent intensity on a log-scale. The proportion of cells in the sorting gate are shown as a percentage. (B) Representative fluorescent profiles confirming the binding of the positive clones (red) identified from the above screen to biotinylated CCL17 and streptavidin-AF647. The fluorescent profile of the negative control, empty vector with the same surface display tag, is shown in blue. The y-axis shows cell count and x-axis shows the fluorescent intensity on a log-scale. Positive cells exceeding that of the control are shown as a percentage.

3.2.3.4. CCL19 FACS screening

CCL19 FACS sorting showed 24.6% of the pooled library yeast cells bound to CCL19, upon enrichment, 41.4% of yeast cells bound to CCL19 (Figure 3. 6. A). The 24-clone binding assay showed all picked clones having MFI more than three-fold higher than their control. Sanger sequencing identified the putative evasins as P1243 (from the vectors D1211 and D1212), P1006 (from the vector D1212). Following transformation of the aforementioned putative evasins into YSD vectors, they were labelled with biotinylated CCL19 and streptavidin-AF64 for re-testing. Flow cytometry analysis confirmed all identified putative evasins bound CCL19 (Figure 3. 6. B, Table 3. 1).

3.2.3.5. CCL20 FACS screening

CCL20 FACS sorting showed 1.13% of the pooled library yeast cells bound to CCL20, upon enrichment, 0.2% of yeast cells bound to CCL20 (Figure 3. 7. A). therefore, a third sort was conducted where 2.35% of yeast cells showed binding to CCL20, showing enrichment. The 24-clone assay showed 4 out of the 24 picked clones showed MFI more than three-fold higher than their control. Sanger sequencing identified the following putative evasins as P1015 (from the vector D1211), P1252 (from the vector D1211) and P993 (from the vector D1211). Following transformation of the aforementioned putative evasins into their respective YSD vectors, they were labelled with biotinylated CCL20 and streptavidin-boundAF64 for re-testing. Flow cytometry analysis confirmed all identified putative evasins do bind CCL20 (Figure 3. 7. B, Table 3. 1).

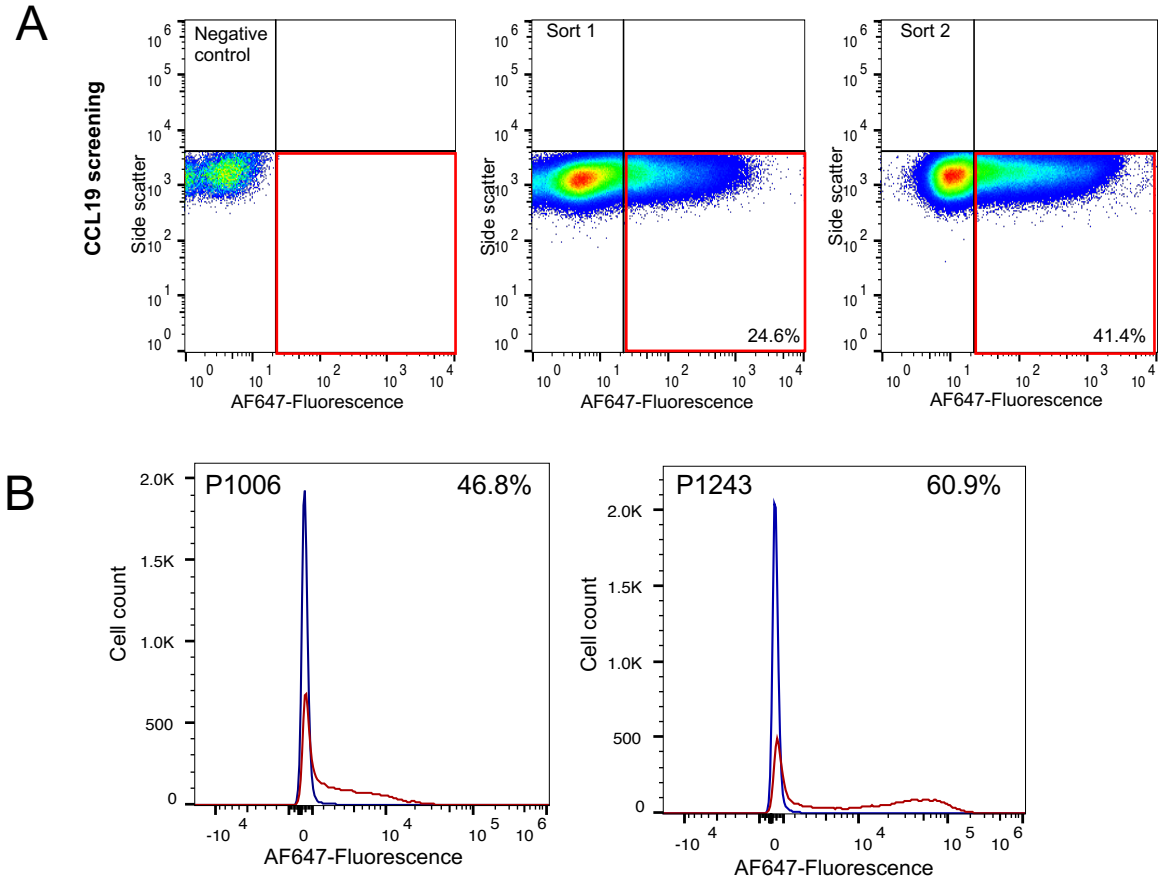


Figure 3. 6. CCL19 yeast surface display screen. (A) Fluorescent profiles of evasin yeast surface display library against human CCL19. Yeast cells were labelled with streptavidin-AF647 alone (negative control, left panel), and with biotinylated CCL19 and streptavidin-AF647 (middle and right panel). Sorting gate was established based on the negative control (red box). All positive cells were sorted (middle panel), re-grown as a pool and sorted again (right panel) to enrich chemokine binding yeast. After the second sort, positive clones were plated at a low-density to allow isolation of single clones. The y-axis shows cell count and x-axis shows the fluorescent intensity on a log-scale. The proportion of cells in the sorting gate are shown as a percentage. (B) Representative fluorescent profiles confirming the binding of the positive clones (red) identified from the above screen to biotinylated CCL19 and streptavidin-AF647. The fluorescent profile of the negative control, empty vector with the same surface display tag, is shown in blue. The y-axis shows cell count and x-axis shows the fluorescent intensity on a log-scale. Positive cells exceeding that of the control are shown as a percentage.

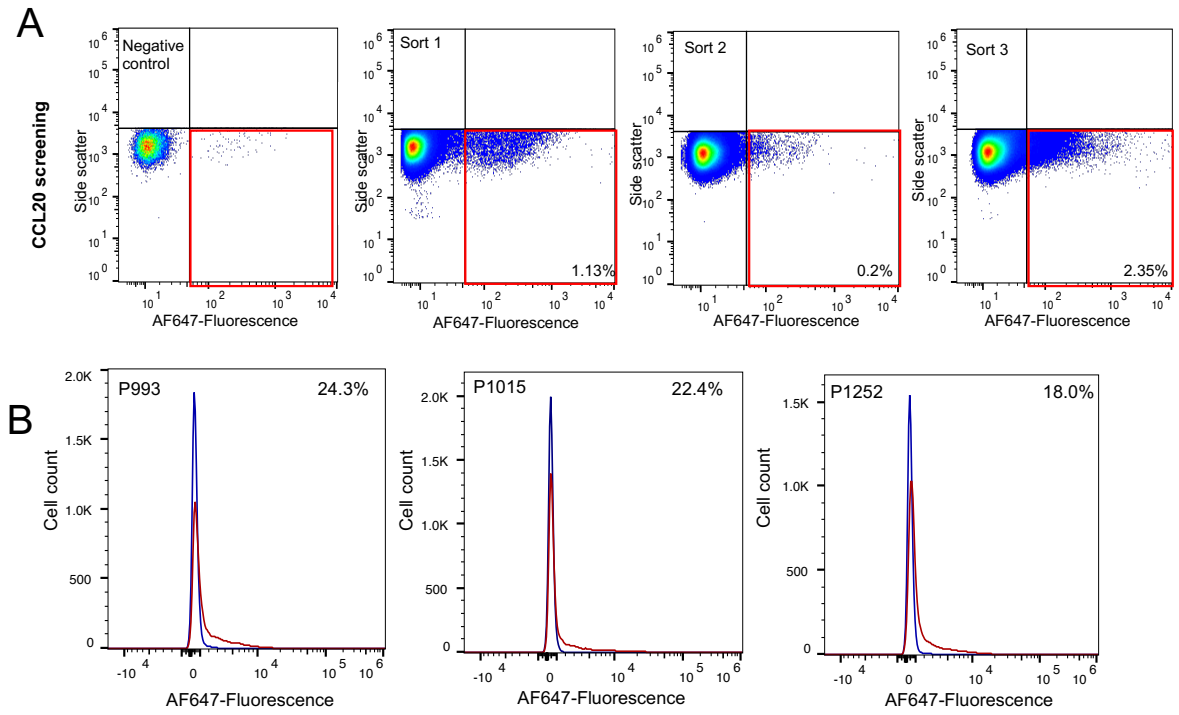


Figure 3. 7. CCL20 yeast surface display screen. (A) Fluorescent profiles of evasin yeast surface display library against human CCL20. Yeast cells were labelled with streptavidin-AF647 alone (negative control, first panel), and with biotinylated CCL20 and streptavidin-AF647 (second, third and fourth panel). Sorting gate was established based on the negative control (red box). All positive cells were sorted (second panel), re-grown as a pool and sorted again (third panel) to enrich chemokine binding yeast. Due to the low number of sorted cells after the second sort, all positive clones were sorted a third time (fourth panel). After the third sort, positive clones were plated at a low-density to allow isolation of single clones. The y-axis shows cell count and x-axis shows the fluorescent intensity on a log-scale. The proportion of cells in the sorting gate are shown as a percentage. (B) Representative fluorescent profiles confirming the binding of the positive clones (red) identified from the above screen to biotinylated CCL20 and streptavidin-AF647. The fluorescent profile of the negative control, empty vector with the same surface display tag, is shown in blue. The y-axis shows cell count and x-axis shows the fluorescent intensity on a log-scale. Positive cells exceeding that of the control are shown as a percentage.

3.2.3.6. CXCL8 FACS screening

CXCL8 FACS sorting showed 1.7% of the pooled library yeast cells bound to CXCL8, upon enrichment, 3.2% of yeast cells bound to CXCL8 (Figure 3. 8. A). Sequencing identified the following putative evasins as P993 (from the vector D1211) and P1156 (from the vector D1212). Following transformation of P993 and P1156 into their respective YSD vectors, they were labelled with biotinylated CXCL8 and streptavidin-AF64 for re-testing. Flow cytometry analysis confirmed both putative evasins bound CXCL8 (Figure 3. 8. B, Table 3. 1).

3.2.3.7. CXCL12 FACS screening

CXCL12 FACS sorting showed 1.7% of the pooled library yeast cells bound to CXCL12, upon enrichment, 66.4% of yeast cells bound to CXCL12 (Figure 3. 9. A). Sanger sequencing identified the following putative evasins as P1015 (from the vector D1211), P1209 (from the vector D1211) and P1215 (from the vector D1213). Following transformation of the aforementioned putative evasins into their respective yeast surface display vectors, they were labelled with biotinylated CXCL12 and streptavidin-AF64 for re-testing. Flow cytometry analysis confirmed all identified putative evasins bound CXCL12 (Figure 3. 9. B, Table 3. 1).

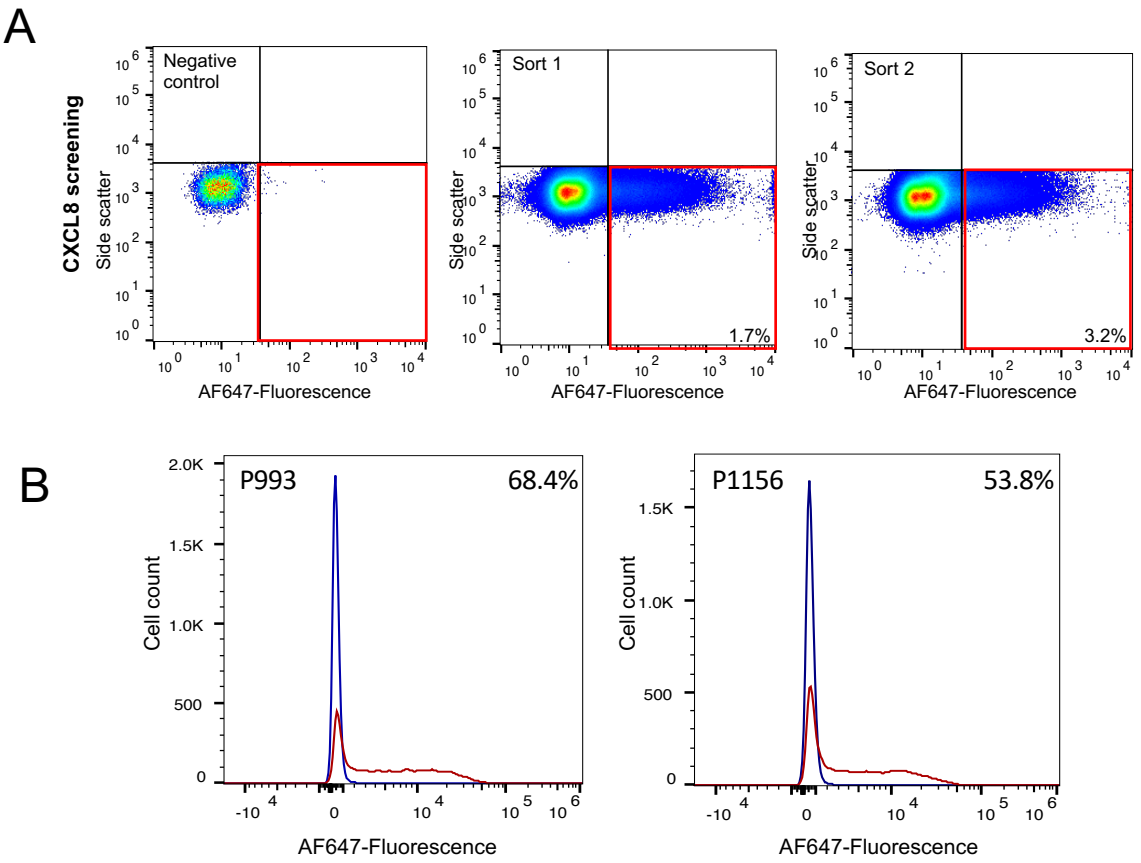


Figure 3. 8. CXCL8 yeast surface display screen. (A) Fluorescent profiles of evasin yeast surface display library against human CXCL8. Yeast cells were labelled with streptavidin-AF647 alone (negative control, left panel), and with biotinylated CXCL8 and streptavidin-AF647 (middle and right panel). Sorting gate was established based on the negative control (red box). All positive cells were sorted (middle panel), re-grown as a pool and sorted again (right panel) to enrich chemokine binding yeast. After the second sort, positive clones were plated at a low-density to allow isolation of single clones. The y-axis shows cell count and x-axis shows the fluorescent intensity on a log-scale. The proportion of cells in the sorting gate are shown as a percentage. (B) Representative fluorescent profiles confirming the binding of the positive clones (red) identified from the above screen to biotinylated CXCL8 and streptavidin-AF647. The fluorescent profile of the negative control, empty vector with the same surface display tag, is shown in blue. The y-axis shows cell count and x-axis shows the fluorescent intensity on a log-scale. Positive cells exceeding that of the control are shown as a percentage.

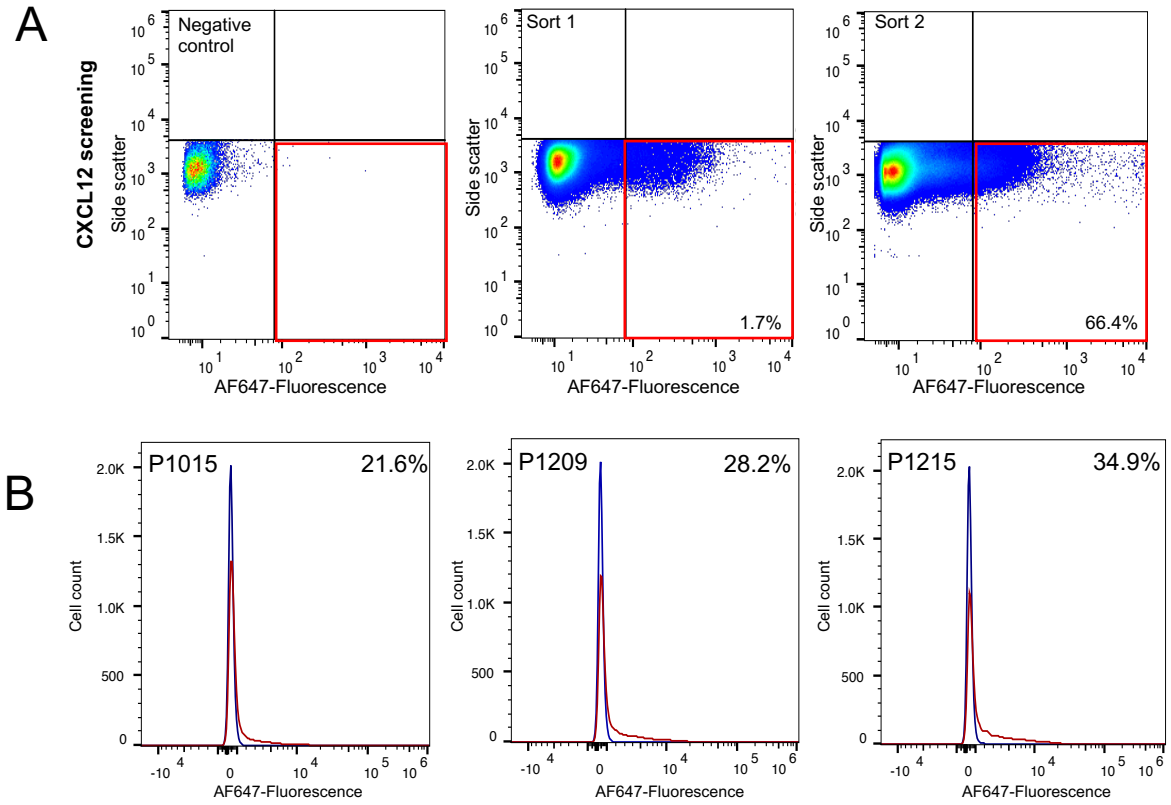


Figure 3. 9. CXCL12 yeast surface display screen. (A) Fluorescent profiles of evasin yeast surface display library against human CXCL12. Yeast cells were labelled with streptavidin-AF647 alone (negative control, left panel), and with biotinylated CXCL12 and streptavidin-AF647 (middle and right panel). Sorting gate was established based on the negative control (red box). All positive cells were sorted (middle panel), re-grown as a pool and sorted again (right panel) to enrich chemokine binding yeast. After the second sort, positive clones were plated at a low-density to allow isolation of single clones. The y-axis shows cell count and x-axis shows the fluorescent intensity on a log-scale. The proportion of cells in the sorting gate are shown as a percentage. (B) Representative fluorescent profiles confirming the binding of the positive clones (red) identified from the above screen to biotinylated CXCL12 and streptavidin-AF647. The fluorescent profile of the negative control, empty vector with the same surface display tag, is shown in blue. The y-axis shows cell count and x-axis shows the fluorescent intensity on a log-scale. Positive cells exceeding that of the control are shown as a percentage.

Table 3. 1. Summary profile of novel evasins. Mean fluorescence intensity (MFI). AMBAM- *Amblyomma americanum*, AMBMA – *Amblyomma maculatum*, AMBTR – *Amblyomma triste*, AMBPA, *Amblyomma parvum*, RHIPU- *Rhipicephalus pulchellus*, AMBCA- *Amblyomma cajennense*, IXORI- *Ixodes ricinus*.

Chemokine	Evasin ID	Tick species	Blast search	Tag	MFI fold-increase
CCL8	P672	RHIPU	Evasin 1/4	D1212	24.3
	P991	AMBCA	Evasin 1/4	D1211	1.52
	P974	AMBCA	Evasin 1/4	D1212	5.7
	P983	AMBCA	Evasin 1/4	D1212	14.9
	P1180	AMBTR	Evasin 1/4	D1212	10.7
	P1182	AMBMA	Evasin 1/4	D1212	4.4
CCL15	P1243	AMBAM	Evasin 1/4	D1212	3.1
CCL17	P974	AMBCA	Evasin 1/4	D1212	2.4
	P991	AMBCA	Evasin 1/4	D1211	3.6
	P1030	AMBPA	Evasin 1/4	D1211	1.6
	P1243	AMBAM	Evasin 1/4	D1212	9.8
CCL19	P1243	AMBAM	Evasin 1/4	D1211	4.5
	P1243	AMBAM	Evasin 1/4	D1212	7.4
CCL20	P993	AMBPA	Evasin 1/4	D1211	2.3
	P1015	AMBCA	Evasin 1/4	D1211	1.6
	P1252	AMBAM	Evasin 1/4	D1211	1.7
CXCL8	P993	AMBPA	Evasin 1/4	D1211	10.7
	P1156	IXORI	Evasin 3	D1212	5.6
CXCL12	P1015	AMBCA	Evasin 1/4	D1211	1.5
	P1209	AMBPA	Evasin 1/4	D1211	2.1
	P1215	AMBPA	Evasin 1/4	D1213	2.1

Table 3. 2. Summary of identified novel evasins and their sequence homology to published evasins. AMBAM- *Amblyomma americanum*, AMBMA – *Amblyomma maculatum*, AMBTR – *Amblyomma triste*, AMBPA, *Amblyomma parvum*, RHIPU- *Rhipicephalus pulchellus*, AMBCA- *Amblyomma cajennense*, IXORI- *Ixodes ricinus*

Evasin ID	Tick species	Accession number	Chemokine screen	Similarity to known sequences (%)		
				Evasin 1	Evasin 3	Evasin 4
P672	RHIPU	JAA60789.1	CCL8	29	-	36
P974	AMBCA	JAC18993.1	CCL8 CCL17	41	-	36
P983	AMBCA	JAC19634.1	CCL8	40	-	25
P991	AMBCA	JAC19654.1	CCL8 CCL17	30	-	26
P1180	AMBTR	JAC29349.1	CCL8	41	-	29
P1182	AMBMA	AEO33551.1	CCL8	44	-	24
P1243	AMBAM	JAG91989.1	CCL15 CCL17 CCL19	33	-	43
P1030	AMBPA	JAC26666.1	CCL17	25	38	-
P1006	AMBCA	JAC23940.1	CCL19	38	40	20
P993	AMBPA	JAC27182.1	CCL20 CXCL8	34	-	36
P1015	AMBCA	JAC24462.1	CCL20 CXCL12	32	-	26
P1252	AMBAM	JAG92346.1	CCL20	30	-	24
P1156	IXORI	JAB72437.1	CXCL8	-	30	-
P1209	AMBPA	JAC26686.1	CXCL12	36	-	22
P1215	AMBPA	JAC26685.1	CXCL12	34	-	21

3.3. Discussion

Inflammation is characterised by the recruitment of inflammatory cells. Chemokines are one of the key mediators responsible for the recruitment of inflammatory cells. Subsequently, this has led to their characterisation and validation as therapeutic targets in inflammatory disease (75). However, targeting these signalling proteins has been largely unsuccessful due to the robustness of their signalling network, which requires targeting multiple nodes in the network. Therefore, evasins, derived from ticks, were further investigated as they are able to overcome the chemokine network by binding to multiple chemokines. Only three evasins have been identified, to date, and were all characterised from the brown-dog tick *Rhipicephalus sanguineus* (192, 193). In this chapter, it was demonstrated that other tick species harbour chemokine binding proteins (CKBP), 16 of which have been confirmed in this study. Furthermore, this chapter has shown that yeast surface display (YSD) is a powerful tool for identifying evasins.

Bioinformatics identifies putative evasins

Anti-chemokine activity, in ticks, was first reported by, Hajnicka *et al*., (191) where they demonstrated salivary gland extracts of Ixodid tick species exhibited anti-CXCL8 activity, on the other hand, Frauenschuh *et al*., (192) generated a cDNA library directly from the salivary gland extracts of the *Rhipicephalus sanguineus* tick and subsequently three evasins were isolated and cloned (192, 193). In this chapter, evasin sequences were identified through homology searches of the published evasin sequences (192, 193), this yielded 352 putative evasin sequences, belonging to eight tick species from the *Amblyomma*, *Rhipicephalus* and *Ixodes* genera. Similarly, Hayward *et al*., (198) recently identified a putative evasin library of 257 sequences through bioinformatic evasin homology searches that also spanned the

Amblyomma, *Rhipicephalus* and *Ixodes* genera. Thus, demonstrating other tick species do have evasins. Considering there are over 900 tick species reported (220), it is likely, with advancements in proteomics and next generation sequencing that more evasin sequences could be identified in the future, as evasins have yet to be isolated from the *Anomalohimalaya*, *Bothriocroton*, *Cosmiomma*, *Cornupalpatum*, *Compluriscutula*, *Dermacentor*, *Haemaphysalis*, *Margaropus*, *Nosomma* and *Rhipicentor* genera. Indeed, anti-CXCL8 activity has been reported in salivary gland extracts of *Dermacentor reticulatus* tick (199), yet no individual evasins has been isolated from this study.

Interestingly, homology searches investigating evasin-like sequences in mammals yielded no results (174), yet CKBP's are not restricted to ticks as CKBP's have been reported in viruses and helminths (172, 180). However, with the exception of a few, the binding nature of these proteins is broadly unrestrained, in that they bind chemokines across multiple classes and lack the specific binding nature exhibited by evasins (174). One of the exceptions is the viral CKBP (vCKBP) vCCI (222), which binds selectively to a broad-range of CC chemokines, a feature shared by Evasin 4 (193). Conversely, vCKBP are typically large proteins, three to four times the size of evasins and can also form dimers, as observed by the vCKBP M3 (223). Moreover, considering not all chemokines are inflammatory and some are essential for homeostasis or exhibit reparative functions (75), generally, the use of viral CKBP's as therapeutics may result in off-target effects. Thus, evasins may be more suitable as their binding to chemokines is more selective.

Yeast surface display (YSD) as a screening tool for evasins

In this study, putative evasins were identified using YSD, a method not used before to identify evasins. Other studies have identified evasins using other forms of peptide display, including

bacterial (198) and mammalian (192, 193). However, unlike mammalian systems, the use of YSD allows the stable transfection of large libraries of secreted proteins easily, as they have the protein disulfide isomerases and chaperones in their secretory pathways (224), contrasting to bacterial systems where they need to be artificially introduced (201).

On the other hand, the results shown in this chapter show many of the evasin-like sequences, identified via bioinformatics, do not have a high enough affinity to bind to chemokines identified by YSD. Whilst this may be a subsequent artefact of the methodology used to identify evasins, it is unlikely to be the case as, similarly, the bioinformatic search performed by Hayward *et al*., (198), which generated a putative evasin library of 257 sequences, yielded only 8 evasins. Considering ticks feed on their hosts for prolonged periods of time whilst evading the hosts immune response (225) and the complexity of the immune response, which involves many mediators (75), evasins may function to bind not only chemokines but also other signalling molecules such as cytokines or complement, although this has not yet been explored in detail. Indeed, studies on tick saliva show it not only exhibits anti-inflammatory and immunosuppressive effects but also anticoagulant, vasodilatory and cytolytic effects (226). Moreover, the evasin library was screened for binders against human chemokines, however considering ticks feed on several species, including mammals, reptiles, birds and amphibians (227), it is fair to assume some of the identified putative evasins, that did not bind to the human chemokines during FACS screening, may bind mediators in the immune responses of other species and not humans.

YSD cell surface expression tags affect the peptide display of evasins on the cell surface of yeast

A common complication of protein-protein interactions is steric hinderance, whereby, in this case, the evasin structure could be masked in such a way that chemokine does not recognise it and cannot bind (228). However, to overcome this, a $(Gly_4S)_3$ linker was placed between the evasin and the surface tag to minimise steric hindrance. Alternative or larger linkers can be used to further increase flexibility and decrease steric hinderance (229).

Previous studies on the published evasins had shown evasins can be displayed on the surface of yeast fused to tags on either the N- or C-terminus (175), however this affected the evasins ability to bind to chemokines (175, 230). It has been previously described that the binding modalities exhibited by the published Evasins 1 and 4, differed based on such parameters (194), Evasin 1 requires both its C- and N-terminus to bind chemokines, whereas Evasin 4 requires the use of only its N-terminus (194). These findings highlight the need for multiple surface display tags when constructing an evasin library, to ensure for more comparable and reproducible results.

Therefore, this study used three vectors that varied in cell surface tags and the orientation of the cell surface tags (Figure 3. 1). Subsequently, the majority of the putative evasins identified were from the vector with the surface tag AGA2 at the C-terminus (D1212, Figure 3. 1, Table 3.1). Despite this, putative evasins were recovered from the other two vectors with the different cell surface tag, SAG1 (D1213), and with the N-terminal AGA2 (D1211), thus showing that the nature and orientation of the tag affects the evasins binding of chemokine unpredictably. For example, the P1243 identified during the CCL19 screening was expressed in the vectors with AGA2 at the N- or C- terminus, suggesting expression on either the N- or C- terminus does not affect P1243 binding to CCL19. However, P1243 recovered from the CCL15 and the

CCL17 screenings were from the expression vector with AGA2 at the N-terminus only, suggesting that for P1243 binding to CCL15 and CCL17, the N-terminus is required. Interestingly, P1243 was the only putative evasin identified from the CCL15 chemokine screen, suggesting it may be a very potent binder of CCL15, however, this result restricted identifying more putative evasins that bound to CCL15.

'One-to-many' binding nature of evasins

The key characteristic feature of evasins is their ability to bind chemokines in a 'one-to-many' fashion. Evasin-1, for example, binds CCL3, CCL4 and CCL18 (174). An encouraging finding observed in this chapter is the same evasin appearing in several chemokine screens, thus showing the evasin binding to multiple chemokines. The evasin P991, from the *Amblyomma cajennense* tick, showed binding to both CCL8 and CCL17 (Figure 3. 3. B, Figure 3. 5. B, Table 3. 1). Additionally, the evasin P1243, from the *Amblyomma americanum* tick, showed binding to CCL15 (Figure 3. 4. B), CCL17 (Figure 3. 5. B) and CCL19, (Figure 3. 6. B, Table 3. 1). These findings support the one-to-many chemokine binding nature exhibited by evasins (192, 193) and the main reason behind their suitability for targeting the chemokine network.

An interesting finding also observed by this chapter was the binding of an evasin to not only a CC chemokine but also a CXC chemokine. For example, P993, binding to CCL20 (Figure 3. 7. B) and CXCL8 (Figure 3. 8. B), and P1015, binding to CCL20 (Figure 3. 7. B) and CXCL12 (Figure 3. 9. B). However, P1015 failed, at re-testing, to show binding to CCL20 nor CXCL12, whereas P993 only showed 'high-affinity' binding to CXCL8 and not CCL20 (Table 3. 1). These finding suggest evasins only show 'high-affinity' binding to chemokines of a certain subgroup and may show low-affinity binding to chemokines of different subgroups.

In summary, this chapter has also shown bioinformatics and YSD present a unique powerful tool for identifying novel evasins. In addition to this, as all the identified novel evasins share less than 50% sequence homology to the published evasins (Table 3. 2), they have subsequently been patented (PCT/GB2017/050563). In order to fully characterise the novel evasins and confirm chemokine binding in mammalian systems, a selection process was required. An obvious candidate was P1243 as this evasin showed binding to multiple chemokines, CCL15, CCL17 and CCL19. Also, P1156, which bound CXCL8, was selected as this was the only evasin that showed sequence homology to Evasin 3 and bound a CXC chemokine, thus implying it may behave in a similar way.

Chapter 4.

Characterising the Novel

Evasin P1243

4.1. Introduction

4.1.1. CC chemokines

Structurally, chemokines that have two, out of their four, cysteine groups adjacent to each other at the N-terminus are termed CC chemokines (1, 84) and encompass the largest of the chemokine subgroups. CC chemokines, their designated CCR-receptors, and the immune cells expressing those receptors, form a robust network that is difficult to overcome, as multiple chemokines can signal through a single receptor, one receptor is able to bind multiple chemokines and multiple receptors are expressed on the surface of immune cells (Figure 4. 1) (1).

Given the role of CC chemokines in the recruitment of immune cells in inflammatory diseases, they have been extensively studied for their roles in disease pathogenesis. Most prominently, CC chemokines recruitment of monocytes (2). Increased levels of monocytes have been associated with a large number of inflammatory diseases including, atherosclerosis (231),

coronary artery disease (232), crohns disease (233) and rheumatoid arthritis (RA) (234). Additionally, increasing levels of circulating monocytes correlate with increasing levels of atherogenic lipids and plaque vulnerability (235). Furthermore, increasing levels CCL2, CCL3, CCL4, CCL5, CCL11, CCL13, CCL15, CCL17, CCL18, CCL19, CCL20, CCL21, CCL22, CCL23 and CCL25 have been found in atherosclerotic lesions (143, 144, 146, 236-241) and in some cases, serve as plasma biomarkers for atherosclerosis (34, 142, 242). Moreover, mouse studies have shown deletions in the CCL2 or CCR2 receptor resulted in reduced atherosclerotic lesion formation (158). Through the recruitment of immune cells, CC chemokines have also been associated with cardiac ischemia, reperfusion injury, fibrosis, acute coronary syndromes, myocarditis and heart failure (53, 243-248), as well as other diseases such as inflammatory bowel disease (249), psoriasis (46) and asthma (43).

4.1.2. Targeting CC chemokines therapeutically

The pharmaceutical industry has long since attempted to target chemokines and eliminate their excessive recruitment of immune cells in disease, however they have been largely unsuccessful. For example, Maraviroc, a CCR5 antagonist, showed no efficacy in treating patients with RA (250). Furthermore, MLN3897, a small molecule targeting CCR1 (169), and ABN912, a monoclonal antibody targeting CCL2 (168), both also showed no clinical improvement and efficacy in RA patients. As discussed above and in Chapter 3, targeting chemokines and their signalling pathway is challenging. The robustness of the chemokine network ensures eliminating a single chemokine or receptor will not eliminate the signalling pathway (2). Thus, targeting the chemokine network requires a multi-nodal approach, one which nature may have found a solution to.

In particular, tick derived evasins are capable of binding multiple chemokines and in doing so are able to overcome the chemokine network. Evasin 1 and 4 are selective CC chemokine binders, however they differ in selectivity. Evasin 1 binds three closely related chemokines CCL3, CCL4 and CCL18, whereas Evasin 4 has a broader binding profile, similar to those seen in viral chemokine binding proteins, such as vCCI (from poxvirus), M3 (from murine gammaherpesvirus 68) (184, 188), Glycoprotein G (gG, from herpes simplex virus) (183) and Crm (from smallpox virus) (251). But unlike gG and Crm, Evasin 4 binds only CC chemokines. A major disadvantage of viral chemokine binding proteins is the non-specific approach to binding chemokines which could have deleterious consequences on other biological functions, as they may target homeostatic chemokines which are crucial to maintenance of internal bodily functions, even in disease (75).

P1243, from the tick species *amblyomma americanum,* was identified bioinformatically in Chapter 3 and was selected for further characterisation, as it bound to multiple chemokines, including CCL15, CCL17 and CCL19. These findings indicate the 'one-to-many' binding nature of P1243 and bodes well for its therapeutic potential as a CKBP. This chapter hypothesises that P1243 is able to bind to multiple chemokines and neutralise their activity. Therefore, this chapter will biochemically and functionally determine the effects of the novel evasin P1243.

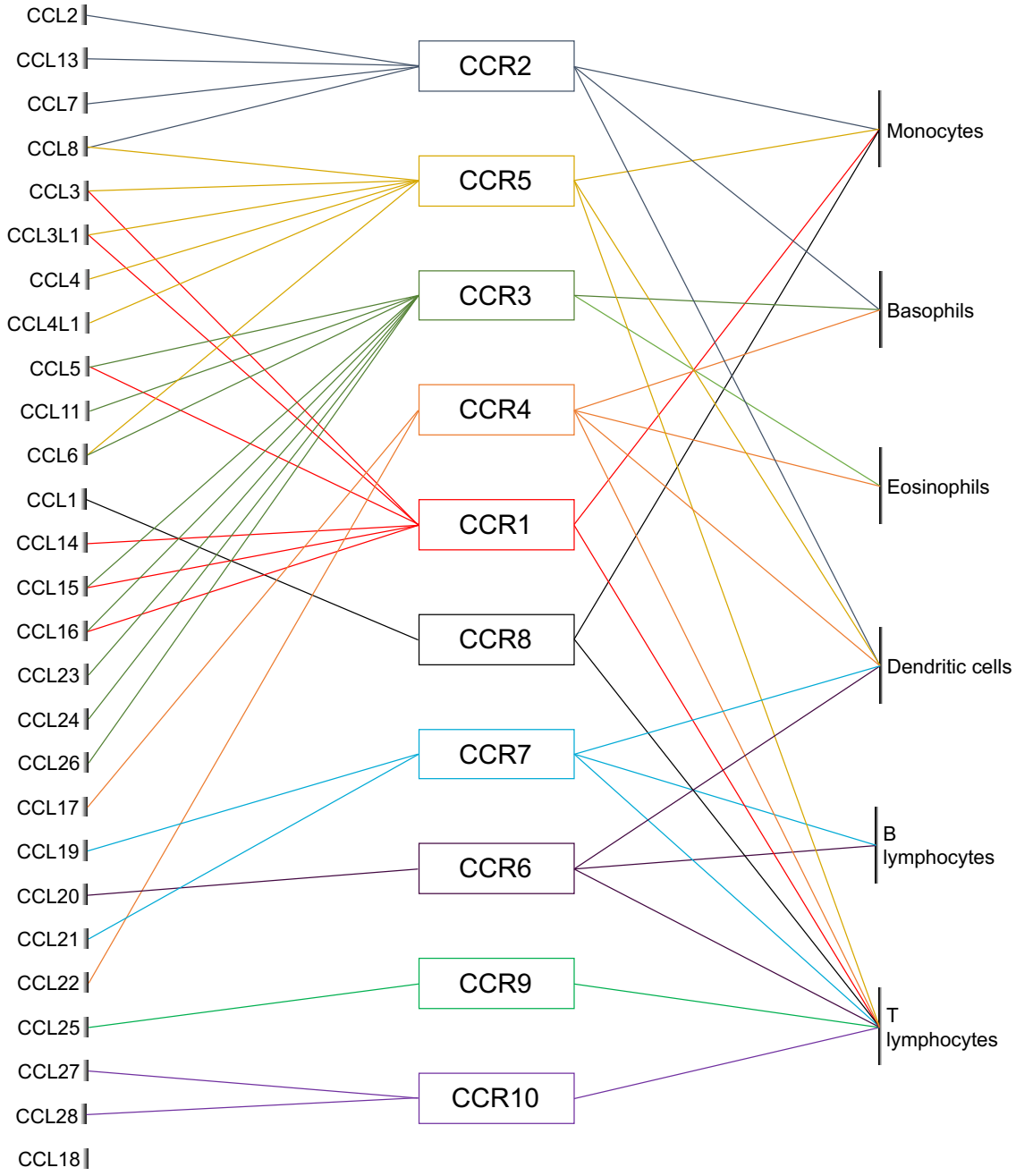


Figure 4. 1. Overview of the CC chemokine network. Network shows CC chemokines, the receptors they signal through and the immune cells they recruit. All interactions are colour coded based on the chemokine receptor interactions. The signalling receptor for CCL18 is not known. All interactions shown have been reported in the literature (1, 2).

4.2. Results

4.2.1. Sequence analysis of P1243 shows sequence homology to Evasins 1 and 4

Sequence analysis showed P1243 has 98 amino acid residues, with a predicted molecular weight of 10.9 kDa and a predicted pI of 6.94. Peptide sequence alignment of P1243 with published evasins shows this evasin retains the 8-Cystine (8-Cys) format that is observed in CC chemokine binding evasins and is predicted to be responsible for forming disulphide bonds (Figure 4. 2, green arrows) (175, 201). The shared motif being C-x(14,17)-C-x(3)-C-x(11,16)-C-x(17,20)-C-x(4)-C-x(4)-C-x(8)-C, where the numbers indicate the spacing between Cys residues (175, 201). P1243 only shares 33% identify with Evasin 1, however it shares a much larger identity with the other evasins, P991, 67% identity over 93 residues, and P983, 48% identity over 89 residues (175, 252). P1243 shares no sequence homology with Evasin 3, the CXC chemokine binding evasin (Figure 4. 2)

4.2.2. P1243 expresses as a highly glycosylated protein

To characterise the P1243 evasin, it was fused to a C-terminal StrepII:His tag, and was expressed as a secreted protein in HEK293F cells. Next, the supernatant from HEK293F cells was filtered and all histidine-tagged protein was isolated using nickel affinity (Ni-NTA) chromatography (Figure 4. 3. A). Subsequently, this was followed by size exclusion chromatography (SEC) to remove contaminating high and low molecular weight proteins from the nickel affinity purification.

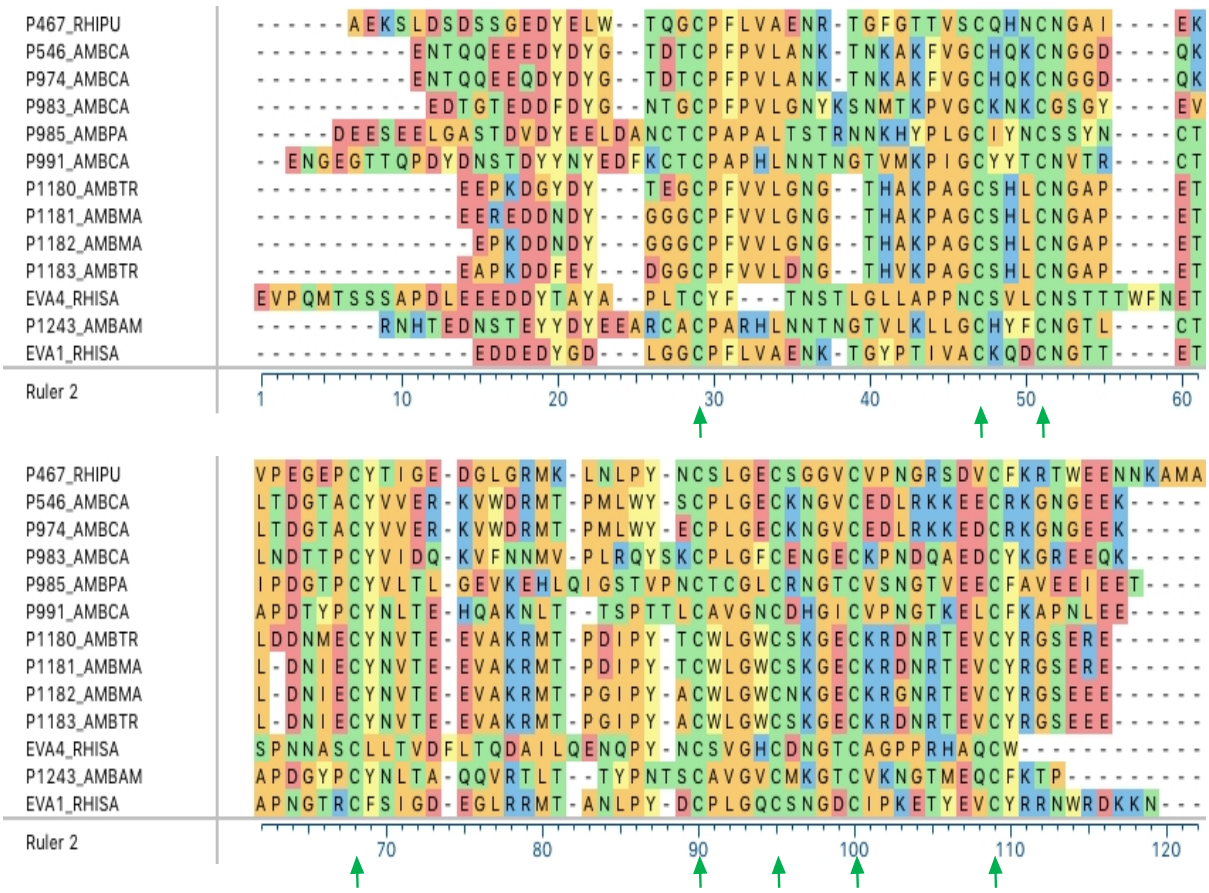


Figure 4. 2. CLUSTAL-W sequence alignment of P1243 with published CC chemokine binding evasins. Proteins sequences are defined as the identity, prefix, followed by tick species, suffix. Tick species are as follows: MBPA, AMBMA, AMBTR, AMBCA, - *Amblyomma parvum*, *maculatum*, *triste* and *cajennense* respectively, and RHIPU and RHISA – *Rhipicephalus pulchellus* and *sanguineus* respectively. Amino acid residues are coloured to show physiochemical properties. Green arrows indicate Cysteine residues (252).

All elutants were then analysed by SDS-PAGE, which showed P1243 expresses as a highly glycosylated protein, with fractions migrating in a range of molecular weights from 20-50 kDa (Figure 4. 3. B). This is consistent with glycosylation servers, which predicted seven N-glycosylation sites for P1243 (Figure 4. 4. A). All fractions containing protein of interest were pooled and concentrated. P1243 protein concentration was determined using the Bicinchoninic acid assay (BCA) and the protein yield from 0.9 L of P1243 transfected cells was typically measured to be 10 mg/L.

The integrity of the C-terminus of P1243 was confirmed using western blotting. P1243 protein, resolved on an SDS-PAGE gel, was transferred onto nitrocellulose blot and labelled with anti-histidine antibody and expression analysed using BioRad ChemiDoc MP system (Figure 4. 3. C).

To examine the peptide sequence of P1243 MS/MS was used, which required de-glycosylated P1243. To produce deglycosylated P1243, HEK293F cells were transfected with the addition of Kifunensine, in the transfection reagent, and incubated for 4-5 days. Following protein purification, using Ni-NTA affinity chromatography and SEC, concentrated P1243 protein was diluted in a 1:1 ratio with 40mM HEPES, 300mM NaCl and 1mM TCEP and then digested overnight using the N-glycosylation enzymes PNGaseF and EndoF1. P1243 was then purified again, using SEC, and protein resolved on SDS-PAGE gel. SDS-PAGE analysis showed treated P1243 migrated at 15 kDa, which is much closer to the expected molecular weight (10.9 kDa) (Figure 4. 4. B). SDS-PAGE gel, containing treated P1243, was then sent to Dr Rod Chalk (Burgess-Brown Laboratory, SGC, University of Oxford) for MS/MS. MS/MS analysis of P1243 recovered 62% of P1243 peptide sequence, including part of the N-terminus (Figure 4. 4. C).

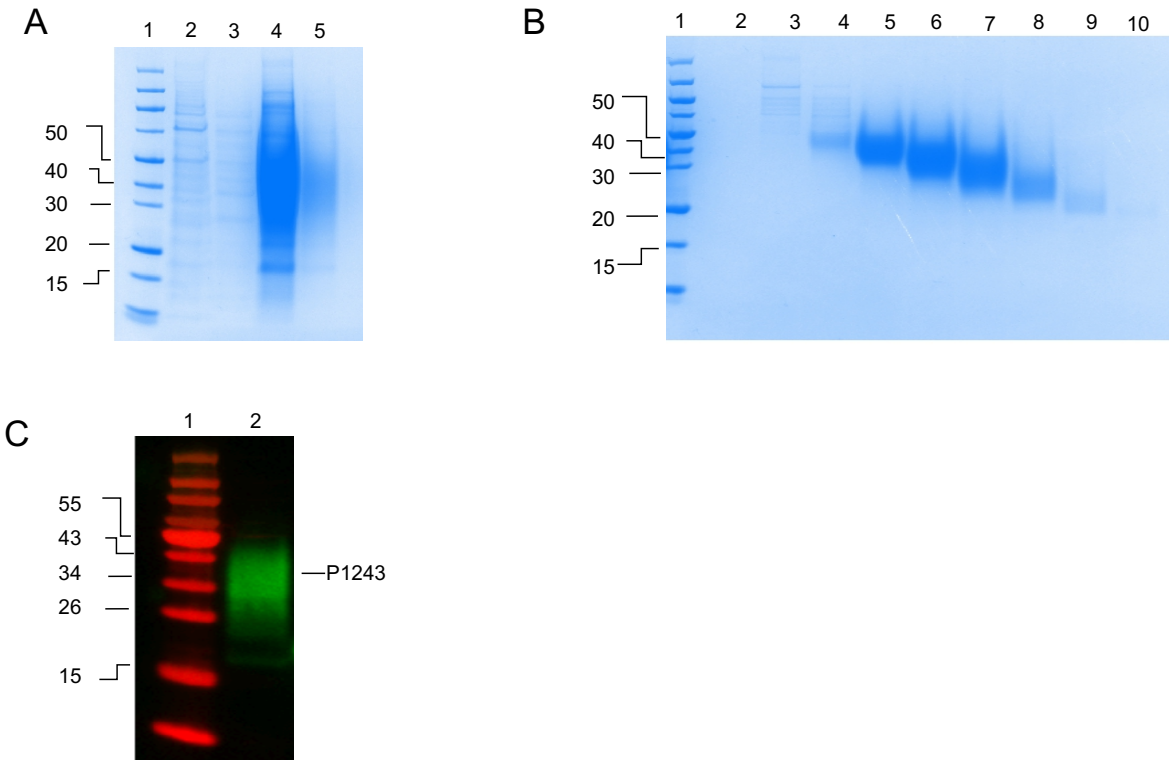
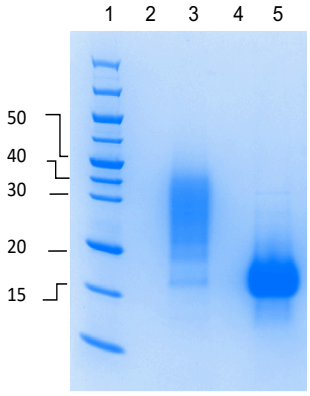


Figure 4. 3. Protein expression of P1243. (A) Colloidal Coomassie stained SDS-PAGE gel showing P1243 protein fractions following nickel affinity chromatography (Ni-NTA). Lane 1 shows protein ladder, lane 2 shows Ni-NTA column flow through, lane 3 shows flow through after washing and lanes 4-5 show elutions containing P1243 protein. (B) Colloidal Coomassie stained SDS-PAGE gel showing P1243 protein fractions (lane 5-9) following size exclusion chromatography. (C) Western blot showing anti-histidine labelling of P1243 protein. Lane 1 shows ladder (red) and lane 2 shows P1243 anti-histidine expression (green) (252).

A

Evasin	Accession	Clone tag	Length	Molecular weight (kDa)	pI	N-linked glycans	O-linked glycans
P1243	JAG91989.1	N	98	10.9	6.94	5, 10, 30, 33, 47, 61, 75, 91	-

B



C

MATRIX SCIENCE **MASCOT Search Results**

Protein View: P1243

P1243

Database:	Evasins
Score:	287
Nominal mass (M_r):	15248
Calculated pI:	6.66

Sequence similarity is available as an NCBI BLAST search of P1243 against nr.

Search parameters

Enzyme:	Trypsin: cuts C-term side of KR unless next residue is P.
Fixed modifications:	Carbamidomethyl (C)
Variable modifications:	Oxidation (M)

Protein sequence coverage: 62%

Matched peptides shown in ***bold red***.

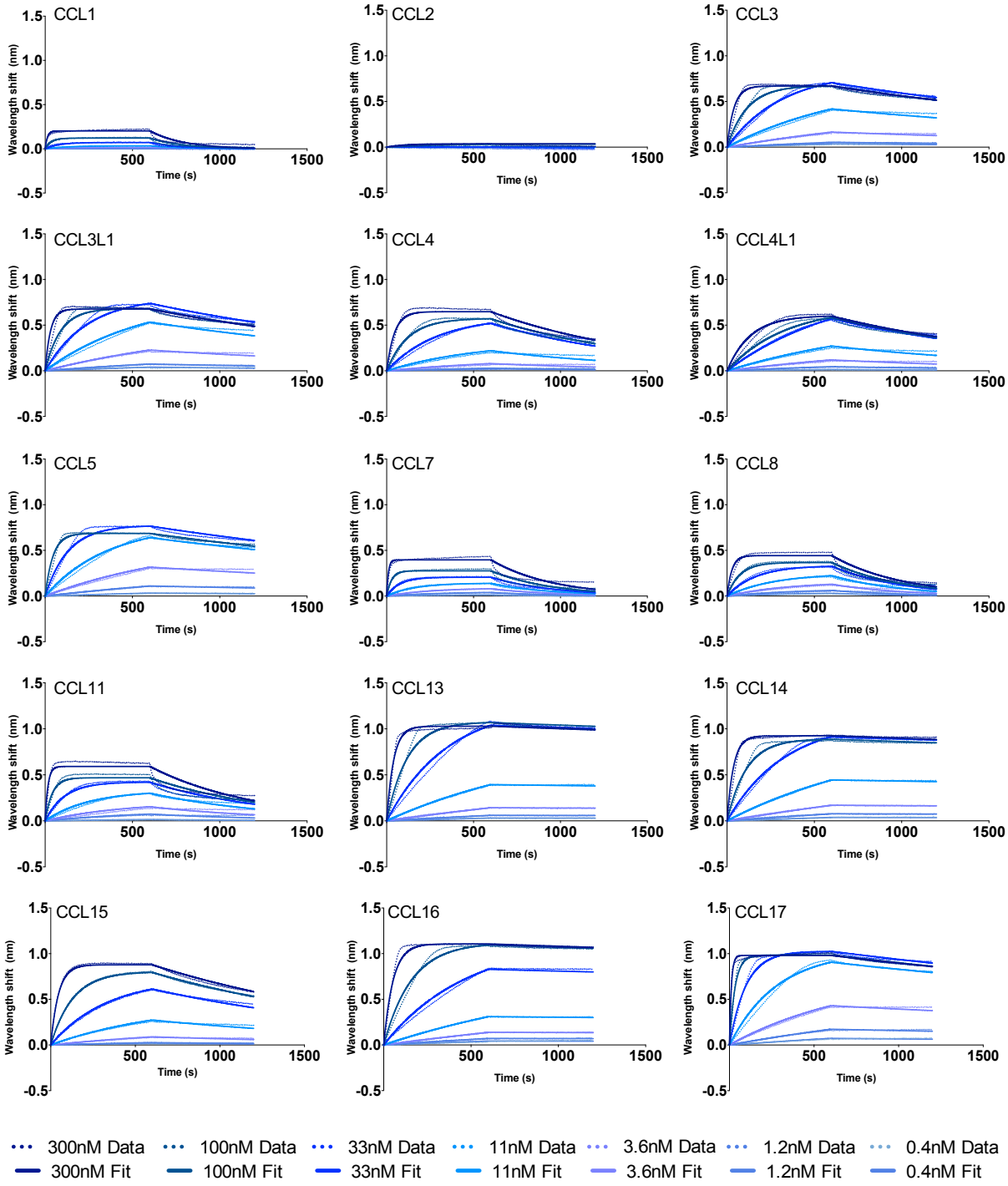
```
  1 ETGRNHTEDN STEYYDYEEA RCACPARHLN NTNGTVLKLL GCHYFCNGTL
 51 CTAPDGYPCY NLTAQQVRTL TTYPNTSCAV GVCMKGTCVK NGTMEQCFKT
101 PTGGGGGSGG GGSGGASAWS HPQFEKLEHH HHHHH
```

Figure 4. 4. Characterisation of the P1243 protein sequence. (A) P1243 protein profile and predicted glycosylation sites, predicted by the NetNGlyc1.0 and NetOGlyc4.0 servers (http://www.cbs.dtu.dk/services). (B) Colloidal Coomassie stained SDS-PAGE stained gel showing glycosylated (lane 3) and deglycosylated (lane 5) P1243. Lane 1 shows protein ladder, lanes 2 and 4 are empty. For deglycosylation, P1243 was treated with PNGaseF and EndoF1. (C) MS/MS analysis of deglycosylated P1243 showing 62% coverage of the peptide sequence. P1243 N-terminal sequence, 'ETG', encodes the start sequence of the pHLSec vector. P1243 C-terminal sequence, 'TGGGGGSGGGGSGGASAWSHPQFEKLEHHHHHHHH', encodes the Strep II-8xHis protein purification tag.

4.2.3. Analysis of the biochemical profile of P1243 shows it is a selective CC chemokine binder

The binding profile of P1243 to human chemokines was investigated in order to identify its potential therapeutic targets. The binding profile of P1243 across human chemokines was established using Bio-layer interferometry (BLI). Firstly, P1243 was immobilised on the nickel-coated sensor through the C-terminal histidine-tag. The sensor was then dipped into a well containing buffer (baseline), then into a well containing chemokine (association) followed by a well containing buffer (dissociation). P1243 was assayed against a panel of human chemokines at 300 nM in the BLI cross-binding assay, which showed P1243 associated, with varying degrees, to a panel of CC and CXC chemokines and XCL1 and CX_3CL1.

Next, binding affinities (K_d) were determined by assaying a fixed concentration of P1243 (1μM) against a titration of chemokine ranging from 0.4 nM to 300 nM. The binding data was fitted using ForteBio Data Analysis 9 software and K_d values were calculated. Analysis of results showed P1243 bound 21 CC chemokines with high affinity. Sensorgrams of CC chemokines that P1243 bound, and a summary of the K_d values are shown in Figure 4.5 and Figure 4.6, respectively. To determine dissociation half-life or target residence time (minutes, RT) for each chemokine P1243 bound, the following calculation was used: 0.693/ ($k_{off} \times 60$), using the off-rate (k_{off}, s^{-1}) obtained from BLI analysis. RT calculations show P1243 binds to chemokines with a broad variation (Figure 4. 6).


CCL1
CCL2
CCL3
CCL3L1
CCL4
CCL4L1
CCL5
CCL7
CCL8
CCL11
CCL13
CCL14
CCL15
CCL16
CCL17
Wavelength shift (nm)
Time (s)
300nM Data
100nM Data
33nM Data
11nM Data
3.6nM Data
1.2nM Data
0.4nM Data
300nM Fit
100nM Fit
33nM Fit
11nM Fit
3.6nM Fit
1.2nM Fit
0.4nM Fit

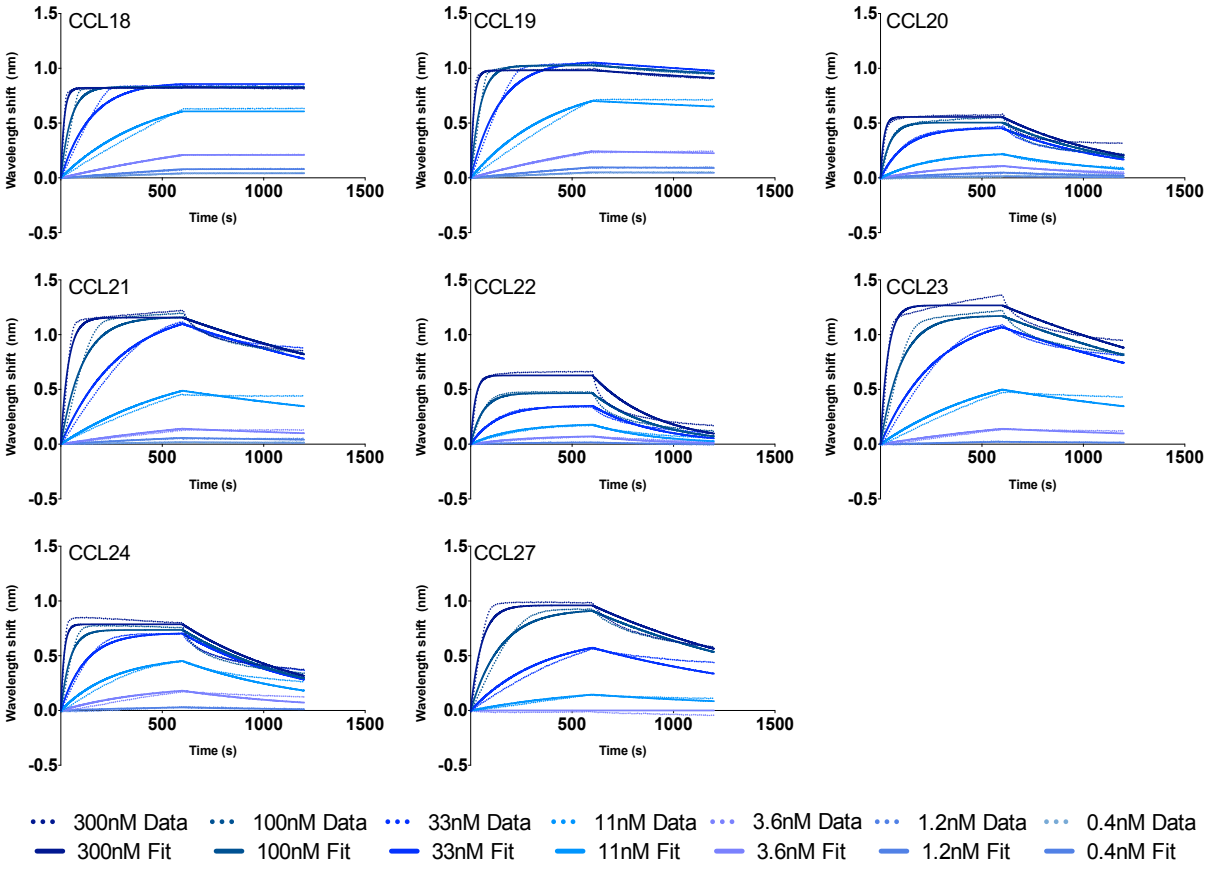


Figure 4. 5. Bio-layer interferometry (BLI) sensograms of P1243 against human chemokines. P1243 protein was assayed against a titration of chemokine (labelled) ranging from 0.4 nM to 300 nM**.** Plots show wavelength shift (nm, y-axis) versus time (seconds, x-axis). Collected data is shown as solid line and fitted data is shown by the dotted line.

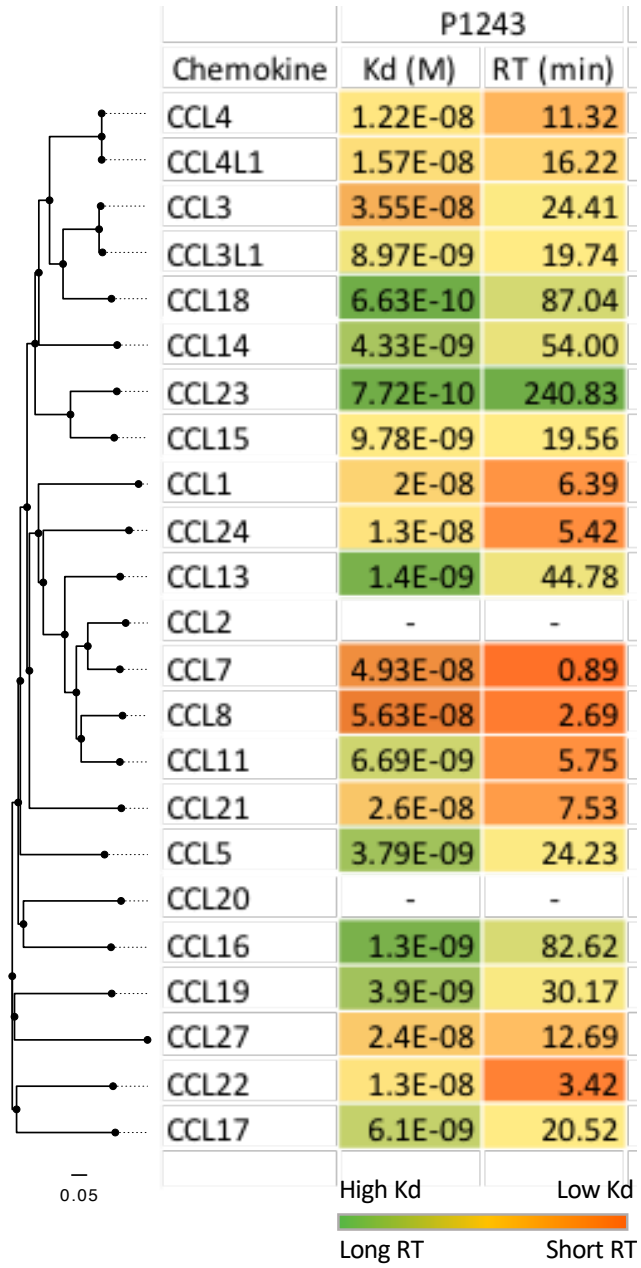


Figure 4. 6. Summary of the biochemical profile of P1243. Binding affinity profile of P1243 against CC chemokines. Binding affinities (K_d, M) and target residence times (RT, minutes) were determined using BLI. Colour gradient indicates high or long (green) to low or short (red) Kd or RT, respectively. Colour gradient established from data in figure. A dash (-) indicates either data could not be fitted, or binding could not be detected.

4.2.4. P1243 neutralises CC chemokines activity

To examine functional profile of P1243 in cells, chemotaxis assays were carried out. Firstly, THP-1 cells were placed in an upper chamber in a the 96-well plate (Corning HTS Transwell 96-well tissue culture system) and the chemoattractant in the lower chamber, separated by a 5 μm pore membrane. Next, cells were allowed to migrate, in response to chemoattractant, for 4 hours at 37^{o}C and migrating cells were then counted on the Attune Nxt Flow Cytometer. THP-1 cells express CCR2 and CCR5 and can migrate in response to CCL2, CCL3, CCL3L1, CCL5, CCL7 and CCL8. The EC_{80} values of chemokines for THP-1 cells determined previously (175): CCL3 is 3.5 nM, CCL3L1 is 0.5 nM, CCL5 is 8.6 nM, CCL7 is 7.2 nM and CCL8 is 7.3 nM. P1243 (0.006 nM to 300 nM) was pre-incubated with chemokines at their EC_{80} in the lower chamber for 30 minutes at 37^{o}C before incubation with the cells.

IC_{50} values were determined using an inhibitor response curve with a 4-parameter fit and are displayed as a mean of three technical and biological repeats (Figure 4. 7). P1243 IC_{50} values against CCL3: 6.5E-09 M, for CCL3L1: 1E-09 M, CCL5: 8.9E-09 M, CCL7: 1.2E-07 M and CCL8: 3.2E-09 M (Figure 4. 7).

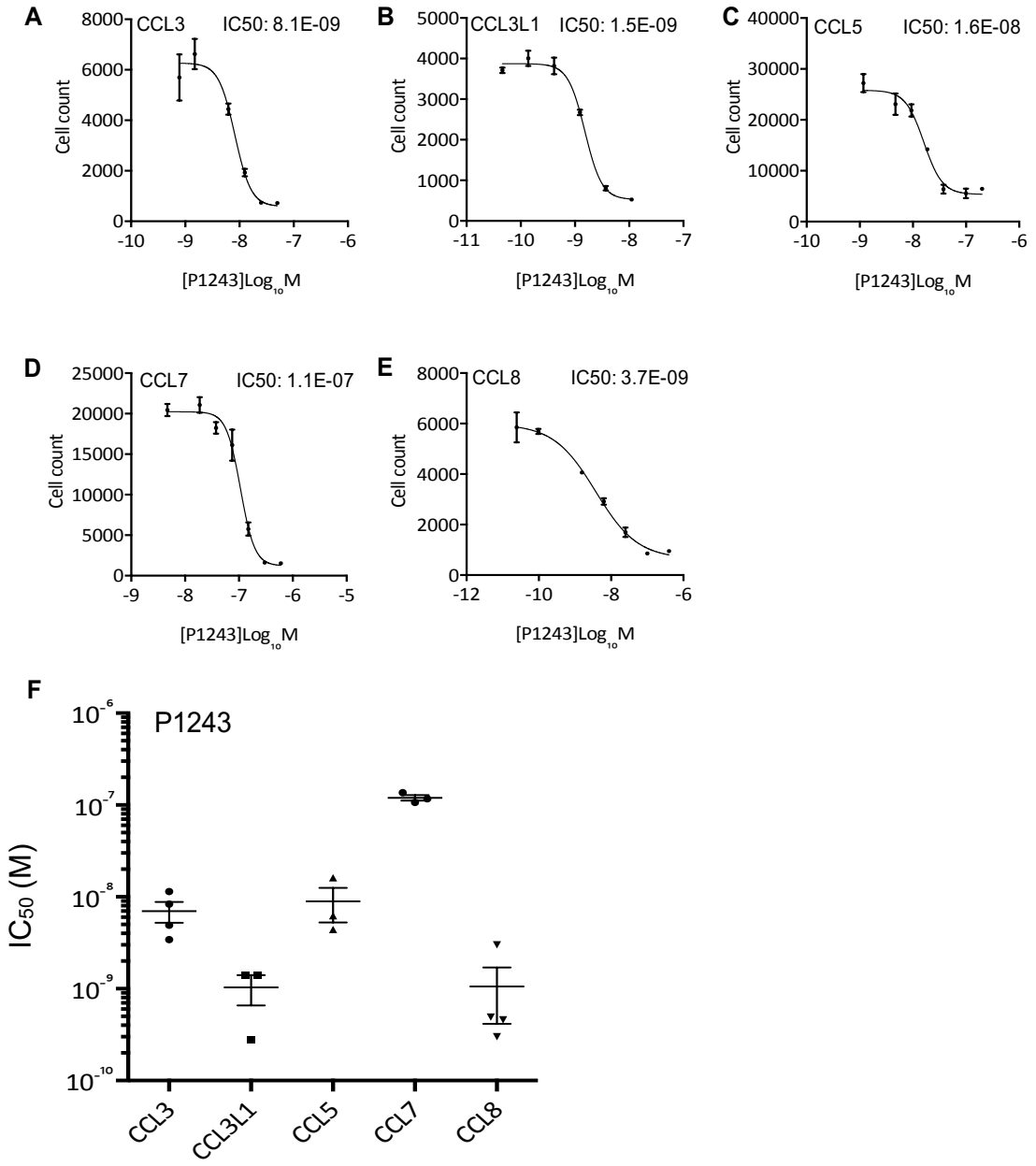


Figure 4. 7. Neutralisation profile of P1243 against CC chemokines. (A-E) Neutralisation of CC chemokine driven chemotaxis of THP-1 cells by P1243. Cell count of migrating THP-1 cells, in response to chemokine EC_{80} indicated, is shown on the y-axis and P1243 concentration ($Log_{10}M$) is shown on the x-axis. In each case, data from a representative experiment is shown mean ± s.e.m. of three technical replicates. IC_{50} (M) values for each chemokine, indicated, were estimated by fitting an agonist response curve with 4 parameters. (F) Summary P1243 IC_{50} data of the chemokines indicated (mean ± s.e.m., and individual data points from three biological replicates). Y-axis shows IC_{50} (logarithmic scale, M), assayed against indicated chemokine EC80, and x-axis shows each CKBP (252).

4.3. Discussion

The process of inflammation is characterised by the influx of immune cells, largely mediated by chemokines (75). This finding has subsequently led to their investigation and validation as therapeutic targets in inflammatory disease (131). Evasins, identified from tick saliva, bind and neutralise chemokines in a class specific manner, either binding and neutralising CC or CXC chemokines (174). To date, only 2 CC chemokine binding evasins have been identified: Evasin 1 and Evasin 4 (192, 193).

Increasing body of evidence shows specific chemokines are associated with inflammatory disease (131), and this study sought to identify further evasins and characterise their own potentially unique binding profile. Chapter 3 showed ticks do indeed harbour many more evasins that have yet to be investigated. From those identified, P1243, from the lone star tick *Amblyomma americanum*, was investigated further as it bound CCL15, CCL17 and CCL19 during yeast surface display (YSD) experiments. In this chapter, the functional properties of P1243 were examined in mammalian systems *in vitro*, and it was demonstrated that P1243 is a functionally active evasin that selectively binds and neutralises the activity of CC chemokines.

P1243 is expressed as a highly glycosylated protein

P1243 is a relatively small protein with a predicted mass of 10.9 kDa, however its expression, using the mammalian HEK293F cells, shows a heavily glycosylated protein, resolving on the SDS-PAGE gel in a number of glyco-forms that range in molecular weight from 20-50 kDa (Figure 4. 3). This finding correlates with all previously published evasins, which are also expressed as heavily glycosylated proteins (193, 200). Furthermore, Dias *et al*., (200) showed glycosylation was not essential for evasin recognition of chemokines. Considering ticks are

able to feed on their hosts for prolonged periods of time (226), this may be an evolutionary protective feature developed by the tick to evade immune detection during feeding, as glycosylation is a known technique of immune-evasion (253).

On the other hand, glycans are one of the biochemical signatures that may be recognised by innate sensors, pattern recognition receptors (PRRs), and labelled as pathogen associated molecular patterns (PAMPs). PAMPs are expressed exclusively on pathogens and are distinct from the hosts molecules. Thus when recognised, a signalling cascade is initiated that results in the recruitment of immune cells and the expression of interferons (IFNs) and pro-inflammatory cytokines (254). The innate sensors recognising PAMPs include toll-like receptors (TLRs), expressed on macrophages and dendritic cells (255). Thus, the glycans present on evasins may be more harmful than beneficial. Although, studies by Dias *et al.,* (200) showed that glycans were not required for the function of evasins, therefore they could be removed if they were to result in immune cell recruitment.

Moreover, it must be considered that evasins are non-human proteins and could potentially be immunogenic, eliciting an immune response, as generally observed when a foreign protein is introduced into a different species (174). Furthermore, an immune response against a therapeutic drug impacts the efficacy of the drug, as antibody induced clinical resistance begins to outweigh the administered doses of drug. However, Russo *et al*., (202) showed the chronic administration of Evasin 1, subcutaneously in mice, over a period of 25 days did not result in an antibody response against the evasin. In addition to this, *in vitro* chemotaxis assays performed in this study showed P1243 had no significant effect on migrating THP-1 cells (Appendix A, Figure A1), showing P1243 alone does not itself induce cell recruitment. Indeed, ticks could be producing evasins as glycosylated proteins in order to create a 'glycan-shield' that defends against neutralising antibodies (256, 257). Moreover, non-human proteins have already been developed and are administered in clinics. For example, Hirudin, a small protein

derived from leeches that inhibits thrombin, is currently used to retreat hip-replacement surgery patients following heparin induced thrombocytopenia (258). Another example is Exenatide, derived from the saliva of the venomous lizard the Gila monster, used as a first-in-class therapy for type 2 diabetes mellitus (259). Also, considering glycosylation as a strategy for immune evasion implies evasins, which are all heavily glycosylated, will likely have reduced immunogenicity (174).

This chapter has also shown P1243 expresses several versions of glyco-forms. All forms (confirmed to be P1243 through positive histidine-tag labelling) were pooled together for subsequent assays. Further work may require examining the effects of each glyco-form on the function of the protein, chemokine binding and neutralisation, as this was not examined in this study. Biopharmaceutically, glycans present on any glycoprotein destined for therapeutic application typically requires individual investigation of each glycan present, to establish whether they affect the activity of the therapeutic and whether it will cause an immune response (260). Moreover, published data on glycosylation having no immediate effect on evasin function (200), nor resulting in an immunogenic response (202) is encouraging. However, each evasin will need to be examined individually as glycosylation is structurally diverse, considering different cell lines exhibit different patterns of glycosylation that depend on not only on the glycosidases and glycosyltransferases present in the endoplasmic reticulum and golgi apparatuses of a cell (261), but also cell media composition and culturing conditions (262).

P1243 selectively binds CC chemokines with high affinity

Peptide sequence alignment of P1243 and the published evasins show it shares most sequence similarity to P991 (175) and Evasins 1 and 4 (192, 193) (Figure 4. 2), thus, suggesting they

may share similar characteristics. Indeed, P1243 exhibited a similar selective binding profile to the aforementioned evasins, in binding to only CC chemokines. However, unlike Evasin 1, P1243 exhibited a 'broad-spectrum' binding profile, which bound to a large subset of CC chemokines, akin to Evasin 4 (193) and P991 (175), as they also bind a broad range of CC chemokines.

Moreover, P1243 and P991, share an almost identical CC chemokine binding profile, with the exception of CCL2 and CCL20, in which P1243 binding affinity to these chemokines could not be established using the BLI assay conditions. However, Hayward *et al.,* (198) recently reported and partially characterised P1243, in which they refer to it as AAM-02, and described it binding to CCL2, CCL7, CCL11, CCL24 and CCL26. The results shown in this chapter, however, show P1243 binds to a much larger subset of CC chemokines (Figure 4.6). Nonetheless, the data reported by Hayward *et al*., (198) describing AAM-02 (or P1243) having a K_d of 1000 nM for CCL2 correlates with the findings shown in this chapter, which show no binding of P1243 to CCL2 could be detected at 300 nM (Appendix A, Figure A2). Moreover, targeting of CCL2, a major monocytic chemoattractant, is a most advantageous therapeutic target and has been implicated in a range of inflammatory diseases including myocarditis (263), atherosclerosis (264), multiple sclerosis (265) and rheumatoid arthritis (266). Therefore, putting P1243 at a disadvantage for monocyte targeted therapy.

Although, P1243 does not bind CCL2, with nanomolar affinity, it still binds the remaining CCR2 ligands: CCL7, CCL8, CCL13, with high affinity. Alternatively, P1243 could be combined with a CCL2 targeted monoclonal antibody to achieve therapeutic ablation of downstream CCR2 pathways and monocyte chemotaxis. For example, P1243 could be combined with ABN912, a CCL2 monoclonal antibody that showed no clinical improvement in rheumatoid arthritis patients (168). However, monocytes can be recruited through chemokine binding, not only through CCR2, but also CCR1, CCR5 and CCR8 (Figure 4.1).

Encouragingly, P1243 binds all the ligands that signal through those receptors. Furthermore, both Evasins 1 and 4 do not bind CCL2 and have proved therapeutically beneficial in a range of disease animal models, including lung inflammation and fibrosis (202), post-infarction myocardial injury (206), psoriasis (193) and graft-versus-host disease (204).

P1243 neutralises CC chemokine activity *in vitro*

The monocytic cell line THP-1 was used to examine and establish the evasins functional effects. THP-1 cells express CCR2 and CCR5, which may signal through CCL2, CCL3, CCL5, CCL7 and CCL8 (Figure 4. 1). This chapter showed that P1243 not only binds to CCL3, CCL3L1, CCL5, CCL7 and CCL8 with high affinity, but also neutralise their activity in the chemotaxis assays with half maximal inhibitory concentration (IC_{50}) values in the nanomolar region (Figure 4. 7). Neutralisation of chemokine activity in the nanomolar region is most advantageous, as this requires fewer administered doses of the evasin, which is most valuable when selecting therapeutic candidates (267).

Although P1243 binds the same chemokines as P991 (175), with the exception of CCL2 and CCL20, it varies quite dramatically in the dissociation half-lives, or target residence times (RT), of the chemokines they bind. RT describes the length of time a ligand interacts with its target (268), in this case, the evasin binding to chemokines and forms part of the pharmacodynamic profile of a drug. The longer the RT, the more attractive the therapeutic is as it likely to be more effective for longer and, thus, requires fewer doses (268).

This chapter showed P1243 has a short RT compared to the CC chemokines it binds, indicating it interacts with chemokines for shorter periods of time. P991, on the other hand, had a much longer RT, indicating it interacts with chemokines over longer periods of time. The RT for CCL7 and P1243 is under 1 minute, whereas for P991 it was reported to be over 8 minutes

(175). However, the only variability observed is P1243 binding to CCL23, where an RT of 240 minutes was calculated, whereas for P991 is was reported to be approximately 32 minutes (175). Thus, highlighting the different binding modalities of evasins to chemokines. Considering these findings, P1243 is most suitable for short-term chemokine inhibition but not long-term inhibition. P1243 would therefore be most suited for therapeutic application in a range of acute diseases driven by inflammation.

In summary, P1243 is a novel evasin, capable of selective binding to 21 CC chemokines with high affinity. Furthermore, P1243 serves as a good candidate for acute responses, due its shorter dissociation times to the chemokines it binds. Additionally, P1243 is functionally effective with IC_{50} values in the nanomolar region, further encouraging its potential as a strong therapeutic. Although this chapter has validated P1243 as an evasin using *in vitro* assays, its physiological effects *in vivo* will need to be examined to determine its therapeutic suitability. Encouragingly, this chapter has shown P1243 binds to the chemokines it bound during the yeast surface display (YSD) experiments (Chapter 3), CCL15, CCL17 and CCL19, with nanomolar affinity, thus validating the use of YSD to identify evasins.

Chapter 5.

Characterising the Novel

Evasin P1156

5.1. Introduction

5.1.1. CXC chemokines

The second largest family of chemokines, after CC chemokines, are the CXC chemokines, defined by a single amino acid group between their N-terminal Cysteines. Genetic mapping of CXC chemokines showed that they all cluster together at a specific locus of chromosome 4 (q12-q21) and share 20-50% homology in their amino acid form (269). This finding suggests these chemokines arose by duplication and divergence from a primordial chemokine gene (269). Despite CXC chemokines existing in other species (270), these developments are most likely to have occurred recently during evolution, as suggested by their limited numbers. For example, there are not as many murine chemokines as there are human, also there is no mouse ortholog to the human CXCL8 (271).

CXC chemokines are further classified based on the presence of a glutamate-leucine-arginine (ELR) motif, immediately before the first cysteine as either ELR+ (with motif) or ELR- (without motif). The ELR+ CXC chemokines include CXCL1, CXCL2, CXCL3, CXCL5,

CXCL6, CXCL7 and CXCL8, and primarily signal via CXCR1 and/or CXCR2. Whereas, the ELR- CXC chemokines, CXCL4, CXCL9, CXCL10, CXCL11 and CXCL12, signal through either CXCR3, CXCR4 or CXCR5 receptors (84).

Furthermore, they also have distinct functions, for example, ELR+ CXC chemokines are chemotactic for neutrophils, whereas ELR- CXC chemokines tend to be chemotactic for lymphocytes (Figure 5. 1) (2). On key feature of chemokine receptor is their binding via a 'one-to-many' approach (described in Chapter 4) (2). In particular, the CXCR2 chemokine receptor is able to bind all seven ELR+ chemokines, CXCL6 and CXCL8 can also signal through CXCR1. To complicate things further CXCR1 and CXCR2 are highly expressed on the surface of neutrophils but are also expressed, to a lesser-extend, on some T cells, mast cells, monocytes and macrophages (2) (Figure 5. 1).

5.1.2. The role of CXC chemokines in inflammatory disease

ELR+ CXC chemokines have been validated as therapeutic targets due to their association with inflammatory disease, especially in those involving acute inflammatory responses (75, 97). For example, ischemic-reperfusion injuries are thought to contribute to the pathologies of myocardial infarctions (272), strokes (273) and acute respiratory distress syndrome (274) through neutrophil involvement, which is part of the acute inflammatory response. In models of ischemic-reperfusion injury, blocking the chemokine receptors CXCR1 and CXCR2 results in an efficacious reduction in neutrophil influx and damage to tissues (97, 160, 162, 275) and increasing numbers of neutrophils post-myocardial infarctions are considered detrimental to patient outcomes (276, 277).

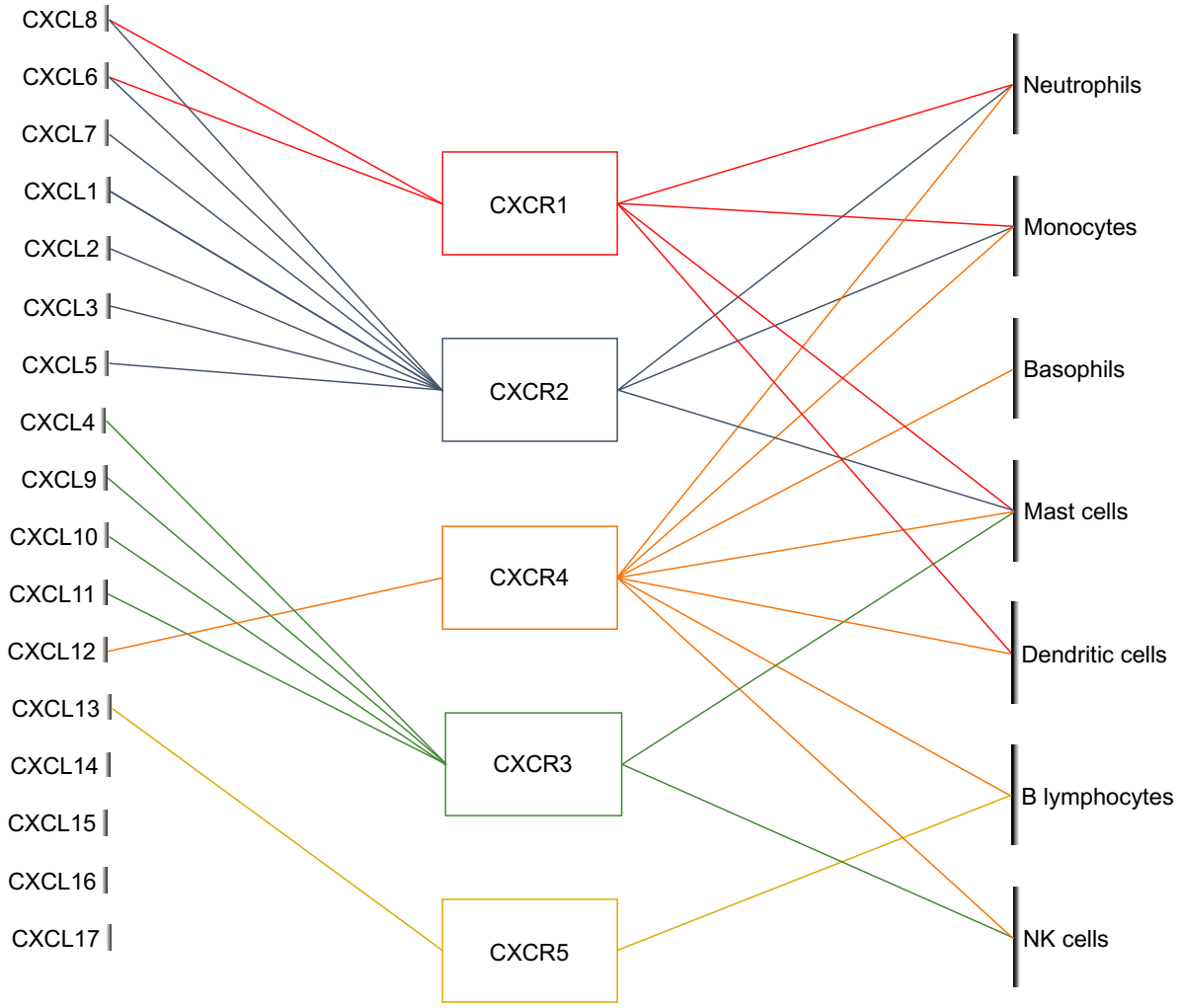


Figure 5. 1. Overview of the CXC chemokine network. The interaction network shows CXC chemokines, the receptors they signal through and the immune cells they recruit. All interactions are colour coded based on the chemokine receptor interactions. The signalling receptors for CXCL7, CXCL14, CXCL15, CXCL16 and CXCL17 are unknown. All interactions shown have been reported in the literature (2).

Furthermore, Yunoki *et al*., showed that neutrophils play a role in plaque destabilization in atherosclerosis, typically presenting in numerous patients with unstable plaques (278). Also, activated macrophages in the atherosclerotic plaques produce chemokines that recruit neutrophils to the lesion site. These neutrophils then release reactive oxidizing species, which activate the endothelium to recruit more neutrophils and result in a looping neutrophil influx and are a source of MMP-8 and MMP-9, further contributing to the destabilization of the plaques (279-281). Recently, the use of a neutrophil chemotaxis inhibitor, Colchicine, in coronary heart disease patients resulted in reduced vascular events (282).

With increasing evidence highlighting the roles of CXC chemokines in inflammatory diseases and lack of efficacious therapies to target them, this chapter sought to characterise P1156 and examine its potential as a neutrophil-targeting therapeutic. The hypothesises was P1156 is able to bind to multiple chemokines and neutralise their ability to recruit inflammatory cells. The aim of this chapter is to biochemically and functionally determine the effects of the novel evasin P1156, identified from *Ixodes ricinus* tick.

5.2. Results

5.2.1. Sequence analysis of P1156

Sequence analysis of P1156 shows the protein is comprised of 80 amino acid residues and has a predicted molecular weight of 8.8 kDa and predicted pI of 4.7. Furthermore, P1156 shares no significant homology with Evasins 1 and 4, but shares 30% sequence homology with Evasin 3, over an alignment of 43 residues. P1156 also exhibits the same number of cysteines observed in Evasin 3, six cysteines (Figure 5. 2, green arrows).

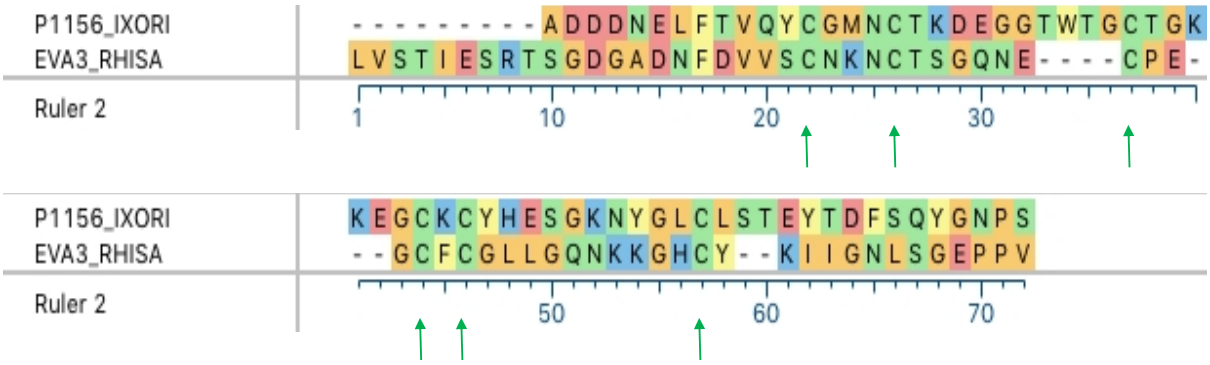


Figure 5. 2. Graphical overview of CLUSTAL-W sequence alignment of P1156 with published CXC chemokine binding evasin, Evasin-3. Proteins sequences are defined as the identity, prefix, followed by tick species, suffix. Tick species are as follows: IXORI- Ixodes Ricinus and RHISA – Rhipicephalus sanguineus. Amino acid residues are coloured to show physiochemical properties. Green arrows indicate Cysteine residues (252).

5.2.2. P1156 expresses as a highly glycosylated protein

To permit the characterization of the P1156 evasin, the protein was fused to a C-terminal StrepII:His tag, and expressed as a secreted protein in HEK293F cells. The protein was then enriched from the HEK293F supernatant by filtration and Histidine-tagged protein were isolated using nickel affinity (Ni-NTA) chromatography (Figure 5. 3. A). Next, size exclusion

chromatography (SEC) was employed to remove contaminating high and low molecular weight proteins from the Ni-NTA purification.

All eluents were then analysed by SDS-PAGE, which showed P1156 is expressed as a highly glycosylated protein, with fractions migrating of a molecular weight of approximately 17 kDa. This is consistent with glycosylation prediction sites, which predicted two N-linked glycosylation sites, at positions 16 and 61, and two O-linked glycosylation sites, at positions 63 and 75 (Figure 5. 4. A). All eluted fractions, containing protein of interest, were pooled and concentrated and is visualised in Figure 5. 3. B. P1156 protein concentration was determined using the Bicinchoninic acid assay (BCA) and the protein yield from 0.9 L of P1156 transfected cells was typically measured to be 3.6 mg/L.

Finally, the C-terminus-tagged P1156 protein was confirmed by western blot analysis and is shown at the correct protein molecular weight in Figure 5. 3. C. In addition to this, the P1156 protein was further confirmed using MS/MS, which required deglycosylated P1156. To produce the deglycosylated P1156, HEK293F cells were transfected, along with the deglycosylation agent Kifunensine, and then purified and digested overnight using the N-glycosylation enzymes PNGaseF and EndoF1. SDS-PAGE analysis showed treated P1156 migrated at 15 kDa, which is closer to the expected molecular weight (8.8 kDa) (Figure 5. 4. B). The identity of the purified P1156 was confirmed by MS/MS by Dr Rod Chalk (Burgess-Brown Laboratory, SGC, University of Oxford). MS/MS analysis showed only 18% coverage of peptide sequence, with only one peptide sequence recovered towards the C-terminus (Figure 5. 4. C). As no coverage of the N-terminus was shown by MS/MS, N-terminal sequencing was performed which showed an intact N-terminus (Figure 5. 4. D).

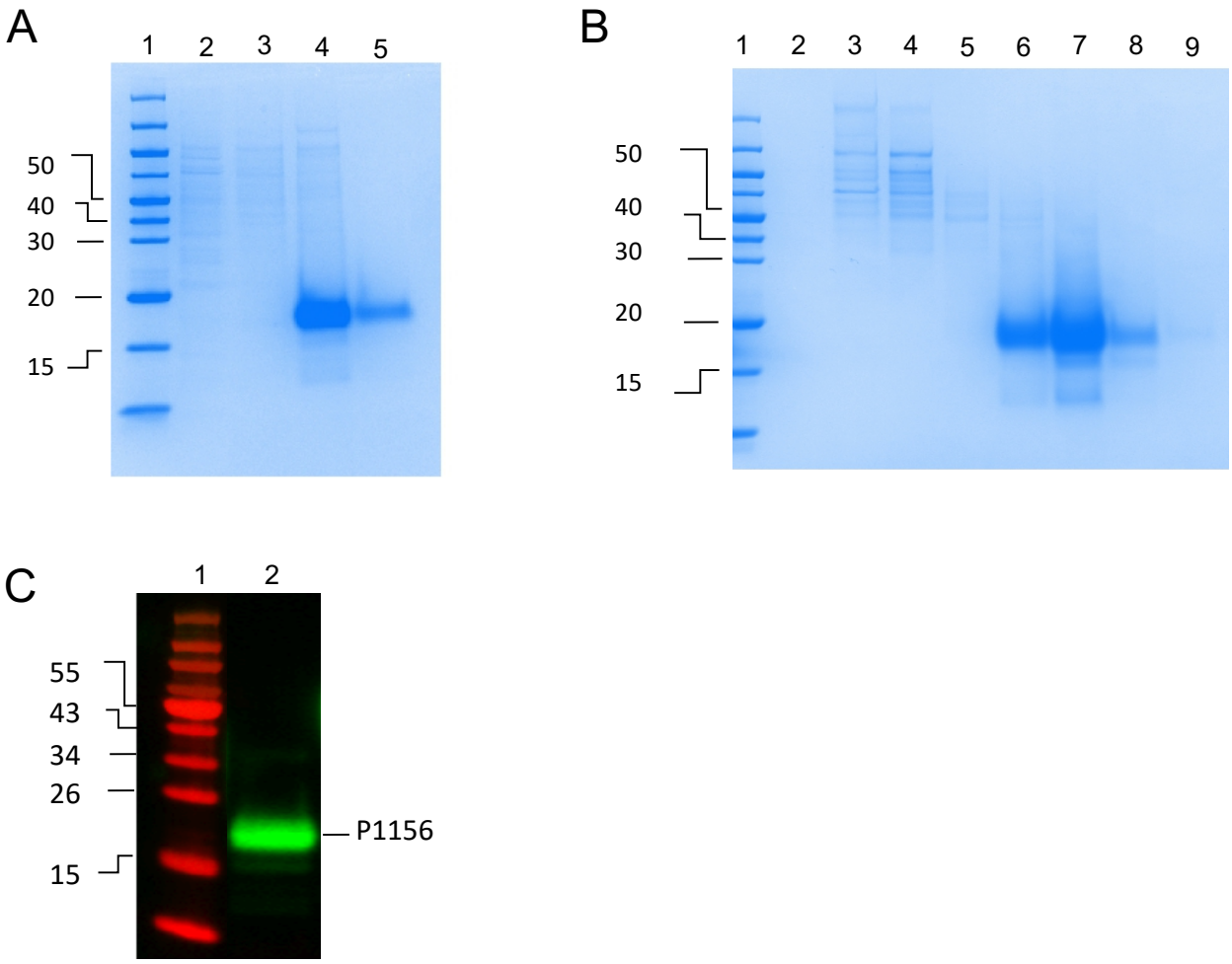
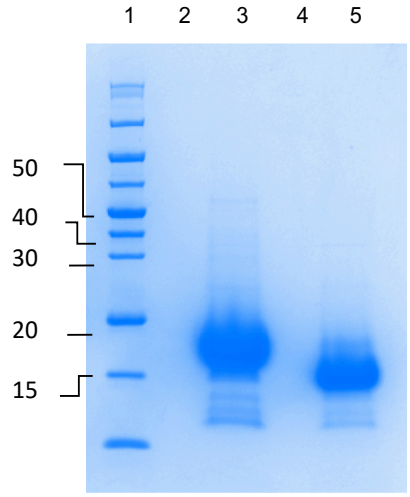


Figure 5. 3. Analysis of Protein expression of histidine-tagged-P1156. (A) Colloidal Coomassie stained SDS-PAGE gel showing P1156 protein fractions following nickel affinity chromatography (Ni-NTA). Lane 1 shows protein ladder, lane 2 shows Ni-NTA column flow through, lane 3 shows flow through after washing and lanes 4-5 show elutions containing P1156 protein. (B) Colloidal Coomassie stained SDS-PAGE gel showing P1156 protein fractions (lane 5-9) following size exclusion chromatography. (C) Western blot showing anti-histidine labelling of P1156 protein. Lane 1 shows ladder (red) and lane 2 shows P1156 anti-histidine expression (green) (252).

A

Evasin	Accession	Clone tag	Length	Molecular weight (kDa)	pI	N-linked glycans	O-linked glycans
P1156	JAB72437.1	N	80	8.8	4.7	16, 61	63, 75

B



C

MATRIX SCIENCE **MASCOT Search Results**

Protein View: Sequence

Sequence

Database: Evasin2
Score: 69
Nominal mass (M_r): 12105
Calculated pI: 5.68

Sequence similarity is available as an NCBI BLAST search of Sequence against nr.

Search parameters

Enzyme: Trypsin: cuts C-term side of KR unless next residue is P
Fixed modifications: Carbamidomethyl (C)
Variable modifications: Oxidation (M)

Protein sequence coverage: 18%

Matched peptides shown in ***bold red***.

```
  1 DGGADDDNEL FTVQYCGMNC TKDEGGIWTG CTGKKEGCKC YHESGKNYGL
 51 CLSTEYTDFS QYGNPSDSEI EAAKPKRSDT LSHGGASAWS HPQFEKLEHH
101 HHHHHH
```

D

Protein sequence report

Alta Bioscience code: S7081
Customer sample code: P1156

N terminus

Residue			
1	**D**		
2	**G**		
3	**G**		
4	**A**		
5	**D**		
6			
7			
8			
9			
10			
11			
12			
13			
14			
15			

Comments:- Strong clear sequence.

Figure 5. 4. Characterising of P1156 protein sequence. (A) P1156 protein profile and predicted glycosylation sites, predicted by the NetNGlyc1.0 and NetOGlyc4.0 servers (http://www.cbs.dtu.dk/services). (B) SDS-PAGE coomassie stained gel showing glycosylated and deglycosylated P1156. Lane 1 shows protein ladder, Lanes 2 is empty, lane 3 shows glycosylated P1156, lane 4 is empty and lane 5 shows deglycosylated P1156. For deglycosylation, P1243 was treated with PNGaseF and EndoF1. The N-terminus of P1156 sequence begins with 'DGG', which encodes the start sequence. The C-terminus contains the sequence 'GGASAWSHPQFEKLEHHHHHHHH', which encodes StrepII:His purification tag (C) MS/MS analysis of deglycosylated P1156. Recovered peptides are shown in red. (D) N-terminal sequencing of P1156 protein (AltaBioscience, Redditch, UK).

5.2.3. Analysis of the biochemical profile of P1156 shows it is a selective CXC chemokine binder

The binding profile of P1156 to human chemokines was investigated in order to identify its potential therapeutic targets. P1156's binding to human chemokines, was established using Bio-layer interferometry (BLI). Firstly, P1156 was immobilised on the nickel-coated sensor, through the C-terminal histidine-tag, then dipped into a well containing buffer (baseline), then into a well containing chemokine (association) followed by a well containing buffer (dissociation).

P1156 was first assayed against human chemokines at 300 nM in the BLI cross-binding assay, which showed P1156 associated with varying degrees, to a panel of CXC chemokines only. Next, binding affinities (K_d) were determined by assaying a fixed concentration of P1156 (1 μM) against a titration of chemokine ranging from 0.4nM to 600 nM. The binding data was fitted using ForteBio Data Analysis 9 software and K_d values were calculated. Analysis of this showed P1156 was bound to six of the ELR+ CXC chemokines: CXCL1, CXCL2, CXCL3, CXCL5, CXCL6 and CXCL8, showing the highest affinity for CXCL1 and CXCL8 (Figure 5. 5 and Figure 5. 6).

To determine dissociation half-life or target residence time (RT, minutes) the following calculation was used: 0.693/ ($k_{off} \times 60$) from the off-rate (k_{off}, s^{-1}) obtained from biolayer interferometry analysis (ForteBio Data Analysis 9 software). RT calculations revealed P1156 had the longest RT for CXCL1 and CXCL8. The remaining chemokines show similar RT's (Figure 5. 6).

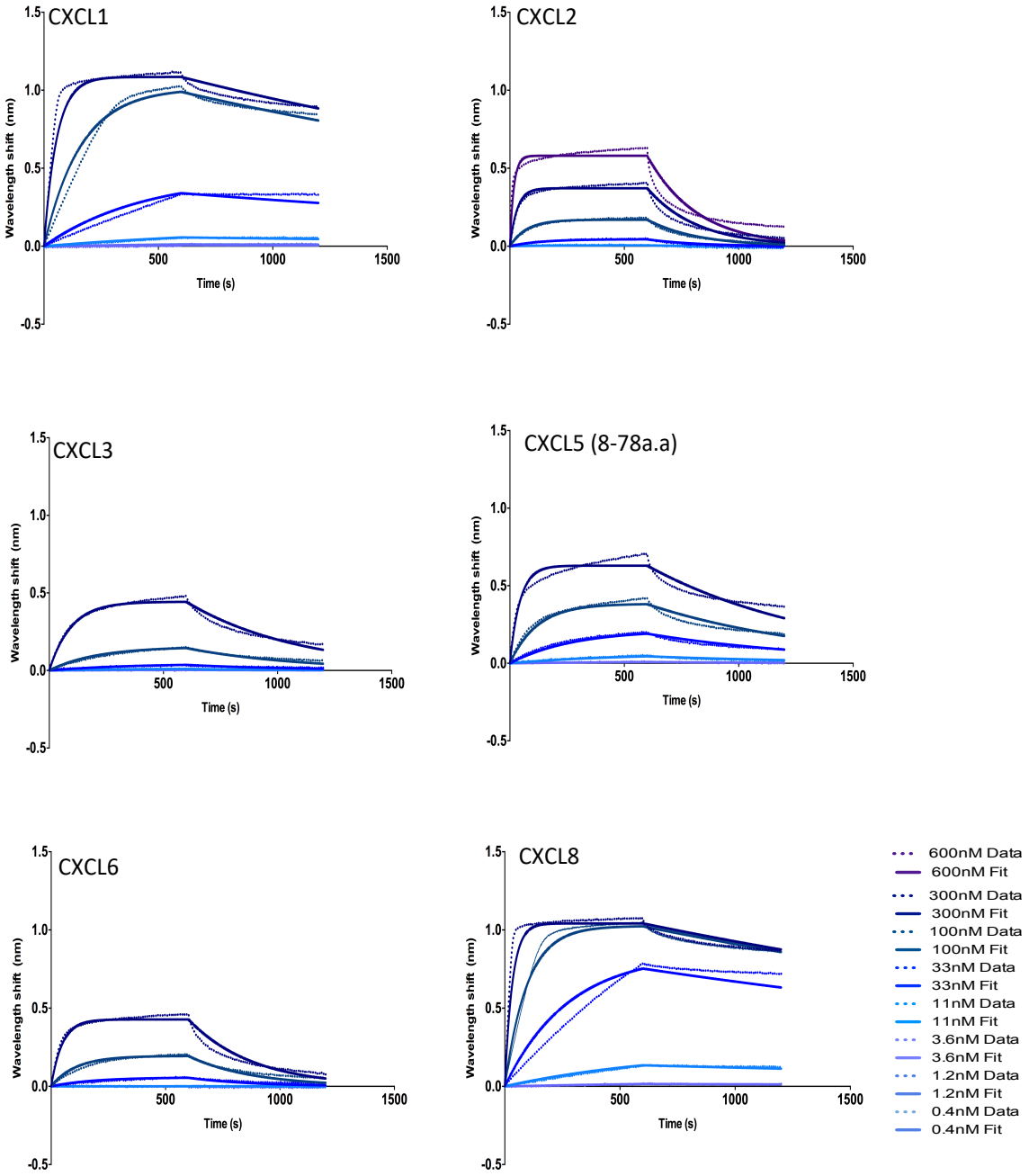


Figure 5. 5. Bio-layer interferometry (BLI) sensograms of P1156 against human CXC chemokines. Plots show wavelength shift of respective chemokines (nm, y-axis) versus time (seconds, x-axis). Collected data is shown as solid line and fitted data is shown by the dotted line.

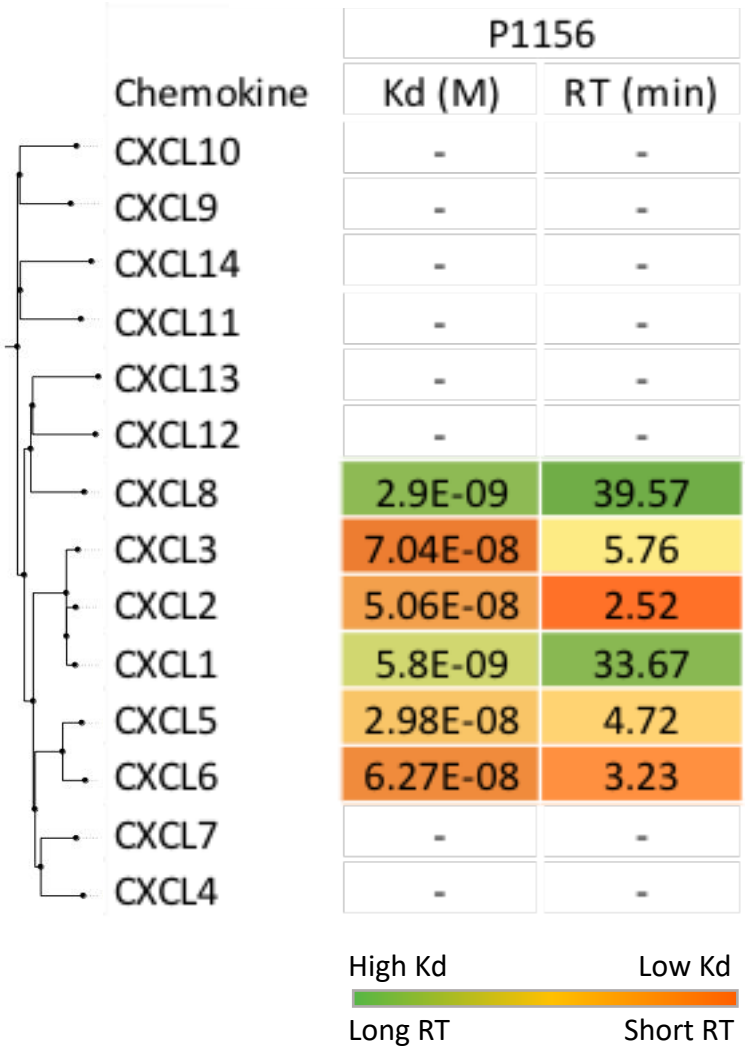


Figure 5. 6. Binding affinity profile of P1156 against CXC chemokines. Binding affinities (K_d, M) and target residence times (RT, minutes) determined using BLI. Colour gradient indicates high or long (green) to low or short (red) Kd or RT, respectively. Colour gradient established from data in figure. A dash (-) indicates either data could not be fitted, or binding could not be detected.

5.2.4. P1156 neutralises CXC chemokine activity *in vitro*

To examine the functional effects of P1156, human granulocytes were used in the cell migration assay. Human granulocytes were placed in an upper chamber in a the Transwell 96-well plate and chemoattractant in the lower chamber, separated by a 3 or 5 μm pore membrane. Cells were allowed to migrate, in response to chemoattractant, for 1 hour at 37^{o}C. Migrating cells were then counted on the Attune Nxt Flow Cytometer.

For the CXCL8 assays, granulocytes were isolated from whole blood of healthy volunteers, by red blood cell depletion followed by red blood cell lysis. For the CXCL1 assays, granulocytes were purified from buffy coat and isolated using the same method. Furthermore, labelling of the granulocyte population of cells shows the neutrophil population to be the most dominant cell population, identified based on the cell surface expression of CXCR2 and not CCR3, which is attributed to eosinophils (Appendix C, Figure C2).

Additionally, the EC_{80} values of chemokines against human granulocytes was determined for each experiment on the day. The CXCL1 EC_{80} ranged from 2-10 nM and the CXCL8 EC_{80} ranged from 0.5-0.9 nM (Figure 5. 7). Titrations of P1156 (0.006 nM to 300 nM) was added to chemokines dosed at EC_{80} and incubated for 30 minutes at 37^{o}C before incubation with the cells. Next, the IC_{50} values were determined using an inhibitor response curve with a 4-parameter fit and displayed as a mean of three technical and biological repeats. P1156 IC_{5o} values against CXCL1 was 8.8E-09 M and CXCL8 was 1.8E-09 M (Figure 5. 8).

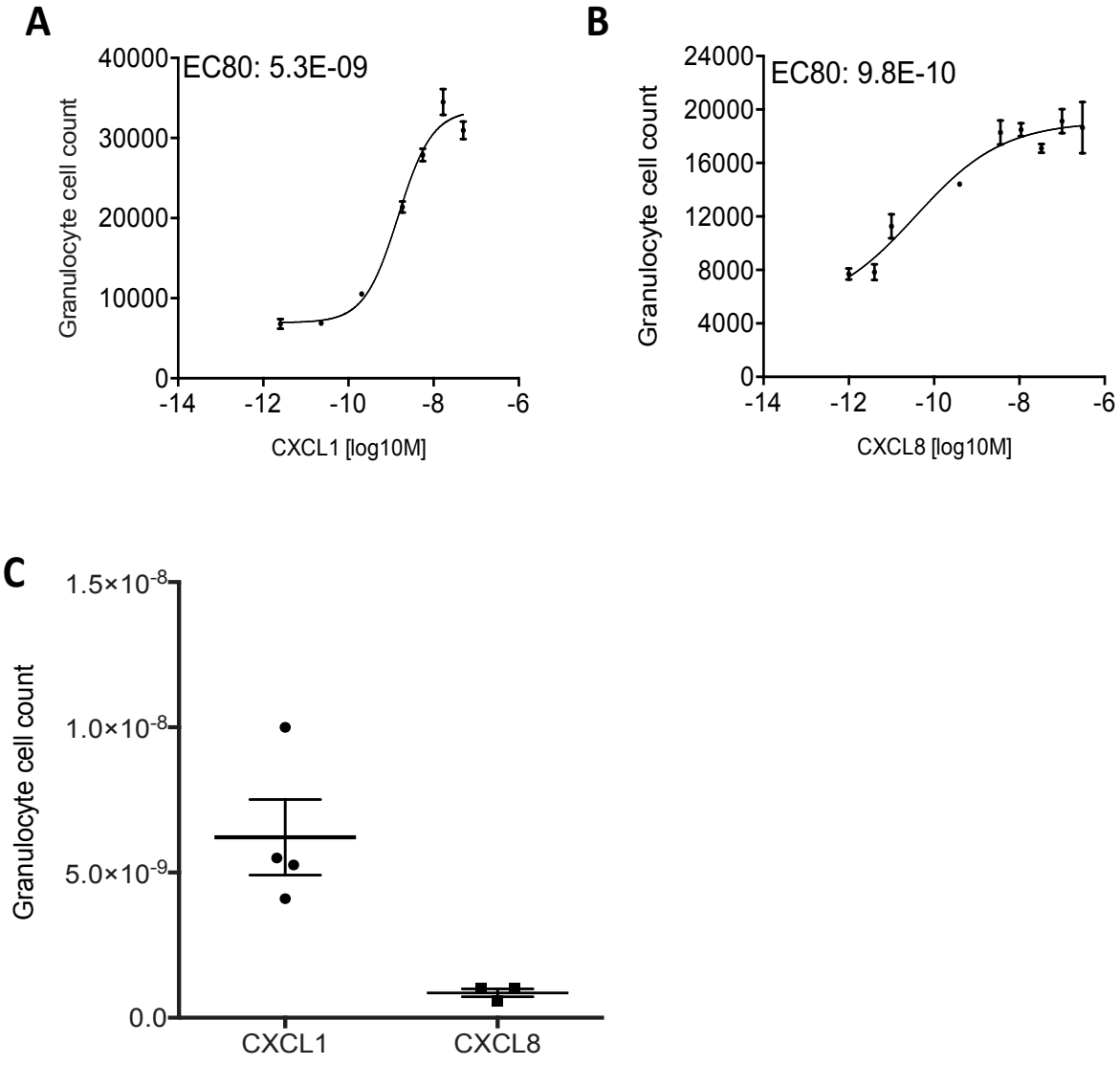


Figure 5. 7. Dose dependant migration of human granulocytes in response to CXCL1 and CXCL8. Human granulocytes were isolated from human whole blood and buffy coat by first depletion of red blood cells, using HetaSep, and lysis, using MACS red blood cell lysis solution. (A-B) Representative trace from single experiment showing human granulocytes migration in response to chemokines indicated. In each case, data from a representative experiment is shown mean ± s.e.m. of three technical replicates, y-axis shows cell count and x-axis shows concertation of chemokine (logarithmic scale, M(Log_{10}M)). EC_{80} (M) values for each chemokine, indicated, were estimated by fitting an agonist response curve with 4 parameters. (C) Summary EC_{80} data of the chemokines indicated (mean ± s.e.m., and individual data points from three biological replicates). Y-axis shows EC_{80} (logarithmic scale, M), and x-axis shows chemokine assayed.

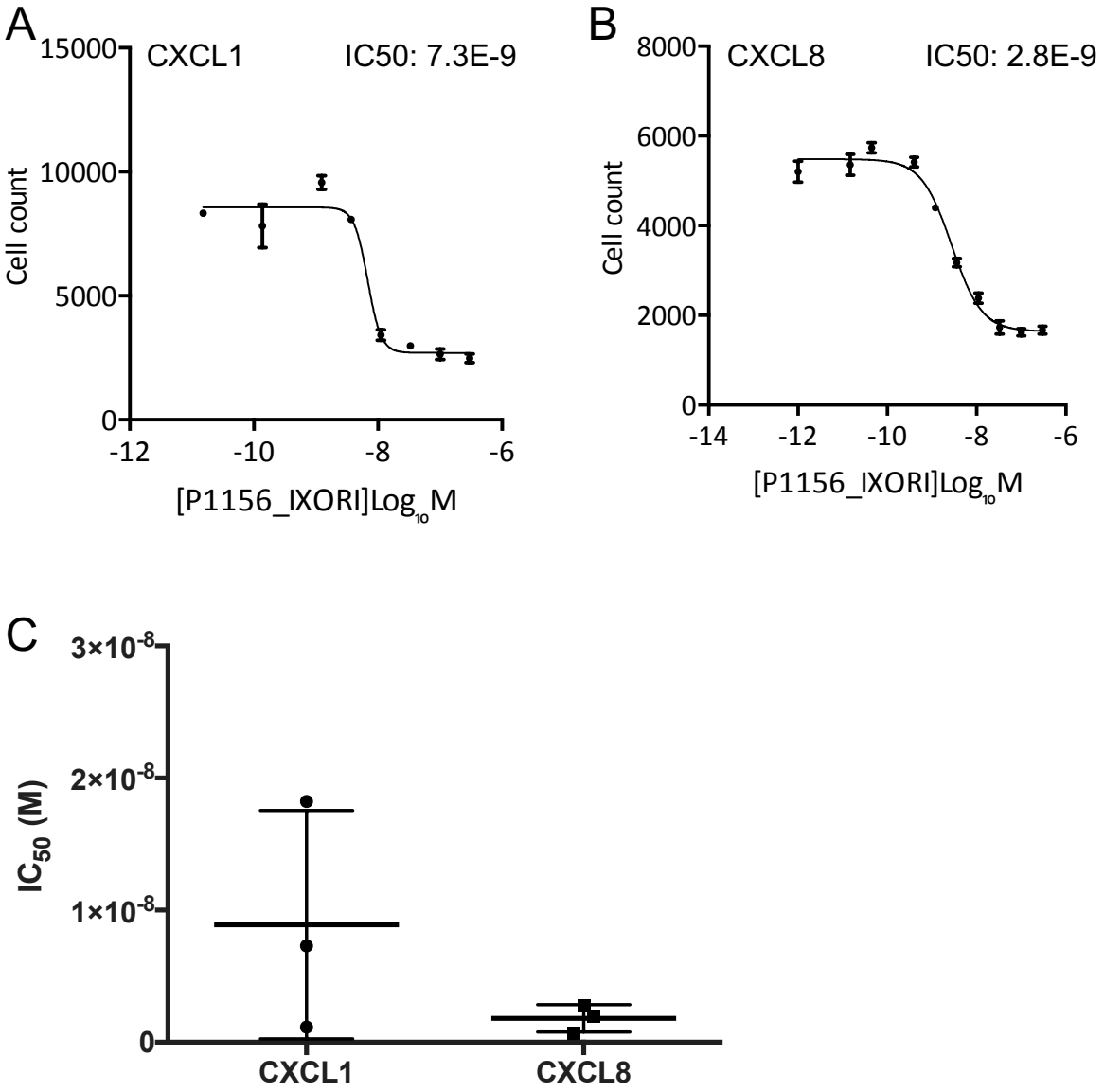


Figure 5. 8. Analysis of the neutralisation profile of P1156 against CXC chemokines. (A-B) Neutralisation of CXC chemokine driven chemotaxis of human granulocytes by P1156. Cell count of migrating granulocytes in response to chemokine EC_{80} indicated is shown on the y-axis and P1156 concentration ($Log_{10}M$) is shown on the x-axis. In each case, data from a representative experiment is shown mean ± s.e.m. of three technical replicates. IC_{50} (M) values for each chemokine, indicated, were estimated by fitting an agonist response curve with 4 parameters. (F) Summary P1156 IC_{50} data of the chemokines indicated (mean ± s.e.m., and individual data points from three biological replicates). Y-axis shows P1156 IC_{50} (logarithmic scale, M) assayed against indicated chemokine EC_{80}, shown on the x-axis.

5. 3. Discussion

Inflammatory diseases are characterised by the influx of immune cells, mediated by chemokines. Thus, chemokines have been investigated and validated as therapeutic targets in inflammatory disease (75). However, targeting chemokines has been challenging due the robustness of the chemokine network. Several clinical trials for antagonists to CXCR1/2 are currently ongoing, such as Schering–Plough's 'SCH527123' for COPD, currently in Phase II and Dompé's 'Reparixin' for reperfusion injury, also in phase II. Amgen, on the other hand, have failed on two separate trials with a CXCL8 neutralising antibody (215), highlighting single node targeting of the chemokine network does not yield promising results. Therefore, a multi-nodal approach is required in order to overcome the robustness of the chemokine network (2). Evasins can target multiple chemokines and neutralise their activity (174), thus overcoming the robustness of the chemokine network.

Chapter 3 highlighted CXC chemokine binding evasins exist in other tick species, and identified P1156 from the *Ixodes ricinus* tick, which bound CXCL8. Targeting CXCL8 is crucial for attenuating neutrophil chemotaxis, as CXCL8 is a potent neutrophil chemoattract (1, 283, 284). Thus, P1156 was chosen to be characterised in order to explore its CXC chemokine neutralising effects further. In this chapter, the functional properties of P1156 were examined in mammalian systems *in vitro*, and it was demonstrated that P1156 is a functionally active evasin that selectively binds and neutralises the activity of CXC chemokines.

P1156 is expressed as a heavily glycosylated protein

Considering all evasins, identified to-date, are relatively small proteins that are expressed as highly glycosylated proteins, it was encouraging to find P1156 also shares these similarities and was expressed as a heavily glycosylated protein. Glycosylated proteins have been

attributed to, as discussed in chapter 4, immune-evasion (253), reduced immunogenicity (174, 256, 257), protein stability (285) and do not appear to be required, by evasins, for chemokine recognition (200).

The treatment of purified P1156 protein with the de-glycosylating enzymes PNGaseF and EndoF1, resulted in a protein resolving on the SDS-PAGE at approximately 15 kDa. This finding suggested partial deglycosylation, which was expected since P1156 contains two O-linked and two N-linked glycosylation sites and the de-glycosylating enzymes used only targeted N-linked. Therefore, it was also not surprising that tandem mass spectrometry (MS/MS) yielded poor coverage of P1156's peptide sequence, only identifying one peptide sequence. Technically, glycoproteins need to have their glycans removed prior to MS/MS, as this can impact matching the fragmented peptide sequences during analysis, as both the protein sequence and the sugar carbohydrate structures (glycans) can fragment resulting in a spectrum of sequences that do not match the peptide sequence (286).

Despite this, the peptide recovered by MS/MS was correct, and the N- and C-terminus integrity of the protein were also validated using N-terminal sequencing and western blotting of the C-terminal histidine-tag. Surprisingly, resolving P1156 on an SDS-PAGE gel showed several low-molecular weight bands below the expected band showing P1156, which label positive for histidine (Figure 5. 3. C). Such findings are usually indicative of protein degradation (287), likely a result of protein handling or contaminating proteases, which may result in fragmented proteins. Although these bands were not explored further in this study, these low molecular weight bands could be investigated by resolving P1156 protein on SDS-PAGE gel, excising the bands and analysis using MS/MS.

P1156 selectively binds the ELR+ CXC chemokines

Similar to Evasin 3, P1156 showed no sequence homology to any of the published evasins that bind CC chemokines, nor did it bind any of the CC chemokines. Peptide sequence alignments showed P1156 shares 30% sequence homology with Evasin 3 (193), indicating it may behave in a similar way. Indeed, P1156 initially showed binding to CXCL8 during the YSD experiments of Chapter 3, and further confirmed in this chapter. Similar to Evasin 3 (193), P1156 binds six of the ELR+ CXC chemokines (84), and signal through the CXCR1 and/or CXCR2 receptors to recruit neutrophils (Figure 5. 1) (2).

More specifically, the bio-layer interferometry (BLI) assay showed P1156 has the highest affinity (K_d) for CXCL8 and CXCL1. Similarly, Deruaz *et al*., (193) reported that Evasin 3 having the highest affinity for CXCL1 and CXCL8, which was determined using Surface Plasma Resonance (SPR). Both SPR and BLI are used to determine the biochemical profile of proteins. BLI applies biosensors to sample and in SPR the sample is applied to the sensor. BLI is a more high-throughput protocol compared to SPR, as it allows the processing of up to 96 samples in parallel and allows the re-use of biosensors and samples. Furthermore, these features allow the same sample well, in this case, containing the evasin, to be assayed against multiple wells containing different chemokines. In addition to this, BLI, unlike SPR, does not have to compete with microfluidics, in which fluid and surface properties of the protein need to be considered (288). Therefore, opting to use BLI, the chemokine binding profile of Evasin 3 to CXC chemokines was examined to allow for a comparison with P1156 without the variability of methodology. Encouragingly, Evasin 3 bound the same chemokines as previously reported (192), however, the highest affinity observed was for CXCL6, closely followed by CXCL8 and CXCL1 (Appendix B. Figure B1).

Interestingly, anti-CXCL8 activity has previously been reported in the saliva extracts of a number of ticks, including *Amblyomma variegatum*, *Rhipicephalus appendiculatus* and

Dermatitis reticulatus ticks. These findings, combined with both Evasin 3 and P1156 also binding CXCL8, confirms anti-CXCL8 activity to be a common feature of *Metastriate Ixodidid* tick species and further encourages the importance of ticks controlling neutrophils to suppress inflammation during feeding (191).

Surprisingly, P1156 and Evasin 3, both bound all the CXCR2 ligands except CXCL7, despite its signalling resulting in the recruitment of neutrophils (2). Although, CXCL7 is only released from activated platelets (289), and tick saliva extracts have shown anti-coagulant effects, preventing platelet aggregation (290). Indeed, Chmelar *et al*., (291) showed tick salivary gland extracts from the *Ixodes ricinus* tick targets thrombin preventing platelet aggregation. Thus, without the platelets being present during tick feeding, CXCL7 is also not present. Subsequently, evasins injected into the hosts that target neutrophil recruitment will not need to target CXCL7, and will focus on the neutrophil recruiting chemokines, such as CXCL1, CXCL2, CXCL3, CXCL5, CXCL6 and CXCL8 (2). Considering ticks have been evolving from the Paleozoic to early Mesozoic eras (292), it is likely they have evolutionarily eliminated their CXCL7 binding abilities.

Furthermore, it comes as no surprise to observe that both P1156 and Evasin 3 are targeting the most potent CXC chemokines responsible for neutrophil recruitment; CXCL1 and CXCL8, with high affinity. Moreover, the similarity observed in binding profile between P1156 and Evasin 3 can be attributed to host association (292), in that both evasins are derived from ticks that feed on the same species (225, 227).

In order to further examine the binding of P1156 to chemokines, the length of time P1156 interacts with the chemokines it binds (the dissociation half-lives or target residence times (RT)) were considered. This chapter showed that the higher the affinity P1156 has for a chemokine, the longer it will bind to that chemokine (Figure 5. 6). Moreover, P1156 not only

has the highest affinities for CXCL1 and CXCL8 but it also interacts with them for the longest time, 33 and 39 minutes, respectively. However, the interaction of P1156 with the remaining chemokines only lasts for several minutes. This is likely a result of CXCL1 and CXCL8 being more potent neutrophil chemoattractants than the remaining neutrophil recruiting ligands (84, 284). On the other hand, Evasin 3 exhibited the longest interaction time with CXCL8, lasting 76 minutes, followed by CXCL6, which it interacted with for 24 minutes.

Furthermore, Evasin 3 also only interacts with the remaining chemokines for only a few minutes, including CXCL1 (Appendix B, Figure B1). These findings highlight the diverse preferences different tick species evasins have for targeting neutrophil recruitment. Neutrophils implication in driving the pathogenesis of diseases such as coronary heart disease (293), myocardial infarction (294), atherosclerosis (35), rheumatoid arthritis (295), inflammatory bowel disease (40) and pulmonary fibrosis (296) and psoriasis (46), suggests P1156 could be therapeutically examined in the clinical models of these diseases.

P1156 binds and neutralises CXC chemokine activity

In accordance with the high affinity binding observed by BLI, P1156 also neutralised the chemotactic activity of CXCL1 and CXCL8 against human granulocytes, *in vitro*, with IC_{50} values recorded in the nanomolar range. In fact, Déruaz *et al*., (193) reported Evasin 3 neutralising CXCL8-induced migration of neutrophils, *in vit*ro, with an IC_{50} of 3.35 nM. On the other hand, IC_{50} values of P1156 for CXCL8 is almost three times less, showing if administered therapeutically fewer doses of P1156 would be required in comparison to Evasin 3, although these findings will need to be examined *in vivo*.

Encouragingly, Evasin 3 has proven positively efficacious in a number of neutrophil-mediated animal models, including ischemic reperfusion injury (174), carotid atherosclerosis and

ischemic stroke (207), and acute pancreatitis (297). Therefore, as P1156 behaves in a similar way to Evasin 3, by binding and neutralizing the same chemokines, it will likely also exhibit similar therapeutic potential *in vivo* and should be investigated further.

In summary, the *Ixodes ricinus* derived evasin P1156 is a novel chemokine binding protein, capable of selective binding to six of the ELR+ CXC chemokines with high affinity. Furthermore, P1156 serves as a good candidate for acute responses, due its shorter dissociation times to the chemokines it binds to and it is functionally effective with IC_{50} values in the nanomolar region, further encouraging its potential as a strong therapeutic target. Although this chapter has validated P1156 as an evasin using *in vitro* assays, its effects *in vivo* will need to be examined. Encouragingly, this chapter has shown P1156 indeed binds CXCL8, with high affinity, as shown during the yeast surface display experiments of Chapter 3, thus validating the use of YSD to identify evasins.

Chapter 6.

Genetically Engineering the Two-Warhead Evasins

6.1. Introduction

6.1.1. Chemokines in inflammatory disease

Inflammatory diseases are characterised by an influx of immune cells, driven primarily by chemokines from multiple classes (75). For example, during cardiac dysfunction, or heart failure, increasing levels of CXCL8 (298), CCL2, and CXCL10 (299) are observed in the damaged myocardium. Furthermore, through the recruitment of immune cells during cardiac ischaemia, the following chemokines have been associated with tissue damage, CCL2 (244), CCL3 (245), CCL4 (245), CCL5 (243), CCL11 (53) and CXCL8 (298). In addition to this, a large number of chemokines have been implicated in the pathogenesis of atherosclerosis, such as CCL2 (300), CCL5 (300), CCL11 (143), CCL13 (300), CXCL8 (301), CXCL10 (147), CXCL12 (302). Moreover, chemokine driven damage in inflammatory disease is not limited to cardiac diseases, as the increased expression of both CC and CXC chemokines is also observed in other inflammatory diseases, such as rheumatoid arthritis (295, 303, 304), lung fibrosis (296, 305), asthma (43), psoriasis (203) and cancer (306).

6.1.2. Evasins

Evasins bind to multiple chemokines in a 'one-to-many' fashion, however they are selective in the class of chemokine they bind. For example, Evasin 1 (193), Evasin 4 (193), P991 (175) and P1243 (characterised in Chapter 4), all selectively bind CC chemokines. On the other hand, Evasin 3 (193) and P1156 (characterised in Chapter 5) selectively bind CXC chemokines. Collectively, these evasins, provide an opportunity, through combinatorial administration, to target inflammatory diseases where selective CC and CXC chemokines are expressed. For example, the administration of P1243 in combination with P1156 will target CCL3, CCL4, CCL5, CCL11 and CXCL8, the chemokines associated with tissue damage in cardiac ischaemia (53, 243, 245, 298).

However, in combinatorial therapeutic approaches the risks and benefits of each single agent and in combination needs to be evaluated (307). More specifically, each evasin will need to be examined for its effects as a single agent followed by its effects in combination with another evasin, thus presenting a lengthy and costly study. For this reason, this study sought to genetically engineer a single agent, capable of dual function, by fusing together two evasins and thus, creating a fusion-evasin, termed the 'two-warhead' evasin. Thus, the two-warhead evasin presents an opportunity to preferentially bind limited subsets of chemokines, from different classes, to provide precision targeting of multiple disease relevant chemokines without unnecessarily affecting other chemokines.

This chapter describes, for the first time, a genetically engineered novel evasin capable of targeting both CC and CXC chemokines at the same time, engineered through fusion of a CC chemokine binder, P1243, and a CXC chemokine binder, P1156. As proof of concept, a second set of two-warhead evasins, fusion of P991 and P1156, were also created and successfully expressed and characterised (Appendix E).

6.2. **Results**

The results described below refer to the two-warheads evasins: P1243:G4S:P1156 and P1156:G4S:P1243, and from henceforth will be referred to as the two-warhead evasins.

6.2.1. Sequence analysis of two-warhead evasins

To create the two-warhead evasins P1243 was fused to P1156 via a GGGS (G4S) linker, to create: P1243:G4S:P1156 and P1156:G4S:P1243 (Figure 6. 1). The resulting peptide is 183 amino acid residues long and has a predicted molecular weight of 20 kDa and a pI of 5.3.



Figure 6. 1. A schematic overview displaying the structure of the two-warhead Evasins expression constructs. P1243 and P1156 evasins are fused together using a GGGGS (G4S) linker. Each expression plasmid also has a StrepII:His (S2:HIS) tag.

6.2.2. Genetically engineering evasins to create a 'two-warhead' fusion

To create a two-warhead evasin, a two-step PCR (programme detailed in Table 2. 3) was performed to fuse P1243 and P1156. The first PCR step amplified the sequences of P1243 and P1156, followed by the second PCR step, which fused the two evasins together, creating the two-warhead fusion-protein sequence. A schematic showing the two-warhead cloning process is shown in Figure 6. 2.

The first PCR, which amplified P1243 and P1156, used specific primers that also incorporate overhangs that encode for the GGGGS (G4S) linker. This overhang is present in both sequences but in different orientations, for example, the P1243:G4S:P1156 plasmid required primers that amplified P1243 and P1156 sequences to create P1243:G4S and G4S:P1156, respectively. Whereas, for P1156:G4S:P1243, the primers were designed to encode for P1156:G4S and G4S:P1243. Thus, when the second PCR is performed, the two sequences fuse together, as the G4S sequence is complementary: P1243:G4S and G4S:P1156 overlap to create P1243:G4S:P1156, and P1156:G4S and G4S:P1243 overlap to create P1156:G4S:P1243 (Figure 6. 2).

For P1243:G4S:P1156 plasmid (plasmid ID: P1694), P1243 was amplified using primers 940 and 1054 (Table 6. 1), to create a PCR product with a size of 309 base-pairs (Figure 6. 3. A). P1156 was amplified using primers 1029 and 926 (Table 6. 1) to create a product with a size of 255 base-pairs (Figure 6. 3. B). The evasins were then fused together in the second PCR step using the primers 940 and 926 to create the fusion sequence, with a size of 549 base-pairs (Table 6. 1, Figure 6. 3. C).

For the P1156:G4S:P1243 plasmid (plasmid ID: P1709), P1156 was amplified using the primers 925 and 1074 (Table 6. 2), to create a PCR product with a size of 255 base-pairs (Figure 6. 4. A). P1243 was amplified using the primers 1075 and 941 (Table 6. 2) to create a PCR product with a size of 309 base-pairs (Figure 6. 4. A). The two amplified evasin sequences were then fused together in the second PCR step using the primers 925 and 1075, to create a PCR product with a size of 549 base-pairs (Table 6. 2, Figure 6. 4. B).

Fusion sequences were then transformed into pHLSec vectors using In-fusion cloning, following the manufacturer's instructions, and transformed into competent DH5α cells. Sequences were then confirmed using restriction enzyme digest the AgeI, showing vector at

1000 base-pairs and insert (fusion sequence) at 549 base-pairs (Figure 6. 3. D, Figure 6. 4. C) and sanger sequencing, confirming DNA sequences had no errors.

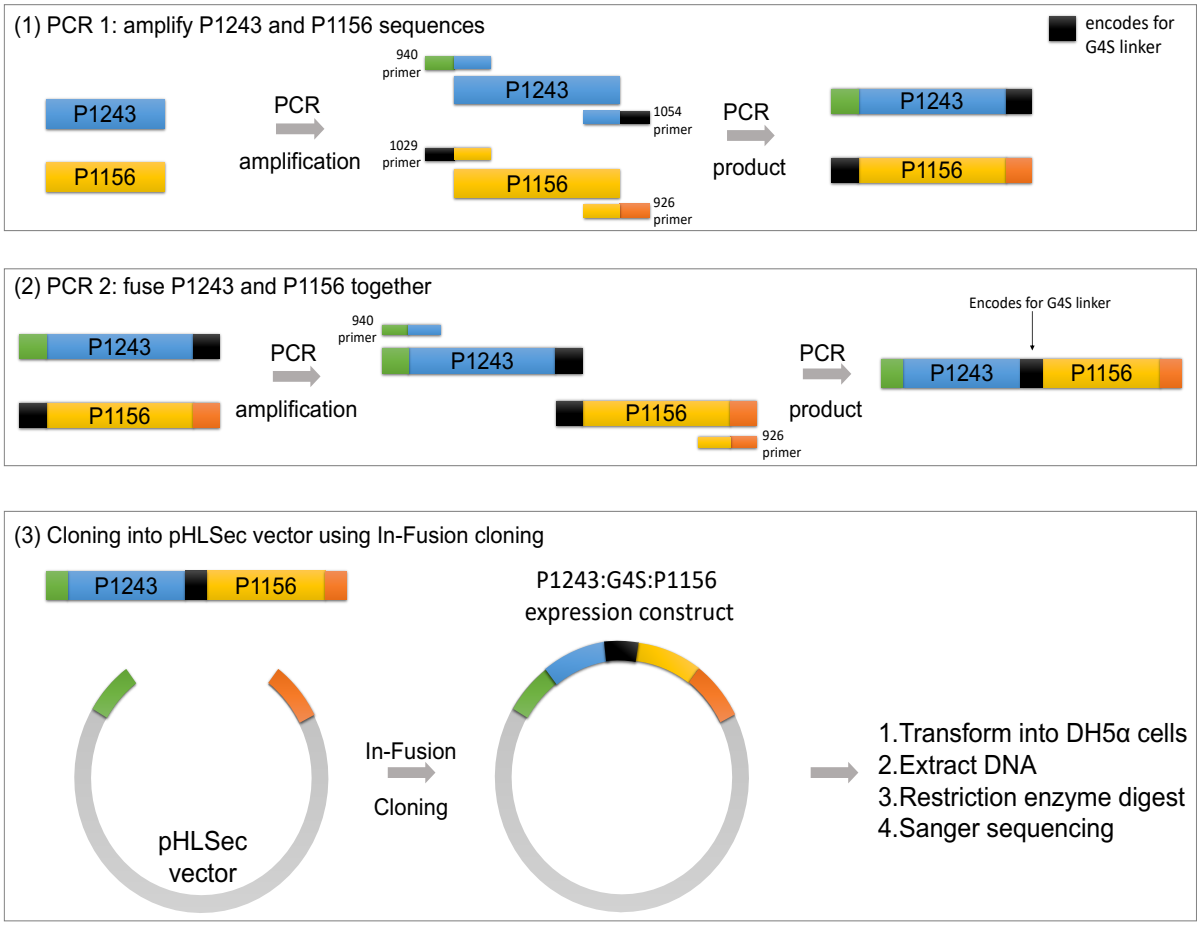


Figure 6. 2. Schematic overview of the steps taken to create the two-warhead evasins. This figure shows P1243:G4S:P1156 as an example, however the same process is applied to the creation of all two-warheads but with specific primers. The create the two-warhead evasins a two-step PCR process is performed. The first PCR (1) amplifies the sequences of P1243 and P1156 using specific primers (shown in Table). The reverse primer overhang of P1243 and forward primer overhand of P1156 are complementary and encode for the GGGGS (G_4S) linker. The second PCR (2) uses the forward primer for P1243 and the reverse primer for P1156 in PCR 1 (1) to fuse together P1243:G4S and G4S:P1156 to create P1243:G4S:P1156. At the end of each PCR stage the PCR products are confirmed by resolving on agarose gel. The third step is cloning the fusion sequence into pHLSec vector using In-Fusion cloning, following the manufacturer's instructions. Once complete plasmid is transformed into DH5α cells, DNA is then extracted, digested using the restriction enzyme AgeI and sequenced to confirm validity.

Sequence amplified	Primer	Primer ID	Primer sequence	Product size (base-pairs)
P1243:G4S	Forward Reverse	940 1054	cgtagctgaaaccggtCGCAATCATACGGAAGATAATTCTACTGAA agagcctcctccaccAGGTGTCTTGAAGCATTGCTCC	309
G4S:P1156	Forward Reverse	1029 926	ggtggaggaggctctGCAGATGACGATAACGAACTCTTTACTGT ctcctccgccaccggtATGAGATAATGTGTCTGAGCGCTTTG	255
P1234:G4S:P1156	Forward Reverse	940 926	cgtagctgaaaccggtCGCAATCATACGGAAGATAATTCTACTGAA ctcctccgccaccggtATGAGATAATGTGTCTGAGCGCTTTG	549

Table 6. 1. PCR primer sets for the two-warhead evasin: P1243:G4S:P1156. Primer sequence complementary to the template DNA is shown in upper-case and overhangs are shown in lower case. Overhangs encoding the GGGGS (G4S) linker are shown in red.

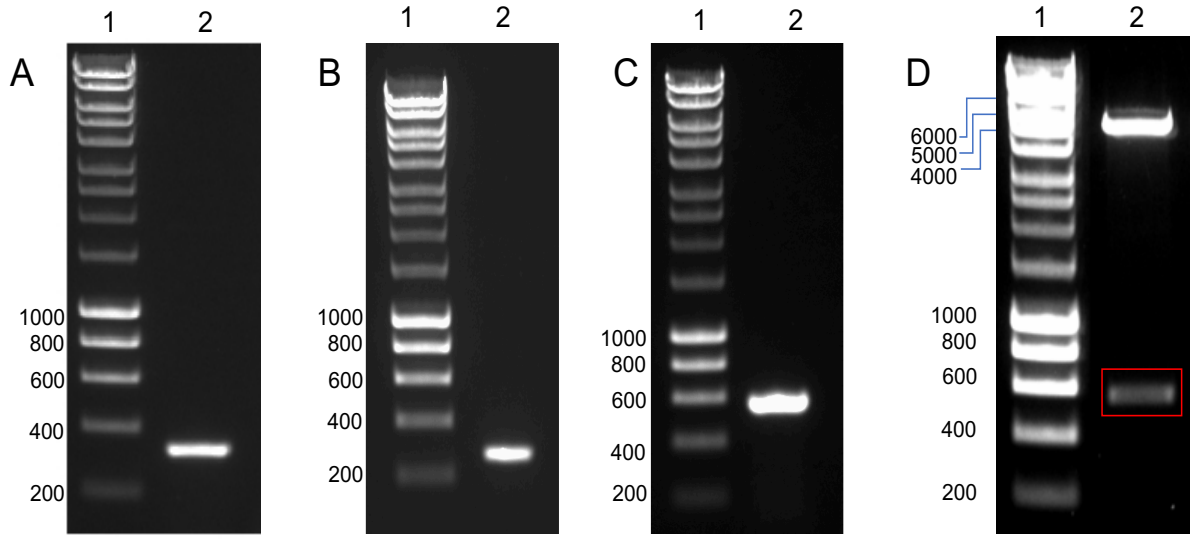


Figure 6. 3. Gel electrophoresis of the steps to create the two-warhead evasin: P1243:G4S:P1156. Lane 1, in each case, shows 1 kilo-base-pair ladder and lane 2 shows DNA. (A) PCR 1: amplification of P1243, expected band size 309 base-pairs (lane 2). (B) PCR 1: amplification of P1156, expected band size 255 base-pairs (lane 2). (C) PCR fusion of P1243 and P1156 to create P1243:G4S:P1156, expected band size is 549 base-pairs. (D) AgeI restriction enzyme digest of P1243:G4S:P1156 DNA plasmid showing vector at 4698 base-pairs and insert (P1243:G4S:P1156) at 549 base-pairs (lane 2, red box).

Sequence amplified	Primer	Primer ID	Primer sequence	Product size (base-pairs)
P1156:G4S	Forward	925	cgtagctgaaaccggtGCAGATGACGATAACGAACTCTTTACTGT	255
	Reverse	1074	agagcctcctccaccATGAGATAATGTGTCTGAGCGCTTTG	
G4S:P1243	Forward	1075	ggtggaggaggctctCGCAATCATACGGAAGATAATTCTACTGAA	309
	Reverse	941	ctcctccgccaccggtAGGTGTCTTGAAGCATTGCTCC	
P1156:G4S:P1243	Forward	925	cgtagctgaaaccggtGCAGATGACGATAACGAACTCTTTACTGT	549
	Reverse	941	ctcctccgccaccggtAGGTGTCTTGAAGCATTGCTCC	

Table 6. 2. PCR primer sets for the two-warhead evasin: P1156:G4S:P1243. Primer sequence complementary to the template DNA is shown in upper-case and overhangs are shown in lower case. Overhangs encoding the GGGGS (G4S) linker are shown in red.

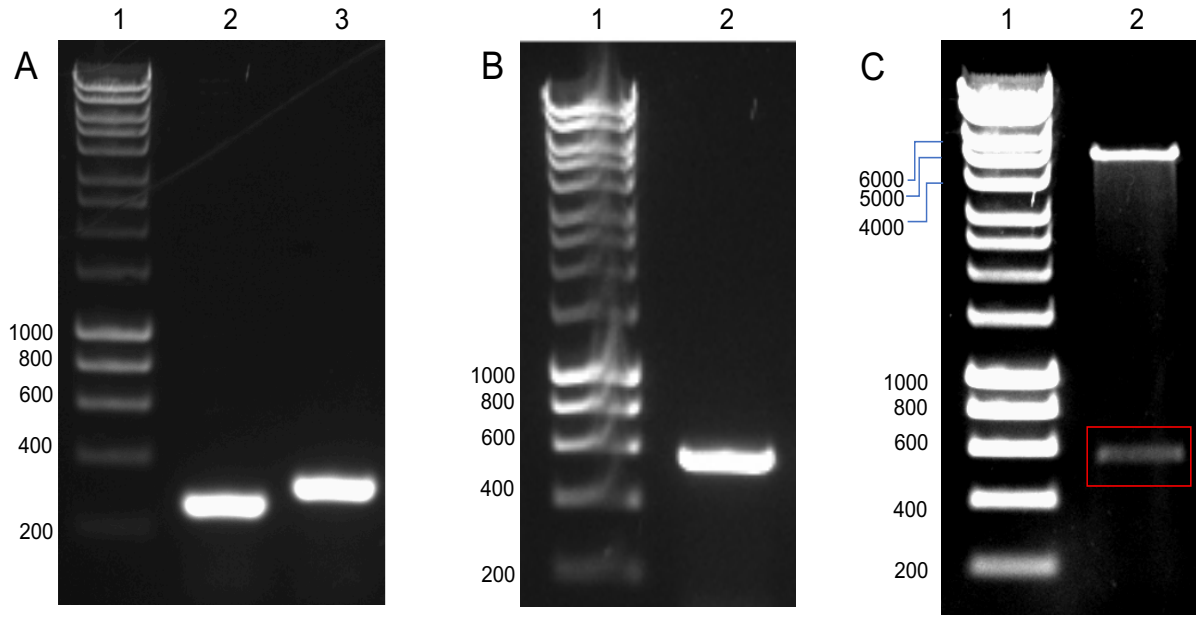


Figure 6. 4. Gel electrophoresis of the steps to create the two-warhead evasin: P1156:G4S:P1243. Lane 1, in each case, shows 1 kilo-base-pair ladder and lane 2 and 3 shows DNA. (A) PCR 1: amplification of P1156 (255 base-pairs, lane 2) and P1243 (309 base-pairs, lane 3). (B) PCR fusion of P1156 and P1243 to create P1156:G4S:P1243, expected band size is 549 base-pairs. (C) AgeI restriction enzyme digest of P1156:G4S:P1243 DNA plasmid showing vector at 4698 base-pairs and insert (P1156:G4S:P1243) at 549 base-pairs (lane 2, red box).

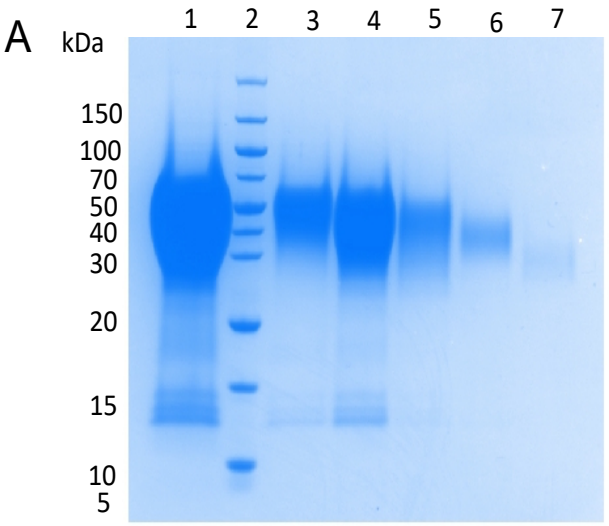
6.2.3. Two-warhead evasins are expressed as highly glycosylated proteins

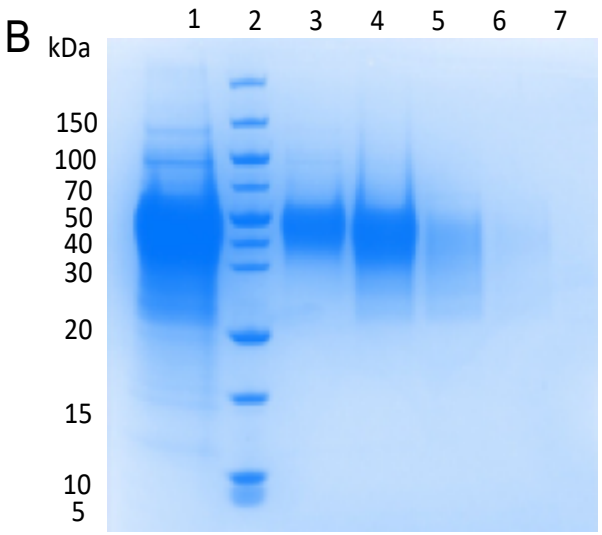
The two-warhead evasins, P1243:G4S:P1156 and P1156:G4S:P1243, were expressed as secreted proteins, using the mammalian HEK293F cells and purified using nickel affinity (Ni-NTA) chromatography and size exclusion chromatography (SEC). All elutions were then analysed on SDS-PAGE gel and all fractions containing protein of interest were pooled and concentrated.

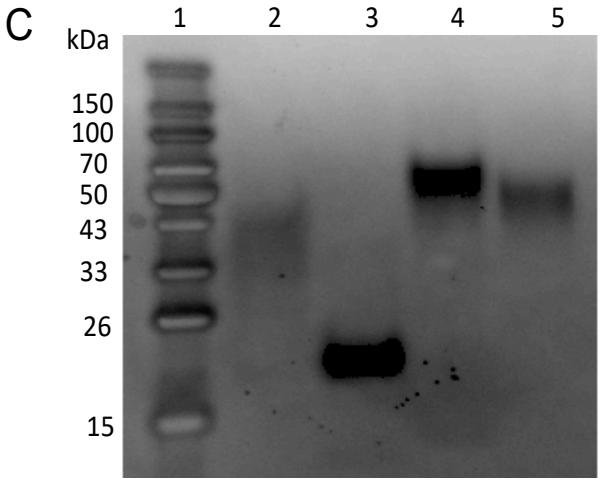
SDS-PAGE analysis showed that the two-warhead evasins migrate at a higher molecular weight than predicted, between 30-60 kDa (Figure 6. 5. A, B). Additionally, N-terminal sequencing identified the first 5 residues of the P1243:G4S:P1156 and P1156:G4S:P1243 two-warhead evasins, confirming the N-terminus of each is intact (Figure 6. 5. D).

To confirm the C-terminal integrity of the protein, proteins were labelled with anti-histidine and confirmed using western blotting. Immunoblots showed glycosylated P1243:G4S:P1156, and deglycosylated P1156:G4S:P1243 could also be detected readily. Deglycosylated P1243:G4S:P1156 and glycosylated P1156:G4S:P1243 could not be detected in this experiment (Appendix D, Figure D1). Glycosylated P1243:G4S:P1156 and P1156:G4S:P1243, alongside their parental evasins P1243 and P1156, were labelled with NiNTA-Atto550 and all evasins could be detected, thus indicating an intact C-terminus (Figure 6. 5. C).

Using tandem mass spectroscopy (MS/MS), the protein sequence of the two-warheads, in both orientations, was analysed. This required producing deglycosylated forms of both proteins. MS/MS analysis showed good coverage of both two-warheads, including coverage of the G4S linkers and adjacent amino acids, confirming correct orientation of both two-warheads (Figure 6. 6. B, Figure 6. 7. B).







D

Protein sequence report

Alta Bioscience code: S7044
Customer sample code: P1694

N terminus

Residue		Minor	
1	-	e	
2	E	t	
3	T	g	
4	G	r	
5	R	-	

Protein sequence report

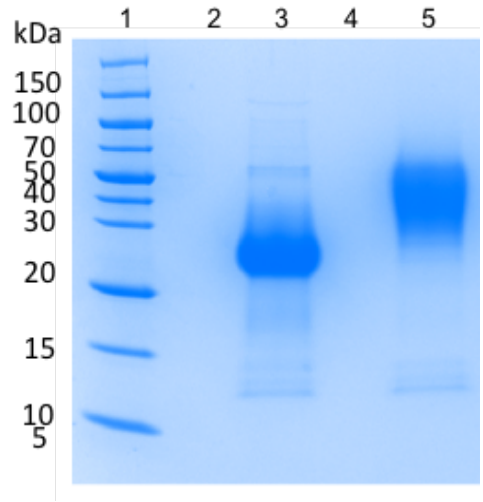
Alta Bioscience code: S7045
Customer sample code: P1709

N terminus

Residue			
1	E		
2	T		
3	G		
4	A		
5	D		

Figure 6. 5. Protein purification and characterisation of the two-warhead evasins. (A-B) Colloidal Coomassie stained SDS-PAGE gel showing P1243:G4S:P1156 (A) and P1156:G4S:P1243 (B) protein fractions following nickel affinity chromatography (Ni-NTA). Lane 2 shows protein ladder, lane 1 shows concentrated Ni-NTA-purified protein and lanes 3-7 show protein purified by size exclusion chromatography. (C) In-gel staining using Ni-NTA-Atto550 of P1243 (lane 2), P1156 (lane 3), P1243:G4S:P1156 (lane 4) and P1156:G4 S:P1243 (lane 5). Lane 1 shows protein ladder. (D) N-terminal sequencing of P1243:G4S:P1156 (P1694) and P1156:G4S:P1243 (P1709) (AltaBioscience, Redditch, UK).

A



B

MATRIX SCIENCE **MASCOT Search Results**

Protein View: P1243-G4S-P1156

P1243-G4S-P1156

Database:	Evasins
Score:	353
Nominal mass (M_r):	24700
Calculated pI:	5.93

Sequence similarity is available as an NCBI BLAST search of P1243-G4S-P1156 against nr.

Search parameters

Enzyme:	Trypsin: cuts C-term side of KR unless next residue is P.
Fixed modifications:	Carbamidomethyl (C)
Variable modifications:	Oxidation (M)

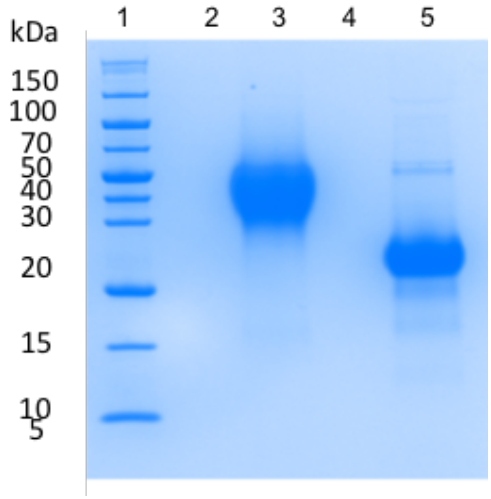
Protein sequence coverage: 47%

Matched peptides shown in ***bold red***.

```
  1 ETGRNHTEDN STEYYDYEEA RCACPARHLN NTNGTVLKLL GCHYFCNGTL
 51 CTAPDGYPCY NLTAQQVRTL TTYPNTSCAV GVCMKGTCVK NGTMEQCFKT
101 PGGGGSADDD NELFTVQYCG MNCTKDEGGT WTGCTGKKEG CKCYHESGKN
151 YGLCLSTEYT DFSQYGNPSD SEIEAAKPKR SDTLSHTGGG GGSGGGGSGG
201 ASAWSHPQFE KLEHHHHHHH H
```

Figure 6. 6. Characterising the peptide sequence of the two-warhead evasin P1243:G4S:P1156. (A) Colloidal Coomassie stained SDS-PAGE stained gel showing deglycosylated P1243:G4S:P1156 (lane 3), glycosylated P1243:G4S:P1156 (lane 5). Lane 1 shows protein ladder, lanes 2 and 4 are empty. For deglycosylation, two-warhead evasins were treated with PNGaseF and EndoF1. (B) MS/MS analysis of deglycosylated two-warhead evasin: P1243:G4S:P1156. Images are cropped to show recovered peptides in red. Uncropped images shown in Appendix D, Figure D2).

A



B

MATRIX SCIENCE **MASCOT Search Results**

Protein View: P1156-G4S-P1243

P1156-G4S-P1243

Database:	Evasins
Score:	403
Nominal mass (M_r):	24700
Calculated pI:	5.93

Sequence similarity is available as an NCBI BLAST search of P1156-G4S-P1243 against nr.

Search parameters

Enzyme:	Trypsin: cuts C-term side of KR unless next residue is P.
Fixed modifications:	Carbamidomethyl (C)
Variable modifications:	Oxidation (M)

Protein sequence coverage: 45%

Matched peptides shown in ***bold red***.

```
  1 ETGADDDNEL FTVQYCGMNC TKDEGGTWTG CTGKKEGCKC YHESGKNYGL
 51 CLSTEYTDFS QYGNPSDSEI EAAKPKRSDT LSHGGGGSRN HTEDNSTEYY
101 DYEEARCACP ARHLNNTNGT VLKLLGCHYF CNGTLCTAPD GYPCYNLTAQ
151 QVRTLTTYPN TSCAVGVCMK GTCVKNGTME QCFKTPTGGG GGSGGGGSGG
201 ASAWSHPQFE KLEHHHHHHH H
```

Figure 6. 7. Characterising the peptide sequence of the two-warhead evasin P1156:G4S:P1243. (A) Colloidal Coomassie stained SDS-PAGE stained gel showing deglycosylated P1156:G4S:P1243 (lane 3), glycosylated P1156:G4S:P1243 (lane 5). Lane 1 shows protein ladder, lanes 2 and 4 are empty. For deglycosylation, two-warhead evasins were treated with PNGaseF and EndoF1. (B) MS/MS analysis of deglycosylated two-warhead evasin: P1156:G4S:P1243. Images are cropped to show recovered peptides in red. Uncropped images shown in Appendix D, Figure D2).

6.2.4. Analysis of the biochemical profile of two-warhead evasins show they bind both CC and CXC chemokines with high affinity

The binding profile of the two-warhead evasins were examined using bio-layer interferometry (BLI). This was initially carried out to determine their interaction and binding affinities. Initial binding assays showed that the two-warhead evasins bound an array of both CC and CXC chemokines. Furthermore, binding affinity (K_d) studies showed that the two-warhead evasins only bound certain CC (Figure 6. 8) and CXC chemokines (Figure 6. 9).

P1243:G4S:P1156 initially showed binding to CXCL4, CXCL7, CXCL12, CXCL13 and CXCL14, however a K_d, which was calculated using 5 different ligand concentrations, could not be determined as binding was only observed at 100 nM, and not the lower concentrations (Appendix F, Figure F1). Thus, these were interpreted as low-affinity binders and not investigated further.

The two-warhead evasins bound the majority of the chemokines their parental evasins bound, with similar affinities. However, binding affinities of the two-warhead evasins could not be determined for CCL1, CCL7, CCL22, CXCL3, CXCL5 and CXCL6, despite binding to the parental evasins, which is discussed further in this chapter (Figure 6. 8, Figure 6. 9).

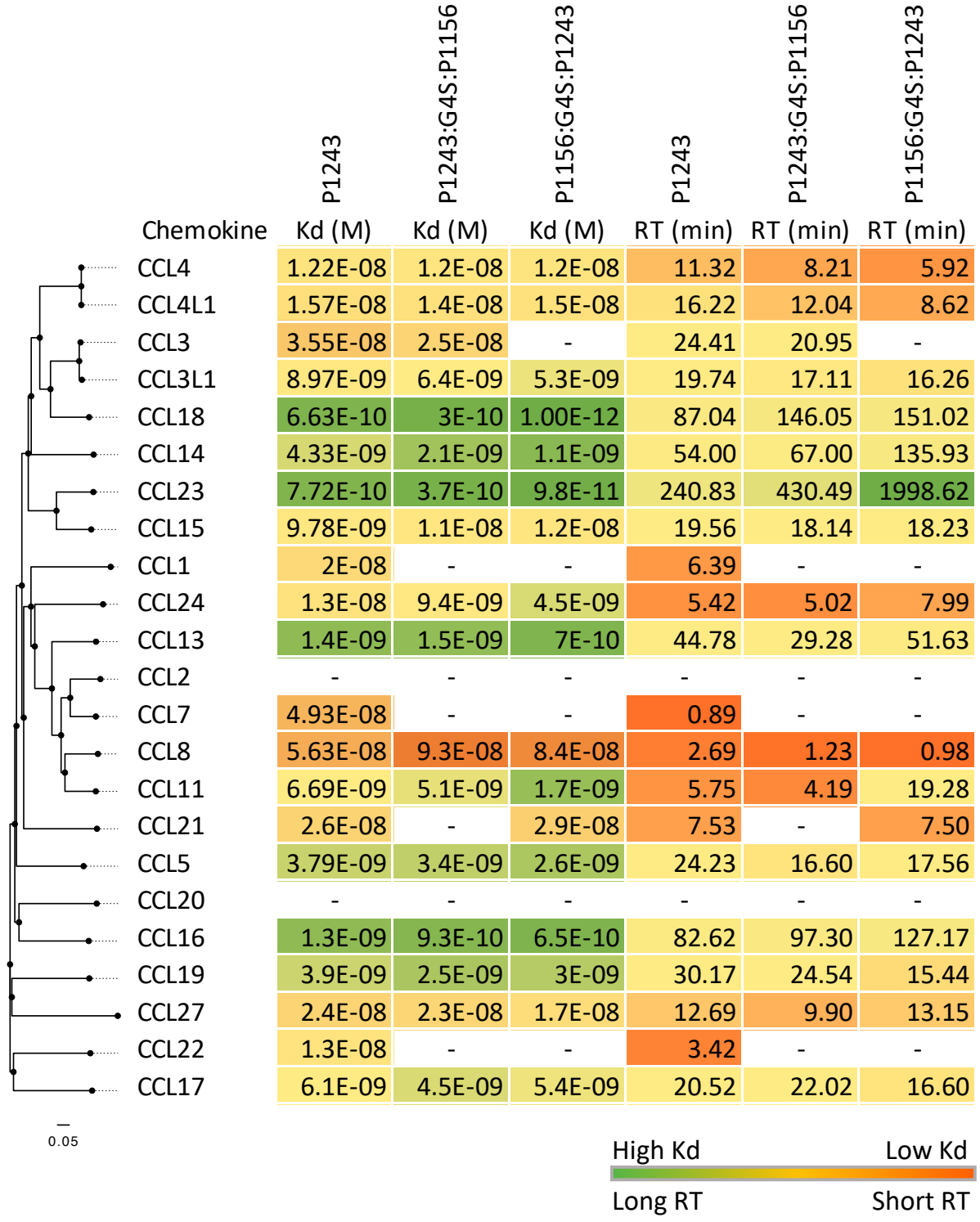


Figure 6. 8. Biochemical profile showing CC chemokine binding to single and two-warhead evasins: P1243:G4S:P1156 and P1156:G4S:P1243. Binding affinities (K_d, M) and target residence times (RT, minutes) were determined once using bio-layer interferometry (BLI). Colour gradient indicates high or long (green) to low or short (red) Kd or RT, respectively. Colour gradient established from data in figure. A dash (-) indicates either data could not be fitted, or binding could not be detected.

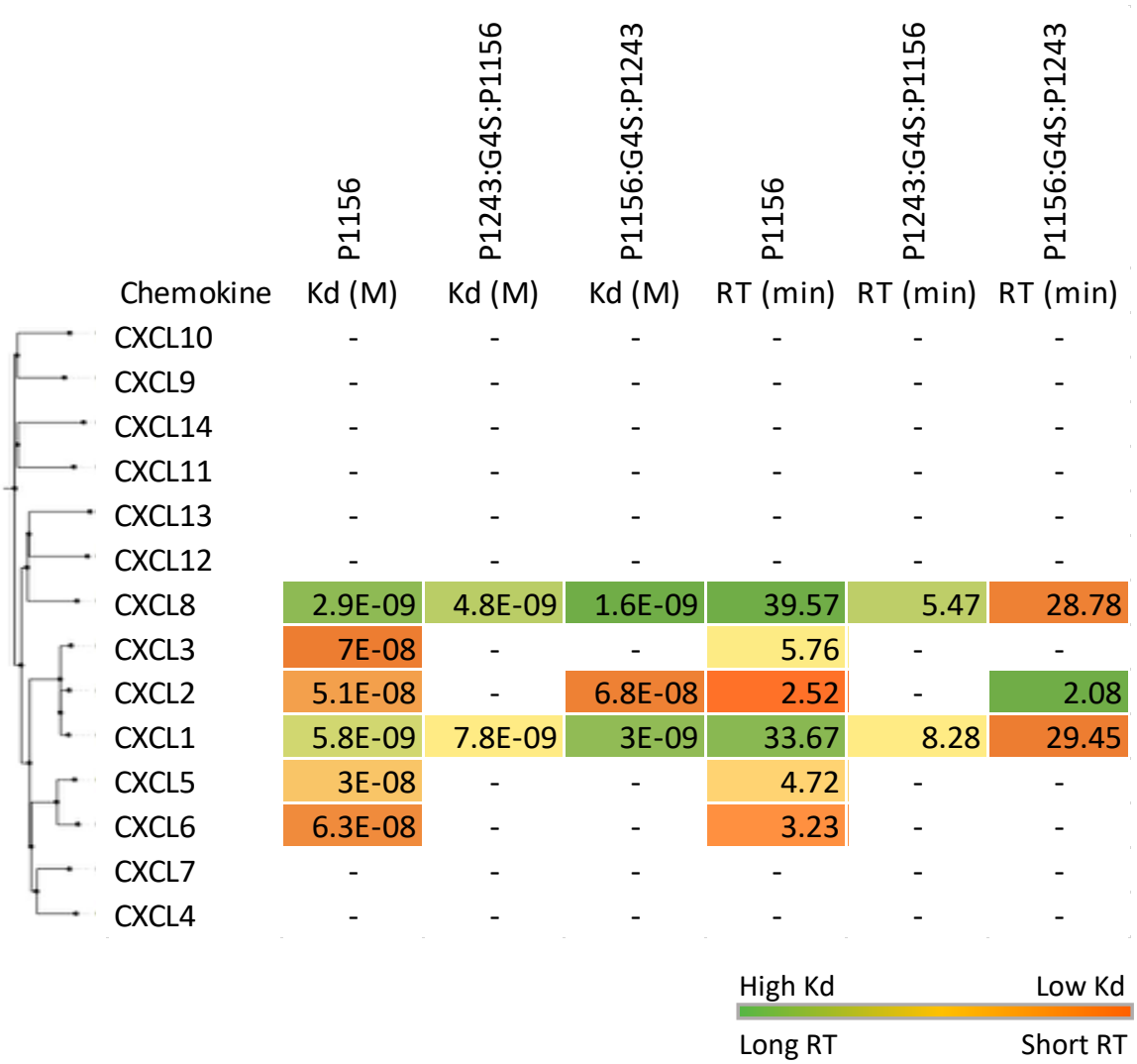


Figure 6. 9. Biochemical profile showing CXC chemokine binding to single and two-warhead evasins: P1243:G4S:P1156 and P1156:G4S:P1243. Binding affinities (K_d, M) and target residence times (RT, minutes) were determined once using bio-layer interferometry (BLI). Colour gradient indicates high or long (green) to low or short (red) Kd or RT, respectively. Colour gradient established from data in figure. A dash (-) indicates either data could not be fitted, or binding could not be detected.

6.2.5. Two-warhead evasins simultaneously bind CC and CXC chemokines

To examine polyvalent binding of chemokines by the two-warheads evasins, the BLI assay was used. The two-warhead evasins were first associated with either CCL3, CCL5, CXCL1 or CXCL8, followed by a second association with either CCL3, CCL5, CXCL1 or CXCL8, followed by dissociation. When the two-warheads evasins bound either CCL3 or CCL5 they could then bind CXCL1 or CXCL8 but not CCL3 or CCL5. On the other hand, the two-warhead evasin associated with CXCL1 or CXCL8 could associate again with CCL3 or CCL5 but not CXCL1 or CXCL8.

This data shows that when the two-warheads evasins are bound to a CC chemokine they can then go on to bind a CXC chemokine but not a second CC chemokine, as all the CC binding sites attributed to P1243 are saturated. Similarly, when the two-warhead evasin is bound to a CXC chemokine it can then bind a CC chemokine but not second CXC chemokine as all the CXC chemokine binding sites attributed to P1156 are saturated. An overview, summarising the data showing CCL5 association, followed by CXCL1, CXCL8 or CCL3 for both two-warheads is shown in Figure 6. 10.

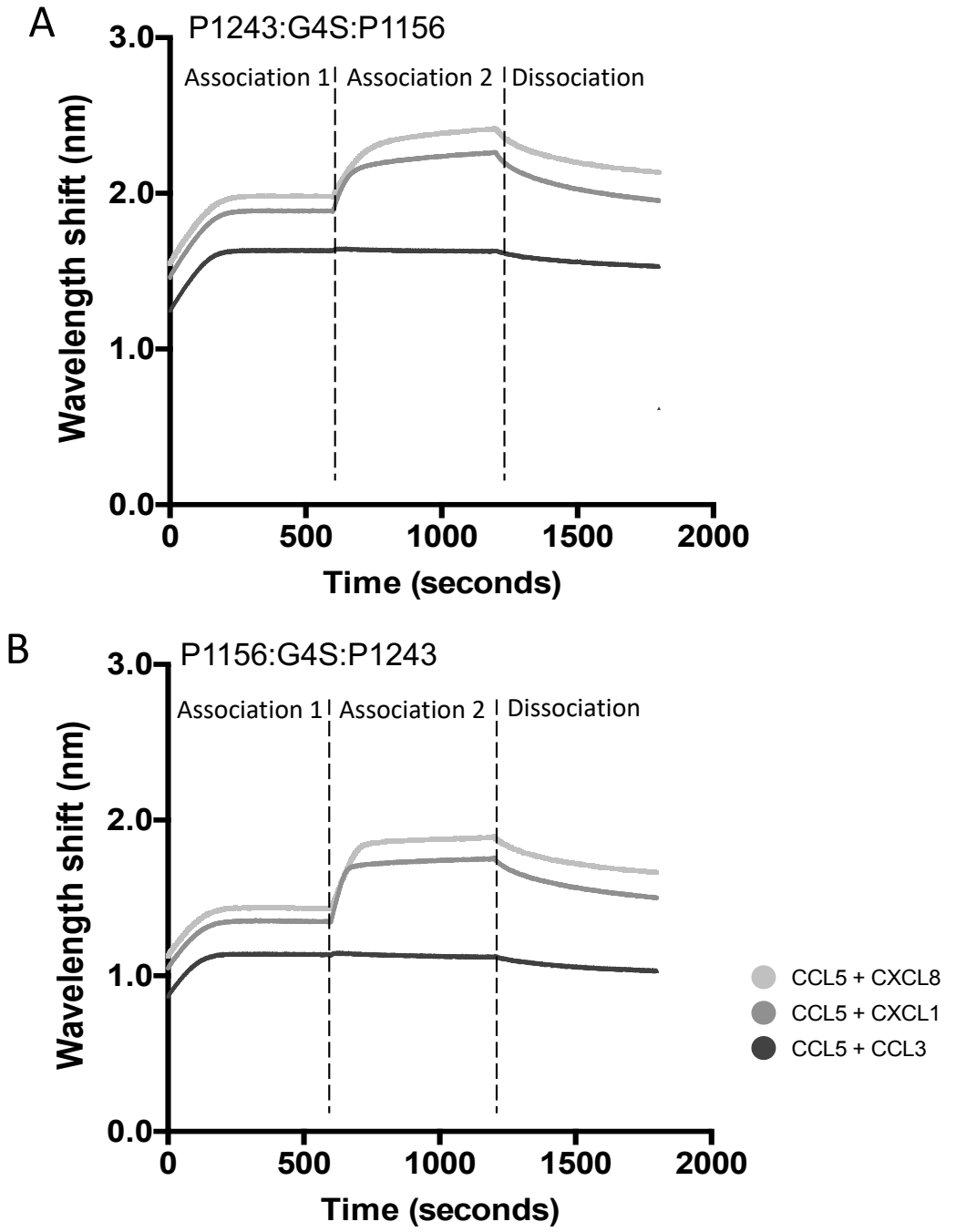


Figure 6. 10. Polyvalent binding of two-warhead evasins P1243:G4S:P1156 and P1156:G4S:P1243 to human CC and CXC chemokines, determined using bio-layer interferometry. Two-warhead evasins were first immobilized onto nickel-coated sensors, associated with human CCL5 (association 1), followed by an association with CCL5 in addition to CXCL8 (light grey trace), CXCL1 (dark grey trace) or CCL3 (black trace) (association 2), and then dissociated in buffer (dissociation).

6.2.6. Two-warhead evasins neutralise CC chemokine activity *in vitro*

To examine the effects of the two-warhead evasins on CC chemokine induced migration, THP-1 cells were used in the 96-well Boyden chamber assays. IC_{50} values of each two-warhead were established by titrating increasing doses of the two-warhead evasin against the EC_{80} dose of each chemokine assayed. The EC_{80} values of each chemokine was determined previously (Chapter 4). The IC_{50} values were then determined as an average of three technical and biological triplicates. IC_{50} values for P1243:G4S:P1156 and P1156:G4S:P1243 against human CCL3 where, 1.2E-8 M, and 8.8E-9 M, respectively, against CCL3L1 they were 1.7E-9 M, and 2.2E-9M, respectively, and against CCL5 they were 7.4E-9 M and 1.2E-8 M, respectively (Figure 6. 11).

6.2.7. Two-warhead evasins neutralise CXC chemokine activity *in vitro*

To examine the effects of the two-warhead evasins on CXC chemokine induced migration, human granulocytes were used in the 96-well Boyden chamber assays. IC_{50} values of each two-warhead evasin were established by titrating increasing doses of the two-warhead evasin against the EC_{80} dose of each chemokine assayed. The EC_{80} values of each chemokine was determined on the day of experiment (Chapter 5, Figure 5. 6). IC_{50} values were determined as an average of three technical and four biological triplicates. IC_{50} values for P1243:G4S:P1156 and P1156:G4S:P1243 against human CXCL1 were determined as 3.4E-08 M and 1.5E-08 M respectively, and against CXCL8 were 3.8E-8 M and 7.5E-9 M, respectively (Figure 6. 12).

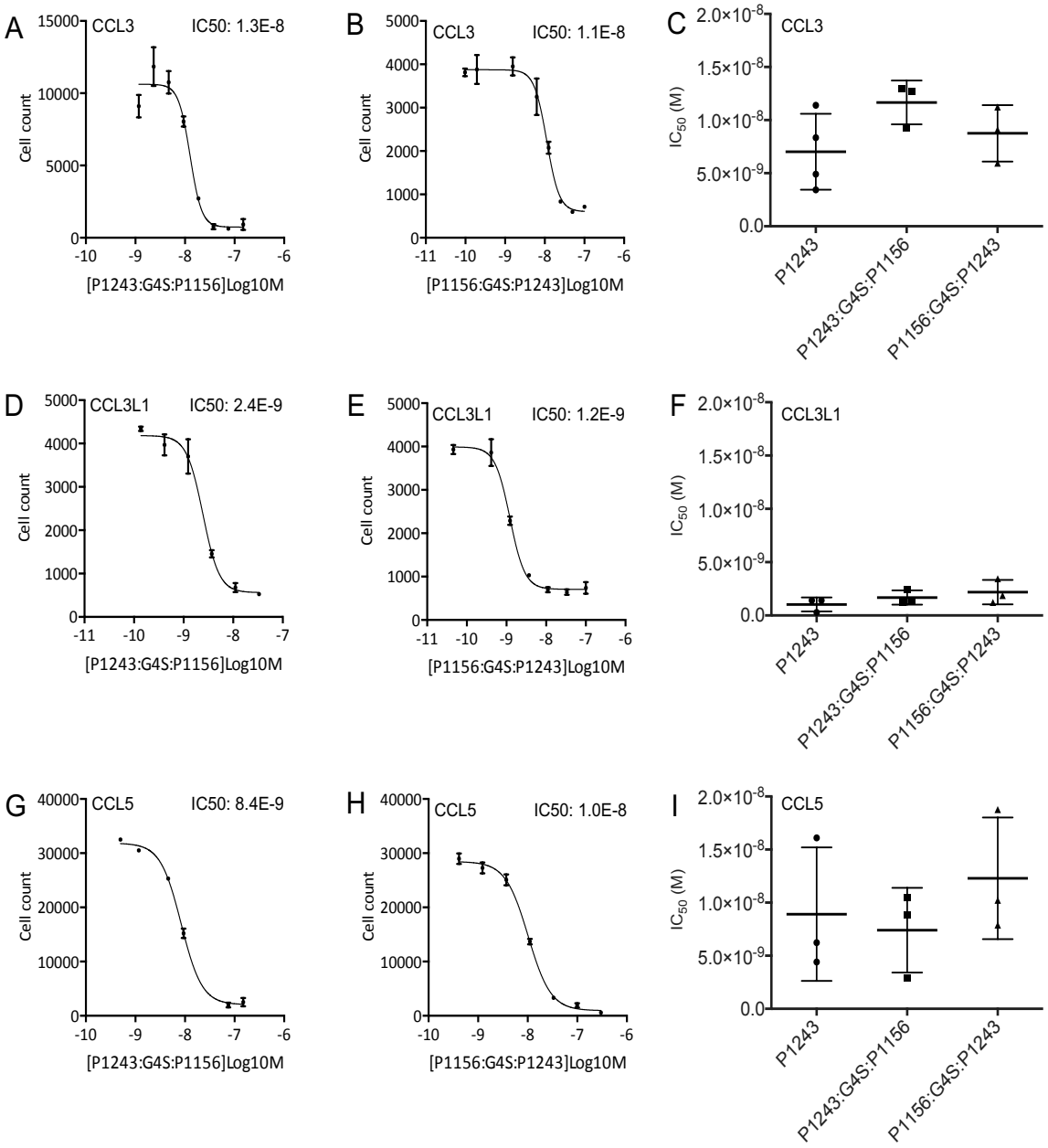


Figure 6. 11. Neutralisation of CC chemokine induced cell migration by two-warhead evasins. (A, B, D, E, G, H) Neutralisation of CC chemokine driven chemotaxis of THP-1 cells by P1243:G4S:P1156 (A, D, G) and P1156:G4S:P1243 (B, E, H). Cell count of migrating THP-1 cells (in response to chemokine EC_{80} indicated) is shown on the y-axis and evasin concentration ($Log_{10}M$) is shown on the x-axis. In each case, data from a representative experiment is shown mean ± s.e.m. of three technical replicates. IC_{50} (M) values for each chemokine, indicated, were estimated by fitting an agonist response curve with 4 parameters. (C, F, I) Summary IC_{50} data of P1243 and two-warhead evasins neutralisation of the chemokines indicated. Data show as mean ± s.e.m., and individual data points from three biological replicates. Y-axis shows IC_{50} (logarithmic scale, M), assayed against indicated chemokine EC80, and x-axis shows each CKBP.

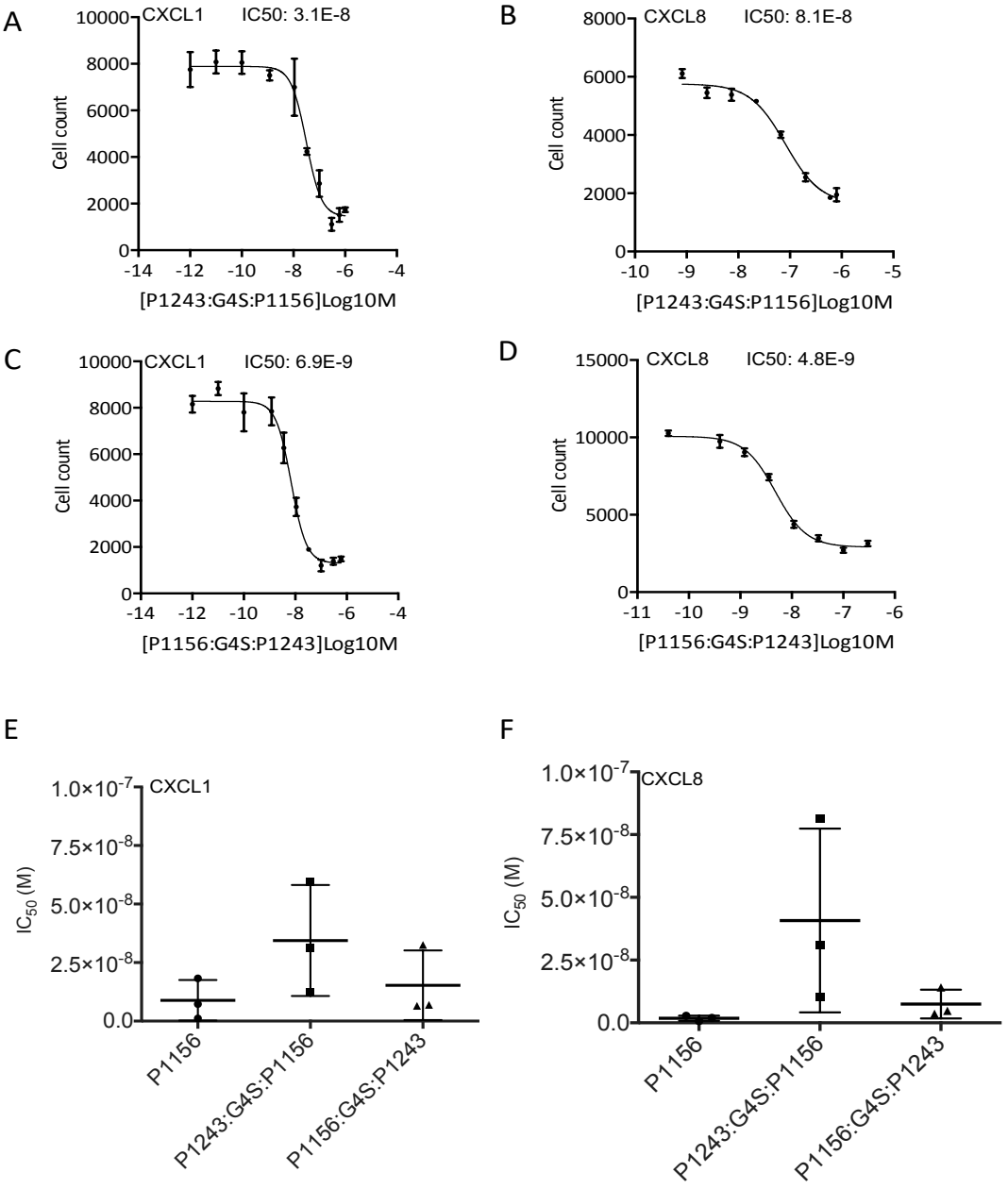


Figure 6. 12. Neutralisation of CXC chemokine induced cell migration by two-warhead evasins. Human granulocytes were isolated from human whole blood and buffy coat by first depletion of red blood cells, using HetaSep, and lysis, using MACS red blood cell lysis solution. (A-D) Neutralisation of CXC chemokine driven chemotaxis of human granulocytes by P1243:G4S:P1156 (A,B) and P1156:G4S:P1243 (C,D). Cell count of migrating granulocytes in response to chemokine EC_{80} indicated is shown on the y-axis and evasin concentration ($Log_{10}M$) is shown on the x-axis. In each case, data from a representative experiment is shown mean ± s.e.m. of three technical replicates. IC_{50} (M) values for each chemokine, indicated, were estimated by fitting an agonist response curve with 4 parameters. (E,F) Summary IC_{50} data P1156 and two-warhead evasins neutralisation of the chemokines indicated. Data show as mean ± s.e.m., and individual data points from three biological replicates. Y-axis shows IC_{50} (logarithmic scale, M), assayed against indicated chemokine EC_{80}, and x-axis shows each CKBP.

6. 3. Discussion

Evasins are small molecular weight proteins that bind chemokines with class-specificity (175, 192, 193, 198, 308). Thus far, this study has characterised a novel CC chemokine binding evasin, P1243 (Chapter 4), and a novel CXC chemokine binding evasin, P1156 (Chapter 5). Targeting chemokines in inflammatory diseases has been validated as a therapeutic approach due to chemokines recruiting immune cells, can drive the pathogenesis of inflammatory diseases (1). However, the expression of CC and CXC chemokines in inflammatory diseases indicates that in order to achieve maximal therapeutic benefit for inflammatory diseases, combinatorial administration of a CC and CXC chemokine binding proteins (CKBP) is required. For example, the administration of P1243 in combination with P1156 will target CCL3, CCL4, CCL5, CCL11 and CXCL8, the chemokines associated with tissue damage in cardiac ischaemia (53, 243, 245, 298). However, the combinatorial administration of multiple evasins present a number of complications that will require examining the risks factors and efficacy of each evasins, individually and in combination (307).

An obvious answer may be to administer viral CKBP (vCKBP), which, for the majority of cases, do not discriminate between the classes of chemokines and simply bind chemokines of multiple classes (180). For example, the viral chemokine protein M3, from the Gammaherpesvirinae virus, binds CC, CXC, XC and CX_3C chemokines (184, 188). However, the use of vCKBP's can potentially result in harmful complications and limit therapeutic benefit, as not all chemokines are inflammatory and associated with disease. Indeed, chemokines can be both pro-inflammatory and anti-inflammatory. For example, CXCL10 and CXCL11 both signal through the CXCR3 chemokine receptor, where CXCL10 results in pro-inflammatory effects and CXCL11 results in anti-inflammatory effects (24). Thus, evasins present advantages, as they offer precision targeting of chemokines and limiting off-target effects.

However, to date no evasin has been identified that is capable of binding to multiple chemokines from different classes. Therefore, this study sought to genetically engineer a novel evasin capable of precision targeting of CC and CXC chemokines. To achieve this, P1243, a CC-CKBP, was fused to P1156, a CXC-CKBP, to create P1243:G4S:P1156 and P1156:G4S:P1243, also termed the 'two-warhead' evasins. Additionally, as proof of concept, a second set of two-warhead evasins were created by fusing, the CC chemokine binding evasin, P991 (175) to P1156, to create P991:G4S:P1156 and P1156:G4S:P991 two-warhead evasins (Appendix E). This chapter has shown two evasins can be fused together, using a series of PCR steps, to create a fusion evasin capable of simultaneously targeting CC and CXC chemokines.

Evasins can be fused together using a G4S linkers to create a two-warhead evasin

Linkers are typically short amino acid sequences separating two functional domains in a single protein (309) and can be used to provide flexibility and rigidity (309, 310). Flexible linkers are commonly used in protein purification, whereby a protein is linked to an affinity tag which can then be used as a tool to purify proteins from crude samples (311). This is also observed in this study, whereby P1243, P1156 and the two-warhead evasins were all purified using the C-terminal histidine affinity tag by Ni-NTA chromatography. This histidine-tag also enabled validation of the proteins using immunolabelling (Figure 6. 5. C). Moreover, biopharmaceuticals have been utilising the use of flexible linkers in the production and enhancement of therapeutic drugs. As observed in Fc domain fusions to antibodies, such as Fc-immunoglobulin G1 (Fc-IgG1) (312), or fusions of therapeutics to carrier proteins, such as serum albumin (313), to improve the half-lives of therapeutics in plasma. Linkers are also used to promote flexibility between the two domains in a fusion protein, ensuring they do not interact

and potentially impede the functional activity of each other (309). Selecting a suitable linker for a fusion protein is crucial, as linkers can sometimes block the interacting regions of a protein (309). The direct fusion of two domains, without a linker, is not recommended as it can result in a number of complications, such as protein misfolding (314), low protein yields (315) and compromised biological activity (316, 317).

Since the interacting regions of P1243 and P1156 are not yet known, the G4S linker was selected. The G4S linker is commonly used as it promotes flexibility and spatial separation between two functional domains (309). Furthermore, previous studies on the published evasins had described that the binding modalities exhibited by evasins differed. Evasin 1 requires both its C- and N-terminus to bind chemokines, whereas Evasin 4 requires the use of only its N-terminus (174). Considering these findings, two-warhead evasins were generated in both orientations, P1243:G4S:P1156 and P1156:G4S:P1243.

Fusion of two evasins to create the two-warhead evasins does not impact protein expression

Encouragingly, the two-warhead evasins expressed well, in both orientations, and yielded proteins with similar sizes and yields. Thus, showing the spacing between the P1243 and P1156 domains, provided by the G4S linker, did not impact production of the protein and was sufficient to allow the proteins to fold correctly.

Moreover, the lower-bands observed in SDS-PAGE analysis of P1156, at 15-20 kDa (Figure 5. 3), were observed in the two-warhead evasin with the orientation that has P1156 closer to the C-terminus (P1243:G4S:P1156). Whereas, in the two-warhead evasin with P1156 closer to the N-terminus (P1156:G4S:P1243) these low molecular weight bands were not observed. Furthermore, these bands were not visible when labelled proteins were labelled with NiNTA-

Atto550 (Figure 6. 5. C), however this may be due to the amount of protein loaded onto the SDS-PAGE gel. Similarly, the low molecular weight bands were also observed in the P991 and P1156 two-warheads, where when P1156 is closer to the C-terminus, they are visible and when P1156 is closer to the N-terminus, they are not (Appendix E, Figure E3).

Although these low-molecular weight bands were not examined in detail, they may be indicative of protein degradation (287). These findings suggest, the further away P1156 is to the C-terminus, the more likely it will be preserved and not degraded. Studies by Mohanty *et al*., (318) have shown the location and length of a histidine-tag affects the expression and production of a protein. Therefore, the degradation observed by P1156 proteins, or fusion proteins contacting P1156, may be a result of the histidine-tag. Contrastingly, histidine-tags are commonly used in proteins and known, for the majority of proteins, not to interfere with expression or function (287, 319). Alternatively, the spacing between P1156 and the C-terminus can be lengthened by lengthening the linker between P1156 and the histidine-tag at the C-terminus.

Two-warhead evasins are expressed as heavily glycosylated proteins

Reassuringly, the two-warhead evasins expressed as heavily glycosylated proteins, a feature exhibited by their parental evasins (P1243 and P1156), and all other published evasins (175, 192, 193). As previously discussed in Chapters 4 and 5, glycans may result in the activation of a signalling cascade that results in the expression of pro-inflammatory cytokines and the recruitment of immune cells (254). However, glycosylation of evasins has no impact of the functional activity of the evasin (200), thus can be removed. However, glycosylation has been attributed to protein stability (285), reduced immunogenicity (174, 256, 257) and immune-evasion (253). Furthermore, treatment of the two-warhead evasins with deglycosylating

enzymes resulted in proteins with molecular weights closer to the expected weight, however this also indicates partial deglycosylation. *In Silico* analysis of glycosylation, using online databases predicted that the two-warhead evasins had the same number of N-linked and O-linked glycans as their parental evasins, thus the partial deglycosylation may be attributed to the O-linked glycans not digesting, as observed in P1156 (Figure 5. 4. B).

Achieving complete deglycosylation will require a combination of deglycosylation enzymes that target both N-linked and O-linked sugars. As described in previous chapters (Chapter 4 and 5), deglycosylation was required for MS/MS. However, despite the two-warhead evasins being partially deglycosylated, there was good coverage of the peptide sequence for both two-warhead evasins. Encouragingly, the G4S linker and adjacent amino acid sequences were also recovered, showing the correct orientation of the evasins in the two-warhead. Although N-terminal sequencing was required to confirm an intact N-terminus.

Surprisingly, immune-labelling of the two-warheads with anti-histidine initially appeared to be glycosylation-dependant. Immunoblotting showed that when P1243:G4S:P1156 was in glycosylated form, it labelled positively with anti-histidine, however when the two-warhead evasin was partially deglycosylated it could not be detected. On the other hand, for the P1156:G4S:P1243 the opposite was observed, whereby only the partially deglycosylated form of the protein could be detected and not the glycosylated form. Studies by Debeljak *et al*., (320) reported variation in immuno-detection of histidine-tagged proteins, thus it is likely the reason behind the variations in histidine expression from the two-warhead evasins. Moreover, labelling of the two-warheads with the NiNTA-Atto550, along with their parental evasins, showed that both two-warhead evasins can be readily detected.

Two-warhead evasins simultaneously bind CC and CXC chemokines

The fusion of two functionally active evasins, generating two-warhead evasins, resulted in an evasins capable of binding and neutralising both CC and CXC chemokines. Ideally, the two-warhead evasin would retain all functional properties the parental evasins exhibited. However, this study has shown the fusion of two domains impacted the two-warhead evasins binding affects to certain chemokines, especially to those the parental evasins bound to with low binding affinity. For example, in Figure 6. 8 and Figure 6. 9, the binding affinities could not be determined for CCL1, CCL7, CCL22, CXCL3, CXCL5 and CXCL6, whereas their binding affinities could be determined for the parental evasins. Despite not detecting an affinity for these chemokines with the two-warhead evasins, binding could be detected at the highest concentration detailed in the assay conditions. Therefore, binding affinities could be determined if a higher chemokine titration was used. The conditions of the binding assay were previously a limiting factor in Chapter 4, in which the binding affinity of P1243 to CCL2 could not be determined. However, Hayward *et al.*, (198) showed the affinity of P1243 for CCL2 could be determined using higher concentrations of CCL2 in the assay. The affinity a drug has for its target relates to the strength of the interaction; the higher the affinity the quicker and stronger the interaction, a quality most advantageous in designing therapeutics (267, 268). Thus, the conditions established in the BLI assay ensured only high affinity interactions are determined and low affinity interactions were not investigated further. Encouragingly, the two-warhead evasins displayed high affinities for the chemokines they interact with, which is designated by their nanomolar affinities (Figure 6. 8 and Figure 6. 9).

In addition to binding to chemokines with high affinity, this study has crucially shown the two-warhead evasins are capable of simultaneous binding of CC and CXC chemokines. Moreover, the two-warhead evasins could only bind chemokines of different classes at the same time and not from the same class. This study showed when the two-warhead evasins first bind CCL5,

they could then bind CXCL1 or CXCL8, but could not bind CCL3. Thus, by binding to CCL5, they have saturated all the CC chemokine binding sites, attributed to P1243, and can no longer bind CCL3 as no binding sites are available. However, the two-warhead evasins could then go on to bind CXCL1 or CXCL8 as the CXC chemokine binding sites, attributed to P1156, are available. Likewise, when the two-warhead evasins bound a CXC chemokine they could then go on to bind a CC chemokine, but not a second CXC chemokine as all the CXC chemokine binding sites are saturated (data not shown). Interestingly, these findings may suggest the mode of binding of both P1243 and P1156 to their chemokines. More specifically, for P1243, it may be interacting with CCL3 and CCL5 using the same binding sites. Likewise, P1156 may be interacting with CXCL1 and CXCL8 using the same binding sites.

Furthermore, certain published evasins, such as P672 (308) and Evasin 1 (192, 193), both show binding to CCL3 but not CCL5, whereas P1243, Evasin 4 (194) and P991 (175) both bind CCL3 and CCL5. Thus, these findings show evasins from different tick species may be interacting with chemokines differently. In order to confirm the method of P1243 and P1156's interaction with chemokines, a methodical approach will need to be adopted, whereby crystal structures of evasins in complex with chemokines need to be determined, as has previously been shown for Evasin 1 and CCL3 (200).

The interaction of two-warhead evasins with chemokines and their target residence time (RT) remained generally similar to what was identified by the parental evasins. However, there were some differences, which were observed with the P1243:G4S:P1156 two-warhead evasin, in affinity and RT, showing reduced affinity and RT for CXCL1 and CXCL8. Whereas for P1156:G4S:P1243, they remained similar to the parental evasin (P1156). These findings suggest that the orientation of the two-warheads may affect their function (discussed in more detail below).

Also, there was a notable increase in affinity and RT, for both two-warheads, for CCL16 and CCL23. The interaction with CCL23 was more affected, as P1243 interacted with CCL23 for 4 hours, whereas P1243:G4S:P1156 interacted with CCL23 for 7 hours and P1156:G4S:P1243 interacted for 33 hours. Generally, the fusion of two evasins showed it impacts binding and RT negatively, therefore this finding was surprising. It is likely the fusion of two evasins may have exposed a region in the P1243 domain that enables improved or more stabilised binding to CCL16 and CCL23. However, these findings will need to be examined functionally as, previously, Deruaz *et al*., (194) observed Evasin 4 bound certain chemokines but did not functionally inhibit their activity *in vitro*. With the exception of CCL16 and CCL23, the two-warhead evasins would be most suited therapeutically in acute disease, due to the length of their interactions with chemokines, similar to their parental evasins.

Two-warhead evasins neutralise CC and CXC chemokine mediated activity

Considering the effects the two-warhead evasins had on chemokine binding, it was paramount to examine if the two-warheads retained the functional effects their parental evasins exhibited. Encouragingly, the two-warhead evasins were capable of neutralising both CC and CXC chemokine induced activity. To provide a comparison between the two-warheads evasins and their parental evasins, the half maximal inhibitory concentrations (IC_{50}) were determined. The findings showed that the two-warhead evasins neutralised chemokine induced activity with IC_{50} values in the nanomolar region (Figure 6. 12). However, similar to the findings observed in the binding assays, a more pronounced difference was observed in CXC chemokine mediated activity by the two-warhead: P1243:G4S:P1156, which exhibited higher IC_{50} to CXCL1 and CXCL8 (Figure 6. 12), compared to the two warhead: P1156:G4S:P1243 and the parental evasin. Whereas, neutralisation of CC chemokine induced migration was not impacted by the orientation of the two-warheads. Nonetheless, the two-warhead evasins not only

exhibited high affinity for chemokines, but also indicate that if they were administered therapeutically, they will require fewer doses to achieve function, thus limiting the likelihood of off-target effects (267).

Orientation of the evasins in the two-warhead evasin impacts functional effects

Previously, studies on the published evasins showed that they differed in their interactions to chemokines. Evasin 1 requires both its C- and N-terminus to bind chemokines, whereas Evasin 4 requires the use of only its N-terminus (201). Furthermore, Eaton *et al*., (308) showed the location of the tag on the evasin P672 affected chemokine binding. Considering these findings, the two-warheads were generated in two orientations. This chapter has shown the orientation of the two-warhead evasins impacted the evasins interaction with chemokines.

Furthermore, there was a general trend whereby the evasin closest to the N-terminus retained a more similar chemokine binding affinity profile to the parental evasin, as opposed to when the same evasin was closer to the C-terminus. For example, P1156 was found to be bound to CXCL2 with a relatively low affinity compared to CXCL1 and CXCL8 (Figure 6. 9). However, in the two-warhead evasin P1243:G4S:P1156, binding affinities could only be determined for CXCL1 and CXCL8. However, for the two-warhead P1156:G4S:P1243, binding affinities to CXCL1, CXCL2 and CXCL8 could be experimentally determined. Likewise, whilst P1243 binding affinity could be determined for CCL3, it could only be determined in the P1243:G4S:P1156 two-warhead evasin and not the P1156:G4S:P1243 orientation (Figure 6. 8, Figure 6. 9).

Therefore, these findings show that the fusion of two functional domains does indeed have impact of the function of the final protein. Whilst this may be a result of steric hinderance

(309), reversing the orientation of the evasins did not alleviate this. Likewise, incorporating the use of the G4S linker, intended to promote flexibility between the two domains, also did not overcome the loss of function. Alternatively, examining the use of longer linker or alternative types of linkers may counteracted this loss of activity (229, 309).

In summary, to-date only viral and helminth derived CKBP's have shown the ability to bind chemokines of multiple classes (180), for example, the myxoma virus derived CKBP M-T7 binds and neutralises the activity of CC, CXC and XC chemokines (321). However, unlike the viral CKBP's, two-warhead evasins provide a more precise method of targeting chemokines, as they were created by fusing naturally selective evasins. Furthermore, the two-warhead evasins are capable of simultaneously binding CC and CXC chemokines, *in vitro*, and subsequently neutralisation of CC and CXC induced activity. Thus, the application of two-warhead evasins may be useful in treating inflammatory diseases associated with CC and CXC chemokine activity. To examine the effects of the two-warhead evasins P1243:G4S:P1156 and P1156:G4S:P1243, *in vivo*, models of atherosclerosis (35), rheumatoid arthritis (167) and inflammatory bowel disease (42) would be most advantageous as they are associated with both CC and CXC chemokines (Appendix F, Table F1).

Chapter 7.

General Discussion

Chemokines are signalling proteins that are categorised into four groups, based on the position of their cysteine residues at the N-terminus, as CC, CXC, CX_3C and XC chemokines (C-cysteine, X-amino acid) (84) (Figure 1. 2). Chemokines are crucial to the immune response as they recruit immune and inflammatory cells to sites of inflammation. Increased expression of chemokines is a key finding in a range of inflammatory diseases (75). Typically, an initial insult results in the expression of various cytokines and chemokines, as observed in myocardial infarction (53) and strokes (39) following ischemia, and in atherosclerosis (322) and non-alcoholic steatohepatitis (323) following lipid deposition. The recruitment of immune cells in disease results in tissue damage and propagation of disease pathogenesis (131). Thus, chemokines are an attractive therapeutic target in inflammation-driven diseases.

Considering this, the pharmaceutical industry developed a range of agents that target chemokines or their receptors, however many of these agents failed at the clinical trial phase, mainly due to a lack in efficacy (167). Largely, the pharmaceutical industry failed to consider the robustness of the chemokine network. Chemokines operate in a network, where multiple chemokines bind a single receptor, single receptors bind multiple chemokines and immune cells

express multiple chemokine receptors (Figure 1. 4) (2). Therefore, targeting a single chemokine or chemokine receptor will likely fail as a therapeutic approach in inflammatory disease (167).

Ticks are parasitic species that are able to feed on their hosts for prolonged periods of time without eliciting their hosts immune response. Ticks do this by injecting more than 3000 peptides into their hosts during feeding (190). Evasins are proteins isolated from tick saliva and thought to reduce inflammation at the site of the tick bite through binding and neutralising multiple chemokines (174, 175, 198). Chemokine binding proteins (CKBPs) have also been reported in viruses (180) and helminths (172), however tick-derived CKBPs (evasins) exclusively bind to chemokines with class-specificity (174, 175, 198). Thus far in the field, three evasins have been isolated from the *Rhipicephalus sanguineus* tick, Evasin 1 and 4, which are selective CC-CKBPs and Evasin 3, which is a selective CXC-CKBP (174). Furthermore, the systemic administration of these evasins in a range of preclinical models of disease proved effective in reducing inflammation in those models (174), thus showing initial proof-of-concept that targeting chemokines may be an effective mode of therapy in inflammatory diseases. However, limitations in these published CKBP's include evasins capable of binding CCL2, CCL13 and CXCL10, and a single evasin capable of binding CC and CXC chemokines. Accordingly, this thesis aimed to expand the chemokine-binding repertoire of identified evasins and hypothesised that other tick species would have novel evasins that are also capable of modulating chemokine activity.

Summary of findings

The findings in this thesis show that both bioinformatics and yeast surface display (YSD) provide powerful tools for identifying novel evasins (Chapter 3). Using bioinformatic analysis of *Amblyomma*, *Rhipicephalus* and *Ixodes* genera of ticks, a library of 352 evasin-like

sequences were identified and subsequently transformed into yeast surface display (YSD) vectors (Figure 3. 1). Next, the evasin library was screened for binders against fluorescently labelled CCL8, CCL15, CCL17, CCL19, CCL20, CXCL8 and CXCL12 using fluorescent-activated cell sorting (FACS). FACS screening identified 16 novel evasins: P672, P974, P983, P991, P1180, P1182, P1243, P1030, P1006, P993, P1015, P1252, P1156, P1209 and P1215 (Table 3. 1). As these evasins were of interest, they were patented in the UK (PCT/GB2017/050563). Following YSD screening experiments, the novel evasins P1243 and P1156 were selected for further characterisation. Each of these evasins exhibited distinct functions, for example, P1156 bound CXCL8, whereas P1243 bound multiple CC chemokines, including CCL15, CCL17 and CCL19.

Expression of both P1243 and P1156, using mammalian cells, showed that they are expressed as heavily glycosylated proteins. Glycans are recognised pathogen associated molecular patterns (PAMPs), which can be recognised by innate sensors, such as toll-like receptors (TLRs), which are expressed on the surface of macrophages and dendritic cells. Upon recognition, a signalling cascade is activated that results in the release of pro-inflammatory cytokines and the recruitment of immune cells. However, glycosylation is typically observed in all evasins published to-date (174, 175) and attributed to reduced immunogenicity (174, 256, 257), immune-evasion (253), and improving protein stability (285). Moreover, studies by Dias *et al.,* (200) showed glycosylation has no impact of the functional activity of the evasin. Therefore, in the event the evasins cause immune cell recruitment, glycans can be removed.

Characterisation of P1243 showed it is a broad-spectrum evasin, that binds with high affinity, 21 CC chemokines, *in vitro* (Chapter 4). P1156 proved to be a narrow-spectrum evasin that binds *in vitro*, to 6 ELR+ CXC chemokines, with high affinity (Chapter 5). Where tested, evasins that bound chemokines also efficiently neutralized their biological activity.

In order to develop agents capable of targeting both CC and CXC chemokines, the two-warhead evasins were created. Through a series of PCR steps, P1243 and P1156 were fused together using a G4S linker, to create P1243:G4S:P1156 and P1156:G4S:P1243. The two-warhead evasins bind and neutralise CC and CXC chemokines with high affinity and retain the majority of the activity exhibited by their parental evasins with minimal loss. Crucially, the two-warhead evasins are capable of simultaneously binding CC and CXC chemokines (Chapter 6). Furthermore, as further proof-of-concept, a second set of two-warhead evasins were produced using the evasins P991 and P1156, creating P991:G4S:P1156 and P1156:G4S:P991 (Appendix E, Figure E1-E2). These two-warhead evasins also bound and neutralised multiple CC and CXC chemokines, to the same effect as their parental evasins (Appendix E, Figure E4-E6). Moreover, they too were capable of simultaneously binding CC and CXC chemokines (Appendix E, Figure E7).

Collectively, these findings show that other tick species also carry novel evasins that are capable of binding to multiple human chemokines and neutralising their activity. Moreover, evasins can be fused together to create a single agent capable of dual-binding to CC and CXC chemokines.

Future directions

One of the key results in this study was the construction of the two-warhead evasins and their functional characterisation *in vitro*. However, the fusion of P1243 and P1156 did result in loss of binding to certain chemokines, especially to those chemokines which the parental evasin bound to with low affinity, such as CCL1, CCL7, CCL22, CXCL3, CXCL5 and CXCL6 (Figure 6. 8, 6. 9). Similarly, the two-warheads created from the fusion of P991 and P1156 also lost binding to some chemokines, including CCL19, CCL20 and CXCL6 (Appendix E, Figure E4-E5). The mechanisms behind this loss was not explored in detail in this study, although

switching orientation of the parental evasins in the two-warhead did improve binding affinity to those chemokines. A possible reason behind this loss in binding affinity may be attributed to the choice of linker used to fuse the two-warheads. In this study, the G4S linker, widely employed due to its flexibility (309), was selected for constructing the two-warhead evasins. However, this may not be the optimal linker and exploring the use of longer or alternative linkers may restore the high-affinity binding lost in the two-warhead evasins (229). For example, the length of linker could be increased with the $(GGGGS)_3$ sequence, which not only promotes flexibility, but has also shown improvements to biological activity (317). On the other hand, an alternative linker, such as $(Gly)_6$ or $(Gly)_8$ could be used (229).

Moreover, the two-warhead evasins are capable of simultaneous binding to CC and CXC chemokines, as shown in the BLI assay (Figure 6. 10), however the functional effects of the two-warheads were only examined on single chemokines. Therefore, *in vitro* assays will need to be developed that explore the simultaneous migration of a mixture of cells in response to a combination of CC and CXC chemokines, and their neutralisation by the two-warhead evasins. The use of buffy coat cells could be incorporated here, as they contain a mixture of monocytes, neutrophils and lymphocytes.

Furthermore, previous studies have shown the administration of evasins systemically proved effective in a range of preclinical models of inflammation (174). However, inflammatory diseases are commonly associated with chemokines from multiple classes (324). For example, increasing levels of CCL3, CCL4, CCL5, CCL11, CCL13 and CXCL8 have all been observed in myocardial infarction (325-327). Moreover, in rheumatoid arthritis (RA) many chemokines are progressively expressed in the sera, synovial fluid and tissues of RA patients and have been associated with propagating disease, these include: CCL2 (44, 328), CCL3 (303, 329), CCL5 (304), CCL7, CCL8 (45), CCL13 (330), CCL14, CCL15 (45), CCL17 (331), CCL18 (332, 333), CCL20 (328, 334), CXCL1, CXCL5, CXCL7 and CXCL8 (329, 335-340). Thus, in order

to achieve maximal therapeutic benefit, a combination of evasins will likely need to be administered, one that targets CC chemokines and another that targets CXC chemokines. This form of therapy will require thorough consideration, as each evasin will need to be examined individually and in combination, in which the risk factors and efficacy of each evasin individually and in combination will need to be examined (307). Therefore, the two-warhead evasins present at an advantage, as they can precisely target both CC and CXC chemokines as a single agent. However, firstly, the effects of the two-warhead evasins on inflammation will need to be examined *in vivo*, as thus far all studies have been performed *in vitro*.

The applications of the two-warhead evasins would primarily be dictated by the chemokine expression patterns in a particular disease. Based on the published literature, and the characteristics of the two-warhead evasins shown in this study, preclinical models driven by both neutrophilic and monocytic migration, would be most suitable. These models would include: myocarditis (341), myocardial infarction (33, 342), atherosclerosis (35), vasculitis (343), idiopathic pulmonary fibrosis (42), inflammatory bowel disease (344) and rheumatoid arthritis (44, 167) (Appendix F, Table F1).

Moreover, *in vivo* models of these diseases have all been established and cited in the literature. However, they are established in mice, therefore, in order to utilise these mouse models, it is crucial that the two-warhead evasins are able to recognise and bind murine chemokines. Therefore, this study has taken initial steps towards this aim by showing that the parental evasin and the two-warhead evasins are all capable of binding to murine chemokines (Appendix G, Figure G1-G2). However, there may be certain complications that need to be considered when using mouse models. As with all evolutionary conservation of genes and proteins, there may be issues with functional conservation of these factors, as the functions of human and murine chemokines are not comparable 1:1 (345). For example, murine CCL3 is chemotactic for

neutrophils (346), whereas human CCL3 signals for monocytes/macrophages and not neutrophils (84).

Prior to examining the function of P1243, P1156 and the two-warhead evasins in disease mouse models, their function against mouse chemokines will need to be examined. Thus, *in vitro* assays, such at the transwell migration assay, will need to be performed using murine cells. Murine immune cells can be extracted from mouse bone marrow, which will contain a mixture of monocytes, neutrophils and lymphocytes. Immune cell populations can be isolated using flow cytometry through size, using forward and side scatter, and through cell surface markers. Once the function of evasins, using mouse cells, has been confirmed, the evasins pharmacodynamic and pharmacokinetic profile will need to be examined. Collectively, these studies will determine the maximal dosage and safety of evasins in mouse models. Evasins can be systemically injected into wild-type mice, as shown for Evasin 1 (202), and blood biochemistry will need to be examined for abnormal changes, such as increasing levels of T and B cells, which would indicate antibodies are being raised against the evasin. Studies by Bonvin *et al.,* (174) used *in silico* methods to predict the potential CD4+ T cell epitopes present in their published evasins, and the predictor showed the evasins have less antigenic sites than Interferon-β, a widely used treatment for multiple sclerosis. Moreover, the half-life of each evasin will need to be determined. In order to achieve this, evasins should be systemically administered, subcutaneously or intravenously, and their levels examined after certain time periods, such as 30 minutes, 1 hour, 6 hours and 24 hours. Examining the levels of evasins will require antibodies targeting specific epitopes of each evasin, which can be designed, or the use of a streptavidin or histidine-antibodies can be used, as the evasins contain a streptavidin-histidine tag.

Nonetheless, the ‘two-warhead’ evasin concept has laid the foundations of generating multiple forms of fusion-evasins. This can take the form of fusing not only CC-CKBPs and CXC-

CKBPs, but also two CC-CKBPs or CXC-CKBPs, thus potentially providing an enhanced response against CC or CXC chemokine activity, respectively. For example, P991 and P1243 could be fused together to provide a more amplified response against CC chemokine activity, which may prove most advantageous in monocytic-driven diseases, such as myocarditis (263). Moreover, the fusion of evasins need not to be limited to only two-warheads, as multi-domain-warheads can be explored and tailored to fit the requirements of disease.

In conclusion, the work in this study has revealed evasins exist in other tick species and are capable of binding multiple chemokines. The work also characterised two novel evasins: P1243, a broad-spectrum selective CC-CKBP, and P1156, a narrow-spectrum CXC-CKBP. Moreover, this study has shown, for the first time, that it is possible to construct genetically engineered two-warhead evasins, capable of simultaneously targeting CC and CXC chemokines. Thus, the novel two-warhead CKBPs provide a concept of achieving precision targeting of disease-relevant CC and CXC chemokine subsets as a single agent. As a result, the applications of the two-warhead evasins will cover a broad range of inflammatory diseases associated with the combinatorial expression of CC and CXC chemokines. Therefore, upon identifying the chemokine-subset associated with a certain disease, a fusion evasin can be tailored to meet the chemokine binding requirements. Such fusion-evasins are likely to be more advantageous to viral and helminth CKBP's as the binding properties can be tailored to fit the disease subset, through the selection of appropriate parental evasins.

Chapter 8.

References

1. Viola A, Luster AD. Chemokines and their receptors: drug targets in immunity and inflammation. Annual review of pharmacology and toxicology. 2008;48:171-97.
2. Zlotnik A, Yoshie O. The chemokine superfamily revisited. Immunity. 2012;36(5):705-16.
3. Medzhitov R. Origin and physiological roles of inflammation. Nature. 2008;454(7203):428-35.
4. Kotas ME, Medzhitov R. Homeostasis, inflammation, and disease susceptibility. Cell. 2015;160(5):816-27.
5. Medzhitov R, Janeway C, Jr. Innate immunity. The New England journal of medicine. 2000;343(5):338-44.
6. Janeway CA, Jr., Medzhitov R. Innate immune recognition. Annual review of immunology. 2002;20:197-216.
7. Charles A Janeway J, Travers P, Walport M, Shlomchik MJ. Principles of innate and adaptive immunity. 2001.
8. Nauseef WM, Borregaard N. Neutrophils at work. Nature immunology. 2014;15(7):602-11.
9. Ward AC, Loeb DM, Soede-Bobok AA, Touw IP, Friedman AD. Regulation of granulopoiesis by transcription factors and cytokine signals. Leukemia. 2000;14(6):973-90.
10. Oelgeschläger M, Nuchprayoon I, Lüscher B, Friedman AD. C/EBP, c-Myb, and PU.1 cooperate to regulate the neutrophil elastase promoter. Molecular and cellular biology. 1996;16(9):4717-25.
11. Geering B, Stoeckle C, Conus S, Simon HU. Living and dying for inflammation: neutrophils, eosinophils, basophils. Trends in immunology. 2013;34(8):398-409.
12. Borregaard N, Cowland JB. Granules of the human neutrophilic polymorphonuclear leukocyte. Blood. 1997;89(10):3503-21.
13. Summers C, Rankin SM, Condliffe AM, Singh N, Peters AM, Chilvers ER. Neutrophil kinetics in health and disease. Trends in immunology. 312010. p. 318-24.
14. Cachat J, Deffert C, Hugues S, Krause KH. Phagocyte NADPH oxidase and specific immunity. Clinical science (London, England : 1979). 2015;128(10):635-48.
15. Towbin AJ, Chaves I. Chronic granulomatous disease. Pediatric radiology. 2010;40(5):657-68; quiz 792-3.

16. Brinkmann V, Zychlinsky A. Neutrophil extracellular traps: is immunity the second function of chromatin? The Journal of cell biology. 2012;198(5):773-83.
17. Brinkmann V, Reichard U, Goosmann C, Fauler B, Uhlemann Y, Weiss DS, et al. Neutrophil extracellular traps kill bacteria. Science (New York, NY). 2004;303(5663):1532-5.
18. Zhang DE, Hetherington CJ, Chen HM, Tenen DG. The macrophage transcription factor PU.1 directs tissue-specific expression of the macrophage colony-stimulating factor receptor. Molecular and cellular biology. 1994;14(1):373-81.
19. van Furth R, Cohn ZA, Hirsch JG, Humphrey JH, Spector WG, Langevoort HL. The mononuclear phagocyte system: a new classification of macrophages, monocytes, and their precursor cells. Bulletin of the World Health Organization. 1972;46(6):845-52.
20. Geissmann F, Jung S, Littman DR. Blood monocytes consist of two principal subsets with distinct migratory properties. Immunity. 2003;19(1):71-82.
21. Tacke F, Randolph GJ. Migratory fate and differentiation of blood monocyte subsets. Immunobiology. 2006;211(6-8):609-18.
22. Saeed L, Patnaik MM, Begna KH, Al-Kali A, Litzow MR, Hanson CA, et al. Prognostic relevance of lymphocytopenia, monocytopenia and lymphocyte-to-monocyte ratio in primary myelodysplastic syndromes: a single center experience in 889 patients. Blood Cancer J. 72017. p. e550-.
23. Dutta P, Nahrendorf M. Regulation and consequences of monocytosis. Immunological reviews. 2014;262(1):167-78.
24. Kumar AH, Martin K, Turner EC, Buneker CK, Dorgham K, Deterre P, et al. Role of CX3CR1 receptor in monocyte/macrophage driven neovascularization. PloS one. 2013;8(2):e57230.
25. Tsou CL, Peters W, Si Y, Slaymaker S, Aslanian AM, Weisberg SP, et al. Critical roles for CCR2 and MCP-3 in monocyte mobilization from bone marrow and recruitment to inflammatory sites. The Journal of clinical investigation. 2007;117(4):902-9.
26. Ziegler-Heitbrock L, Ancuta P, Crowe S, Dalod M, Grau V, Hart DN, et al. Nomenclature of monocytes and dendritic cells in blood. Blood. 2010;116(16):e74-80.
27. Hijdra D, Vorselaars AD, Grutters JC, Claessen AM, Rijkers GT. Differential expression of TNFR1 (CD120a) and TNFR2 (CD120b) on subpopulations of human monocytes. J Inflamm (Lond). 92012. p. 38.
28. Shi C, Pamer EG. Monocyte recruitment during infection and inflammation. Nat Rev Immunol.11(11):762-74.
29. Swirski FK, Nahrendorf M, Etzrodt M, Wildgruber M, Cortez-Retamozo V, Panizzi P, et al. Identification of splenic reservoir monocytes and their deployment to inflammatory sites. Science (New York, NY). 2009;325(5940):612-6.
30. Geissmann F, Manz MG, Jung S, Sieweke MH, Merad M, Ley K. Development of monocytes, macrophages, and dendritic cells. Science (New York, NY). 2010;327(5966):656-61.
31. Murray PJ, Wynn TA. Protective and pathogenic functions of macrophage subsets. Nat Rev Immunol. 2011;11(11):723-37.
32. Roszer T. Understanding the Mysterious M2 Macrophage through Activation Markers and Effector Mechanisms. Mediators Inflamm. 2015;2015:816460.
33. Frangogiannis NG, Entman ML. Targeting the chemokines in myocardial inflammation. Circulation. 110. United States2004. p. 1341-2.
34. Aukrust P, Halvorsen B, Yndestad A, Ueland T, Oie E, Otterdal K, et al. Chemokines and cardiovascular risk. Arteriosclerosis, thrombosis, and vascular biology. 2008;28(11):1909-19.
35. Zernecke A, Weber C. Chemokines in the vascular inflammatory response of atherosclerosis. Cardiovascular research. 2010;86(2):192-201.

36. Liu J, Wang H, Li J. Inflammation and Inflammatory Cells in Myocardial Infarction and Reperfusion Injury: A Double-Edged Sword. Clin Med Insights Cardiol. 102016. p. 79-84.
37. Wyss-Coray T, Rogers J. Inflammation in Alzheimer Disease—A Brief Review of the Basic Science and Clinical Literature. Cold Spring Harb Perspect Med. 22012.
38. Frischer JM, Bramow S, Dal-Bianco A, Lucchinetti CF, Rauschka H, Schmidbauer M, et al. The relation between inflammation and neurodegeneration in multiple sclerosis brains. Brain. 1322009. p. 1175-89.
39. Anrather J, Iadecola C. Inflammation and Stroke: An Overview. Neurotherapeutics. 132016. p. 661-70.
40. Danese S, Gasbarrini A. Chemokines in inflammatory bowel disease. J Clin Pathol. 582005. p. 1025-7.
41. Habtezion A. Inflammation in acute and chronic pancreatitis. Current opinion in gastroenterology. 2015;31(5):395-9.
42. Sahin H, Wasmuth HE. Chemokines in tissue fibrosis. Biochimica et biophysica acta. 2013;1832(7):1041-8.
43. Palmqvist C, Wardlaw AJ, Bradding P. Chemokines and their receptors as potential targets for the treatment of asthma. British journal of pharmacology. 1512007. p. 725-36.
44. Szekanecz Z, Kim J, Koch AE. Chemokines and chemokine receptors in rheumatoid arthritis. Seminars in immunology. 2003;15(1):15-21.
45. Haringman JJ, Smeets TJ, Reinders-Blankert P, Tak PP. Chemokine and chemokine receptor expression in paired peripheral blood mononuclear cells and synovial tissue of patients with rheumatoid arthritis, osteoarthritis, and reactive arthritis. Annals of the rheumatic diseases. 2006;65(3):294-300.
46. Lowes MA, Suárez-Fariñas M, Krueger JG. Immunology of Psoriasis. Annual review of immunology. 2014;32:227-55.
47. Lafyatis R, York M. Innate immunity and inflammation in systemic sclerosis. Current opinion in rheumatology. 2009;21(6):617-22.
48. Middleton J, Patterson AM, Gardner L, Schmutz C, Ashton BA. Leukocyte extravasation: chemokine transport and presentation by the endothelium. Blood. 2002;100(12):3853-60.
49. Wendt E, Keshav S. CCR9 antagonism: potential in the treatment of Inflammatory Bowel Disease. Clinical and experimental gastroenterology. 2015;8:119-30.
50. Herrington W, Lacey B, Sherliker P, Armitage J, Lewington S. Epidemiology of Atherosclerosis and the Potential to Reduce the Global Burden of Atherothrombotic Disease. Circulation research. 2016;118(4):535-46.
51. Braunersreuther V, Mach F, Steffens S. The specific role of chemokines in atherosclerosis. Thromb Haemost. 2007;97(5):714-21.
52. Schwartz CJ, Valente AJ, Sprague EA, Kelley JL, Nerem RM. The pathogenesis of atherosclerosis: an overview. Clinical cardiology. 1991;14(2 Suppl 1):I1-16.
53. Libby P. Inflammation and cardiovascular disease mechanisms. The American journal of clinical nutrition. 2006;83(2):456s-60s.
54. Moore KJ, Freeman MW. Scavenger receptors in atherosclerosis: beyond lipid uptake. Arteriosclerosis, thrombosis, and vascular biology. 2006;26(8):1702-11.
55. Jones CB, Sane DC, Herrington DM. Matrix metalloproteinases: a review of their structure and role in acute coronary syndrome. Cardiovascular research. 2003;59(4):812-23.
56. Croce K, Libby P. Intertwining of thrombosis and inflammation in atherosclerosis. Current opinion in hematology. 2007;14(1):55-61.
57. Soehnlein O. Multiple roles for neutrophils in atherosclerosis. Circulation research. 2012;110(6):875-88.

58. Drechsler M, Megens RT, van Zandvoort M, Weber C, Soehnlein O. Hyperlipidemia-triggered neutrophilia promotes early atherosclerosis. Circulation. 2010;122(18):1837-45.
59. Zernecke A, Bot I, Djalali-Talab Y, Shagdarsuren E, Bidzhekov K, Meiler S, et al. Protective role of CXC receptor 4/CXC ligand 12 unveils the importance of neutrophils in atherosclerosis. Circulation research. 2008;102(2):209-17.
60. Yvan-Charvet L, Ranalletta M, Wang N, Han S, Terasaka N, Li R, et al. Combined deficiency of ABCA1 and ABCG1 promotes foam cell accumulation and accelerates atherosclerosis in mice. The Journal of clinical investigation. 2007;117(12):3900-8.
61. Seimon TA, Nadolski MJ, Liao X, Magallon J, Nguyen M, Feric NT, et al. Atherogenic lipids and lipoproteins trigger CD36-TLR2-dependent apoptosis in macrophages undergoing endoplasmic reticulum stress. Cell metabolism. 2010;12(5):467-82.
62. Soehnlein O, Zernecke A, Eriksson EE, Rothfuchs AG, Pham CT, Herwald H, et al. Neutrophil secretion products pave the way for inflammatory monocytes. Blood. 2008;112(4):1461-71.
63. Hosokawa T, Kumon Y, Kobayashi T, Enzan H, Nishioka Y, Yuri K, et al. Neutrophil infiltration and oxidant-production in human atherosclerotic carotid plaques. Histol Histopathol. 2011;26(1):1-11.
64. Smith JD, Trogan E, Ginsberg M, Grigaux C, Tian J, Miyata M. Decreased atherosclerosis in mice deficient in both macrophage colony-stimulating factor (op) and apolipoprotein E. Proceedings of the National Academy of Sciences of the United States of America. 1995;92(18):8264-8.
65. de Villiers WJ, Smith JD, Miyata M, Dansky HM, Darley E, Gordon S. Macrophage phenotype in mice deficient in both macrophage-colony-stimulating factor (op) and apolipoprotein E. Arteriosclerosis, thrombosis, and vascular biology. 1998;18(4):631-40.
66. Rajavashisth T, Qiao JH, Tripathi S, Tripathi J, Mishra N, Hua M, et al. Heterozygous osteopetrotic (op) mutation reduces atherosclerosis in LDL receptor- deficient mice. The Journal of clinical investigation. 1998;101(12):2702-10.
67. Prabhu SD, Frangogiannis NG. The Biological Basis for Cardiac Repair After Myocardial Infarction: From Inflammation to Fibrosis. Circulation research. 2016;119(1):91-112.
68. Bergmann O, Bhardwaj RD, Bernard S, Zdunek S, Barnabe-Heider F, Walsh S, et al. Evidence for cardiomyocyte renewal in humans. Science (New York, NY). 2009;324(5923):98-102.
69. Saparov A, Ogay V, Nurgozhin T, Chen WCW, Mansurov N, Issabekova A, et al. Role of the immune system in cardiac tissue damage and repair following myocardial infarction. Inflammation research : official journal of the European Histamine Research Society [et al]. 2017;66(9):739-51.
70. Soehnlein O, Lindbom L. Phagocyte partnership during the onset and resolution of inflammation. Nat Rev Immunol. 2010;10(6):427-39.
71. Elahi MM, Kong YX, Matata BM. Oxidative stress as a mediator of cardiovascular disease. Oxidative medicine and cellular longevity. 2009;2(5):259-69.
72. Dutta P, Courties G, Wei Y, Leuschner F, Gorbatov R, Robbins C, et al. Myocardial infarction accelerates atherosclerosis. Nature. 2012;487(7407):325-9.
73. Goldstein JA, Demetriou D, Grines CL, Pica M, Shoukfeh M, O'Neill WW. Multiple complex coronary plaques in patients with acute myocardial infarction. The New England journal of medicine. 2000;343(13):915-22.
74. Milonas C, Jernberg T, Lindback J, Agewall S, Wallentin L, Stenestrand U. Effect of Angiotensin-converting enzyme inhibition on one-year mortality and frequency of repeat acute myocardial infarction in patients with acute myocardial infarction. The American journal of cardiology. 2010;105(9):1229-34.

75. Raman D, Sobolik-Delmaire T, Richmond A. Chemokines in health and disease. Experimental cell research. 2011;317(5):575-89.
76. Uguccioni M, Teixeira MM, Locati M, Mantovani A. Editorial: Regulation of Inflammation, Its Resolution and Therapeutic Targeting. Frontiers in immunology. 2017;8.
77. Ridker PM, Everett BM, Thuren T, MacFadyen JG, Chang WH, Ballantyne C, et al. Antiinflammatory Therapy with Canakinumab for Atherosclerotic Disease. The New England journal of medicine. 2017;377(12):1119-31.
78. Godessart N. Chemokine receptors: attractive targets for drug discovery. Annals of the New York Academy of Sciences. 2005;1051:647-57.
79. Baggiolini M. Chemokines and leukocyte traffic. Nature. 1998;392(6676):565-8.
80. Youn BS, Mantel C, Broxmeyer HE. Chemokines, chemokine receptors and hematopoiesis. Immunological reviews. 2000;177:150-74.
81. Belperio JA, Keane MP, Arenberg DA, Addison CL, Ehlert JE, Burdick MD, et al. CXC chemokines in angiogenesis. Journal of leukocyte biology. 2000;68(1):1-8.
82. Rossi D, Zlotnik A. The biology of chemokines and their receptors. Annual review of immunology. 2000;18:217-42.
83. Sallusto F, Mackay CR, Lanzavecchia A. The role of chemokine receptors in primary, effector, and memory immune responses. Annual review of immunology. 2000;18:593-620.
84. Fernandez EJ, Lolis E. Structure, function, and inhibition of chemokines. Annual review of pharmacology and toxicology. 2002;42:469-99.
85. DeVries ME, Kelvin AA, Xu L, Ran L, Robinson J, Kelvin DJ. Defining the origins and evolution of the chemokine/chemokine receptor system. Journal of immunology (Baltimore, Md : 1950). 2006;176(1):401-15.
86. Colobran R, Pujol-Borrell R, Armengol MP, Juan M. The chemokine network. I. How the genomic organization of chemokines contains clues for deciphering their functional complexity. Clinical and experimental immunology. 2007;148(2):208-17.
87. Petkovic V, Moghini C, Paoletti S, Uguccioni M, Gerber B. Eotaxin-3/CCL26 is a natural antagonist for CC chemokine receptors 1 and 5. A human chemokine with a regulatory role. J Biol Chem. 2004;279(22):23357-63.
88. Ogilvie P, Paoletti S, Clark-Lewis I, Uguccioni M. Eotaxin-3 is a natural antagonist for CCR2 and exerts a repulsive effect on human monocytes. Blood. 2003;102(3):789-94.
89. Nomiyama H, Fukuda S, Iio M, Tanase S, Miura R, Yoshie O. Organization of the chemokine gene cluster on human chromosome 17q11.2 containing the genes for CC chemokine MPIF-1, HCC-2, HCC-1, LEC, and RANTES. Journal of interferon & cytokine research : the official journal of the International Society for Interferon and Cytokine Research. 1999;19(3):227-34.
90. Menten P, Wuyts A, Van Damme J. Macrophage inflammatory protein-1. Cytokine & growth factor reviews. 2002;13(6):455-81.
91. Maurer M, von Stebut E. Macrophage inflammatory protein-1. The international journal of biochemistry & cell biology. 2004;36(10):1882-6.
92. Gunn MD, Tangemann K, Tam C, Cyster JG, Rosen SD, Williams LT. A chemokine expressed in lymphoid high endothelial venules promotes the adhesion and chemotaxis of naive T lymphocytes. Proceedings of the National Academy of Sciences of the United States of America. 1998;95(1):258-63.
93. Kim CH, Pelus LM, White JR, Applebaum E, Johanson K, Broxmeyer HE. CK beta-11/macrophage inflammatory protein-3 beta/EBI1-ligand chemokine is an efficacious chemoattractant for T and B cells. Journal of immunology (Baltimore, Md : 1950). 1998;160(5):2418-24.
94. Homey B, Alenius H, Muller A, Soto H, Bowman EP, Yuan W, et al. CCL27-CCR10 interactions regulate T cell-mediated skin inflammation. Nature medicine. 2002;8(2):157-65.

95. Yang D, Chertov O, Bykovskaia SN, Chen Q, Buffo MJ, Shogan J, et al. Beta-defensins: linking innate and adaptive immunity through dendritic and T cell CCR6. Science (New York, NY). 1999;286(5439):525-8.
96. Huising MO, Stet RJ, Kruiswijk CP, Savelkoul HF, Lidy Verburg-van Kemenade BM. Molecular evolution of CXC chemokines: extant CXC chemokines originate from the CNS. Trends in immunology. 2003;24(6):307-13.
97. Bizzarri C, Beccari AR, Bertini R, Cavicchia MR, Giorgini S, Allegretti M. ELR+ CXC chemokines and their receptors (CXC chemokine receptor 1 and CXC chemokine receptor 2) as new therapeutic targets. Pharmacology & therapeutics. 2006;112(1):139-49.
98. Loetscher P, Pellegrino A, Gong JH, Mattioli I, Loetscher M, Bardi G, et al. The ligands of CXC chemokine receptor 3, I-TAC, Mig, and IP10, are natural antagonists for CCR3. J Biol Chem. 2001;276(5):2986-91.
99. Gunn MD, Ngo VN, Ansel KM, Ekland EH, Cyster JG, Williams LT. A B-cell-homing chemokine made in lymphoid follicles activates Burkitt's lymphoma receptor-1. Nature. 1998;391(6669):799-803.
100. Kurth I, Willimann K, Schaerli P, Hunziker T, Clark-Lewis I, Moser B. Monocyte selectivity and tissue localization suggests a role for breast and kidney-expressed chemokine (BRAK) in macrophage development. The Journal of experimental medicine. 2001;194(6):855-61.
101. Shurin GV, Ferris RL, Tourkova IL, Perez L, Lokshin A, Balkir L, et al. Loss of new chemokine CXCL14 in tumor tissue is associated with low infiltration by dendritic cells (DC), while restoration of human CXCL14 expression in tumor cells causes attraction of DC both in vitro and in vivo. Journal of immunology (Baltimore, Md : 1950). 2005;174(9):5490-8.
102. Matloubian M, David A, Engel S, Ryan JE, Cyster JG. A transmembrane CXC chemokine is a ligand for HIV-coreceptor Bonzo. Nature immunology. 2000;1(4):298-304.
103. Bazan JF, Bacon KB, Hardiman G, Wang W, Soo K, Rossi D, et al. A new class of membrane-bound chemokine with a CX3C motif. Nature. 1997;385(6617):640-4.
104. Kelner GS, Kennedy J, Bacon KB, Kleyensteuber S, Largaespada DA, Jenkins NA, et al. Lymphotactin: a cytokine that represents a new class of chemokine. Science (New York, NY). 1994;266(5189):1395-9.
105. Muller G, Hopken UE, Lipp M. The impact of CCR7 and CXCR5 on lymphoid organ development and systemic immunity. Immunological reviews. 2003;195:117-35.
106. Strydom N, Rankin SM. Regulation of circulating neutrophil numbers under homeostasis and in disease. Journal of innate immunity. 2013;5(4):304-14.
107. Williams JL, Holman DW, Klein RS. Chemokines in the balance: maintenance of homeostasis and protection at CNS barriers. Frontiers in cellular neuroscience. 2014;8:154.
108. Harrison JK, Jiang Y, Chen S, Xia Y, Maciejewski D, McNamara RK, et al. Role for neuronally derived fractalkine in mediating interactions between neurons and CX3CR1-expressing microglia. Proceedings of the National Academy of Sciences of the United States of America. 951998. p. 10896-901.
109. Mantovani A, Cassatella MA, Costantini C, Jaillon S. Neutrophils in the activation and regulation of innate and adaptive immunity. Nat Rev Immunol. 2011;11(8):519-31.
110. Moser B, Wolf M, Walz A, Loetscher P. Chemokines: multiple levels of leukocyte migration control. Trends in immunology. 2004;25(2):75-84.
111. Kufareva I. Chemokines and their receptors: insights from molecular modeling and crystallography. Current opinion in pharmacology. 2016;30:27-37.
112. Clark-Lewis I, Kim KS, Rajarathnam K, Gong JH, Dewald B, Moser B, et al. Structure-activity relationships of chemokines. Journal of leukocyte biology. 1995;57(5):703-11.

113. Deshmane SL, Kremlev S, Amini S, Sawaya BE. Monocyte Chemoattractant Protein-1 (MCP-1): An Overview. Journal of interferon & cytokine research : the official journal of the International Society for Interferon and Cytokine Research. 292009. p. 313-26.
114. Kufareva I, Gustavsson M, Zheng Y, Stephens BS, Handel TM. What Do Structures Tell Us About Chemokine Receptor Function and Antagonism? Annual review of biophysics. 2017;46:175-98.
115. Mantovani A, Bonecchi R, Locati M. Tuning inflammation and immunity by chemokine sequestration: decoys and more. Nat Rev Immunol. 2006;6(12):907-18.
116. Ulvmar MH, Hub E, Rot A. Atypical chemokine receptors. Experimental cell research. 2011;317(5):556-68.
117. Cotton M, Claing A. G protein-coupled receptors stimulation and the control of cell migration. Cellular signalling. 2009;21(7):1045-53.
118. Griffith JW, Sokol CL, Luster AD. Chemokines and chemokine receptors: positioning cells for host defense and immunity. Annual review of immunology. 2014;32:659-702.
119. Ritter SL, Hall RA. Fine-tuning of GPCR activity by receptor-interacting proteins. Nature reviews Molecular cell biology. 2009;10(12):819-30.
120. Neves SR, Ram PT, Iyengar R. G protein pathways. Science (New York, NY). 2002;296(5573):1636-9.
121. Arai H, Charo IF. Differential regulation of G-protein-mediated signaling by chemokine receptors. J Biol Chem. 1996;271(36):21814-9.
122. Kufareva I, Salanga CL, Handel TM. Chemokine and chemokine receptor structure and interactions: implications for therapeutic strategies. Immunol Cell Biol. 2015;93(4):372-83.
123. Crump MP, Gong JH, Loetscher P, Rajarathnam K, Amara A, Arenzana-Seisdedos F, et al. Solution structure and basis for functional activity of stromal cell-derived factor-1; dissociation of CXCR4 activation from binding and inhibition of HIV-1. The EMBO journal. 1997;16(23):6996-7007.
124. Campanella GS, Lee EM, Sun J, Luster AD. CXCR3 and heparin binding sites of the chemokine IP-10 (CXCL10). J Biol Chem. 2003;278(19):17066-74.
125. Comerford I, Litchfield W, Harata-Lee Y, Nibbs RJ, McColl SR. Regulation of chemotactic networks by 'atypical' receptors. BioEssays : news and reviews in molecular, cellular and developmental biology. 2007;29(3):237-47.
126. Locati M, Torre YM, Galliera E, Bonecchi R, Bodduluri H, Vago G, et al. Silent chemoattractant receptors: D6 as a decoy and scavenger receptor for inflammatory CC chemokines. Cytokine & growth factor reviews. 2005;16(6):679-86.
127. Mantovani A. The chemokine system: redundancy for robust outputs. Immunology today. 1999;20(6):254-7.
128. Hartwell L. Theoretical biology. A robust view of biochemical pathways. Nature. 1997;387(6636):855, 7.
129. Barkai N, Leibler S. Robustness in simple biochemical networks. Nature. 1997;387(6636):913-7.
130. Ben-Baruch A, Michiel DF, Oppenheim JJ. Signals and receptors involved in recruitment of inflammatory cells. J Biol Chem. 1995;270(20):11703-6.
131. Garin A, Proudfoot AE. Chemokines as targets for therapy. Experimental cell research. 2011;317(5):602-12.
132. Szalai C, Duba J, Prohaszka Z, Kalina A, Szabo T, Nagy B, et al. Involvement of polymorphisms in the chemokine system in the susceptibility for coronary artery disease (CAD). Coincidence of elevated Lp(a) and MCP-1 -2518 G/G genotype in CAD patients. Atherosclerosis. 2001;158(1):233-9.

133. Kim MP, Wahl LM, Yanek LR, Becker DM, Becker LC. A monocyte chemoattractant protein-1 gene polymorphism is associated with occult ischemia in a high-risk asymptomatic population. Atherosclerosis. 2007;193(2):366-72.
134. Alonso-Villaverde C, Coll B, Parra S, Montero M, Calvo N, Tous M, et al. Atherosclerosis in patients infected with HIV is influenced by a mutant monocyte chemoattractant protein-1 allele. Circulation. 2004;110(15):2204-9.
135. Bai J, Song H, Cai C, Zhang M, Xu S, Tan J. The association of monocyte chemotactic protein-1 and CC chemokine receptor 2 gene variants with chronic obstructive pulmonary disease. DNA and cell biology. 2012;31(6):1058-63.
136. Simeoni E, Winkelmann BR, Hoffmann MM, Fleury S, Ruiz J, Kappenberger L, et al. Association of RANTES G-403A gene polymorphism with increased risk of coronary arteriosclerosis. European heart journal. 2004;25(16):1438-46.
137. Boger CA, Fischereder M, Deinzer M, Aslanidis C, Schmitz G, Stubanus M, et al. RANTES gene polymorphisms predict all-cause and cardiac mortality in type 2 diabetes mellitus hemodialysis patients. Atherosclerosis. 2005;183(1):121-9.
138. Nakamura H, Luster AD, Nakamura T, In KH, Sonna LA, Deykin A, et al. Variant eotaxin: its effects on the asthma phenotype. J Allergy Clin Immunol. 2001;108(6):946-53.
139. Zee RY, Cook NR, Cheng S, Erlich HA, Lindpaintner K, Lee RT, et al. Threonine for alanine substitution in the eotaxin (CCL11) gene and the risk of incident myocardial infarction. Atherosclerosis. 2004;175(1):91-4.
140. Strimbu K, Tavel JA. What are Biomarkers? Curr Opin HIV AIDS. 2010;5(6):463-6.
141. Tiffany HL, Lautens LL, Gao JL, Pease J, Locati M, Combadiere C, et al. Identification of CCR8: a human monocyte and thymus receptor for the CC chemokine I-309. The Journal of experimental medicine. 1997;186(1):165-70.
142. Ardigo D, Assimes TL, Fortmann SP, Go AS, Hlatky M, Hytopoulos E, et al. Circulating chemokines accurately identify individuals with clinically significant atherosclerotic heart disease. Physiological genomics. 2007;31(3):402-9.
143. Haley KJ, Lilly CM, Yang JH, Feng Y, Kennedy SP, Turi TG, et al. Overexpression of eotaxin and the CCR3 receptor in human atherosclerosis: using genomic technology to identify a potential novel pathway of vascular inflammation. Circulation. 2000;102(18):2185-9.
144. Weber C, Meiler S, Doring Y, Koch M, Drechsler M, Megens RT, et al. CCL17-expressing dendritic cells drive atherosclerosis by restraining regulatory T cell homeostasis in mice. The Journal of clinical investigation. 2011;121(7):2898-910.
145. Damas JK, Smith C, Oie E, Fevang B, Halvorsen B, Waehre T, et al. Enhanced expression of the homeostatic chemokines CCL19 and CCL21 in clinical and experimental atherosclerosis: possible pathogenic role in plaque destabilization. Arteriosclerosis, thrombosis, and vascular biology. 2007;27(3):614-20.
146. Calvayrac O, Rodriguez-Calvo R, Alonso J, Orbe J, Martin-Ventura JL, Guadall A, et al. CCL20 is increased in hypercholesterolemic subjects and is upregulated by LDL in vascular smooth muscle cells: role of NF-kappaB. Arteriosclerosis, thrombosis, and vascular biology. 2011;31(11):2733-41.
147. Mach F, Sauty A, Iarossi AS, Sukhova GK, Neote K, Libby P, et al. Differential expression of three T lymphocyte-activating CXC chemokines by human atheroma-associated cells. The Journal of clinical investigation. 1999;104(8):1041-50.
148. Lehrke M, Millington SC, Lefterova M, Cumaranatunge RG, Szapary P, Wilensky R, et al. CXCL16 is a marker of inflammation, atherosclerosis, and acute coronary syndromes in humans. Journal of the American College of Cardiology. 2007;49(4):442-9.
149. Zhang X, Feng X, Cai W, Liu T, Liang Z, Sun Y, et al. Chemokine CX3CL1 and its receptor CX3CR1 are associated with human atherosclerotic lesion volnerability. Thrombosis research. 2015;135(6):1147-53.

150. Savioli B, Abdulahad WH, Brouwer E, Kallenberg CGM, de Souza AWS. Are cytokines and chemokines suitable biomarkers for Takayasu arteritis? Autoimmunity reviews. 2017;16(10):1071-8.
151. Damas JK, Gullestad L, Ueland T, Solum NO, Simonsen S, Froland SS, et al. CXC-chemokines, a new group of cytokines in congestive heart failure--possible role of platelets and monocytes. Cardiovascular research. 2000;45(2):428-36.
152. Fujita K, Matsui N, Takahashi Y, Iwasaki Y, Yoshida M, Yuasa T, et al. Increased interleukin-17 in the cerebrospinal fluid in sporadic Creutzfeldt-Jakob disease: a case-control study of rapidly progressive dementia. J Neuroinflammation. 102013. p. 135.
153. Bo SH, Davidsen EM, Gulbrandsen P, Dietrichs E, Bovim G, Stovner LJ, et al. Cerebrospinal fluid cytokine levels in migraine, tension-type headache and cervicogenic headache. Cephalalgia : an international journal of headache. 2009;29(3):365-72.
154. Biber K, Zuurman MW, Dijkstra IM, Boddeke HW. Chemokines in the brain: neuroimmunology and beyond. Current opinion in pharmacology. 2002;2(1):63-8.
155. de Jager W, Hoppenreijs EP, Wulffraat NM, Wedderburn LR, Kuis W, Prakken BJ. Blood and synovial fluid cytokine signatures in patients with juvenile idiopathic arthritis: a cross-sectional study. Annals of the rheumatic diseases. 2007;66(5):589-98.
156. Kukielka GL, Smith CW, LaRosa GJ, Manning AM, Mendoza LH, Daly TJ, et al. Interleukin-8 gene induction in the myocardium after ischemia and reperfusion in vivo. The Journal of clinical investigation. 1995;95(1):89-103.
157. Ono K, Matsumori A, Furukawa Y, Igata H, Shioi T, Matsushima K, et al. Prevention of myocardial reperfusion injury in rats by an antibody against monocyte chemotactic and activating factor/monocyte chemoattractant protein-1. Laboratory investigation; a journal of technical methods and pathology. 1999;79(2):195-203.
158. Boring L, Gosling J, Cleary M, Charo IF. Decreased lesion formation in CCR2-/- mice reveals a role for chemokines in the initiation of atherosclerosis. Nature. 1998;394(6696):894-7.
159. Gu L, Okada Y, Clinton SK, Gerard C, Sukhova GK, Libby P, et al. Absence of monocyte chemoattractant protein-1 reduces atherosclerosis in low density lipoprotein receptor-deficient mice. Molecular cell. 1998;2(2):275-81.
160. Harada A, Sekido N, Akahoshi T, Wada T, Mukaida N, Matsushima K. Essential involvement of interleukin-8 (IL-8) in acute inflammation. Journal of leukocyte biology. 1994;56(5):559-64.
161. Wada T, Tomosugi N, Naito T, Yokoyama H, Kobayashi K, Harada A, et al. Prevention of proteinuria by the administration of anti-interleukin 8 antibody in experimental acute immune complex-induced glomerulonephritis. The Journal of experimental medicine. 1994;180(3):1135-40.
162. Sekido N, Mukaida N, Harada A, Nakanishi I, Watanabe Y, Matsushima K. Prevention of lung reperfusion injury in rabbits by a monoclonal antibody against interleukin-8. Nature. 1993;365(6447):654-7.
163. Broaddus VC, Boylan AM, Hoeffel JM, Kim KJ, Sadick M, Chuntharapai A, et al. Neutralization of IL-8 inhibits neutrophil influx in a rabbit model of endotoxin-induced pleurisy. Journal of immunology (Baltimore, Md : 1950). 1994;152(6):2960-7.
164. Lappano R, Maggiolini M. Pharmacotherapeutic Targeting of G Protein-Coupled Receptors in Oncology: Examples of Approved Therapies and Emerging Concepts. Drugs. 2017;77(9):951-65.
165. Scholten DJ, Canals M, Maussang D, Roumen L, Smit MJ, Wijtmans M, et al. Pharmacological modulation of chemokine receptor function. British journal of pharmacology. 2012;165(6):1617-43.

166. A. Klarenbeek DM, C. Blanchetot, M. Saunders, S. van der Woning, M. Smit, et al. Targeting chemokines and chemokine receptors with antibodies. Drug discovery today Technologies. 2012;9(4):e227-314.
167. Szekanecz Z, Koch AE. Successes and failures of chemokine-pathway targeting in rheumatoid arthritis. Nature reviews Rheumatology. 2016;12(1):5-13.
168. Haringman JJ, Gerlag DM, Smeets TJ, Baeten D, van den Bosch F, Bresnihan B, et al. A randomized controlled trial with an anti-CCL2 (anti-monocyte chemotactic protein 1) monoclonal antibody in patients with rheumatoid arthritis. Arthritis and rheumatism. 2006;54(8):2387-92.
169. Vergunst CE, Gerlag DM, von Moltke L, Karol M, Wyant T, Chi X, et al. MLN3897 plus methotrexate in patients with rheumatoid arthritis: safety, efficacy, pharmacokinetics, and pharmacodynamics of an oral CCR1 antagonist in a phase IIa, double-blind, placebo-controlled, randomized, proof-of-concept study. Arthritis and rheumatism. 2009;60(12):3572-81.
170. Zipp F, Hartung HP, Hillert J, Schimrigk S, Trebst C, Stangel M, et al. Blockade of chemokine signaling in patients with multiple sclerosis. Neurology. 2006;67(10):1880-3.
171. Proudfoot AE, Bonvin P, Power CA. Targeting chemokines: Pathogens can, why can't we? Cytokine. 2015;74(2):259-67.
172. Smith P, Fallon RE, Mangan NE, Walsh CM, Saraiva M, Sayers JR, et al. Schistosoma mansoni secretes a chemokine binding protein with antiinflammatory activity. The Journal of experimental medicine. 2005;202(10):1319-25.
173. Alcami A, Lira SA. Modulation of chemokine activity by viruses. Current opinion in immunology. 2010;22(4):482-7.
174. Bonvin P, Power CA, Proudfoot AEI. Evasins: Therapeutic Potential of a New Family of Chemokine-Binding Proteins from Ticks. Frontiers in immunology. 2016;7.
175. Singh K, Davies G, Alenazi Y, Eaton JRO, Kawamura A, Bhattacharya S. Yeast surface display identifies a family of evasins from ticks with novel polyvalent CC chemokine-binding activities. Sci Rep. 2017;7(1):4267.
176. Hotez PJ, Brindley PJ, Bethony JM, King CH, Pearce EJ, Jacobson J. Helminth infections: the great neglected tropical diseases. The Journal of clinical investigation. 2008;118(4):1311-21.
177. McSorley HJ, Maizels RM. Helminth Infections and Host Immune Regulation. Clin Microbiol Rev. 252012. p. 585-608.
178. Pearce EJ, MacDonald AS. The immunobiology of schistosomiasis. Nat Rev Immunol. 2002;2(7):499-511.
179. Lucas M, Karrer U, Lucas A, Klenerman P. Viral escape mechanisms--escapology taught by viruses. International journal of experimental pathology. 2001;82(5):269-86.
180. Seet BT, McFadden G. Viral chemokine-binding proteins. Journal of leukocyte biology. 2002;72(1):24-34.
181. Heidarieh H, Hernaez B, Alcami A. Immune modulation by virus-encoded secreted chemokine binding proteins. Virus research. 2015;209:67-75.
182. Lubman OY, Fremont DH. Parallel Evolution of Chemokine Binding by Structurally Related Herpesvirus Decoy Receptors. Structure (London, England : 1993). 2016;24(1):57-69.
183. Bryant NA, Davis-Poynter N, Vanderplasschen A, Alcami A. Glycoprotein G isoforms from some alphaherpesviruses function as broad-spectrum chemokine binding proteins. The EMBO journal. 222003. p. 833-46.
184. van Berkel V, Barrett J, Tiffany HL, Fremont DH, Murphy PM, McFadden G, et al. Identification of a gammaherpesvirus selective chemokine binding protein that inhibits chemokine action. Journal of virology. 2000;74(15):6741-7.

185. Pyo R, Jensen KK, Wiekowski MT, Manfra D, Alcami A, Taubman MB, et al. Inhibition of intimal hyperplasia in transgenic mice conditionally expressing the chemokine-binding protein M3. Am J Pathol. 2004;164(6):2289-97.
186. Martin AP, Alexander-Brett JM, Canasto-Chibuque C, Garin A, Bromberg JS, Fremont DH, et al. The chemokine binding protein M3 prevents diabetes induced by multiple low doses of streptozotocin. Journal of immunology (Baltimore, Md : 1950). 2007;178(7):4623-31.
187. Liu L, Lalani A, Dai E, Seet B, Macauley C, Singh R, et al. The viral anti-inflammatory chemokine-binding protein M-T7 reduces intimal hyperplasia after vascular injury. The Journal of clinical investigation. 1052000. p. 1613-21.
188. Parry CM, Simas JP, Smith VP, Stewart CA, Minson AC, Efstathiou S, et al. A broad spectrum secreted chemokine binding protein encoded by a herpesvirus. The Journal of experimental medicine. 2000;191(3):573-8.
189. Cupp EW. Biology of ticks. The Veterinary clinics of North America Small animal practice. 1991;21(1):1-26.
190. Francischetti IM, Sá-Nunes A, Mans BJ, Santos IM, Ribeiro JM. THE ROLE OF SALIVA IN TICK FEEDING. Front Biosci.14:2051-88.
191. Hajnicka V, Kocakova P, Slavikova M, Slovak M, Gasperik J, Fuchsberger N, et al. Anti-interleukin-8 activity of tick salivary gland extracts. Parasite Immunol. 2001;23(9):483-9.
192. Frauenschuh A, Power CA, Deruaz M, Ferreira BR, Silva JS, Teixeira MM, et al. Molecular cloning and characterization of a highly selective chemokine-binding protein from the tick Rhipicephalus sanguineus. J Biol Chem. 2007;282(37):27250-8.
193. Deruaz M, Frauenschuh A, Alessandri AL, Dias JM, Coelho FM, Russo RC, et al. Ticks produce highly selective chemokine binding proteins with antiinflammatory activity. The Journal of experimental medicine. 2008;205(9):2019-31.
194. Deruaz M, Bonvin P, Severin IC, Johnson Z, Krohn S, Power CA, et al. Evasin-4, a tick-derived chemokine-binding protein with broad selectivity can be modified for use in preclinical disease models. FEBS J. 2013;280(19):4876-87.
195. Karim S, Singh P, Ribeiro JM. A deep insight into the sialotranscriptome of the gulf coast tick, Amblyomma maculatum. PloS one. 2011;6(12):e28525.
196. Radulovic ZM, Kim TK, Porter LM, Sze SH, Lewis L, Mulenga A. A 24-48 h fed Amblyomma americanum tick saliva immuno-proteome. BMC genomics. 2014;15:518.
197. Vancova I, Hajnicka V, Slovak M, Nuttall PA. Anti-chemokine activities of ixodid ticks depend on tick species, developmental stage, and duration of feeding. Veterinary parasitology. 2010;167(2-4):274-8.
198. Hayward J, Sanchez J, Perry A, Huang C, Rodriguez Valle M, Canals M, et al. Ticks from diverse genera encode chemokine-inhibitory evasin proteins. J Biol Chem. 2017;292(38):15670-80.
199. Vancova I, Hajnicka V, Slovak M, Kocakova P, Paesen GC, Nuttall PA. Evasin-3-like anti-chemokine activity in salivary gland extracts of ixodid ticks during blood-feeding: a new target for tick control. Parasite Immunol. 2010;32(6):460-3.
200. Dias JM, Losberger C, Deruaz M, Power CA, Proudfoot AE, Shaw JP. Structural basis of chemokine sequestration by a tick chemokine binding protein: the crystal structure of the complex between Evasin-1 and CCL3. PloS one. 2009;4(12):e8514.
201. Bonvin P, Dunn SM, Rousseau F, Dyer DP, Shaw J, Power CA, et al. Identification of the pharmacophore of the CC chemokine-binding proteins Evasin-1 and -4 using phage display. J Biol Chem. 2014;289(46):31846-55.
202. Russo RC, Alessandri AL, Garcia CC, Cordeiro BF, Pinho V, Cassali GD, et al. Therapeutic effects of evasin-1, a chemokine binding protein, in bleomycin-induced pulmonary fibrosis. Am J Respir Cell Mol Biol. 2011;45(1):72-80.

203. Nedoszytko B, Sokołowska-Wojdyło M, Ruckemann-Dziurdzińska K, Roszkiewicz J, Nowicki RJ. Chemokines and cytokines network in the pathogenesis of the inflammatory skin diseases: atopic dermatitis, psoriasis and skin mastocytosis. Postepy Dermatol Alergol. 312014. p. 84-91.
204. Castor MG, Rezende B, Resende CB, Alessandri AL, Fagundes CT, Sousa LP, et al. The CCL3/macrophage inflammatory protein-1alpha-binding protein evasin-1 protects from graft-versus-host disease but does not modify graft-versus-leukemia in mice. Journal of immunology (Baltimore, Md : 1950). 2010;184(5):2646-54.
205. Wysocki CA, Panoskaltsis-Mortari A, Blazar BR, Serody JS. Leukocyte migration and graft-versus-host disease. Blood. 1052005. p. 4191-9.
206. Braunersreuther V, Montecucco F, Pelli G, Galan K, Proudfoot AE, Belin A, et al. Treatment with the CC chemokine-binding protein Evasin-4 improves post-infarction myocardial injury and survival in mice. Thromb Haemost. 2013;110(4):807-25.
207. Copin JC, da Silva RF, Fraga-Silva RA, Capettini L, Quintao S, Lenglet S, et al. Treatment with Evasin-3 reduces atherosclerotic vulnerability for ischemic stroke, but not brain injury in mice. J Cereb Blood Flow Metab. 2013;33(4):490-8.
208. Montecucco F, Mach F, Lenglet S, Vonlaufen A, Gomes Quindere AL, Pelli G, et al. Treatment with Evasin-3 abrogates neutrophil-mediated inflammation in mouse acute pancreatitis. Eur J Clin Invest. 2014;44(10):940-50.
209. Zhao Y, Bishop B, Clay JE, Lu W, Jones M, Daenke S, et al. Automation of large scale transient protein expression in mammalian cells. Journal of structural biology. 2011;175(2):209-15.
210. Schmidt TG, Skerra A. The Strep-tag system for one-step purification and high-affinity detection or capturing of proteins. Nature protocols. 2007;2(6):1528-35.
211. Ho M, Nagata S, Pastan I. Isolation of anti-CD22 Fv with high affinity by Fv display on human cells. Proceedings of the National Academy of Sciences of the United States of America. 2006;103(25):9637-42.
212. Bendtsen JD, Nielsen H, von Heijne G, Brunak S. Improved prediction of signal peptides: SignalP 3.0. Journal of molecular biology. 2004;340(4):783-95.
213. Altschul SF, Madden TL, Schaffer AA, Zhang J, Zhang Z, Miller W, et al. Gapped BLAST and PSI-BLAST: a new generation of protein database search programs. Nucleic acids research. 1997;25(17):3389-402.
214. Rod Chalk GB, Leela Shrestha, Claire Strain-Damerell, Pravin Mahajan, Wyatt W. Yue, Opher Gileadi and Nicola A. Burgess-Brown. High-Throughput Mass Spectrometry Applied to Structural Genomics. Chromatography2014. p. 159-75.
215. Horuk R. Chemokine receptor antagonists: overcoming developmental hurdles. Nature reviews Drug discovery. 2009;8(1):23-33.
216. Proudfoot AE, Uguccioni M. Modulation of Chemokine Responses: Synergy and Cooperativity. Frontiers in immunology. 2016;7:183.
217. Brandes M, Klauschen F, Kuchen S, Germain RN. A systems analysis identifies a feedforward inflammatory circuit leading to lethal influenza infection. Cell. 2013;154(1):197-212.
218. Hütter G, Bodor J, Ledger S, Boyd M, Millington M, Tsie M, et al. CCR5 Targeted Cell Therapy for HIV and Prevention of Viral Escape. Viruses. 72015. p. 4186-203.
219. Hovius JW. Spitting image: tick saliva assists the causative agent of Lyme disease in evading host skin's innate immune response. The Journal of investigative dermatology. 2009;129(10):2337-9.
220. Barker SC, Murrell A. Systematics and evolution of ticks with a list of valid genus and species names. Parasitology. 2004;129 Suppl:S15-36.

221. Sarrion-Perdigones A, Falconi EE, Zandalinas SI, Juarez P, Fernandez-del-Carmen A, Granell A, et al. GoldenBraid: an iterative cloning system for standardized assembly of reusable genetic modules. PloS one. 2011;6(7):e21622.
222. Burns JM, Dairaghi DJ, Deitz M, Tsang M, Schall TJ. Comprehensive mapping of poxvirus vCCI chemokine-binding protein. Expanded range of ligand interactions and unusual dissociation kinetics. J Biol Chem. 2002;277(4):2785-9.
223. Alexander JM, Nelson CA, van Berkel V, Lau EK, Studts JM, Brett TJ, et al. Structural basis of chemokine sequestration by a herpesvirus decoy receptor. Cell. 2002;111(3):343-56.
224. Boder ET, Wittrup KD. Yeast surface display for screening combinatorial polypeptide libraries. Nature biotechnology. 1997;15(6):553-7.
225. Wikel SK, Ramachandra RN, Bergman DK. Tick-induced modulation of the host immune response. International journal for parasitology. 1994;24(1):59-66.
226. Šimo L, Kazimirova M, Richardson J, Bonnet SI. The Essential Role of Tick Salivary Glands and Saliva in Tick Feeding and Pathogen Transmission. Front Cell Infect Microbiol. 2017;7.
227. Kiewra D, Lonc E. Epidemiological consequences of host specificity of ticks (Ixodida). Annals of parasitology. 2012;58(4):181-7.
228. Hlavacek WS, Posner RG, Perelson AS. Steric effects on multivalent ligand-receptor binding: exclusion of ligand sites by bound cell surface receptors. Biophys J. 1999;76(6):3031-43.
229. Reddy Chichili VP, Kumar V, Sivaraman J. Linkers in the structural biology of protein-protein interactions. Protein science : a publication of the Protein Society. 2013;22(2):153-67.
230. Pepper LR, Cho YK, Boder ET, Shusta EV. A decade of yeast surface display technology: where are we now? Combinatorial chemistry & high throughput screening. 2008;11(2):127-34.
231. Wildgruber M, Lee H, Chudnovskiy A, Yoon TJ, Etzrodt M, Pittet MJ, et al. Monocyte subset dynamics in human atherosclerosis can be profiled with magnetic nano-sensors. PloS one. 2009;4(5):e5663.
232. Schlitt A, Heine GH, Blankenberg S, Espinola-Klein C, Dopheide JF, Bickel C, et al. CD14+CD16+ monocytes in coronary artery disease and their relationship to serum TNF-alpha levels. Thromb Haemost. 2004;92(2):419-24.
233. Grip O, Bredberg A, Lindgren S, Henriksson G. Increased subpopulations of CD16(+) and CD56(+) blood monocytes in patients with active Crohn's disease. Inflammatory bowel diseases. 2007;13(5):566-72.
234. Kawanaka N, Yamamura M, Aita T, Morita Y, Okamoto A, Kawashima M, et al. CD14+,CD16+ blood monocytes and joint inflammation in rheumatoid arthritis. Arthritis and rheumatism. 2002;46(10):2578-86.
235. Rothe G, Gabriel H, Kovacs E, Klucken J, Stohr J, Kindermann W, et al. Peripheral blood mononuclear phagocyte subpopulations as cellular markers in hypercholesterolemia. Arteriosclerosis, thrombosis, and vascular biology. 1996;16(12):1437-47.
236. Haque NS, Zhang X, French DL, Li J, Poon M, Fallon JT, et al. CC chemokine I-309 is the principal monocyte chemoattractant induced by apolipoprotein(a) in human vascular endothelial cells. Circulation. 2000;102(7):786-92.
237. Yu R, Kim CS, Kawada T, Kwon TW, Lim TH, Kim YW, et al. Involvement of leukotactin-1, a novel CC chemokine, in human atherosclerosis. Atherosclerosis. 2004;174(1):35-42.
238. Erbel C, Sato K, Meyer FB, Kopecky SL, Frye RL, Goronzy JJ, et al. Functional profile of activated dendritic cells in unstable atherosclerotic plaque. Basic research in cardiology. 2007;102(2):123-32.

239. Kimura S, Tanimoto A, Wang KY, Shimajiri S, Guo X, Tasaki T, et al. Expression of macrophage-derived chemokine (CCL22) in atherosclerosis and regulation by histamine via the H2 receptor. Pathology international. 2012;62(10):675-83.
240. Kim CS, Kang JH, Cho HR, Blankenship TN, Erickson KL, Kawada T, et al. Potential involvement of CCL23 in atherosclerotic lesion formation/progression by the enhancement of chemotaxis, adhesion molecule expression, and MMP-2 release from monocytes. Inflammation research : official journal of the European Histamine Research Society [et al]. 2011;60(9):889-95.
241. Abd Alla J, Langer A, Elzahwy SS, Arman-Kalcek G, Streichert T, Quitterer U. Angiotensin-converting enzyme inhibition down-regulates the pro-atherogenic chemokine receptor 9 (CCR9)-chemokine ligand 25 (CCL25) axis. J Biol Chem. 2010;285(30):23496-505.
242. Castillo L, Rohatgi A, Ayers CR, Owens AW, Das SR, Khera A, et al. Associations of four circulating chemokines with multiple atherosclerosis phenotypes in a large population-based sample: results from the dallas heart study. Journal of interferon & cytokine research : the official journal of the International Society for Interferon and Cytokine Research. 2010;30(5):339-47.
243. Montecucco F, Braunersreuther V, Lenglet S, Delattre BM, Pelli G, Buatois V, et al. CC chemokine CCL5 plays a central role impacting infarct size and post-infarction heart failure in mice. European heart journal. 2012;33(15):1964-74.
244. Frangogiannis NG, Youker KA, Rossen RD, Gwechenberger M, Lindsey MH, Mendoza LH, et al. Cytokines and the microcirculation in ischemia and reperfusion. Journal of molecular and cellular cardiology. 1998;30(12):2567-76.
245. Nossuli TO, Frangogiannis NG, Knuefermann P, Lakshminarayanan V, Dewald O, Evans AJ, et al. Brief murine myocardial I/R induces chemokines in a TNF-alpha-independent manner: role of oxygen radicals. American journal of physiology Heart and circulatory physiology. 2001;281(6):H2549-58.
246. de Jager SC, Bongaerts BW, Weber M, Kraaijeveld AO, Rousch M, Dimmeler S, et al. Chemokines CCL3/MIP1alpha, CCL5/RANTES and CCL18/PARC are independent risk predictors of short-term mortality in patients with acute coronary syndromes. PloS one. 2012;7(9):e45804.
247. Finsen AV, Ueland T, Sjaastad I, Ranheim T, Ahmed MS, Dahl CP, et al. The homeostatic chemokine CCL21 predicts mortality in aortic stenosis patients and modulates left ventricular remodeling. PloS one. 2014;9(11):e112172.
248. Marino AP, Silva AA, Santos PV, Pinto LM, Gazinelli RT, Teixeira MM, et al. CC-chemokine receptors: a potential therapeutic target for Trypanosoma cruzi-elicited myocarditis. Memorias do Instituto Oswaldo Cruz. 2005;100 Suppl 1:93-6.
249. Wéra O, Lancellotti P, Oury C. The Dual Role of Neutrophils in Inflammatory Bowel Diseases. J Clin Med. 52016.
250. Fleishaker DL, Garcia Meijide JA, Petrov A, Kohen MD, Wang X, Menon S, et al. Maraviroc, a chemokine receptor-5 antagonist, fails to demonstrate efficacy in the treatment of patients with rheumatoid arthritis in a randomized, double-blind placebo-controlled trial. Arthritis research & therapy. 2012;14(1):R11.
251. Alejo A, Ruiz-Arguello MB, Ho Y, Smith VP, Saraiva M, Alcami A. A chemokine-binding domain in the tumor necrosis factor receptor from variola (smallpox) virus. Proceedings of the National Academy of Sciences of the United States of America. 2006;103(15):5995-6000.
252. Alenazi Y, Singh K, Davies G, Eaton JRO, Elders P, Kawamura A, et al. Genetically engineered two-warhead evasins provide a method to achieve precision targeting of disease-relevant chemokine subsets. Sci Rep. 82018.

253. Schmolke M, Garcia-Sastre A. Evasion of innate and adaptive immune responses by influenza A virus. Cellular microbiology. 2010;12(7):873-80.
254. Mahla RS, Reddy MC, Prasad DVR, Kumar H. Sweeten PAMPs: Role of Sugar Complexed PAMPs in Innate Immunity and Vaccine Biology. Frontiers in immunology. 2013;4.
255. Kawai T, Akira S. The role of pattern-recognition receptors in innate immunity: update on Toll-like receptors. Nature immunology. 2010;11(5):373-84.
256. Sommerstein R, Flatz L, Remy MM, Malinge P, Magistrelli G, Fischer N, et al. Arenavirus Glycan Shield Promotes Neutralizing Antibody Evasion and Protracted Infection. PLoS pathogens. 2015;11(11):e1005276.
257. Wei X, Decker JM, Wang S, Hui H, Kappes JC, Wu X, et al. Antibody neutralization and escape by HIV-1. Nature. 2003;422(6929):307-12.
258. Greinacher A, Warkentin TE. The direct thrombin inhibitor hirudin. Thromb Haemost. 2008;99(5):819-29.
259. Parkes DG, Mace KF, Trautmann ME. Discovery and development of exenatide: the first antidiabetic agent to leverage the multiple benefits of the incretin hormone, GLP-1. Expert opinion on drug discovery. 2013;8(2):219-44.
260. Sola RJ, Rodriguez-Martinez JA, Griebenow K. Modulation of protein biophysical properties by chemical glycosylation: biochemical insights and biomedical implications. Cellular and molecular life sciences : CMLS. 2007;64(16):2133-52.
261. Ohtsubo K, Marth JD. Glycosylation in cellular mechanisms of health and disease. Cell. 2006;126(5):855-67.
262. Croset A, Delafosse L, Gaudry JP, Arod C, Glez L, Losberger C, et al. Differences in the glycosylation of recombinant proteins expressed in HEK and CHO cells. Journal of biotechnology. 2012;161(3):336-48.
263. Fuse K, Kodama M, Hanawa H, Okura Y, Ito M, Shiono T, et al. Enhanced expression and production of monocyte chemoattractant protein-1 in myocarditis. Clinical and experimental immunology. 2001;124(3):346-52.
264. Kusano KF, Nakamura K, Kusano H, Nishii N, Banba K, Ikeda T, et al. Significance of the level of monocyte chemoattractant protein-1 in human atherosclerosis. Circulation journal : official journal of the Japanese Circulation Society. 2004;68(7):671-6.
265. Sorensen TL, Ransohoff RM, Strieter RM, Sellebjerg F. Chemokine CCL2 and chemokine receptor CCR2 in early active multiple sclerosis. European journal of neurology. 2004;11(7):445-9.
266. Hayashida K, Nanki T, Girschick H, Yavuz S, Ochi T, Lipsky PE. Synovial stromal cells from rheumatoid arthritis patients attract monocytes by producing MCP-1 and IL-8. Arthritis research. 2001;3(2):118-26.
267. Hefti FF. Requirements for a lead compound to become a clinical candidate. BMC Neurosci. 92008. p. S7.
268. Copeland RA, Pompliano DL, Meek TD. Drug-target residence time and its implications for lead optimization. Nature reviews Drug discovery. 2006;5(9):730-9.
269. Oppenheim JJ, Zachariae CO, Mukaida N, Matsushima K. Properties of the novel proinflammatory supergene "intercrine" cytokine family. Annual review of immunology. 1991;9:617-48.
270. Nomiyama H, Osada N, Yoshie O. Systematic classification of vertebrate chemokines based on conserved synteny and evolutionary history. Genes Cells. 2013;18(1):1-16.
271. Rollins BJ. Chemokines. Blood. 1997;90(3):909-28.
272. Jordan JE, Zhao ZQ, Vinten-Johansen J. The role of neutrophils in myocardial ischemia-reperfusion injury. Cardiovascular research. 1999;43(4):860-78.

273. Lin L, Wang X, Yu Z. Ischemia-reperfusion Injury in the Brain: Mechanisms and Potential Therapeutic Strategies. Biochem Pharmacol (Los Angel). 2016;5(4).
274. Grommes J, Soehnlein O. Contribution of Neutrophils to Acute Lung Injury. Mol Med. 172011. p. 293-307.
275. Kaneider NC, Agarwal A, Leger AJ, Kuliopulos A. Reversing systemic inflammatory response syndrome with chemokine receptor pepducins. Nature medicine. 2005;11(6):661-5.
276. Kyne L, Hausdorff JM, Knight E, Dukas L, Azhar G, Wei JY. Neutrophilia and congestive heart failure after acute myocardial infarction. American heart journal. 2000;139(1 Pt 1):94-100.
277. Chia S, Nagurney JT, Brown DF, Raffel OC, Bamberg F, Senatore F, et al. Association of leukocyte and neutrophil counts with infarct size, left ventricular function and outcomes after percutaneous coronary intervention for ST-elevation myocardial infarction. The American journal of cardiology. 2009;103(3):333-7.
278. Yunoki K, Naruko T, Komatsu R, Ehara S, Shirai N, Sugioka K, et al. Enhanced expression of haemoglobin scavenger receptor in accumulated macrophages of culprit lesions in acute coronary syndromes. European heart journal. 2009;30(15):1844-52.
279. Naruko T, Ueda M, Haze K, van der Wal AC, van der Loos CM, Itoh A, et al. Neutrophil infiltration of culprit lesions in acute coronary syndromes. Circulation. 2002;106(23):2894-900.
280. Tavora FR, Ripple M, Li L, Burke AP. Monocytes and neutrophils expressing myeloperoxidase occur in fibrous caps and thrombi in unstable coronary plaques. BMC cardiovascular disorders. 2009;9:27.
281. Ionita MG, van den Borne P, Catanzariti LM, Moll FL, de Vries JP, Pasterkamp G, et al. High neutrophil numbers in human carotid atherosclerotic plaques are associated with characteristics of rupture-prone lesions. Arteriosclerosis, thrombosis, and vascular biology. 2010;30(9):1842-8.
282. Nidorf SM, Eikelboom JW, Budgeon CA, Thompson PL. Low-dose colchicine for secondary prevention of cardiovascular disease. Journal of the American College of Cardiology. 2013;61(4):404-10.
283. Zlotnik A, Yoshie O. Chemokines: a new classification system and their role in immunity. Immunity. 2000;12(2):121-7.
284. Sadik CD, Kim ND, Luster AD. Neutrophils cascading their way to inflammation. Trends in immunology. 2011;32(10):452-60.
285. SolÁ RJ, Griebenow K. Effects of Glycosylation on the Stability of Protein Pharmaceuticals. J Pharm Sci. 2009;98(4):1223-45.
286. Zhang H, Aebersold R. Isolation of glycoproteins and identification of their N-linked glycosylation sites. Methods in molecular biology (Clifton, NJ). 2006;328:177-85.
287. S G. Protein production and purification. Nat Methods. 2008;5(2):135-46.
288. Yang D, Singh A, Wu H, Kroe-Barrett R. Determination of High-affinity Antibody-antigen Binding Kinetics Using Four Biosensor Platforms. Journal of visualized experiments : JoVE. 2017(122).
289. Gleissner CA, von Hundelshausen P, Ley K. Platelet chemokines in vascular disease. Arteriosclerosis, thrombosis, and vascular biology. 2008;28(11):1920-7.
290. Aleman MM, Wolberg AS. Tick Spit Shines a Light on the Initiation of Coagulation. Circulation. 2013;128(3).
291. Chmelar J, Oliveira CJ, Rezacova P, Francischetti IM, Kovarova Z, Pejler G, et al. A tick salivary protein targets cathepsin G and chymase and inhibits host inflammation and platelet aggregation. Blood. 2011;117(2):736-44.
292. Klompen JS, Black WCt, Keirans JE, Oliver JH, Jr. Evolution of ticks. Annual review of entomology. 1996;41:141-61.

293. de Oliveira RT, Mamoni RL, Souza JR, Fernandes JL, Rios FJ, Gidlund M, et al. Differential expression of cytokines, chemokines and chemokine receptors in patients with coronary artery disease. International journal of cardiology. 2009;136(1):17-26.
294. Carbone F, Nencioni A, Mach F, Vuilleumier N, Montecucco F. Pathophysiological role of neutrophils in acute myocardial infarction. Thromb Haemost. 2013;110(3):501-14.
295. Wright HL, Moots RJ, Edwards SW. The multifactorial role of neutrophils in rheumatoid arthritis. Nature reviews Rheumatology. 2014;10(10):593-601.
296. Strieter RM, Gomperts BN, Keane MP. The role of CXC chemokines in pulmonary fibrosis. The Journal of clinical investigation. 1172007. p. 549-56.
297. Montecucco F, Lenglet S, Braunersreuther V, Pelli G, Pellieux C, Montessuit C, et al. Single administration of the CXC chemokine-binding protein Evasin-3 during ischemia prevents myocardial reperfusion injury in mice. Arteriosclerosis, thrombosis, and vascular biology. 2010;30(7):1371-7.
298. Kukielka GL, Youker KA, Michael LH, Kumar AG, Ballantyne CM, Smith CW, et al. Role of early reperfusion in the induction of adhesion molecules and cytokines in previously ischemic myocardium. Molecular and cellular biochemistry. 1995;147(1-2):5-12.
299. Tarzami ST. Chemokines and inflammation in heart disease: adaptive or maladaptive? Int J Clin Exp Med. 2011;4(1):74-80.
300. Reape TJ, Rayner K, Manning CD, Gee AN, Barnette MS, Burnand KG, et al. Expression and cellular localization of the CC chemokines PARC and ELC in human atherosclerotic plaques. Am J Pathol. 1999;154(2):365-74.
301. Boisvert WA, Curtiss LK, Terkeltaub RA. Interleukin-8 and its receptor CXCR2 in atherosclerosis. Immunologic research. 2000;21(2-3):129-37.
302. Abi-Younes S, Sauty A, Mach F, Sukhova GK, Libby P, Luster AD. The stromal cell-derived factor-1 chemokine is a potent platelet agonist highly expressed in atherosclerotic plaques. Circulation research. 2000;86(2):131-8.
303. Villiger PM, Terkeltaub R, Lotz M. Production of monocyte chemoattractant protein-1 by inflamed synovial tissue and cultured synoviocytes. Journal of immunology (Baltimore, Md : 1950). 1992;149(2):722-7.
304. Volin MV, Shah MR, Tokuhira M, Haines GK, Woods JM, Koch AE. RANTES expression and contribution to monocyte chemotaxis in arthritis. Clinical immunology and immunopathology. 1998;89(1):44-53.
305. Smith RE, Strieter RM, Zhang K, Phan SH, Standiford TJ, Lukacs NW, et al. A role for C-C chemokines in fibrotic lung disease. Journal of leukocyte biology. 1995;57(5):782-7.
306. Chow MT, Luster AD. Chemokines in Cancer. Cancer Immunol Res. 2014;2(12):1125-31.
307. Woodcock J, Griffin JP, Behrman RE. Development of novel combination therapies. The New England journal of medicine. 2011;364(11):985-7.
308. Eaton JRO, Alenazi Y, Singh K, Davies G, Geis-Asteggiante L, Kessler B, et al. The N-terminal domain of a tick evasin is critical for chemokine binding and neutralization and confers specific binding activity to other evasins. J Biol Chem. 2018;293(16):6134-46.
309. Chen X, Zaro JL, Shen WC. Fusion protein linkers: property, design and functionality. Advanced drug delivery reviews. 2013;65(10):1357-69.
310. George RA, Heringa J. An analysis of protein domain linkers: their classification and role in protein folding. Protein engineering. 2002;15(11):871-9.
311. Lichty JJ, Malecki JL, Agnew HD, Michelson-Horowitz DJ, Tan S. Comparison of affinity tags for protein purification. Protein expression and purification. 2005;41(1):98-105.
312. Dumont JA, Low SC, Peters RT, Bitonti AJ. Monomeric Fc fusions: impact on pharmacokinetic and biological activity of protein therapeutics. BioDrugs : clinical immunotherapeutics, biopharmaceuticals and gene therapy. 2006;20(3):151-60.

313. Weimer T, Wormsbacher W, Kronthaler U, Lang W, Liebing U, Schulte S. Prolonged in-vivo half-life of factor VIIa by fusion to albumin. Thromb Haemost. 2008;99(4):659-67.
314. Zhao HL, Yao XQ, Xue C, Wang Y, Xiong XH, Liu ZM. Increasing the homogeneity, stability and activity of human serum albumin and interferon-alpha2b fusion protein by linker engineering. Protein expression and purification. 2008;61(1):73-7.
315. Amet N, Lee HF, Shen WC. Insertion of the designed helical linker led to increased expression of tf-based fusion proteins. Pharmaceutical research. 2009;26(3):523-8.
316. Bai Y, Ann DK, Shen WC. Recombinant granulocyte colony-stimulating factor-transferrin fusion protein as an oral myelopoietic agent. Proceedings of the National Academy of Sciences of the United States of America. 2005;102(20):7292-6.
317. Bai Y, Shen WC. Improving the oral efficacy of recombinant granulocyte colony-stimulating factor and transferrin fusion protein by spacer optimization. Pharmaceutical research. 2006;23(9):2116-21.
318. Mohanty AK, Wiener MC. Membrane protein expression and production: effects of polyhistidine tag length and position. Protein expression and purification. 2004;33(2):311-25.
319. Uhlen M, Forsberg G, Moks T, Hartmanis M, Nilsson B. Fusion proteins in biotechnology. Current opinion in biotechnology. 1992;3(4):363-9.
320. Debeljak N, Feldman L, Davis KL, Komel R, Sytkowski AJ. Variability in the immunodetection of His-tagged recombinant proteins. Analytical biochemistry. 2006;359(2):216-23.
321. Graham KA, Lalani AS, Macen JL, Ness TL, Barry M, Liu LY, et al. The T1/35kDa family of poxvirus-secreted proteins bind chemokines and modulate leukocyte influx into virus-infected tissues. Virology. 1997;229(1):12-24.
322. Linton MF, Yancey PG, Davies SS, Jerome WGJ, Linton EF, Vickers KC. The Role of Lipids and Lipoproteins in Atherosclerosis. 2015.
323. Braunersreuther V, Viviani GL, Mach F, Montecucco F. Role of cytokines and chemokines in non-alcoholic fatty liver disease. World J Gastroenterol. 2012;18(8):727-35.
324. Turner MD, Nedjai B, Hurst T, Pennington DJ. Cytokines and chemokines: At the crossroads of cell signalling and inflammatory disease. Biochimica et biophysica acta. 2014;1843(11):2563-82.
325. de Lemos JA, Morrow DA, Blazing MA, Jarolim P, Wiviott SD, Sabatine MS, et al. Serial measurement of monocyte chemoattractant protein-1 after acute coronary syndromes: results from the A to Z trial. Journal of the American College of Cardiology. 2007;50(22):2117-24.
326. Orn S, Breland UM, Mollnes TE, Manhenke C, Dickstein K, Aukrust P, et al. The chemokine network in relation to infarct size and left ventricular remodeling following acute myocardial infarction. The American journal of cardiology. 2009;104(9):1179-83.
327. Parissis JT, Adamopoulos S, Venetsanou KF, Mentzikof DG, Karas SM, Kremastinos DT. Serum profiles of C-C chemokines in acute myocardial infarction: possible implication in postinfarction left ventricular remodeling. Journal of interferon & cytokine research : the official journal of the International Society for Interferon and Cytokine Research. 2002;22(2):223-9.
328. Koch AE, Kunkel SL, Harlow LA, Johnson B, Evanoff HL, Haines GK, et al. Enhanced production of monocyte chemoattractant protein-1 in rheumatoid arthritis. The Journal of clinical investigation. 1992;90(3):772-9.
329. Hosaka S, Akahoshi T, Wada C, Kondo H. Expression of the chemokine superfamily in rheumatoid arthritis. Clinical and experimental immunology. 1994;97(3):451-7.
330. Iwamoto T, Okamoto H, Kobayashi S, Ikari K, Toyama Y, Tomatsu T, et al. A role of monocyte chemoattractant protein-4 (MCP-4)/CCL13 from chondrocytes in rheumatoid arthritis. Febs j. 2007;274(18):4904-12.

331. Okamoto H, Koizumi K, Yamanaka H, Saito T, Kamatani N. A role for TARC/CCL17, a CC chemokine, in systemic lupus erythematosus. The Journal of rheumatology. 2003;30(11):2369-73.
332. Auer J, Blass M, Schulze-Koops H, Russwurm S, Nagel T, Kalden JR, et al. Expression and regulation of CCL18 in synovial fluid neutrophils of patients with rheumatoid arthritis. Arthritis research & therapy. 2007;9(5):R94.
333. Momohara S, Okamoto H, Iwamoto T, Mizumura T, Ikari K, Kawaguchi Y, et al. High CCL18/PARC expression in articular cartilage and synovial tissue of patients with rheumatoid arthritis. The Journal of rheumatology. 2007;34(2):266-71.
334. Matsui T, Akahoshi T, Namai R, Hashimoto A, Kurihara Y, Rana M, et al. Selective recruitment of CCR6-expressing cells by increased production of MIP-3 alpha in rheumatoid arthritis. Clinical and experimental immunology. 2001;125(1):155-61.
335. Koch AE, Kunkel SL, Shah MR, Hosaka S, Halloran MM, Haines GK, et al. Growth-related gene product alpha. A chemotactic cytokine for neutrophils in rheumatoid arthritis. Journal of immunology (Baltimore, Md : 1950). 1995;155(7):3660-6.
336. Koch AE, Volin MV, Woods JM, Kunkel SL, Connors MA, Harlow LA, et al. Regulation of angiogenesis by the C-X-C chemokines interleukin-8 and epithelial neutrophil activating peptide 78 in the rheumatoid joint. Arthritis and rheumatism. 2001;44(1):31-40.
337. Koch AE, Kunkel SL, Burrows JC, Evanoff HL, Haines GK, Pope RM, et al. Synovial tissue macrophage as a source of the chemotactic cytokine IL-8. Journal of immunology (Baltimore, Md : 1950). 1991;147(7):2187-95.
338. Koch AE, Kunkel SL, Harlow LA, Mazarakis DD, Haines GK, Burdick MD, et al. Epithelial neutrophil activating peptide-78: a novel chemotactic cytokine for neutrophils in arthritis. The Journal of clinical investigation. 1994;94(3):1012-8.
339. Deleuran B, Lemche P, Kristensen M, Chu CQ, Field M, Jensen J, et al. Localisation of interleukin 8 in the synovial membrane, cartilage-pannus junction and chondrocytes in rheumatoid arthritis. Scandinavian journal of rheumatology. 1994;23(1):2-7.
340. Castor CW, Smith EM, Hossler PA, Bignall MC, Aaron BP. Connective tissue activation. XXXV. Detection of connective tissue activating peptide-III isoforms in synovium from osteoarthritis and rheumatoid arthritis patients: patterns of interaction with other synovial cytokines in cell culture. Arthritis and rheumatism. 1992;35(7):783-93.
341. Leuschner F, Katus HA, Kaya Z. Autoimmune myocarditis: past, present and future. Journal of autoimmunity. 2009;33(3-4):282-9.
342. Frangogiannis NG. The inflammatory response in myocardial injury, repair, and remodelling. Nature reviews Cardiology. 2014;11(5):255-65.
343. Eardley KS, Smith SW, Cockwell P. Chemokines in vasculitis. Frontiers in bioscience (Elite edition). 2009;1:26-35.
344. Leiman DA, Lichtenstein GR. Therapy of inflammatory bowel disease: what to expect in the next decade. Current opinion in gastroenterology. 2014;30(4):385-90.
345. Mestas J, Hughes CC. Of mice and not men: differences between mouse and human immunology. Journal of immunology (Baltimore, Md : 1950). 2004;172(5):2731-8.
346. Bonville CA, Percopo CM, Dyer KD, Gao J, Prussin C, Foster B, et al. Interferon-gamma coordinates CCL3-mediated neutrophil recruitment in vivo. BMC Immunol. 102009. p. 14.
347. Lehmann MH, Kuhnert H, Muller S, Sigusch HH. Monocyte chemoattractant protein 1 (MCP-1) gene expression in dilated cardiomyopathy. Cytokine. 1998;10(10):739-46.
348. Satoh M, Tamura G, Segawa I, Tashiro A, Hiramori K, Satodate R. Expression of cytokine genes and presence of enteroviral genomic RNA in endomyocardial biopsy tissues of myocarditis and dilated cardiomyopathy. Virchows Archiv : an international journal of pathology. 1996;427(5):503-9.

349. Brix SR, Stege G, Disteldorf E, Hoxha E, Krebs C, Krohn S, et al. CC Chemokine Ligand 18 in ANCA-Associated Crescentic GN. Journal of the American Society of Nephrology : JASN. 2015;26(9):2105-17.
350. Blaschke S, Brandt P, Wessels JT, Muller GA. Expression and function of the C-class chemokine lymphotactin (XCL1) in Wegener's granulomatosis. The Journal of rheumatology. 2009;36(11):2491-500.
351. Dallos T, Heiland GR, Strehl J, Karonitsch T, Gross WL, Moosig F, et al. CCL17/thymus and activation-related chemokine in Churg-Strauss syndrome. Arthritis and rheumatism. 2010;62(11):3496-503.
352. Eriksson P, Andersson C, Cassel P, Nystrom S, Ernerudh J. Increase in Th17-associated CCL20 and decrease in Th2-associated CCL22 plasma chemokines in active ANCA-associated vasculitis. Scandinavian journal of rheumatology. 2015;44(1):80-3.
353. Corbera-Bellalta M, Planas-Rigol E, Lozano E, Terrades-Garcia N, Alba MA, Prieto-Gonzalez S, et al. Blocking interferon gamma reduces expression of chemokines CXCL9, CXCL10 and CXCL11 and decreases macrophage infiltration in ex vivo cultured arteries from patients with giant cell arteritis. Annals of the rheumatic diseases. 2016;75(6):1177-86.
354. Bhatia M, Moochhala S. Role of inflammatory mediators in the pathophysiology of acute respiratory distress syndrome. The Journal of pathology. 2004;202(2):145-56.
355. Schmidt K, Martinez-Gamboa L, Meier S, Witt C, Meisel C, Hanitsch LG, et al. Bronchoalveoloar lavage fluid cytokines and chemokines as markers and predictors for the outcome of interstitial lung disease in systemic sclerosis patients. Arthritis research & therapy. 2009;11(4):R111.
356. Izzo RS, Witkon K, Chen AI, Hadjiyane C, Weinstein MI, Pellecchia C. Neutrophil-activating peptide (interleukin-8) in colonic mucosa from patients with Crohn's disease. Scandinavian journal of gastroenterology. 1993;28(4):296-300.
357. Puleston J, Cooper M, Murch S, Bid K, Makh S, Ashwood P, et al. A distinct subset of chemokines dominates the mucosal chemokine response in inflammatory bowel disease. Alimentary pharmacology & therapeutics. 2005;21(2):109-20.
358. Mahida YR, Ceska M, Effenberger F, Kurlak L, Lindley I, Hawkey CJ. Enhanced synthesis of neutrophil-activating peptide-1/interleukin-8 in active ulcerative colitis. Clinical science (London, England : 1979). 1992;82(3):273-5.
359. Ahrens R, Waddell A, Seidu L, Blanchard C, Carey R, Forbes E, et al. Intestinal macrophage/epithelial cell-derived CCL11/eotaxin-1 mediates eosinophil recruitment and function in pediatric ulcerative colitis. Journal of immunology (Baltimore, Md : 1950). 2008;181(10):7390-9.
360. Kotarsky K, Sitnik KM, Stenstad H, Kotarsky H, Schmidtchen A, Koslowski M, et al. A novel role for constitutively expressed epithelial-derived chemokines as antibacterial peptides in the intestinal mucosa. Mucosal immunology. 2010;3(1):40-8.
361. Banks C, Bateman A, Payne R, Johnson P, Sheron N. Chemokine expression in IBD. Mucosal chemokine expression is unselectively increased in both ulcerative colitis and Crohn's disease. The Journal of pathology. 2003;199(1):28-35.
362. Uguccioni M, Gionchetti P, Robbiani DF, Rizzello F, Peruzzo S, Campieri M, et al. Increased expression of IP-10, IL-8, MCP-1, and MCP-3 in ulcerative colitis. Am J Pathol. 1999;155(2):331-6.
363. Mazzucchelli L, Hauser C, Zgraggen K, Wagner HE, Hess MW, Laissue JA, et al. Differential in situ expression of the genes encoding the chemokines MCP-1 and RANTES in human inflammatory bowel disease. The Journal of pathology. 1996;178(2):201-6.

Chapter 9.

Appendices

Appendix A.

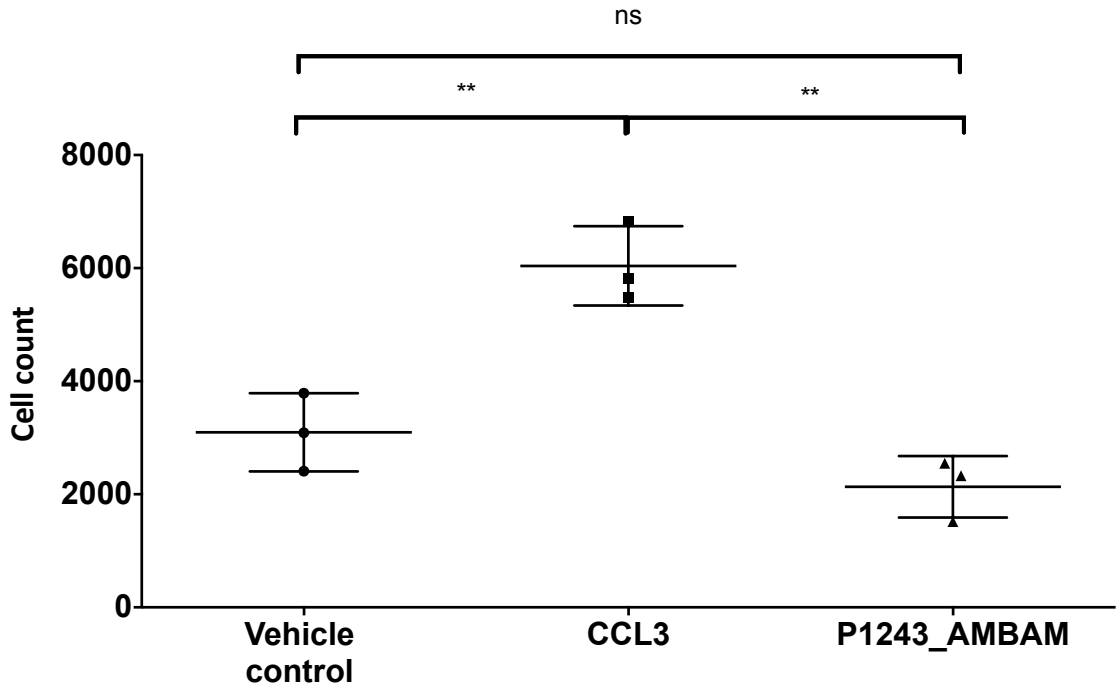


Figure A1. Effect of P1243 alone on cell migration. Y-axis shows cell count of THP-1 cells migrating through to the bottom chamber in response to vehicle control, CCL3 (EC80 dose, positive control) and P1243 (X-axis). Evasin was added at a dose of 100 nM (the maximum doses used the corresponding IC_{50} experiments). Data are presented as mean ± s.e.m, and individual data points from technical replicates. All samples contained 0.5% fetal bovine serum. A reduction in cell migration was observed by P1243 in comparison to the vehicle control, but this was not statistically significant (ns) (252).

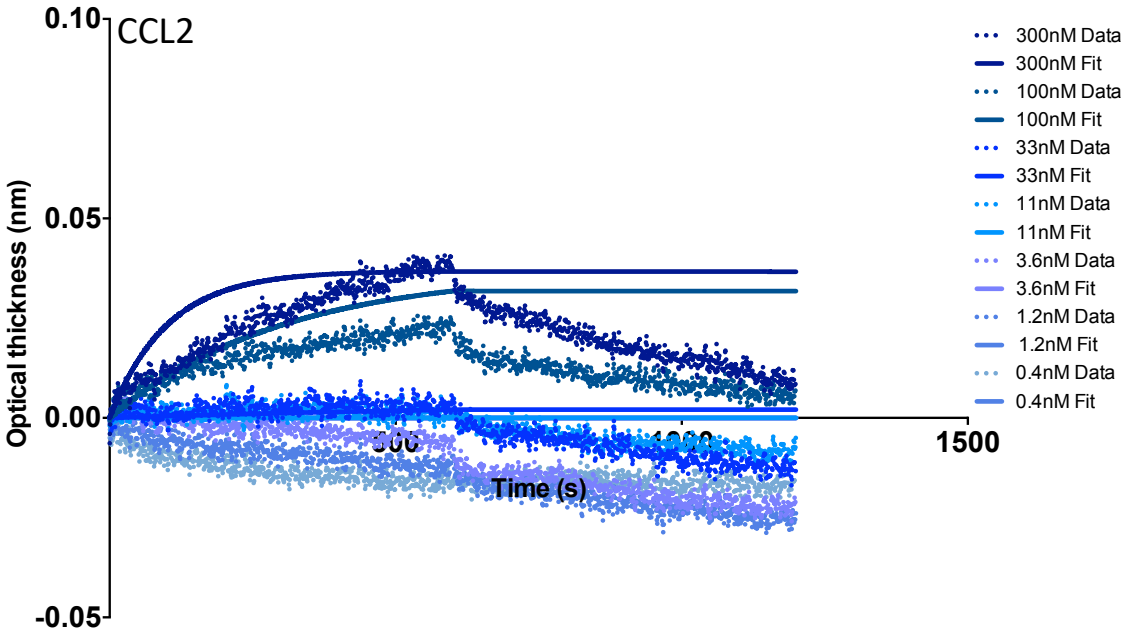


Figure A2. Bio-layer interferometry (BLI) sensogram of P1243 against human CCL2. Plots show wavelength shift (nm, y-axis) versus time (seconds, x-axis). Collected data is shown as solid line and fitted data is shown by the dotted line.

Appendix B.

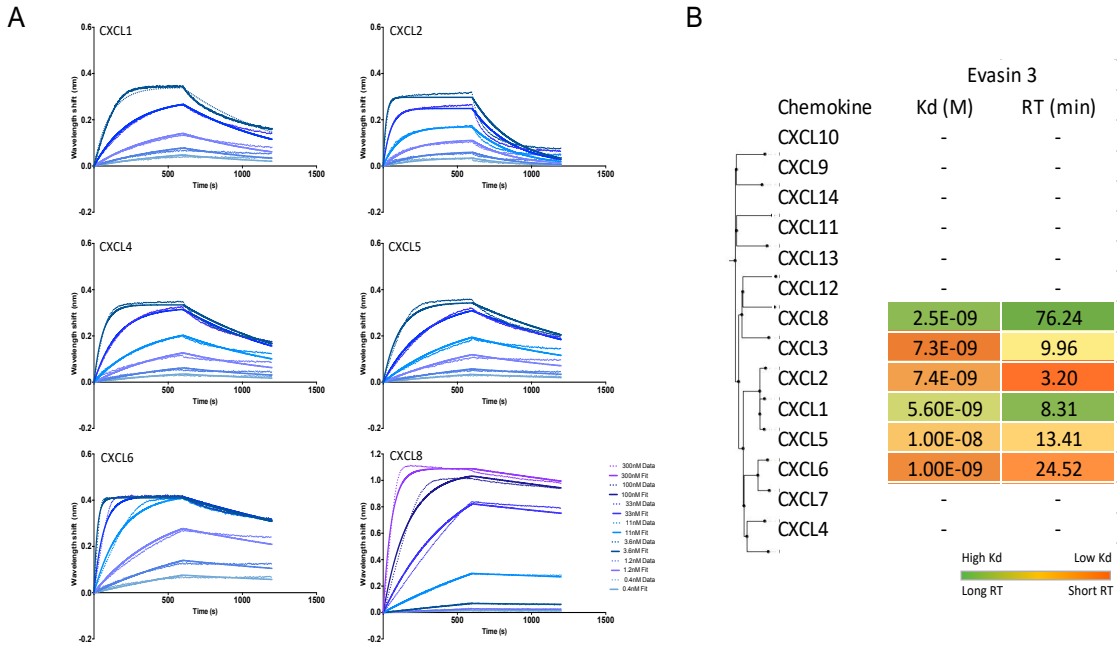
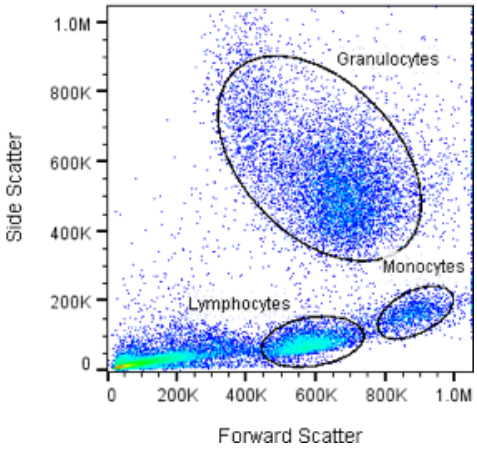


Figure B1. Biochemical profile of Evasin 3. (A) Bio-layer interferometry (BLI) sensograms of Evasin 3 against human chemokines labelled. Plots show wavelength shift (nm, y-axis) versus time (seconds, x-axis). Collected data is shown as solid line and fitted data is shown by the dotted line. (B) Binding affinity profile of Evasin 3 against CXC chemokines. Binding affinities (K_d, M) and target residence times (RT, minutes) determined using BLI. High affinity binding is indicated by shades of green, medium affinity in shades of yellow and low affinity in shades of orange. Longest RT is shown in shades of green, medium RT in shades of yellow and shortest RT is shown in shades of orange.

Appendix C.

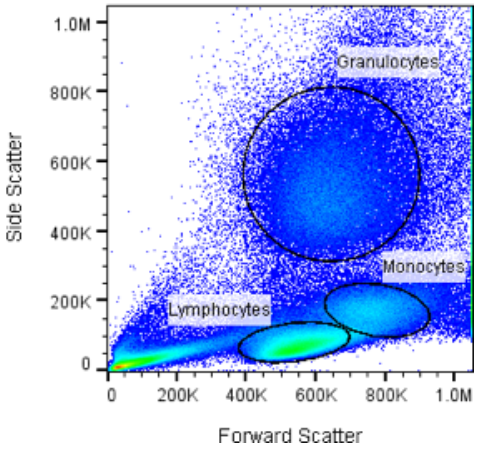
A



Whole Blood

Cell type	Cell count
Granulocytes	2.90E+06
Monocytes	4.00E+05
Lymphocytes	1.80E+06

B



Buffy Coat

Cell type	Cell count
Granulocytes	2.00E+07
Monocytes	1.30E+07
Lymphocytes	4.70E+07

Figure C1. Fluorescence-activated cell sorting (FACS) dot blots showing cell populations obtained from human whole blood (A) or buffy coat (B). Gates showing granulocytes, monocytes and lymphocytes, were determined using forward scatter (x-axis) and side scatter (y-axis) on the Attune Nxt Flow Cytometer. Cell counts were determined using FlowJo software.

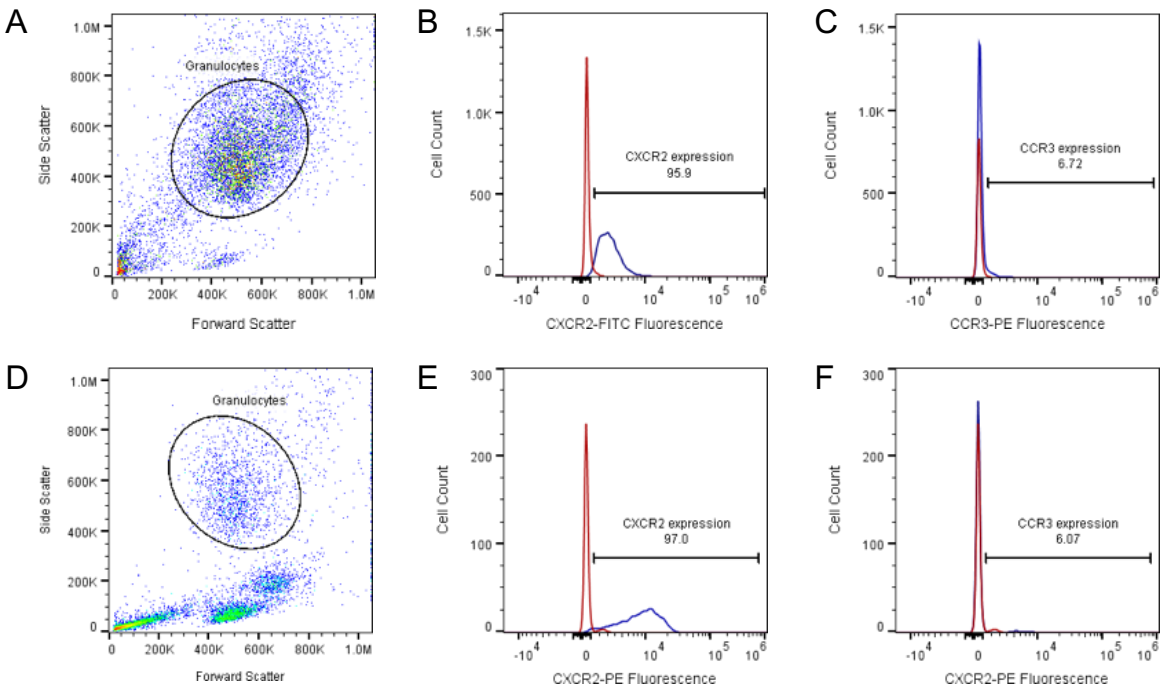


Figure C2. Labelling cell surface of granulocytes for CXCR2 and CCR3. Granulocyte population isolated from whole blood (A) and buffy coat (D) and was determined using forward and side scatter dot blots on the Attune Nxt Flow Cytometer. (B, C, E, F) Fluorescence profiles showing granulocyte cells expression of CXCR2 or CCR3 (red). Granulocytes were isolated from whole blood (B, C) and buffy coat (E, F) by red blood cell depletion and lysis. 1 x 10^6 granulocyte cells were labelled with CXCR2 (B, E) or CCR3 (C, F). Cells labelled with isotype control are shown in blue. Y-axis shows cell count and x-axis shows chemokine receptor fluorescence. The bar shows the gate used to identify positive cells with fluorescence exceeding that of the control, indicated as a percentage A11above the bar.

Appendix D.

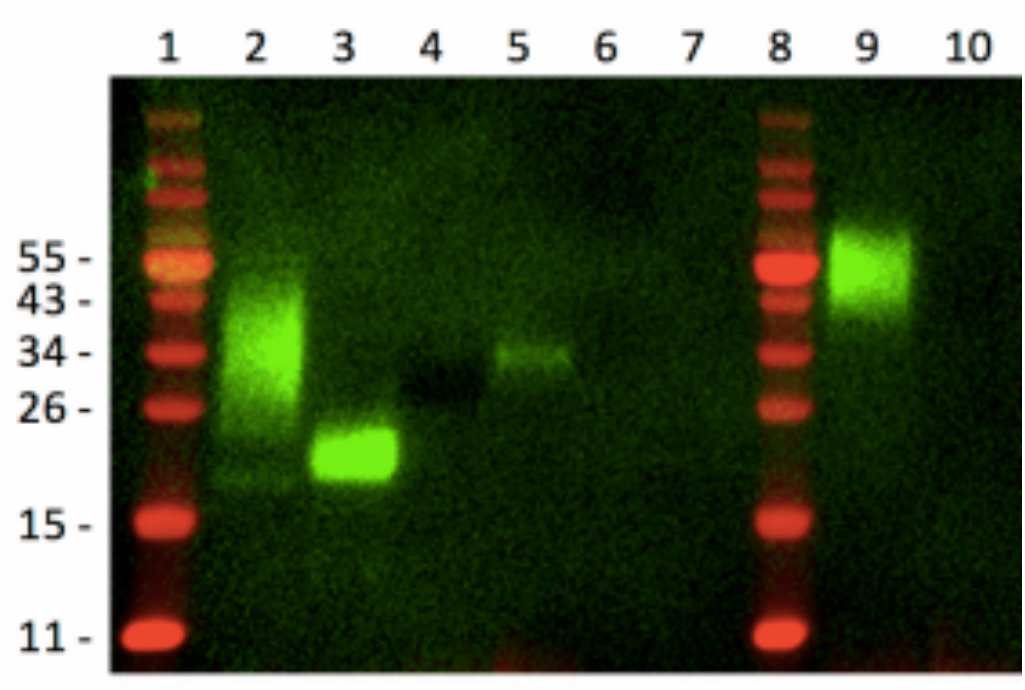


Figure D1. Western blotting of P1243, P1156 and the two-warheads P1243:G4S:P1156 and P1156:G4S:P1243. Lane 1 and lane 8 show molecular weight markers (kDa). Lane 2 shows P1243, lane 3 shows P1156, lane 4 shows P1243:G4S:P1156 (deglycosylated), lane 5 shows P1156:G4S:P1243 (deglycosylated), lane 9 shows P1243:G4S:P1156 (glycosylated), lane 10 shows P1156:G4S:P1243 (glycosylated). Three ug of protein was loaded in each lane (252).



Figure D2. Uncropped images of the MS/MS analysis of the two-warhead Evasins P1243:G4S:P1156 and P1156:G4S:P1243.

Appendix E. Genetically engineering the two-warhead evasins: P991:G4S:P1156 and P1156:G4S:P991

A

Sequence amplified	Primer	Primer ID	Primer sequence	Product size (base-pairs)
P991:G4S	Forward	915	cgtagctgaaaccggtGAGAATGGTGAAGGCACTACTCAACC	339
	Reverse	1028	agagcctcctccaccTTCTTCTAGATTAGGTGCCTTGAAGCATAG	
G4S:P1156	Forward	1029	ggtggaggaggctctGCAGATGACGATAACGAACTCTTTACTGT	255
	Reverse	926	ctcctccgccaccggtATGAGATAATGTGTCTGAGCGCTTTG	
P991:G4S:P1156	Forward	915	cgtagctgaaaccggtGAGAATGGTGAAGGCACTACTCAACC	579
	Reverse	926	ctcctccgccaccggtATGAGATAATGTGTCTGAGCGCTTTG	

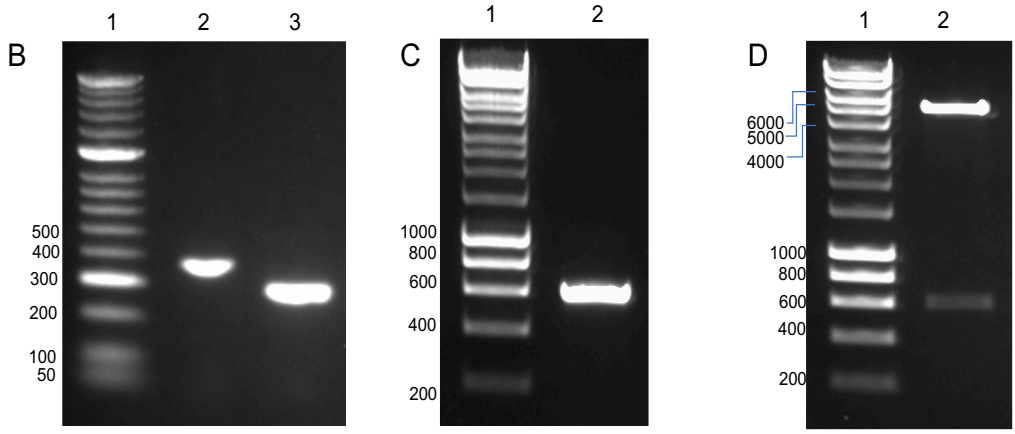


Figure E1. Gel electrophoresis of the steps to create the two-warhead evasin: P991:G4S:P1156. (A) PCR primer sets for the two-warhead P991:G4S:P1156. Primer sequence complementary to the template DNA is shown in upper-case and overhangs are shown in lower case. Overhangs encoding the GGGGS (G4S) linker are shown in red. Lane 1, in each case, shows 1 kilo-base-pair ladder and lanes 2-3 shows DNA. (A) PCR 1: amplification of P991 (339 base-pairs, lane 2) and P1156 (255 base-pairs, lane 3). (B) PCR fusion of P991 and P1156 to create P991:G4S:P1156, expected band size is 579 base-pairs. (C) AgeI restriction enzyme digest of P991:G4S:P1156 DNA plasmid showing vector at 4698 base-pairs and insert (P991:G4S:P1156) at 579 base-pairs (lane 2).

A

Sequence amplified	Primer	Primer ID	Primer sequence	Product size (base-pairs)
P1156:G4S	Forward	925	cgtagctgaaaccggtGCAGATGACGATAACGAACTCTTTACTGT	255
	Reverse	1074	agagcctcctccaccATGAGATAATGTGTCTGAGCGCTTTG	
G4S:P991	Forward	1076	ggtggaggaggctctGAGAATGGTGAAGGCACTACTCAACC	339
	Reverse	916	ctcctccgccaccggtTTCTTCTAGATTAGGTGCCTTGAAGCATAG	
P1156:G4S:P991	Forward	925	cgtagctgaaaccggtGCAGATGACGATAACGAACTCTTTACTGT	579
	Reverse	916	ctcctccgccaccggtTTCTTCTAGATTAGGTGCCTTGAAGCATAG	

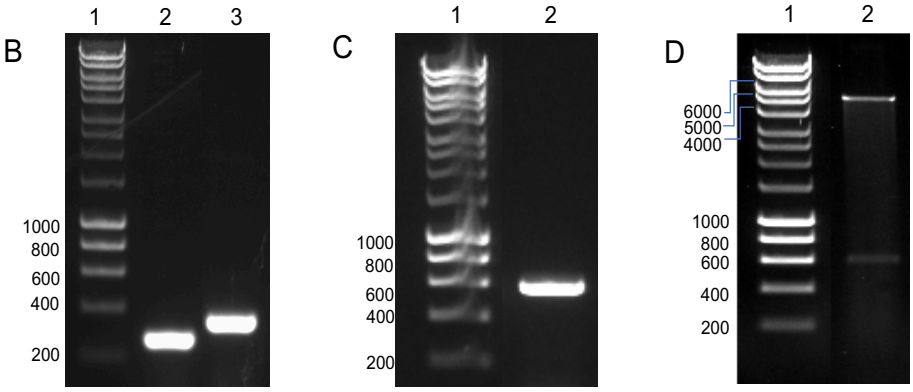


Figure E2. Gel electrophoresis of the steps to create the two-warhead evasin: P1156:G4S:P991. PCR primer sets for the two-warhead P1156:G4S:P991. Primer sequence complementary to the template DNA is shown in upper-case and overhangs are shown in lower case. Overhangs encoding the GGGGS (G4S) linker are shown in red. Lane 1, in each case, shows 1 kilo-base-pair ladder and lanes 2-3 shows DNA. (A) PCR 1: amplification of P1156 (255 base-pairs, lane 2) and P991 (339 base-pairs, lane 3). (B) PCR fusion of P1156 and P991 to create P1156:G4S:P991, expected band size is 579 base-pairs. (C) AgeI restriction enzyme digest of P1156:G4S:P991 DNA plasmid showing vector at 4698 base-pairs and insert (P1156:G4S:P991) at 579 base-pairs (lane 2).

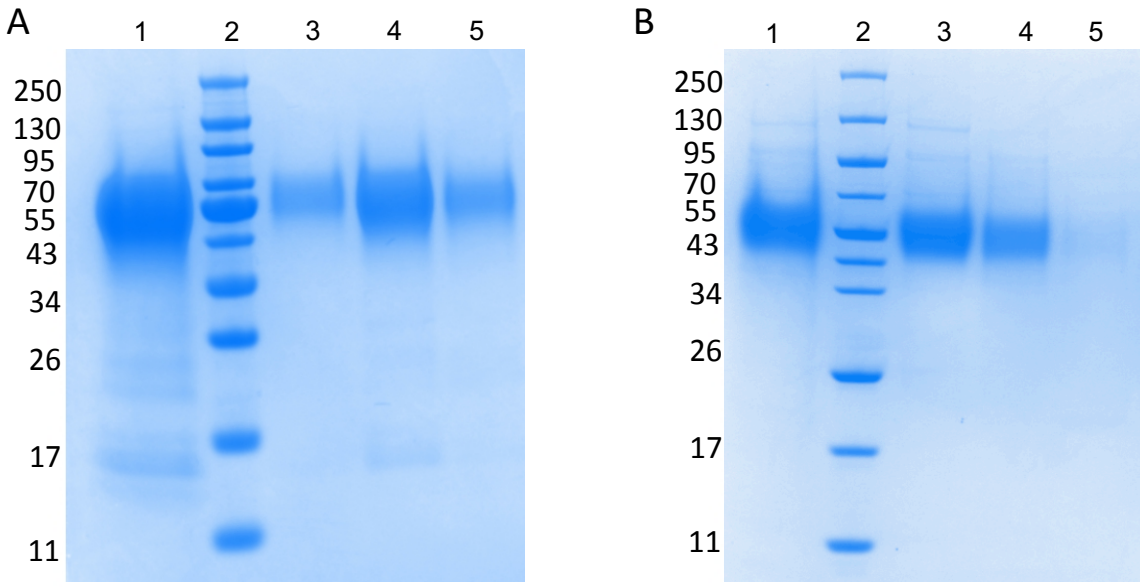
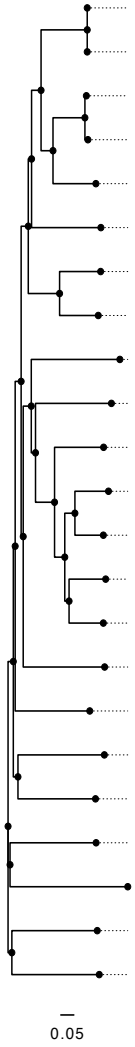


Figure E3. SDS-PAGE analysis of the two-warhead evasins: P991:G4S:P1156 and P1156:G4S:P991. (A) P991:G4S:P1156. (B) P1156:G4S:P991. Lane 1 shows pooled and concentrated nickel affinity (Ni-NTA) chromatography purified protein, lane 2 shows protein ladder and lanes 3-5 show protein elutions, following Ni-NTA chromatography and size exclusion chromatography (SEC). SDS-PAGE analysis shows both two-warheads express as highly glycosylated proteins migrating at approximately 40-60 kDa. In each case, SEC elutions 3-5 from both proteins were pooled and concentrated for subsequent experiments.



Chemokine	P991 KD (M)	P991:G4S:P1156 KD (M)	P1156:G4S:P991 KD (M)	P991 RT (min)	P991:G4S:P1156 RT (min)	P1156:G4S:P991 RT (min)
CCL4	3.68E-09	3.54E-09	3.55E-09	32.25	28.08	26.55
CCL4L1	1.34E-09	1.24E-09	1.28E-09	42.78	38.33	33.79
CCL3	2.24E-09	2.22E-09	1.89E-09	42.57	37.08	38.16
CCL3L1	2.99E-09	2.91E-09	3.09E-09	52.05	43.82	34.70
CCL18	2.52E-10	1.43E-10	2.01E-10	185.33	293.22	182.29
CCL14	7.11E-10	8.35E-10	6.64E-10	191.51	134.85	158.94
CCL23	5.87E-09	5.13E-09	7.00E-09	32.27	35.25	28.48
CCL15	1.09E-07	1.27E-07	1.66E-07	1.08	0.87	0.66
CCL1	8.60E-09	7.66E-09	1.66E-08	5.37	4.13	2.01
CCL24	5.42E-09	3.18E-09	3.58E-09	7.07	8.52	6.75
CCL13	1.91E-10	1.76E-10	2.07E-10	290.35	275.85	221.22
CCL2	2.47E-08	2.48E-08	3.21E-08	4.17	4.02	3.25
CCL7	2.41E-10	2.87E-10	4.35E-10	507.69	374.76	231.23
CCL8	1.59E-08	7.89E-09	7.45E-09	10.77	16.56	15.27
CCL11	1.90E-09	1.39E-09	1.54E-09	24.95	30.55	24.83
CCL21	2.61E-08	1.82E-08	1.99E-08	12.09	17.73	15.26
CCL5	8.69E-10	9.47E-10	7.54E-10	112.90	91.96	103.31
CCL20	1.54E-08	-	-	7.03	-	-
CCL16	5.36E-10	6.36E-10	5.03E-10	101.85	72.41	92.55
CCL19	1.20E-08	-	-	7.00	-	-
CCL27	3.95E-08	4.26E-08	3.62E-08	4.14	2.91	3.40
CCL22	3.01E-09	2.36E-09	2.18E-09	16.76	15.62	15.84
CCL17	7.37E-09	5.80E-09	7.44E-09	10.27	11.62	8.60

High Kd — Low Kd

Long RT — Short RT

Figure E4. Biochemical profile showing CC chemokine binding to single and two-warhead evasins: P991:G4S:P1156 and P1156:G4S:P991. Binding affinities (K_d, M) and target residence times (RT, minutes) were determined using bio-layer interferometry (BLI). Colour gradient indicates high or long (green) to low or short (red) Kd or RT, respectively. Colour gradient established from data in figure. A dash (-) indicates either data could not be fitted, or binding could not be detected.

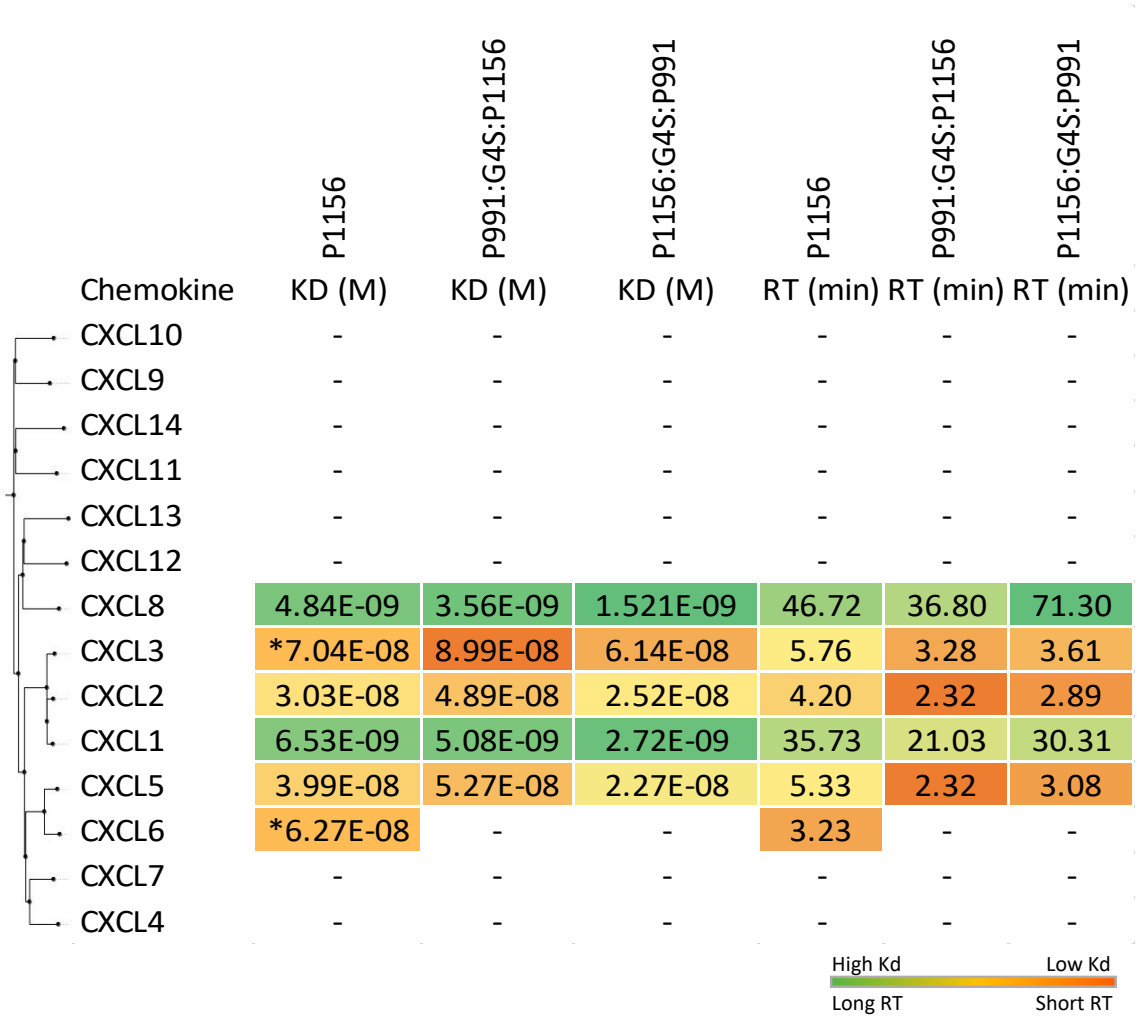


Figure E5. Biochemical profile showing CXC chemokine binding to single and two-warhead evasins: P991:G4S:P1156 and P991:G4S:P1243. Binding affinities (K_d, M) and target residence times (RT, minutes) were determined using BLI. Colour gradient indicates high or long (green) to low or short (red) Kd or RT, respectively. Colour gradient established from data in figure. A dash (-) indicates either data could not be fitted, or binding could not be detected. An asterisk (*) indicates the K_d could not be determined during this experiment because of difficulty in fitting the data in the software, so previous data has been shown instead.

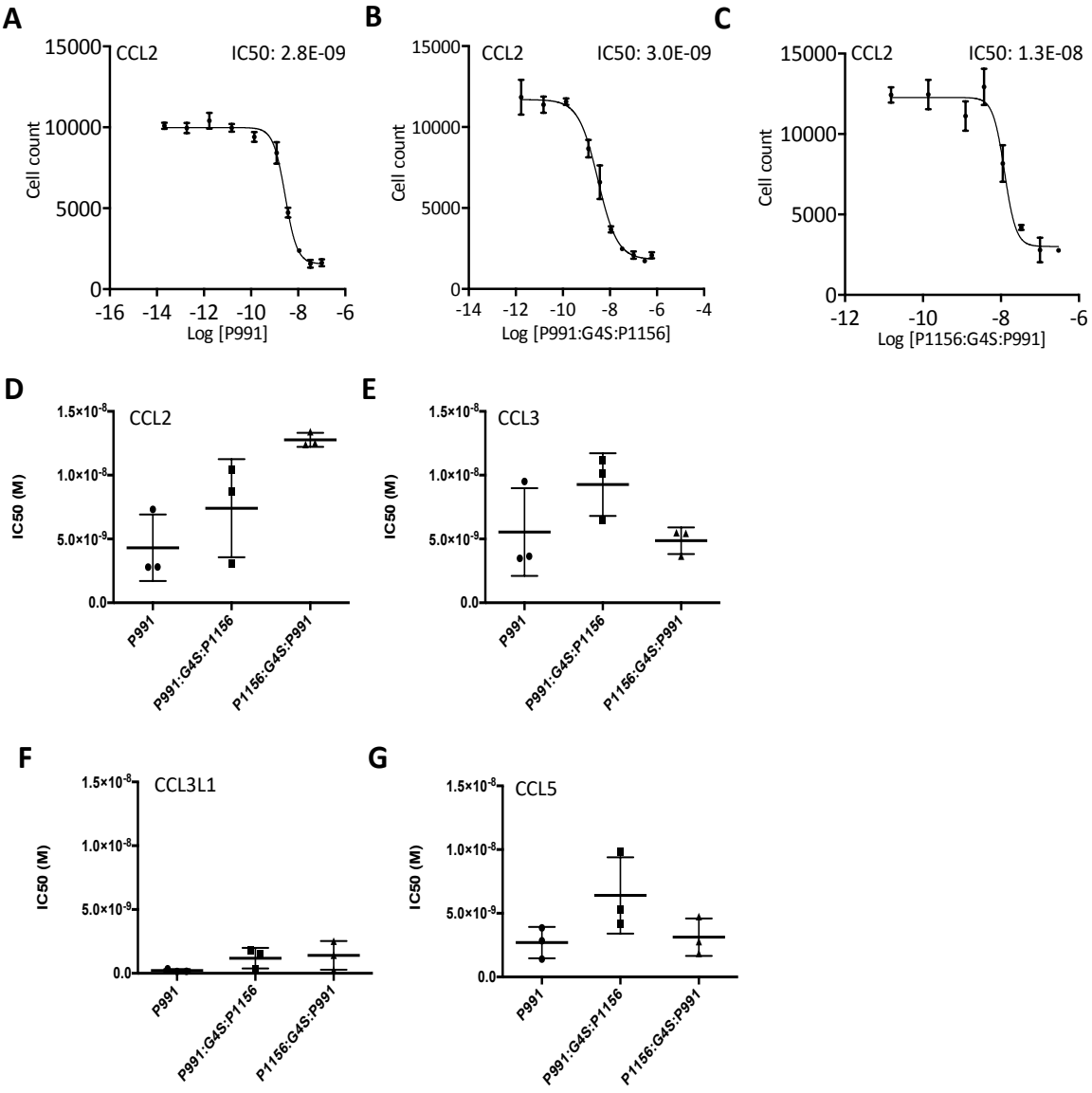


Figure E6. Functional inhibition of CC chemokines by individual and 'two-warhead' evasins. (A-C) Neutralization of CCL2-induced migration of THP-1 cells by P991, P991:G4S:P1156 and P1156:G4S:P991. Y-axis shows migration of THP-1 cells in response to EC_{80} dose of human CC chemokine shown. X-axis shows evasin concentration (Log_{10} Molar). In each case, data from a representative experiment is shown as mean ± s.e.m. of three technical replicates. IC_{50}'s (M) shown in each figure were estimated by fitting an agonist response curve with 4 parameters. (D-G) Summary IC_{50} data of indicated CC chemokines, CCL2, CCL3, CCL3L1 and CCL5. IC_{50}'s were determined for P991, P991:G4S:P1156 and P1156:G4S:P991 against CCL2, which were 4.3E-9 M, 7.4E-9 M and 1.3E-8 M, against CCL3, which were 5.5E-9 M, 9.3E-9 M and 4.9E-9 M, against CCL3L1, which were 2.2E-10 M, 1.2E-9 M and1.4E-9 M, and against CCL5, which were 2.7E-9 M, 6.4E-9 M and 3.1E-9 M. Y-axis shows IC_{50} (logarithmic scale, M) and X-axis shows each Evasin. In each case, data from a representative experiment is shown as mean ± s.e.m. of three biological replicates. Each evasin was assayed against the CC chemokines EC_{80} in the THP-1 migration assay.

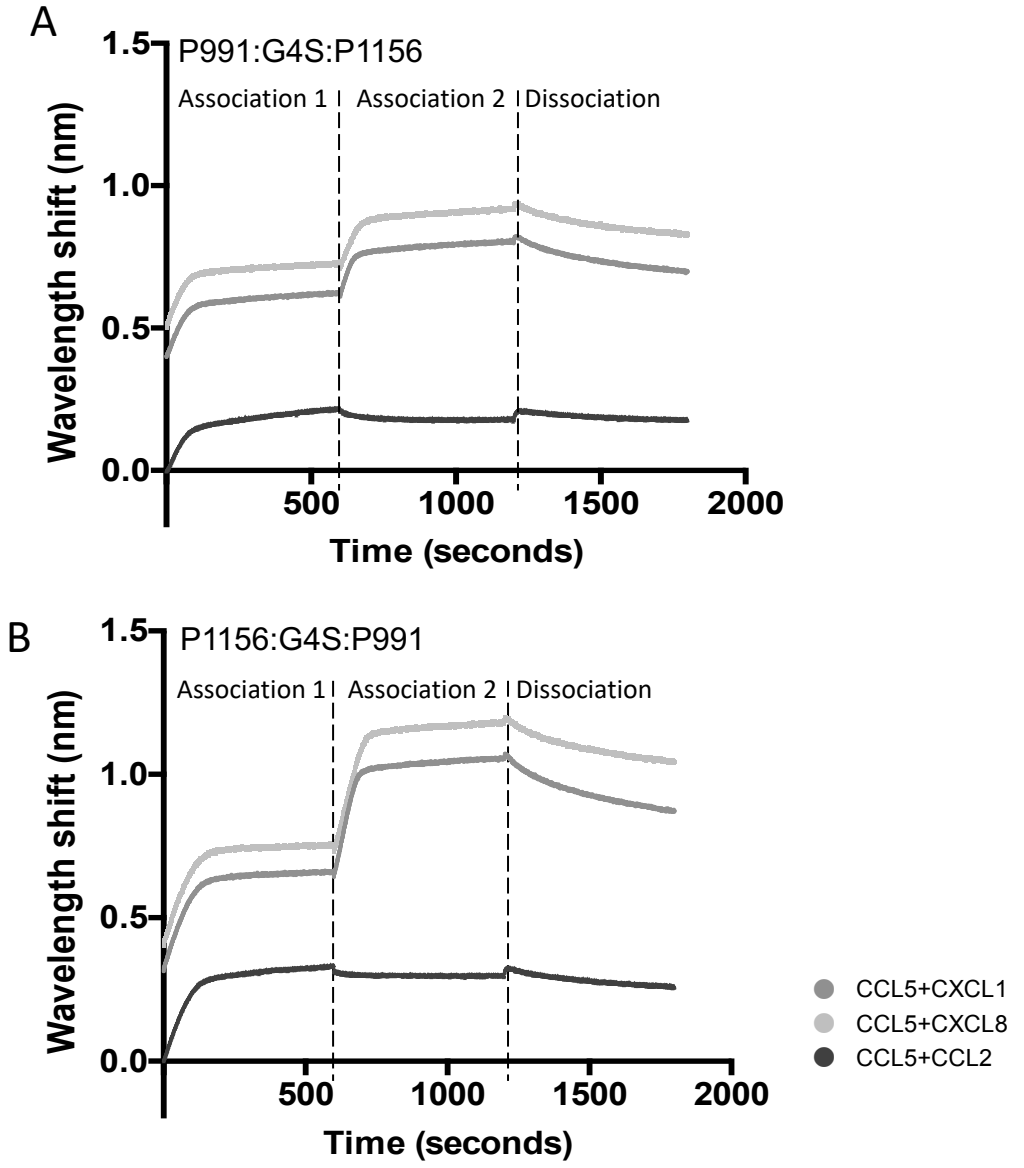


Figure E7. Binding assay showing two-warhead evasins: P991:G4S:P1156 and P1156:G4S:P991, polyvalent binding to human CC and CXC chemokines, determined using bio-layer interferometry. Two-warhead evasins were first immobilized onto nickel-coated sensors, associated with human CCL5 (association 1), followed by an association with CCL5 in addition to CXCL8 (light grey trace), CXCL1 (dark grey trace) or CCL2 (black trace) (association 2), and then dissociated in buffer (dissociation).

Appendix F.

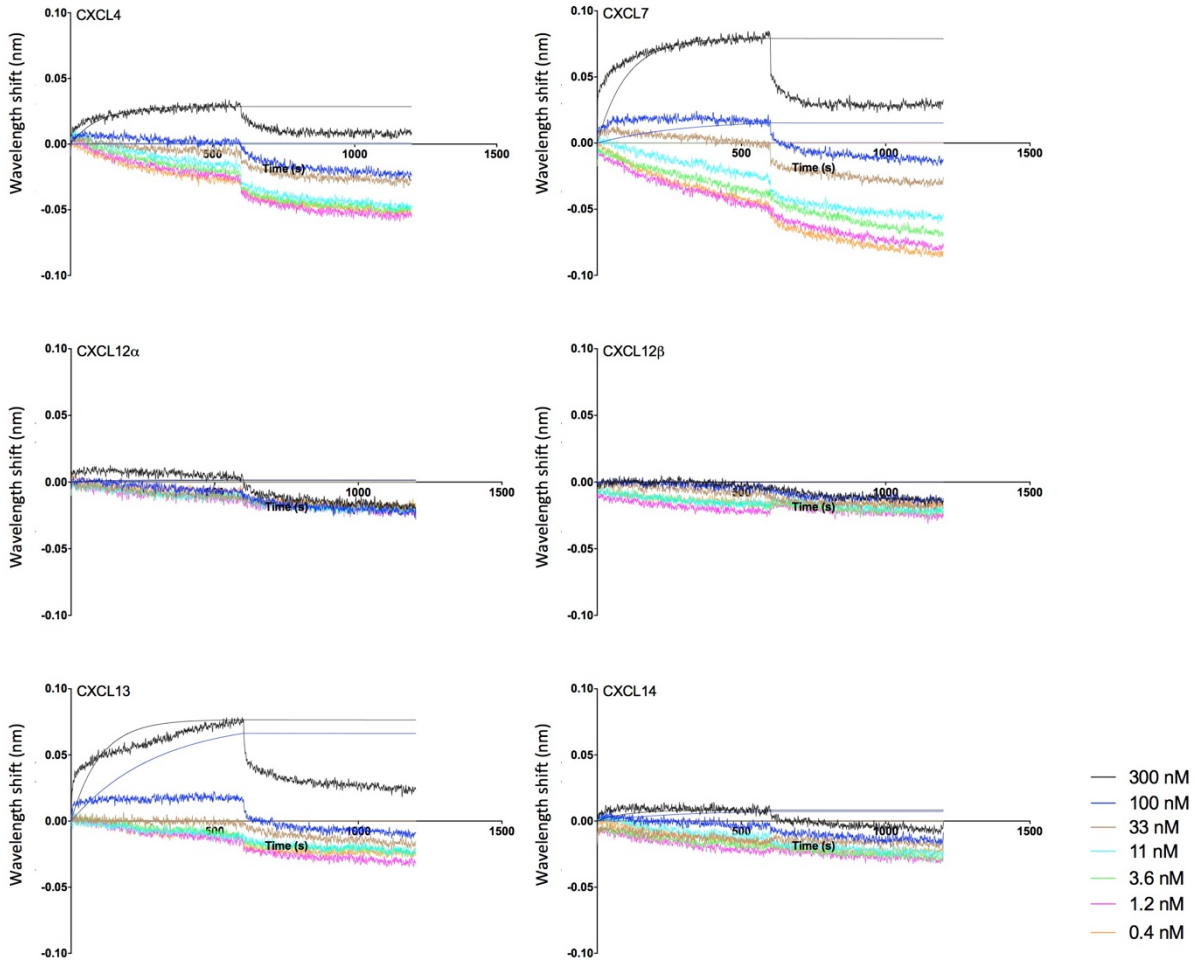


Figure F1. Biolayer interferometry sensorgrams of P1243:G4S:P1156 binding to indicated chemokines. Plots display wavelength shift (y-axis, nm) versus time (x-axis, seconds). Solid lines indicate collected data, dashed lines indicate fitted data.

Disease	Chemokines targeted by P1243:G4S:P1156
Myocarditis	CCL5, CCL13, CCL17, CCL18, CCL19, CXCL8
Myocardial infarction	CCL3, CCL4, CCL5, CCL11, CCL13, CXCL8
Vasculitis	CCL3, CCL4, CCL5, CCL13, CCL17, CCL18, CCL19, CXCL1, CXCL8
Atherosclerosis	CCL3, CCL4, CCL5, CCL11, CCL13, CCL15, CCL17, CCL18, CCL19, CCL23, CXCL1, CXCL8
Idiopathic pulmonary disease	CCL3, CCL4, CCL5, CCL8, CCL11, CCL13, CCL17, CCL18, CCL19, CXCL1, CXCL8
Inflammatory bowel disease	CCL3, CCL4, CCL5, CCL8, CCL11, CCL14, CCL15, CXCL1, CXCL8
Rheumatoid arthritis	CCL3, CCL5, CCL7, CCL8, CCL13, CCL14, CCL15, CCL17, CCL18, CCL20, CXCL1, CXCL5, CXCL8

Table F1. Table showing chemokines associated with specified human disease that can be targeted by the two-warhead evasin: P1243:G4S:P1156. Chemokines association with diseases was identified based on literature searches of Myocarditis (347, 348), Myocardial Infarction (325-327), Vasculitis (349-353), Atherosclerosis (44, 45, 303, 304, 328-340), Idiopathic pulmonary disease (296, 305, 354, 355), Inflammatory bowel disease(356-363) and Rheumatoid arthritis (44, 45, 167, 303, 304, 329-335, 337-340).

Appendix G.

	P1243 kd (M)	P1243:G4S:P1156 kd (M)	P1156:G4S:P1243 kd (M)	P1243 RT (min)	P1243:G4S:P1156 RT (min)	P1156:G4S:P1243 RT (min)
mCCL2	-	-	-	-	-	-
mCCL3	2.99E-08	1.25E-08	1.08E-08	13.86	8.31	8.02
mCCL4	6.74E-09	5.74E-09	6.05E-09	25.23	19.85	17.59
mCCL5	5.20E-08	1.03E-08	1.02E-08	23.17	7.78	5.99
mCCL6	2.84E-09	3.75E-08	2.83E-08	14.59	9.23	12.56
mCCL7	-	-	-	-	-	-
mCCL8	-	2.51E-08	1.83E-08	6.82	2.71	2.6
mCCL9/10	7.15E-10	2.10E-09	9.61E-10	198.97	62.81	116.68
mCCL11	9.85E-10	9.30E-09	7.85E-09	92.25	9.18	8.99
mCCL12	1.40E-08	-	-	-	-	-
mCCL19	1.95E-08	-		80.88	-	-
mCCL20	1.81E-09	-	-	2.74	-	-
mCCL21	-	-	-	-	-	-
mCCL22	8.57E-10	5.52E-09	-	133.84	21.35	-
mCCL24	3.81E-09	5.25E-09	4.68E-09	29.46	9.76	8.38
mCCL27	1.14E-08	3.94E-09	2.88E-09	15.95	14.02	20.42
mCCL28	-	-	-	-	-	-



Figure G1. Summary data of 'two-warhead' evasins binding to murine (m) CC chemokines using bio-layer interferometry. Binding affinities (K_d, M) and target residence times (RT, minutes) were determined using BLI. Colour gradient indicates high or long (green) to low or short (red) Kd or RT, respectively. Colour gradient established from data in figure. A dash (-) indicates either data could not be fitted, or binding could not be detected.

	P1243 kd (M)	P1243:G4S:P1156 kd (M)	P1156:G4S:P1243 kd (M)	P1243 RT (min)	P1243:G4S:P1156 RT (min)	P1156:G4S:P1243 RT (min)
mCXCL1	-	-	-	-	-	-
mCXCL2	6.33E-08	1.31E-07	8.14E-08	4.86	7.17	6.49
mCXCL4	-	-	-	-	-	-
mCXCL6	-	-	-	-	-	-
mCXCL9	-	-	-	-	-	-
mCXCL10	-	-	-	-	-	-
mCXCL11	-	-	-	-	-	-
mCXC12α	-	-	-	-	-	-
mCXCL12β	-	-	-	-	-	-
mCXCL13	-	-	-	-	-	-
mCXCL15	-	-	-	-	-	-
mCXCL16	-	-	-	-	-	-

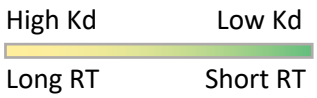


Figure G2. Summary data of 'two-warhead' evasins binding to murine (m) CXC chemokines using bio-layer interferometry. Binding affinities (Kd, M) and target residence times (RT, minutes) were determined using BLI. Colour gradient indicates high or long (green) to low or short (red) Kd or RT, respectively. Colour gradient established from data in figure. A dash (-) indicates either data could not be fitted, or binding could not be detected.

Appendix H. Publications leading to this research

SCIENTIFIC REPORTS

OPEN

Genetically engineered two-warhead evasins provide a method to achieve precision targeting of disease-relevant chemokine subsets

Received: 16 November 2017
Accepted: 6 April 2018
Published online: 20 April 2018

Yara Alenazi[1], Kamayani Singh[1], Graham Davies[1], James R. O. Eaton[1,2], Philip Elders[1], Akane Kawamura[1,2] & Shoumo Bhattacharya[1]

Both CC and CXC-class chemokines drive inflammatory disease. Tick salivary chemokine-binding proteins (CKBPs), or evasins, specifically bind subsets of CC- or CXC-chemokines, and could precisely target disease-relevant chemokines. Here we have used yeast surface display to identify two tick evasins: a CC-CKBP, P1243 from *Amblyomma americanum* and a CXC-CKBP, P1156 from *Ixodes ricinus*. P1243 binds 11 CC-chemokines with $K_d < 10$ nM, and 10 CC-chemokines with K_d between 10 and 100 nM. P1156 binds two ELR + CXC-chemokines with $K_d < 10$ nM, and four ELR + CXC-chemokines with K_d between 10 and 100 nM. Both CKBPs neutralize chemokine activity with $IC_{50} < 10$ nM in cell migration assays. As both CC- and CXC-CKBP activities are desirable in a single agent, we have engineered "two-warhead" CKBPs to create single agents that bind and neutralize subsets of CC and CXC chemokines. These results show that tick evasins can be linked to create non-natural proteins that target subsets of CC and CXC chemokines. We suggest that "two-warhead" evasins, designed by matching the activities of parental evasins to CC and CXC chemokines expressed in disease, would achieve precision targeting of inflammatory disease-relevant chemokines by a single agent.

The 47 structurally related secreted proteins that form the chemokine family differ in the spacing of cysteine residues at the N-terminus, and based on this, are classified as CC, CXC, CX3C or XC[1]. Of these, the 27 CC and 17 CXC chemokines[1] form the majority. Multiple CC and CXC chemokines are typically expressed in tissues affected in inflammatory disease[2]. The combinatorial effects of these chemokines are responsible for the recruitment of innate and adaptive immune cells including monocytes, neutrophils, eosinophils, and lymphocytes to sites of inflammation[3–5]. The synergistic effects between certain CC and CXC chemokines are well documented, for instance, in monocyte, lymphocyte and neutrophil migration (reviewed in[6]), and the functional importance of certain CC-CXC chemokine interactions has recently been demonstrated[7]. The chemokine network has been difficult to therapeutically target using monovalent agents such as monoclonal antibodies or small molecules[8,9]. Mechanisms underlying the robustness of the network include expression of multiple chemokines in tissues affected by inflammatory disease, the ability of chemokines to interact with several chemokine receptors, expression of multiple receptor types on leukocytes and immune cells[10], synergy and interactions between different chemokines[6,7], and feed-forward loops where inflammatory cells recruited to diseased tissue secrete more chemokines, thereby amplifying the inflammatory response[11].

A number of pathogens and parasitic organisms, including viruses, helminths and ticks, produce structurally unrelated chemokine binding proteins (CKBPs) that target multiple chemokines (reviewed in[9,12]). Viral and helminth CKBPs studied to date, with the exceptions of R17[13] and 35-kDa/vCCI[14], typically do not discriminate between CC and CXC chemokines[12,15–17]. Tick CKBPs or evasins, originally identified by Proudfoot *et al.* from *Rhipicephalus sanguineus*[18], fall into two structurally unrelated classes that do discriminate between CC and CXC

[1]RDM Division of Cardiovascular Medicine, University of Oxford, Oxford, United Kingdom. [2]Department of Chemistry, University of Oxford, Oxford, United Kingdom. Correspondence and requests for materials should be addressed to S.B. (email: sbhattac@well.ox.ac.uk)

chemokines, and moreover, are also selective in their binding within either chemokine class. Evasins 1 and 4 solely bind distinctive subsets of CC chemokines, whereas evasin 3 binds only a subset of CXC chemokines. The convergent evolution of structurally unrelated peptides in diverse organisms that target the multiple nodes in the chemokine network, provides strong evidence that such one-to-many targeting is an effective strategy to disrupt chemokine-driven inflammation. Supporting this idea, the potential therapeutic efficacy of viral[15], helminth[16] and tick[9] CKBPs in inflammatory disease provides proof-of-concept of targeting of the chemokine network as a therapeutic approach.

The inadvertent targeting of chemokines that are not involved in the disease process by CKBPs could however increase the likelihood of off-target effects. The preferential binding of tick evasins to limited subsets of CC or CXC chemokines could provide a method to precisely target multiple disease-relevant chemokines without unnecessarily affecting other chemokines. To achieve this there is a great need to identify further tick CKBPs that bind different subsets of CC and CXC chemokines. Putative evasins have been identified in a variety of tick species using bioinformatic analyses of salivary transcriptome data[19–21]. To rapidly identify tick CKBPs that bind chemokines with high-affinity, we screened yeast surface display libraries, constructed to express putative tick evasins, with fluorescently labelled chemokines, and cloned 10 further evasins from *Rhipicephalus* and *Amblyomma* genera[22]. We also showed that these new evasins bound with high affinity to subsets of CC chemokines that range in number from 8–20 chemokines, and not to CXC chemokines. Similar to evasins 1 and 4, these new evasins share eight conserved cysteine residues. A common unifying feature of the these 10 evasins was the ability to bind CCL2 and CCL13, properties which were not observed in evasins 1 and 4[22]. Further novel evasins that bind CC chemokines were identified more recently from *Ixodes, Rhipicephalus* and *Amblyomma* genera by Hayward *et al.*[23].

Here we describe the functional properties of two evasins identified by yeast surface display, P1243 from *Amblyomma americanum* (also described in Hayward *et al.*[23] as AAM-02), which is a CC-chemokine binding CKBP homologous to previously described CC-CKBPs, and P1156 from *Ixodes ricinus*, a novel CXC-binding CKBP that is homologous to evasin 3. We show that P1243 has a distinctive CC-chemokine-binding specificity, binding a large number of CC-chemokines including CCL13, but not binding CCL2. P1156 binds CXCL1 and CXCL8 strongly, but in addition binds CXCL2, 3, 5 and 6. The availability of different evasins that target subsets of CC and CXC chemokines in a one-to-many fashion provides the opportunity to use them in combination to treat inflammatory disease characterized by CC and CXC chemokine expression. The development of such therapeutics is however complicated by performance issues including risks and benefits of each individual agent in a combination[24]. These considerations prompted us to explore the possibility that the two distinct classes of tick evasins could be fused into a single agent. We show here, for the first time, that tick CC- and CXC- CKBPs can be fused together into a single entity we term a "two-warhead" evasin that binds subsets of both CC and CXC chemokines.

Results

Screening of a yeast surface display library. We screened a yeast surface display library expressing 352 putative tick CKBPs[22] using fluorescence activated cell sorting (FACS) with biotinylated CC and CXC chemokines followed by streptavidin–AlexaFluor (AF)647 to label and sort yeast cells that had bound the chemokine. The 352 putative CKBPs were cloned as a pool into yeast surface display vectors, with either N-terminus (AGA2) or C-terminus (SAG1 or AGA2) surface display tags. The pooled library was transformed into yeast, and cells were labelled with biotinylated chemokine and streptavidin-AF647. Labelled cells were sorted by FACS. We used a gate determined by omitting the chemokine to identify and recover a population of positive cells (Fig. 1A,C). Positive cells recovered in the first round were plated and re-grown, and sorted once again as above to further enrich for true positive clones. The sorted cells were plated at low density to enable picking of individual yeast clones. As part of our established screening protocol, the individual yeast clones were next re-tested by labelling with the biotinylated chemokine used in the screen and streptavidin – Alexa 647, and compared to negative control yeast that only expressed the relevant surface display tag (Fig. 1B,D). Consistent with observations from our previous studies[22], and other yeast display methods[25], we noted that a proportion of yeast do not display the protein. Library plasmids were recovered from clones that successfully re-tested positive, and were sequenced to identify the peptide. Through the screening process we identified two novel evasins, P1243 and P1156. P1243 was identified in screens that used CCL19 (Fig. 1A,B), and also CCL17, CCL4, CCL15, and CCL18 (data not shown). P1156 was identified in a screen performed using CXCL8 (Fig. 1C,D).

Sequence analysis of P1243. P1243 has 98 amino acid residues with a predicted molecular weight of 10.9 kDa, and predicted pI of 6.94. Glycosylation site prediction indicates seven N-glycosylation sites. Alignment of P1243 with that of other published CC-chemokine binding tick CKBPs shows that it retains the eight Cys residues predicted to form disulfide bonds in evasin 1, and their arrangement is consistent with motif C-x(14,17)-C-x(3)-C-x(11,16)-C-x(17,20)-C-x(4)-C-x(4)-C-x(8)-C that we have previously described[22] (Fig. 2A). Sequence-based phylogeny reveals that P1243 is most closely related to P991 (Fig. 2B), with which it shares 67% identity over an alignment length of 93 residues and P985 with which it shares 48% identity over 89 residues. It shares only 33% identity with evasin 1, over an alignment length of 62 residues. There is no significant homology to evasin 3. The Pro residue in evasin 1 that immediately follows the first Cys and targets the disulfide bond in CCL3[13] is conserved in P1243. The conservation of the Cys residues in P1243 with evasin 1 suggested that they could potentially form a similar backbone disulfide bonded architecture. We explored this using homology modelling using the structure of evasin 1 in complex with the chemokine CCL3[26]. The Cys disulfide bond architecture observed in evasin 1 is conserved in P1243 (Supplementary Material Fig. S1).

Sequence analysis of P1156. P1156 has 80 amino acid residues, with a predicted molecular weight of 8.8 kDa, and predicted pI of 4.7. It has two predicted N (at positions 16 and 61) and two predicted O-glycosylation

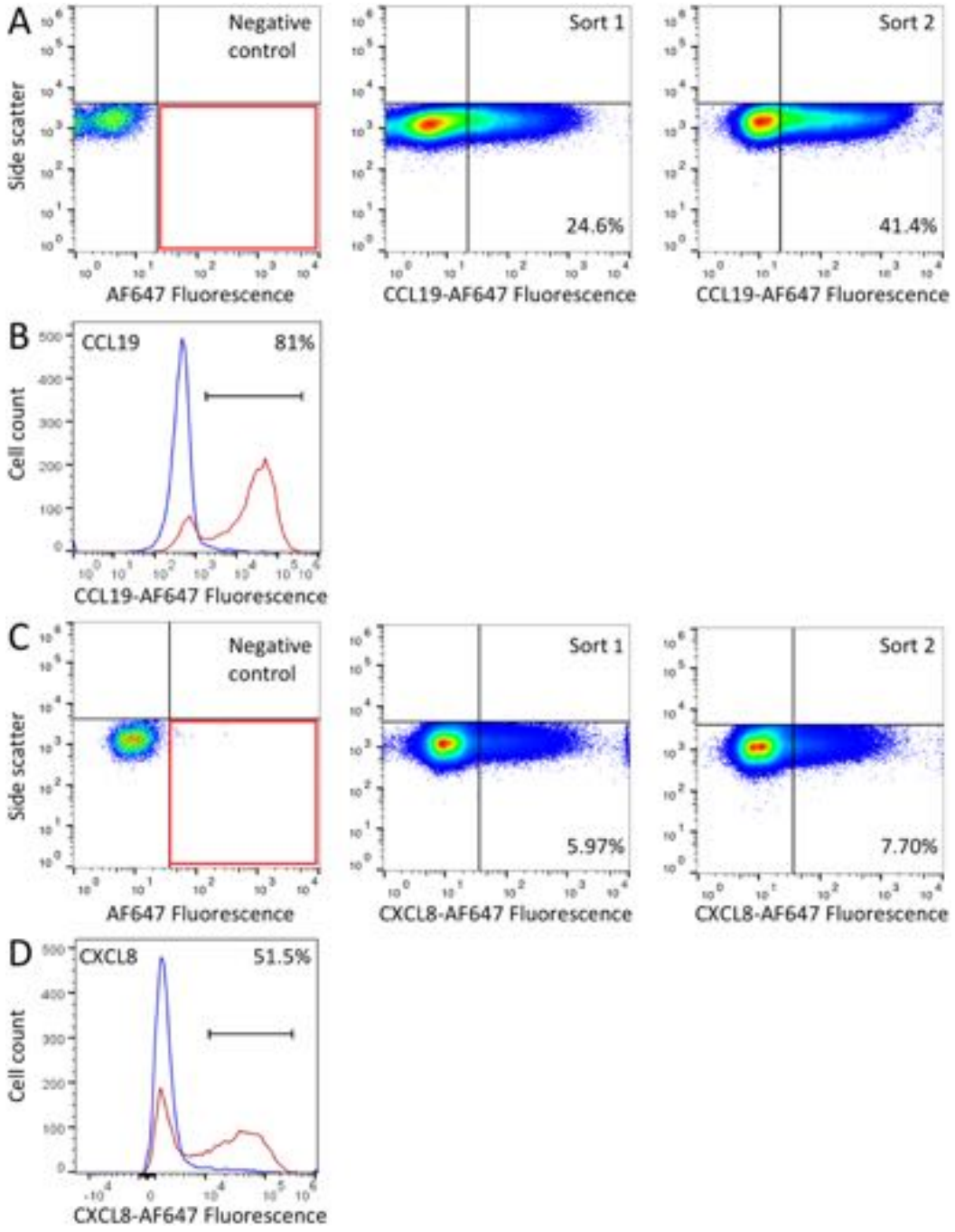


Figure 1. Yeast surface display screens. (**A**) Fluorescence profiles of tick putative CKBP yeast surface display library incubated with streptavidin-AF647 (negative control, left panel)) and with biotinylated CCL19 plus streptavidin-AF647, middle panel. The sorting gate (red box) was defined based on the negative control and was used to sort CKBP expressing yeast that bound biotinylated CCL19. The positive cells identified in the first sort were re-grown as a pool, and sorted once again to further enrich for chemokine binding yeast (right panel), and plated at low density to recover single clones. The y-axis shows side scatter and x-axis the fluorescence intensity on a log-scale. The proportions of cells within the sorting gate are indicated as a percentage. (**B**) Representative fluorescence profile (red) confirming the binding of a P1243 expressing yeast clone isolated in the above screen to biotinylated CCL19 and streptavidin-AF647. The fluorescence profile of control yeast with vector expressing the surface display tag alone are shown in blue. Y-axis shows cell count, and x-axis shows the fluorescence intensity on a log-scale. Positive cells with fluorescence exceeding that of the control are indicated as a percentage. The bar indicates the gate used. (**C**) Fluorescence profiles as above in (**A**), but using biotinylated CXCL8 plus streptavidin-AF647 as probe. (**D**) Representative fluorescence profile (red) confirming the binding of a P1156 expressing yeast clone isolated in the above screen to biotinylated CXCL8 and streptavidin-AF647. The fluorescence profile of control yeast with vector expressing the surface display tag alone are shown in blue. Y-axis shows cell count, and x-axis shows the fluorescence intensity on a log-scale. Positive cells with fluorescence exceeding that of the control are indicated as a percentage. The bar indicates the gate used.

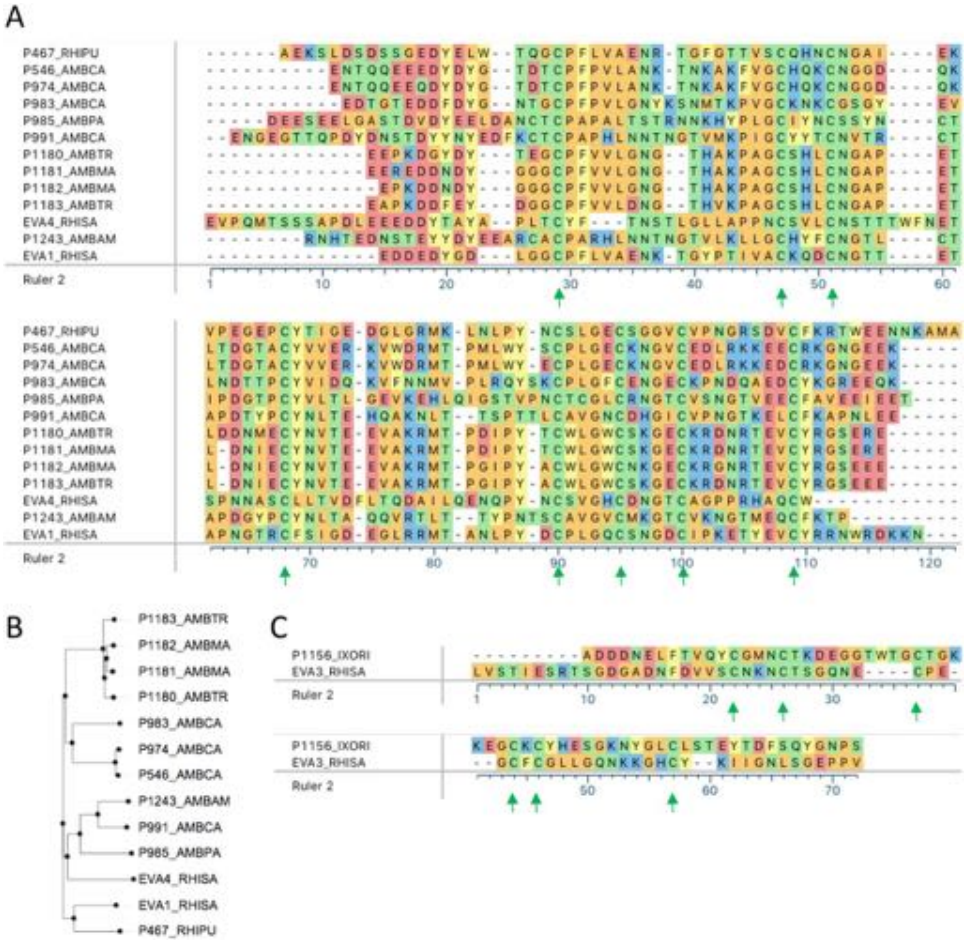


Figure 2. Analysis of P1243 and P1156. (**A**) CLUSTAL-W alignment of P1243 together with published CC-chemokine binding evasins. Protein sequence prefix indicates the identity, and suffix indicate the tick species as follows: AMBPA, AMBMA, AMBTR, AMBCA, - *Amblyomma parvum, maculatum, triste* and *cajennense* respectively, and RHIPU and RHISA – *Rhipicephalus pulchellus* and *sanguineus* respectively. Physicochemical properties are used to color code amino acid residues. Green arrows indicate the eight conserved Cys residues that form disulfide bonds in EVA1_RHISA (evasin 1). (**B**) Sequence similarity based phylogenetic tree of the "C8" CKBPs. (**C**) CLUSTAL-W alignment of P1156 together with EVA3_RHISA. Protein sequence prefix indicates the identity, and suffix indicate the tick species as follows: IXORI – *Ixodes ricinus*, and RHISA – *Rhipicephalus sanguineus*. Physicochemical properties are used to color code amino acid residues. The green arrows indicate the six Cys residues that are conserved in EVA3_RHISA (evasin 3).

sites at positions 63 and 75. It has 30% identity with evasin 3 over an alignment length of 43 residues, but no significant homology to evasins 1 or 4. An alignment of P1156 with EVA3_RHISA (evasin 3) is shown in Fig. 2C, and shows that it has six Cys residues like evasin 3.

Expression of P1243 and P1156. P1243 was expressed as a secreted protein from mammalian cells essentially as described previously[22], and purified using a C-terminal StrepII:His purification tag by Ni-NTA affinity followed by size exclusion chromatography. P1243 protein in the size exclusion fractions migrated in a range of molecular weights ranging from 20–50 kDa (Fig. 3A). This is significantly greater than the predicted molecular weight of 10.9 kDa, and is consistent with the predicted glycosylation at multiple sites, and also with the range of molecular weights observed for other evasins expressed in mammalian cells reported by others and us previously[22,27]. The size exclusion fractions containing protein were pooled for subsequent assays. P1156 was expressed and purified (Fig. 4A), as described above for P1243. P1156 protein in the size exclusion column fractions migrated at ~17 kDa, significantly larger than its predicted molecular weight of 8.8 kDa, and again consistent with its predicted glycosylation. Fractions 4 and 5 were pooled and used for further assays.

Characterization of P1243. We next assayed the binding of P1243 to a panel of chemokines using biolayer interferometry[28]. P1243 was immobilized on the sensor through the C-terminal His tag. An initial cross-binding screening assay performed at 300 nM chemokine concentration indicated that P1243 bound a number of CC chemokines, certain CXC chemokines, and also CX3CL1 and XCL1 (Supplementary Material Fig. S2, Table S2). Binding affinities (K_d) for P1243 were next determined using biolayer interferometry titration studies to chemokines identified as potentially binding P1243 in the cross-binding screen. In the titration assay, for several chemokines, binding was only detected

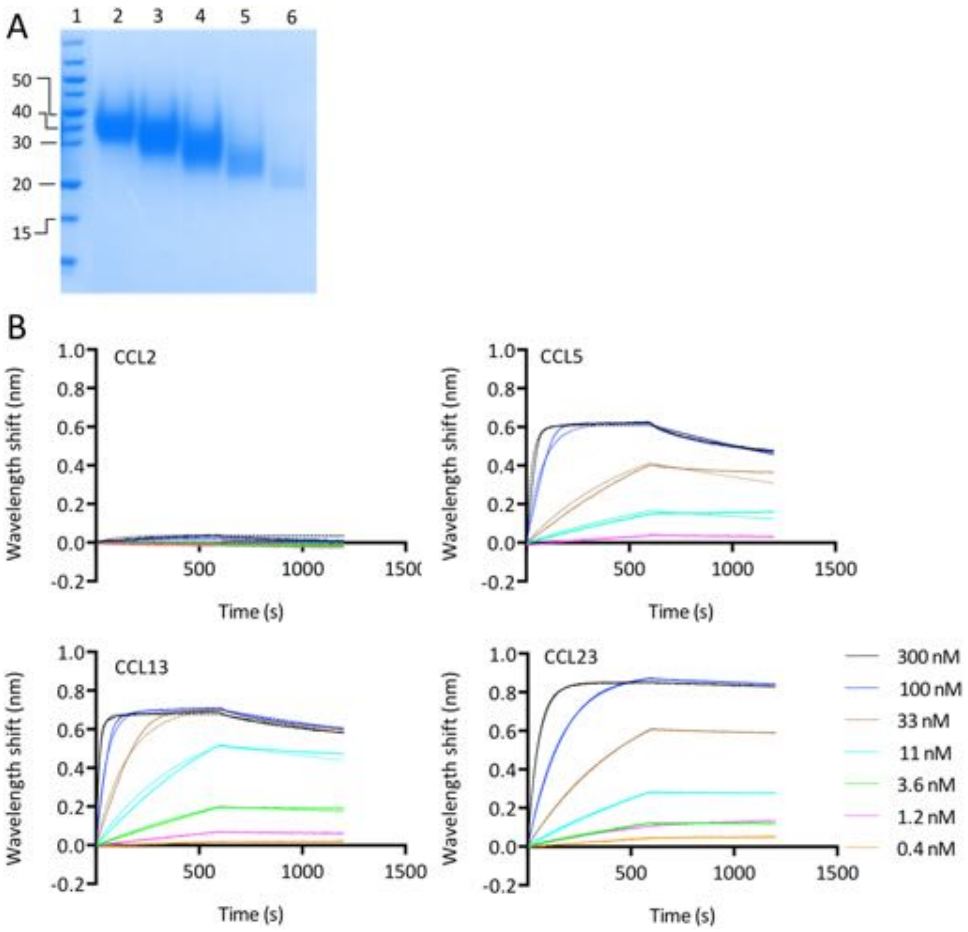


Figure 3. Characterization of P1243. (**A**) Colloidal Coomassie stained SDS-polyacrylamide gel showing size exclusion column fractions (lanes 2–6) obtained following nickel affinity chromatography for P1243. Molecular weight ladder (kDa) is shown in lane 1. The gel image was cropped for clarity and the uncropped image is provided in Fig.S5. (**B**) Biolayer interferometry sensorgrams of P1243 binding to indicated chemokines. Plots display wavelength shift (y-axis, nm) versus time (x-axis, seconds). Solid lines indicate collected data, dashed lines indicate fitted data.

at 300 nM and not at lower concentrations (data not shown). These were XCL1, CX3CL1, CXCL4, CXCL5 CXCL7, CXCL9, CXCL12 and CXCL14, and as curve fitting could not be performed, and we interpret these as low affinity binding and did not investigate them further. Higher affinity binding was identified for 21 CC chemokines where curve fitting could be performed. Example sensorgrams are shown in Fig. 3B, with summary K_d and target residence time data shown Fig. 5C. Notably, and in contrast to CC-binding evasins previously identified[22,26,29,30], P1243 bound CCL13, but did not bind CCL2. We also noted that there was a remarkable variation in target residence time (calculated from the off rate) ranging from under one minute for CCL7, to over 240 minutes for CCL23.

Characterization of P1156. We next assayed the binding of P1156 to a panel of chemokines using biolayer interferometry as described above. An initial screening assay performed at 300 nM chemokine concentration indicated that P1156 bound only certain ELR + CXC chemokines and not CC, XC or CX3C chemokines (Supplementary Material Fig. S2). Binding affinities (K_d) for P1156 were next determined using biolayer interferometry titration studies against CXC chemokines that were identified as potential binders in the cross-binding screen. P1156 bound a number of closely related human ELR + CXC chemokines, including CXCL1, 2, 3, 5, 6 and 8. Example sensorgrams are shown in Fig. 4B, with summary K_d and target residence time data shown in Fig. 6.

Development of "two-warhead" evasins. We fused P1243 to P1156 via a flexible GGGGS linker in order to create the "two-warhead" evasins P1243:G4S:P1156 and P1156:G4S:P1243 (Fig. 5A). The length of the peptide in each case is 183 amino acid residues, with a predicted molecular weight of 20 kDa, and pI of 5.3. The "two-warhead" evasins were expressed and purified using a C-terminal His tag using Ni-NTA affinity purification as described previously for the individual evasins. To confirm that full length proteins were produced we performed N-terminal sequencing of the expressed proteins. This confirmed that the predicted first four residues matched the first four residues observed by N-terminal sequencing in each case (Supplementary Material Fig. S6). To confirm the integrity of the C-termini we used western blotting of glycosylated and deglycosylated two-warheads using anti-His antibody (Supplementary Material Fig. S7). This showed that glycosylated

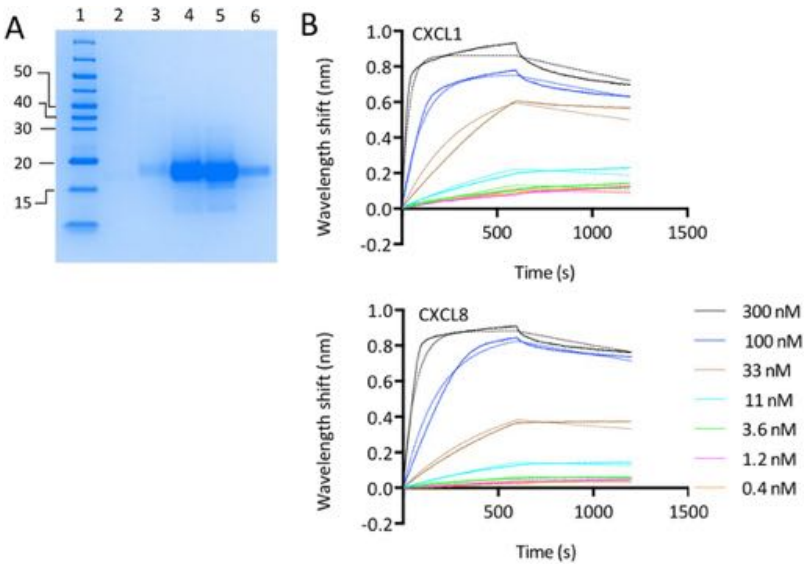


Figure 4. Characterization of P1156. (**A**) Colloidal Coomassie stained SDS-polyacrylamide gel showing size exclusion column fractions (lanes 3–6) obtained following nickel affinity chromatography for P1156. Molecular weight ladder (kDa) is shown in lane 1. The gel image was cropped for clarity and the uncropped image is provided in Fig.S5. (**B**) Biolayer interferometry sensorgrams of P1156 binding to indicated chemokines. Plots display wavelength shift (y-axis, nm) versus time (x-axis, seconds). Solid lines indicate collected data, dashed lines indicate fitted data.

P1243:G4S:P1156 and deglycosylated P1156:G4S:P1243 could be detected readily. Surprisingly, deglycosylated P1243:G4S:P1156 and glycosylated P1156:G4S:P1243 could not be detected in these experiments. We do not have an explanation for this glycosylation-dependent variability except that such immunodetection issues have also been noted with other His-tagged recombinant proteins[31]. However, the purification on Ni-NTA affinity column, binding to the biolayer interferometry Ni-NTA sensor, together with the western blot data indicate that the C-terminal His-tag was intact. Together these experiments showed that the full-length two-warhead proteins were produced in each case. Analysis of the purified protein fractions showed that they migrated at higher molecular weights (between 30–60 kDa) than the expected molecular weight of 20 kDa (Fig. 5B). This is consistent with the predicted glycosylation for P1243 and for P1156. The purified protein fractions obtained for each "two-warhead" evasin were pooled for further analysis.

Binding of "two-warhead" evasins to CC and CXC chemokines. We next assayed the binding of the "two-warhead" evasins to a panel of CC and CXC chemokines using biolayer interferometry, initially by determining if they bound at 100 nM chemokine concentration in a cross-binding screen (Supplementary Material Fig. S2). This suggested binding to several CC and CXC chemokines. In these studies, we found that P1243:G4S:P1156 appeared to bind certain chemokines (CXCL4, 7, 12, 13, 14) that were not bound by the parental evasins. In titration experiments we however found that this binding could not be confirmed (Supplementary Material Fig. S8), and did not follow this up further. No appreciable binding could be observed for XC or CX3C chemokines for either two-warhead evasin. We next performed titration assays in parallel to compare the binding of the parental evasins to the "two-warhead" evasins. The results showed that the "two-warhead" evasins bound several, but not all of the chemokines bound by the parental evasins (Figs 5C, 6). The chemokines most affected by the fusion were the ones that bound the parental evasin with lower affinity. For instance, the two-warhead evasins did not bind CCL1, CCL7, CCL22, CXCL3, CXCL5 or CXCL6, whereas the parental evasins clearly did. We also observed that the relative position of the two evasins in the construction affected the binding patterns to some extent. For example, P1156:G4S:P1243 bound CCL21 and CXCL2, but P1243:G4S:P1156 did not.

Inhibition of CC chemokine function by individual and "two-warhead" evasins. To explore if individual and "two-warhead" evasins would inhibit CC chemokine function, we monitored their effects on the migration of THP-1 human monocyte cells in response to human CC chemokines in 96 well Boyden chamber assays. We determined the effect of titrating in progressively increasing doses of evasins at the EC_{80} dose of each chemokine. Individual dose-response experiments against CCL5 are shown in Fig. 7A–C, from which IC_{50} data were calculated. Summary IC_{50} data for CCL3, CCL3L1 and CCL5, obtained from three biological replicates of such dose-response experiments are presented in Fig. 7D–F. Consistent with their ability to bind CCL3, CCL3L1, and CCL5, we found that the parental P1243 and "two-warhead" evasins also inhibited the function of these chemokines in a dose-dependent manner. Analysis of the summary data (Fig. 7D–F) indicated that the mean IC_{50} values for P1243, P1243:G4S:P1156, and P1156:G4S:P1243 respectively against CCL5 were 8.9E-9, 7.4E-9 and 1.2E-8 M, against CCL3 were 6.5E-9, 1.2E-8, and 8.8E-9 M, and against CCL3L1 were 1E-9, 1.7E-9, and 2.2E-9 M. There was no statistically significant difference in the ability of either "two-warhead" to inhibit these CC chemokines in comparison to the parental evasin P1243.

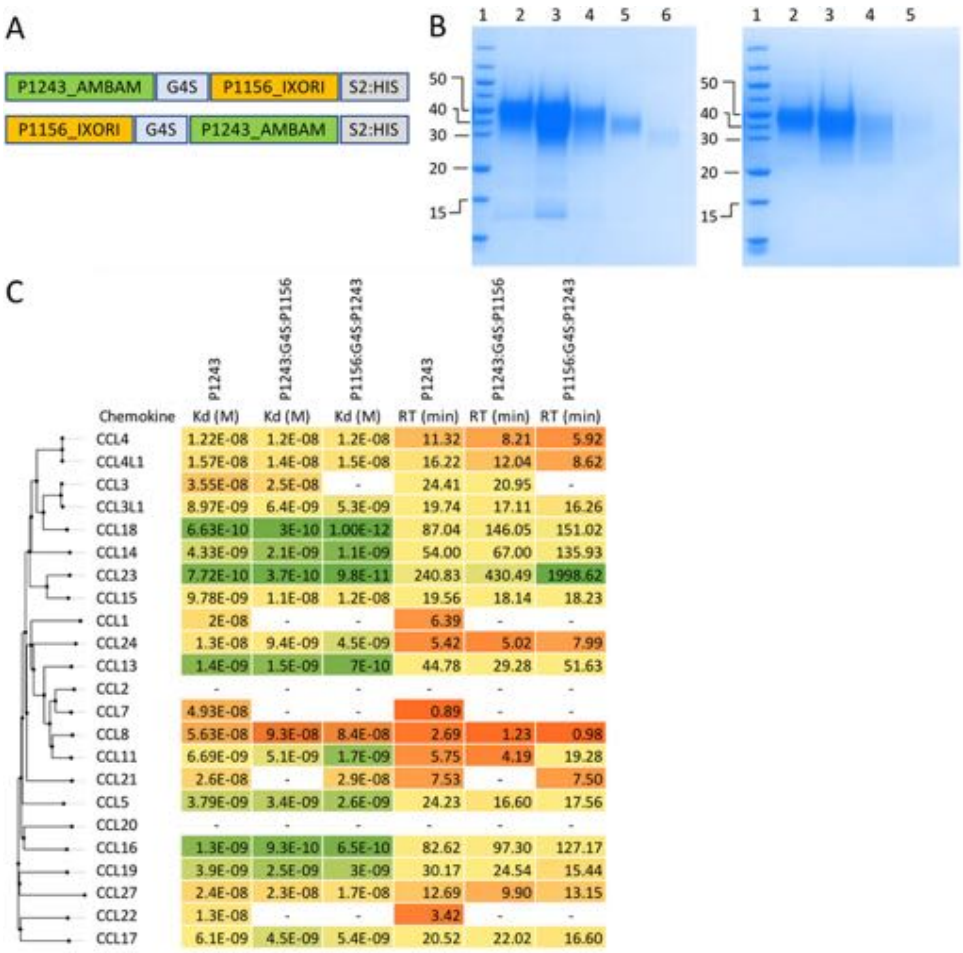


Figure 5. Characterization of single and "two-warhead" evasins. (**A**) Arrangement of the 2-warhead expression constructs P1243:G4S:P1156 and P1156:G4S:P1243 (not to scale). P1243 was engineered in-frame with a GGGGS (G4S) flexible linker to P1156. The construct was tagged at the C-terminus with a StrepII:8xHis purification tag (S2:HIS). (**B**) Colloidal Coomassie stained SDS-polyacrylamide gels showing size exclusion column fractions of P1243:G4S:P1156 (left) and P1156:G4S:P1243 (right) obtained following nickel affinity chromatography. Molecular weight ladder (kDa) is indicated in lane 1. The gel images were cropped for clarity and the uncropped images are provided in Fig.S5. (**C**) Binding affinities (K_d, M) and target residence times (RT, minutes) of P1243, P1243:G4S:P1156 and P1156:G4S:P1243 to human CC-chemokines using biolayer interferometry. High affinity binding is indicated as shades of green, medium affinity as yellow, and low affinity as shades of orange. Chemokines are arranged by sequence-similarity based phylogeny. A dash (-) indicates that binding was either not detected (CCL2) or that K_d could not be determined. Affinity and target residence time in each case was calculated on data obtained at five or more chemokine concentrations.

Inhibition of CXC chemokine function by individual and "two-warhead" evasins. We next examined the effect of the parental P1156 and "two-warhead" evasins on the migration of primary human granulocyte cells in response to CXCL8. Individual dose-response experiments are shown in Fig. 8A–C, from which IC_{50} data were calculated. Summary IC_{50} data obtained from three biological replicates of dose-response experiments are presented in Fig. 8D. Consistent with their ability to bind CXCL8, we found that the parental P1156 and "two-warhead" evasins also inhibited the function of CXCL8 in a dose-dependent manner. Analysis of the summary data (Fig. 8D) indicated that the mean IC_{50} values for P1156, P1243:G4S:P1156, and P1156:G4S:P1243 against CXCL8 were 1.8E-9, 3.8E-8 and 7.5E-9 M respectively. The differences between the evasins were not statistically significant.

Discussion

Chemokine-driven inflammation plays a major role in pathogenesis of disease[2]. These include cardiovascular disorders such as myocardial infarction[32], myocarditis[33], atherosclerotic plaque[34], and vasculitis[35], neurological disorders such as stroke[36,37], multiple sclerosis[38], and Alzheimer disease[37], gastrointestinal disorders including inflammatory bowel disease[37], pancreatitis[39], non-alcoholic steatohepatitis[40] and other inflammatory

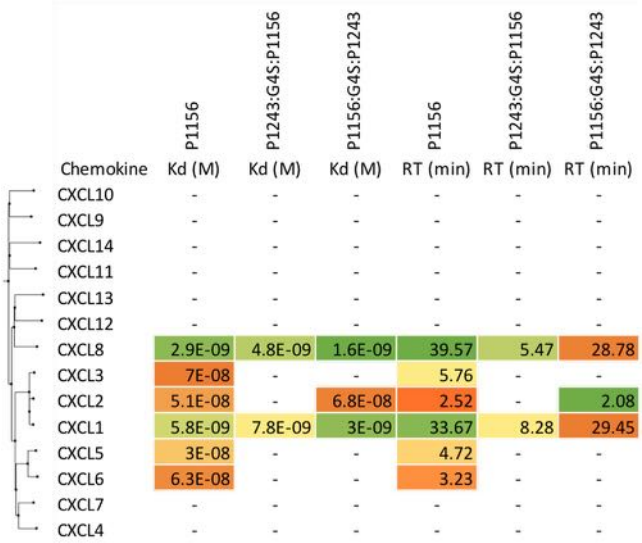


Figure 6. Characterization of CXC chemokine binding by single and "two-warhead" evasins. Binding affinities (K_d, M) and target residence times (RT, minutes) of P1156, P1243:G4S:P1156 and P1156:G4S:P1243 to human CXC-chemokines using biolayer interferometry. High affinity binding is indicated as shades of green, medium affinity as yellow, and low affinity as shades of orange. Chemokines are arranged by sequence-similarity based phylogeny. A dash (-) indicates that either a titration study was not performed in this experiment (CXCL4, 7, 9, 10, 11, 12, 13, 14), or that binding could not be detected. Affinity and target residence time in each case was calculated on data obtained at five or more chemokine concentrations.

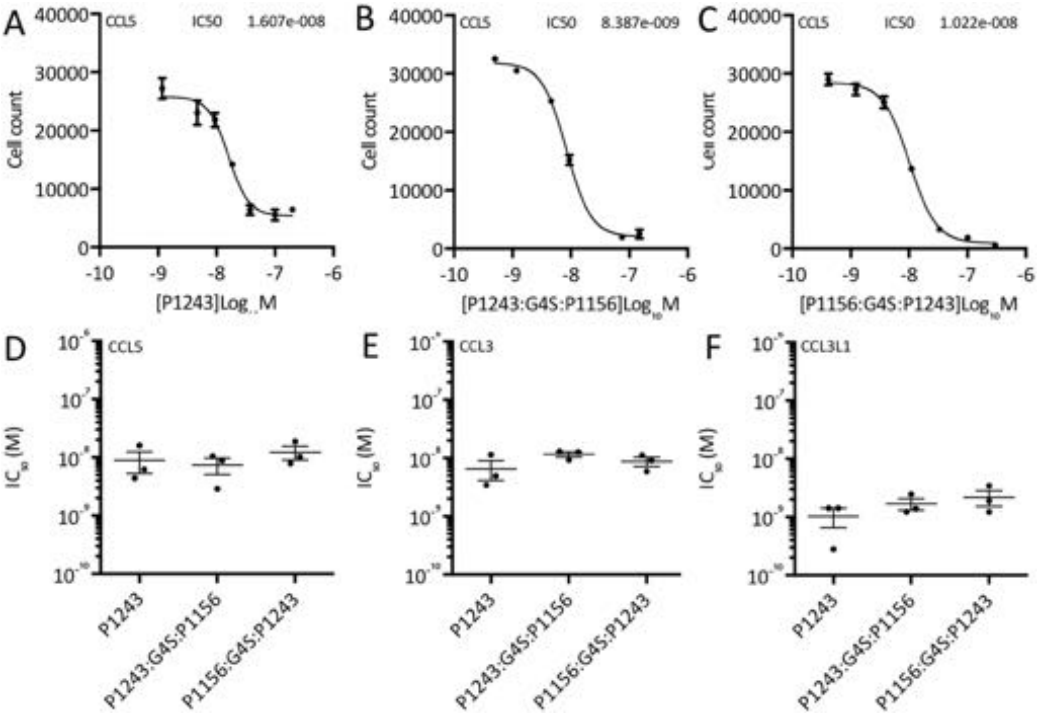


Figure 7. Functional inhibition of CC chemokines by individual and "two-warhead" evasins. (**A**–**C**) Neutralization of CCL5 induced THP-1 cell migration by P1243, P1243:G4S:P1156, and P1156:G4S:P1243 respectively. Y-axis shows cell count of THP-1 cells migrating through to the bottom chamber in response to EC_{80} dose of CCL5. In each case, data from a representative experiment are shown as mean ± s.e.m. of three technical replicates. X-axis shows CKBP concentration (Log_{10} Molar). IC_{50} values (M) indicated in each figure were estimated by fitting an agonist response curve with 4 parameters[22]. (**D**–**F**) Summary IC_{50} data (mean ± s.e.m., and individual data points from three biological replicates) of the indicated CKBPs against CCL5, CCL3 and CCL3L1 respectively. Y-axis shows IC_{50} (logarithmic scale, M), and x-axis shows each CKBP. CC chemokines were assayed using THP-1 cell migration. Each chemokine was assayed at its EC_{80} dose. There were no statistically significant differences between the mean IC_{50} values in each figure.

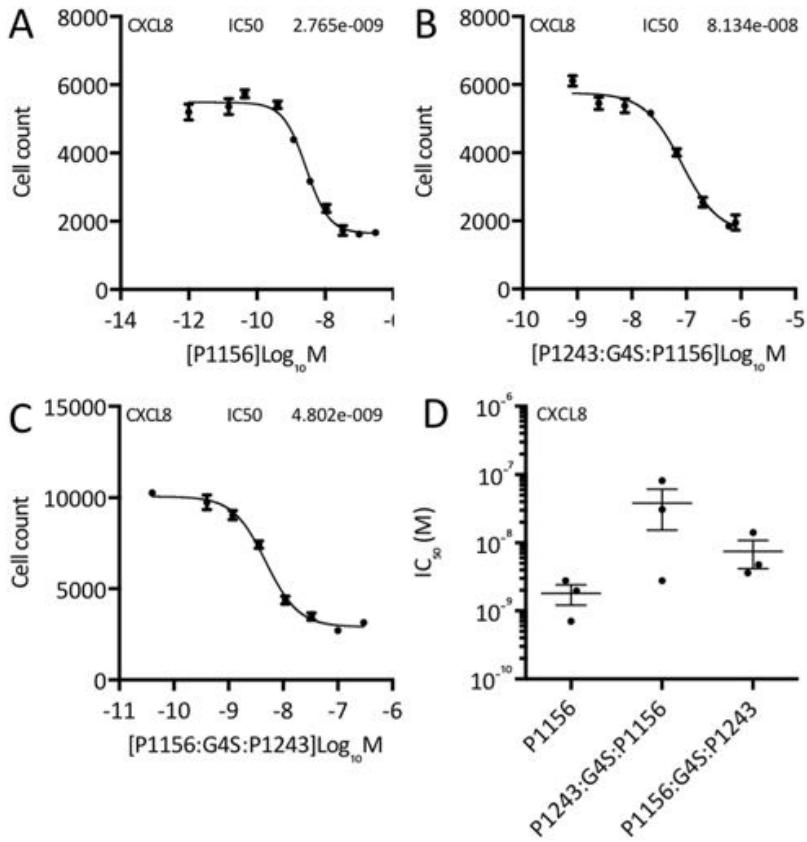


Figure 8. Functional inhibition of CXC chemokines by individual and "two-warhead" evasins. (**A**–**C**) Neutralization of CXCL8 induced granulocyte cell migration by P1156, P1243:G4S:P1156 and P1156:G4S:P1243 respectively. Y-axis shows cell count of granulocytes migrating through to the bottom chamber in response to EC_{80} dose of CXCL8. Data from a representative experiment are shown as mean ± s.e.m. of three technical replicates. X-axis shows CKBP concentration (Log_{10} Molar). IC_{50} values (M) indicated in each figure were estimated by fitting an agonist response curve with 4 parameters[22]. (**D**) Summary IC_{50} data (mean ± s.e.m., and individual data points from three biological replicates) of the indicated CKBPs against CXCL8. Y-axis shows IC_{50} (logarithmic scale, M), and x-axis shows each CKBP. CXCL8 was assayed using granulocyte cell migration at its EC_{80} dose. There were no statistically significant differences between the mean IC_{50} values.

hepatobiliary diseases[41–43], lung diseases including idiopathic pulmonary fibrosis[44], influenza[45,46] and acute lung injury[47], joint diseases such as rheumatoid arthritis[8], and disorders of the skin including psoriasis[48] and scleroderma[44]. Many of these disorders are characterized by an initiating insult such as ischemia in myocardial infarction and stroke, a viral infection in myocarditis and influenza, lipid deposition in the atherosclerotic plaque and non-alcoholic steatohepatitis, toxins such as paracetamol or alcohol in liver injury. The initiating insult results in the expression of chemokines and cytokines, and the ensuing inflammation can cause further additional damage to organs resulting in a vicious cycle of damage and further inflammation.

Typically, in these diseases, multiple CC and CXC class chemokines are expressed, and function synergistically to recruit different types of inflammatory cells. Examples of diseases where multiple CC and CXC chemokines are expressed include atherosclerosis[34], rheumatoid arthritis[8], and idiopathic pulmonary fibrosis[44]. The expression of multiple synergistically acting chemokines from different classes in diseased tissues is a factor that contributes to the difficulty in targeting chemokines using monovalent anti-chemokine therapeutics[8,9]. A wide range of pathogens and parasitic organisms ranging from viruses[15], helminths[16] and ticks[9] produce structurally distinct chemokine-binding proteins (CKBPs) that target multiple chemokines. Pre-clinical trials using these CKBPs has provided proof-of-concept that targeting of multiple chemokines could be effective in inflammatory disease. In particular, tick CKBPs have been shown to be effective in pre-clinical models of arthritis, lung inflammation, colitis, pancreatitis, ischemia-reperfusion injury, plaque vulnerability, and psoriasis (reviewed in[9]).

Putative tick CKBPs have been identified in a variety of tick species using bioinformatic analyses of salivary transcriptome data[19–21]. In an effort to develop a therapeutic armamentarium of tick CKBPs that would provide the ability to target only disease-relevant chemokines without unnecessarily targeting irrelevant chemokines we have developed a yeast surface display approach to identify high-affinity interactors out of libraries of bioinformatically identified putative tick CKBPs[22]. Using this approach we identified 10 novel evasins, from *Rhipicephalus* and *Amblyomma* genera[22]. We also showed that these new evasins bound specifically to between eight (i.e.

"narrow spectrum") to 20 (i.e. "broad-spectrum") CC chemokines, but not to CXC chemokines. A common unifying feature of the these 10 new evasins was their ability to bind CCL2 and CCL13, properties which were not observed in evasins 1 and 4[22]. These evasins contain eight cysteine residues that are conserved in evasins 1 and 4. Further novel eight cysteine or "C8" evasins that bind CC chemokines were identified more recently from *Ixodes, Rhipicephalus* and *Amblyomma* genera by Hayward *et al.*[23].

In this study, we have identified and characterized a further C8 CC-CKBP, P1243. This was also recently reported and partially characterized by Hayward *et al.*[23] as AAM-02, and shown to bind CCL11, CCL24, CCL26, CCL2, and CCL7. Our results indicate that P1243 binds 21 CC chemokines, of which 11 are bound with $K_d < 10$ nM, and so can be regarded as a "broad-spectrum" CC-chemokine inhibitor, akin to EVA4_RHISA[29] and P991[22]. However, P1243, unlike P991, does not bind CCL2 at 300 nM, and we were unable to determine a K_d using our assay conditions (data not shown). This is consistent with data from Hayward *et al.*[23] who show that the K_d for AAM-02 binding to CCL2 is 1000 nM. In comparison to P991, P1243 has a far shorter target residence time for chemokines that are bound in common, suggesting that a potential use may be to achieve short-term inhibition of the chemokine system, whereas P991 would achieve a longer-term inhibition. Analysis of CC-CKBPs show that they all retain the eight cysteine residues that form disulfide bonds in evasin 1[22]. Homology modelling of P1243 and other CC-CKBPs reported previously by us[22] indicates that these Cys residues likely form disulfide bonds, and we thus refer to them as "C8" tick CKBPs. Like previously characterized CC-CKBPs, P1243 has multiple predicted glycosylation sites, and in keeping with this, migrates significantly slower than predicted by the calculated molecular weight of the peptide. As glycosylation does not appear to be required for chemokine recognition[26], it may instead have other functions for instance reducing immunogenicity by creating a "glycan-shield"[49,50], or improving protein stability[51].

In this study, we have also identified a novel CXC-CKBP, P1156, which binds six ELR + CXC class chemokines, CXCL1, 2, 3, 5, 6 and 8, which have, in common, a Glu-Leu-Arg motif immediately preceding the first Cys residue, the ability to bind the receptors CXCR1 and/or CXCR2, and neutrophil trafficking activity[1]. P1156 is homologous to EVA3_RHISA[30], and like it, binds CXCL1 and CXCL8 strongly. We have subsequently identified a number of additional evasins that have six Cys residues that align well with the six Cys residues of evasin 3 and bind CXC-chemokines. We therefore refer to these tick CKBPs collectively as "C6" CKBPs. It should be noted that the "C6" evasin P1156 described in this study is distinct from those described in Hayward *et al.*[23]. Like EVA3_RHISA, P1156 is also predicted to be glycosylated, and migrates significantly slower than predicted by the calculated molecular weight of the peptide.

The availability of several evasins that bind multiple CC and CXC chemokines provides an opportunity to match disease-relevant subsets of both CC and CXC chemokines, and develop novel therapeutics that would not target irrelevant chemokines. A disadvantage of tick CKBPs, however, is that their inability to target both CC and CXC chemokines would mean that combinations of "C8" CC- and "C6" CXC-CKBPs would need to be used. Such combinations of one or more agents require evaluation of the risks and benefits of each agent in the combination[24], rendering the development of combination therapeutics more difficult. Inspired by the development of bispecific antibodies[52], we explored the possibility that the two distinct classes of tick CKBPs could be fused into a single "two-warhead" agent. To achieve this, we linked P1243 with P1156 using a GGGGS linker to minimize steric hindrance and misfolding. The resultant "two-warhead" CKBPs retain most of the properties of the parental CKBPs, and can bind and neutralize subsets of both CC and CXC-chemokines. The mechanism of loss of some chemokine binding in the "two-warhead" CKBPs is unclear at present. One possible explanation is steric hindrance, and although this was not overcome by swapping the relative positions of P1243 and P1156, it could potentially be overcome by adopting longer linkers or other linker types[53]. A limitation of our current work is that we have only shown the effects of the two-warhead evasins in assays that measure chemokine effects on single cell types such as monocytes or granulocytes. In future work it would be important to develop *in vitro* assays that use different combinations of white blood cell types, for instance present in whole blood, and a mixture of chemokines, and also validate the two-warhead evasins usng *in vivo* assays of inflammation.

Applications of a "two-warhead" tick CKBP that binds both a CC chemokine and a CXC chemokine may include the therapeutic inhibition of chemokine signalling in any inflammatory disease associated with both CC and CXC chemokines. By examination of chemokine expression patterns in disease and the binding characteristics of the two-warhead CKBP P1243:G4S:P1156 reported in this paper, certain exemplar therapeutic indications would thus include myocarditis, myocardial infarction, atherosclerosis, vasculitis, idiopathic pulmonary fibrosis, inflammatory bowel disease and rheumatoid arthritis (Table S1). An alternative approach would be to combine a CC chemokine binding evasin with a CXCR1/CXCR2 antagonist such as SCH527123/diaminocyclobutandione-1[54], which would block signalling by the neutrophil attracting chemokines blocked by P1156. However, as discussed previously, the development of such combination therapeutics is complicated by issues involving risks and benefits of each individual agent in a combination[24].

In conclusion, we have shown that it is possible to target specific CC- and CXC-chemokine subsets by using a single agent that is created by a fusion of a tick CC- and a tick CXC-CKBP. As each tick CC- and CXC-CKBP has a remarkably distinctive chemokine binding profile, including narrow and broad-spectrum binding activities, the single agent created by fusing the two will also have a unique and distinctive CC and CXC-chemokine binding profile. This ability to tailor the chemokine binding profile of a "two-warhead" evasin by selecting parental evasins with appropriate CC and CXC binding activity, may provide a significant advantage over viral or helminth CKBPs where such ability to tailor binding properties has not yet been demonstrated. We suggest that novel "two-warhead" CKBPs, designed by matching the chemokine-subset binding properties of parental CKBPs to the CC and CXC chemokines expressed in a particular inflammatory disease, would achieve precision targeting of disease-relevant CC and CXC chemokine subsets by a single agent. We predict that such agents would be useful in the therapy of a broad range of inflammatory disease that are characterised by the combinatorial expression of CC and CXC chemokines.

Experimental procedures

Yeast surface display. Yeast surface display was performed exactly as described previously[22]. Briefly, EBY100 yeast transformed with tick transcriptome library plasmids were induced with galactose and labelled with biotinylated chemokines (Almac) and streptavidin-AF647, and then sorted using a MoFlo FACS system based on a gate defined by a negative control that omitted the chemokine. Cells obtained were regrown, and a second round of sorting was performed, following which cells were plated at low dilution to facilitate recovery of individual clones. Plasmid inserts from individual clones were amplified by PCR and sequenced to identify the insert. Individual yeast clones were also re-tested to confirm chemokine binding by FACS analyses using a 96-well ATTUNE NXT system (Life Technologies).

Plasmids. P1243, P1243:G4S:P1156 and P1156:G4S:P1243 expression plasmids were constructed in plasmid pHLSec[55] using PCR and infusion cloning as described[22] and contained a C-terminal G4S linker, a strep II-8xHis protein purification tag (GGGGGSGGGGSGGASAWSHPQFEKLEHHHHHHHH[56]), and an N-terminal ETG sequence from pHLSec.The P1156 expression plasmid was constructed using idempotent parts using our laboratory's adaptation of the GoldenGate/GoldenBraid cloning method[22]. Parts included the CAGGS promoter (from GenBank Sequence AB281497), Igk signal peptide[57], StrepII:His tag (GGASAWSHPQFEKLEHHHHHHHH, pQE-Trisystem, Qiagen), and bovine growth hormone terminator (pcDNA3, Invitrogen). Following signal peptide cleavage the expected sequence at the N-terminus is DGG predicted by SignalP 3.0[58].

Protein sequence analysis. We used Clustal-W in Megalign Pro (DNAStar version 12.3.1, DNAStar Inc.), to construct CKBP sequence alignments and generate a sequence-similarity based phylogenetic tree which was exported to FigTree (version 1.4.2, http://tree.bio.ed.ac.uk/software/figtree/). Glycosylation sites were predicted using NetNGlyc1.0 (http://www.cbs.dtu.dk/services/NetNGlyc/) and NetOGlyc4.0 (http://www.cbs.dtu.dk/services/NetOGlyc/)[59]. Molecular weight and isoelectric point (pI) of proteins were calculated at ExPASy(http://web.expasy.org/compute_pi/). We used MUSCLE in Megalign Pro to construct chemokine sequence alignments and sequence-similarity based phylogenetic trees. Homology modelling was performed using MODELLER[60], within PYMOD2.0[61], using the evasin 1: CCL3 structure 3FPU[26] as template. Disulfide bonds were identified using using the Protein Interaction Calculator[62].

Cell lines. HEK293F cells were a gift from Nicola Burgess-Brown (University of Oxford). THP-1 cells were purchased from Sigma. A MycoAlert™ (Lonza) kit was used to confirm freedom from mycoplasma contamination. Cells were functionally authenticated by protein production and chemokine – induced migration for HEK293F and THP-1 respectively.

CKBP production. CKBPs were produced as described previously[22] from HEK293F cells using Nickel charged IMAC Sepharose 6 Fast Flow resin (GE Healthcare), and further purified by size exclusion chromatography. Fractions showing absorption at 280 nm were analyzed by electrophoresis on a 12% SDS-PAGE gel, and stained with colloidal Coomassie. Yields obtained (mg/L culture supernatant volume) were 10.1 for P1243, 3.6 for P1156, 46.4 for P1243:G4S:P1156, and 13.1 for P1156:G4S:1243. N-terminal sequencing of two-warhead proteins was performed using Edman degradation at Alta Bioscience, Birmingham.

Deglycosylation. Two-warhead CKBPs were prepared as above except that kifunensine was added to a final concentration of 7.5μg/mL following transfection. Purified protein was diluted 1:1 with 40 mM HEPES, 300 mM NaCl and 1 mM TCEP, and then treated with PNGaseF (NEB) and EndoF1 (gift from C. Siebold, STRUBI) at a ratio of 1:1000 and incubated overnight at 37 °C. Degylcosylated protein was purified by size exclusion chromatography. Western blotting was performed using standard protocols[63], using a mouse monoclonal anti-His primary antibody (R&D Systems) and HRP-tagged goat anti-mouse secondary antibody (Jackson), and Western Lightning ECL Pro (Perkin Elmer kit), and imaged on a BioRad ChemiDoc MP system following the manufacturer's instructions.

Biolayer interferometry cross-binding screen. Biolayer interferometry was performed as described previously[22]. Briefly, we used an OctetRed® system using dip and read Ni-NTA biosensors (ForteBio). The assay buffer contained 10 mM Na_2HPO_4, 1.8 mM KH_2PO_4, 2.7 mM KCl, 500 mM NaCl, 0.1% BSA, 0.002% TWEEN-20, pH 7.4. Assay buffer was used to establish the response baseline (180 seconds). The temperature condition (30 °C) was recommended by the manufacturer. Purified evasin (His-tagged) was immobilized on the Ni-NTA sensor using 1 μM evasin in assay buffer for 500 seconds. The sensor was washed with assay buffer for 60 seconds, and then exposed to 300 nM chemokine in assay buffer to record the association phase. As low affinity binders were identified by this assay, for the two-warheads we used a 100 nM chemokine concentration for the cross-binding screen. The cross-binding screen was performed as a single experiment against all human chemokines with the exception of CCL25, CCL26, and CXCL16, where chemokine non-specifically bound to the sensor, and CXCL17, CXCL4L1, and XCL2, which were not available from Peprotech. The sensor was exposed to assay buffer to measure dissociation. The sensor was regenerated as described previously before re-use[22]. Reference experiments were performed by placing a sensor with evasin alone loaded into buffer to account for baseline drift which was then subtracted. Data was processed in ForteBio Data Analysis 9 software.

Biolayer interferometry. Titration experiments were carried as described previously[22]. Briefly, each experiment was performed once with chemokine concentration ranging from 300 nM to 0.4 nM, (except for CXCL2 where a range of 600 nM to 1.2 nM was used due to issues with data fitting) and using a non-interacting reference protein (of sequence DGGQRNAICRLPPDEGICRASIPRFYFNPAEGKCSFFIYGGCEGNENNFETIEECEKTC

GEPERPSDFEGADFETGCAPKPQRGFCKGFLDHWFFNVTSGECEAFLYSGCGGNDNNYESKEECEIACKL TGGASAWSHPQFEKLEHHHHHHHHH) to allow for non-specific binding to the sensor. For each titration assay, at least five chemokine concentrations were studied. ForteBio Data Analysis 9 software was used to process the data and calculate association (k_{on}), dissociation (k_{off}), and affinity (K_d) constant using a one-site binding fit. The off-rate (k_{off}, s^{-1}) obtained from biolayer interferometry was used to calculate the target residence time or dissociation half-life as described[22,64]. For certain chemokine-evasin interactions where a curve fit was not possible, a steady state analysis was performed using ForteBio Data Analysis 9 software to obtain the $K_{d,}$ from the equilibrium response, and here k_{off} and k_{on}, and hence target residence times were not calculated. Data with poor curve fits ($R^2 < 0.9$) were excluded.

THP-1 cell migration assays. THP-1 monocyte migration assays were performed as described previously[22]. Briefly, chemokine (EC_{80} dose) and evasin (0.006–300 nM doses, in 0.5% fetal bovine serum) were added to the bottom chamber of a 96-well transwell migration plate (5 μM pore size, Corning) and incubated for 30 min at 37 °C before beginning the cell migration assay by adding 5E5 cells to the top chamber. Three technical replicates for each IC_{50} determination were analysed in GraphPad Prism fitting an inhibitor response curve with 4 parameters. The mean IC_{50} from three biological replicates was then calculated. In control experiments (Fig. S3A) we observed that evasins inhibited the small degree of migration induced in vehicle alone controls, we attribute this to neutralization of naturally occurring chemokines in serum[65].

Granulocyte migration assays. Human granulocyte migration assays (see Supplementary Material Figs S3 and S4) were performed using 96 well transwell migration plates (3 μM pore size, Corning). Fresh whole blood was collected from healthy individuals each day of experiment. To collect granulocytes, red blood cells were first depleted, from whole blood, using HetaSep™ (StemCell Technologies) following instructions of the manufacturer. All nucleated cells were then collected and any remaining red blood cells lysed using MACS Red Lysis Buffer (MACS, Miltenyi Biotec). Cells were counted on a ATTUNE flow cytometer using a forward scatter (FSC) versus side scatter (SSC) dot plot. Effective concentrations (EC) EC_{80} and EC_{50} for each chemokine was determined each day, for each batch of blood, in three technical replicates. Chemokines (0–100 nM (Peprotech), in 150 μl RPMI-1640 + L-glu (2 mM) + 0.5% heat treated fetal bovine serum (all from Sigma) were placed in the bottom chamber. Cells (2E5, in 50 μl RPMI- 1640 + L-glu (2 mM) + 0.5% heat treated fetal bovine serum) were placed in the top chamber, and incubated at 37 °C, 5% CO2 for one hour. The migration plate was shaken at 850 r.p.m. for 10 minutes, and media from bottom plate transferred to a U-bottomed 96 well plate. Cells were counted on a ATTUNE flow cytometer using a FSC versus SSC dot plot, and data analysed in GraphPad Prism fitting an agonist response curve with 4 parameters. IC_{50} for each evasin was determined in three technical and three biological replicates using the above system. Chemokine (EC_{80} dose determined on day of experiment) and evasin (0.01 nM-600 nM concentration) were added to the bottom chamber and incubated for 30 min 37 °C, before beginning the cell migration assay. Data (three technical replicates for each IC_{50} determination) were analysed in GraphPad Prism fitting an inhibitor response curve with four parameters. The mean IC_{50} from three biological replicates was then calculated. In control experiments (Supplementary Material Fig. S3B) we observed that evasins inhibited the small degree of migration induced in vehicle alone controls, we attribute this to neutralization of naturally occurring chemokines in serum[65]. The experiments performed on human blood samples were done according to University of Oxford guidelines. Specifically, this study did not require institutional ethical approval as the human tissue was being used solely as a reagent to assay evasin activity. Verbal informed consent was taken from all volunteers who donated the blood samples. All samples were anonymised before use, and no samples were stored. Formal review of the process was obtained from the University of Oxford Medical Sciences Interdivisional Research Ethics Committee (MS IDREC).

Statistical analyses. GraphPad Prism was used to calculate summary statistics. Tests of significance were calculated using ordinary one-way ANOVA, assuming Gaussian distribution and equal variance, in GraphPad Prism, with Tukey's correction for multiple testing.

Data availability. The authors declare that data supporting this manuscript are available either within the manuscript or as Supplementary Information.

Nucleotide accession numbers. JAG91989.1 (P1243) and JAB72437.1 (P1156)

Note added in proof: A further novel C8 evasin that binds CC chemokines was reported by us while this manuscript was under review[66].

References

1. Bachelerie, F. *et al*. International Union of Basic and Clinical Pharmacology. LXXXIX. Update on the extended family of chemokine receptors and introducing a new nomenclature for atypical chemokine receptors. *Pharmacol Rev* **66**, 1–79 (2014).
2. Garin, A. & Proudfoot, A. E. I. Chemokines as targets for therapy. *Experimental Cell Research* **317**, 602–612 (2011).
3. Allen, S. J., Crown, S. E. & Handel, T. M. Chemokine:Receptor Structure, Interactions, and Antagonism. *Annu. Rev. Immunol.* **25**, 787–820 (2007).
4. Fernandez, E. J. & Lolis, E. Structure, function, and inhibition of chemokines. *Annu. Rev. Pharmacol. Toxicol.* **42**, 469–499 (2002).
5. Szpakowska, M. *et al*. Function, diversity and therapeutic potential of the N-terminal domain of human chemokine receptors. *Biochemical Pharmacology* **84**, 1366–1380 (2012).
6. Gouwy, M., Schiraldi, M., Struyf, S., Van Damme, J. & Uguccioni, M. Possible mechanisms involved in chemokine synergy fine tuning the inflammatory response. *Immunol. Lett.* **145**, 10–14 (2012).
7. von Hundelshausen, P. *et al*. Chemokine interactome mapping enables tailored intervention in acute and chronic inflammation. *Sci Transl Med* **9** (2017).

8. Szekanecz, Z. & Koch, A. E. Successes and failures of chemokine-pathway targeting in rheumatoid arthritis. *Nat Rev Rheumatol* **12**, 5–13 (2016).
9. Proudfoot, A. E., Bonvin, P. & Power, C. A. Targeting chemokines: Pathogens can, why can't we? *Cytokine* **74**, 259–267 (2015).
10. Horuk, R. Chemokine receptor antagonists: overcoming developmental hurdles. *Nature Reviews Drug Discovery* **8**, 23–33 (2009).
11. Brandes, M., Klauschen, F., Kuchen, S. & Germain, R. N. A systems analysis identifies a feedforward inflammatory circuit leading to lethal influenza infection. *Cell* **154**, 197–212 (2013).
12. Gonzalez-Motos, V., Kropp, K. A. & Viejo-Borbolla, A. Chemokine binding proteins: An immunomodulatory strategy going viral. *Cytokine & growth factor reviews* **30**, 71–80 (2016).
13. Lubman, O. Y. & Fremont, D. H. Parallel Evolution of Chemokine Binding by Structurally Related Herpesvirus Decoy Receptors. *Structure* **24**, 57–69 (2016).
14. Burns, J. M., Dairaghi, D. J., Deitz, M., Tsang, M. & Schall, T. J. Comprehensive mapping of poxvirus vCCI chemokine-binding protein. Expanded range of ligand interactions and unusual dissociation kinetics. *The Journal of biological chemistry* **277**, 2785–2789 (2002).
15. Heidarieh, H., Hernaez, B. & Alcami, A. Immune modulation by virus-encoded secreted chemokine binding proteins. *Virus Res* **209**, 67–75 (2015).
16. Smith, P. *et al*. Schistosoma mansoni secretes a chemokine binding protein with antiinflammatory activity. *J. Exp. Med.* **202**, 1319–1325 (2005).
17. Counago, R. M. *et al*. Structures of Orf Virus Chemokine Binding Protein in Complex with Host Chemokines Reveal Clues to Broad Binding Specificity. *Structure* **23**, 1199–1213 (2015).
18. Bonvin, P., Power, C. A. & Proudfoot, A. E. Evasins: therapeutic potential of a new Family of Chemokine-Binding proteins from ticks. *Front Immunol* **7**, 1–7 (2016).
19. Karim, S. & Ribeiro, J. M. An Insight into the Sialome of the Lone Star Tick, Amblyomma americanum, with a Glimpse on Its Time Dependent Gene Expression. *PLoS One* **10**, e0131292 (2015).
20. Karim, S., Singh, P. & Ribeiro, J. M. C. A Deep Insight into the Sialotranscriptome of the Gulf Coast Tick, Amblyomma maculatum. *PLoS ONE* **6**, e28525 (2011).
21. Garcia, G. R. *et al*. The sialotranscriptome of Amblyomma triste, Amblyomma parvum and Amblyomma cajennense ticks, uncovered by 454-based RNA-seq. *Parasit Vectors* **7**, 430 (2014).
22. Singh, K. *et al*. Yeast surface display identifies a family of evasins from ticks with novel polyvalent CC chemokine-binding activities. *Sci Rep* **7**, 4267 (2017).
23. Hayward, J. *et al*. Ticks from diverse genera encode chemokine-inhibitory evasin proteins. *The Journal of biological chemistry* **292**, 15670–15680 (2017).
24. Woodcock, J., Griffin, J. P. & Behrman, R. E. Development of novel combination therapies. *The New England journal of medicine* **364**, 985–987 (2011).
25. Chao, G. *et al*. Isolating and engineering human antibodies using yeast surface display. *Nat Protoc* **1**, 755–768 (2006).
26. Dias, J. M. *et al*. Structural Basis of Chemokine Sequestration by a Tick Chemokine Binding Protein: The Crystal Structure of the Complex between Evasin-1 and CCL3. *PLoS ONE* **4**, e8514 (2009).
27. Frauenschuh, A. *et al*. Molecular cloning and characterization of a highly selective chemokine-binding protein from the tick Rhipicephalus sanguineus. *J. Biol. Chem.* **282**, 27250–27258 (2007).
28. Concepcion, J. *et al*. Label-free detection of biomolecular interactions using BioLayer interferometry for kinetic characterization. *Comb Chem High Throughput Screen* **12**, 791–800 (2009).
29. Déruaz, M. *et al*. Evasin-4, a tick-derived chemokine-binding protein with broad selectivity can be modified for use in preclinical disease models. *FEBS Journal* **280**, 4876–4887 (2013).
30. Deruaz, M. *et al*. Ticks produce highly selective chemokine binding proteins with antiinflammatory activity. *Journal of Experimental Medicine* **205**, 2019–2031 (2008).
31. Debeljak, N., Feldman, L., Davis, K. L., Komel, R. & Sytkowski, A. J. Variability in the immunodetection of His-tagged recombinant proteins. *Anal Biochem* **359**, 216–223 (2006).
32. Frangogiannis, N. G. The inflammatory response in myocardial injury, repair, and remodelling. *Nat Rev Cardiol* **11**, 255–265 (2014).
33. Leuschner, F., Katus, H. A. & Kaya, Z. Autoimmune myocarditis: past, present and future. *Journal of autoimmunity* **33**, 282–289 (2009).
34. Zernecke, A. & Weber, C. Chemokines in atherosclerosis: proceedings resumed. *Arteriosclerosis, thrombosis, and vascular biology* **34**, 742-750 (2014).
35. Eardley, K. S., Smith, S. W. & Cockwell, P. Chemokines in vasculitis. *Front Biosci (Elite Ed)* **1**, 26–35 (2009).
36. Mirabelli-Badenier, M. *et al*. CC and CXC chemokines are pivotal mediators of cerebral injury in ischaemic stroke. *Thrombosis and haemostasis* **105**, 409–420 (2011).
37. Leiman, D. A. & Lichtenstein, G. R. Therapy of inflammatory bowel disease: what to expect in the next decade. *Curr Opin Gastroenterol* **30**, 385–390 (2014).
38. Cheng, W. & Chen, G. Chemokines and chemokine receptors in multiple sclerosis. *Mediators Inflamm* **2014**, 659206 (2014).
39. Manohar, M., Verma, A. K., Venkateshaiah, S. U., Sanders, N. L. & Mishra, A. Pathogenic mechanisms of pancreatitis. *World J Gastrointest Pharmacol Ther* **8**, 10–25 (2017).
40. Braunersreuther, V., Viviani, G. L., Mach, F. & Montecucco, F. Role of cytokines and chemokines in non-alcoholic fatty liver disease. *World J Gastroenterol* **18**, 727–735 (2012).
41. Dyson, J. K. *et al*. Novel therapeutic targets in primary biliary cirrhosis. *Nat Rev Gastroenterol Hepatol* **12**, 147–158 (2015).
42. Aron, J. H. & Bowlus, C. L. The immunobiology of primary sclerosing cholangitis. *Semin Immunopathol* **31**, 383–397 (2009).
43. Marra, F. & Tacke, F. Roles for chemokines in liver disease. *Gastroenterology* **147**, 577–594 e571 (2014).
44. Sahin, H. & Wasmuth, H. E. Chemokines in tissue fibrosis. *Biochim. Biophys. Acta* **1832**, 1041–1048 (2013).
45. Ramos, I. & Fernandez-Sesma, A. Modulating the Innate Immune Response to Influenza A Virus: Potential Therapeutic Use of Anti-Inflammatory Drugs. *Front Immunol* **6**, 361 (2015).
46. Tisoncik, J. R. *et al*. Into the eye of the cytokine storm. *Microbiol Mol Biol Rev* **76**, 16–32 (2012).
47. Bhatia, M. & Moochhala, S. Role of inflammatory mediators in the pathophysiology of acute respiratory distress syndrome. *The Journal of pathology* **202**, 145–156 (2004).
48. Mabuchi, T., Chang, T. W., Quinter, S. & Hwang, S. T. Chemokine receptors in the pathogenesis and therapy of psoriasis. *J. Dermatol. Sci.* **65**, 4–11 (2012).
49. Sommerstein, R. *et al*. Arenavirus Glycan Shield Promotes Neutralizing Antibody Evasion and Protracted Infection. *PLoS Pathog* **11**, e1005276 (2015).
50. Wei, X. *et al*. Antibody neutralization and escape by HIV-1. *Nature* **422**, 307–312 (2003).
51. Sola, R. J. & Griebenow, K. Effects of glycosylation on the stability of protein pharmaceuticals. *J Pharm Sci* **98**, 1223–1245 (2009).
52. Tiller, K. E. & Tessier, P. M. Advances in Antibody Design. *Annu Rev Biomed Eng* **17**, 191–216 (2015).
53. Reddy Chichili, V. P., Kumar, V. & Sivaraman, J. Linkers in the structural biology of protein-protein interactions. *Protein Sci* **22**, 153–167 (2013).
54. Planaguma, A. *et al*. Combined anti CXC receptors 1 and 2 therapy is a promising anti-inflammatory treatment for respiratory diseases by reducing neutrophil migration and activation. *Pulm Pharmacol Ther* **34**, 37–45 (2015).

55. Zhao, Y. *et al.* Automation of large scale transient protein expression in mammalian cells. *J. Struct. Biol.* **175**, 209–215 (2011).
56. Schmidt, T. G. & Skerra, A. The Strep-tag system for one-step purification and high-affinity detection or capturing of proteins. *Nat Protoc* **2**, 1528–1535 (2007).
57. Ho, M., Nagata, S. & Pastan, I. Isolation of anti-CD22 Fv with high affinity by Fv display on human cells. *Proc. Natl. Acad. Sci. USA* **103**, 9637–9642 (2006).
58. Bendtsen, J. D., Nielsen, H., von Heijne, G. & Brunak, S. Improved prediction of signal peptides: SignalP 3.0. *Journal of molecular biology* **340**, 783–795 (2004).
59. Steentoft, C. *et al.* Precision mapping of the human O-GalNAc glycoproteome through SimpleCell technology. *The EMBO journal* **32**, 1478–1488 (2013).
60. Webb, B. & Sali, A. Protein structure modeling with MODELLER. *Methods Mol Biol* **1137**, 1–15 (2014).
61. Janson, G., Zhang, C., Prado, M. G. & Paiardini, A. PyMod 2.0: improvements in protein sequence-structure analysis and homology modeling within PyMOL. *Bioinformatics* **33**, 444–446 (2017).
62. Tina, K. G., Bhadra, R. & Srinivasan, N. PIC: Protein Interactions Calculator. *Nucleic Acids Res* **35**, W473–476 (2007).
63. Ausubel, F. M. *et al.* Short Protocols in Molecular Biology. Hoboken: John Wiley & Sons, Inc Third Edition (1995).
64. Copeland, R. A., Pompliano, D. L. & Meek, T. D. Drug-target residence time and its implications for lead optimization. *Nature reviews. Drug discovery* **5**, 730–739 (2006).
65. Wilkinson, P. C., Borel, J. F., Stecher-Levin, V. J. & Sorkin, E. Macrophage and neutrophil specific chemotactic factors in serum. *Nature* **222**, 244–247 (1969).
66. Eaton, J. R. O. *et al.* The N-terminal domain of a tick evasin is critical for chemokine binding and neutralization and confers specific binding activity to other evasins. *J Biol Chem*. 2018 Feb 27. pii:jbc.RA117.000487. https://doi.org/10.1074/jbc.RA117.000487. [Epub ahead of print] PubMed PMID: 29487134.

Acknowledgements

This research was funded by British Heart Foundation Chair Award to SB (CH/09/003/26631), Oxford BHF Centre of Research Excellence (RE/13/1/30181), BHF Oxbridge Centre for Regenerative Medicine (AVMEBCA1), Radcliffe Department of Medicine University of Oxford, and Wellcome Trust Core Award (203141/Z/16/Z) to the Wellcome Trust Centre for Human Genetics. YA is supported by a studentship from the Saudi Arabian Cultural Bureau, JE by a studentship from the Oxford BHF Centre of Research Excellence, and AK by a Royal Society Dorothy Hodgkin Fellowship.

Author Contributions

Y.A., G.D., K.S., J.E. and P.E. designed, performed and interpreted yeast, protein interaction and cell-based experiments. S.B. conceived and designed the yeast surface display and two-warhead approach, and performed bioinformatic and statistical analyses, plasmid library construction, peptide sequence analysis and homology modelling A.K. and S.B. supervised and interpreted experiments and all authors contributed to writing the manuscript.

Additional Information

Supplementary information accompanies this paper at https://doi.org/10.1038/s41598-018-24568-9.

Competing Interests: The two-warhead sequences and concept form part of the basis of a patent application. SB has received funding from LAB282 for development of evasins as therapeutics in partnership with Evotec AG.

Publisher's note: Springer Nature remains neutral with regard to jurisdictional claims in published maps and institutional affiliations.

Open Access This article is licensed under a Creative Commons Attribution 4.0 International License, which permits use, sharing, adaptation, distribution and reproduction in any medium or format, as long as you give appropriate credit to the original author(s) and the source, provide a link to the Creative Commons license, and indicate if changes were made. The images or other third party material in this article are included in the article's Creative Commons license, unless indicated otherwise in a credit line to the material. If material is not included in the article's Creative Commons license and your intended use is not permitted by statutory regulation or exceeds the permitted use, you will need to obtain permission directly from the copyright holder. To view a copy of this license, visit http://creativecommons.org/licenses/by/4.0/.

© The Author(s) 2018

JBC Papers in Press. Published on February 27, 2018 as Manuscript RA117.000487
The latest version is at http://www.jbc.org/cgi/doi/10.1074/jbc.RA117.000487

The N-terminal domain of a tick evasin is critical for chemokine binding and neutralization and confers specific binding activity to other evasins

James R.O. Eaton[1,2], Yara Alenazi[1], Kamayani Singh[1], Graham Davies[1], Lucia Geis-Asteggiante[2], Benedikt Kessler[3], Carol V. Robinson[2], Akane Kawamura[1,2] & Shoumo Bhattacharya[1]*.

From the [1]RDM Division of Cardiovascular Medicine; [2]Department of Chemistry; [3]Nuffield Department of Medicine, University of Oxford, Oxford, United Kingdom

Running title: *Hybrid evasins*

*To whom correspondence should be addressed: Shoumo Bhattacharya: Wellcome Trust Centre for Human Genetics, University of Oxford, Roosevelt Drive, Oxford OX3 7BN, UK; sbhattac@well.ox.ac.uk; Tel: (01865)287771.

Keywords: chemokine, chemotaxis, evasin, tick, inflammation, protein-protein interaction, mass spectrometry, homology modeling, domain swapping, anti-inflammatory therapy

ABSTRACT

Tick chemokine-binding proteins (evasins) are an emerging class of biologicals that target multiple chemokines and have shown anti-inflammatory activities in preclinical disease models. Using yeast surface display, we identified a CCL8-binding evasin, P672, from the tick *Rhipicephalus pulchellus*. We found that P672 binds CCL8 and eight other CC-class chemokines with a K_d < 10 nM and four other CC chemokines with a K_d between 10 and 100 nM, and neutralizes CCL3, CCL3L1, and CCL8 with an IC_{50} < 10 nM. The CC chemokine–binding profile was distinct from that of evasin 1 (EVA1), which does not bind CCL8. We also show that P672's binding activity can be markedly modulated by the location of a StrepII:His purification tag. Combining native MS and bottom-up proteomics, we further demonstrated that P672 is glycosylated and forms a 1:1 complex with CCL8, disrupting CCL8 homodimerization. Homology modeling of P672 using the crystal structure of the EVA1 and CCL3 complex as template suggested that 44 N-terminal residues of P672 form most of the contacts with CCL8. Replacing the 29 N-terminal residues of EVA1 with the 44 N-terminal residues of P672 enabled this hybrid evasin to bind and neutralize CCL8, indicating that the CCL8-binding properties of P672 reside, in part, in its N-terminal residues. This study shows that the function of certain tick evasins can be manipulated simply by adding a tag. We conclude that homology modeling helps identify regions with transportable chemokine-binding functions within evasins, which can be used to construct hybrid evasins with altered properties.

Introduction

Chemokines are a family of secreted proteins that are major drivers of both physiological and pathological inflammation (1). They fall into four groups - CC, CXC, XC and CX3C which are defined by the spacing between their N-terminal cysteine residues (2). Structural features common to all chemokines include, a flexible N-terminus, followed by the double cysteine motif, the N-loop, a helix, a three-stranded sheet with 30S (between β1-β2) and 40S (between β2-β3) loops, and a C-terminal helix. The distal N-terminus of the chemokine binds to the chemokine recognition site 2 (CRS2) pocket of GPCR chemokine receptors, whereas the proximal N-terminus and N-loop/40S loop grooves bind chemokine recognition site 1 (CRS1) in the extracellular N-terminus of the receptor (3,4). Binding to the CRS2 pocket results in conformational changes in the GPCR that activates signaling. Binding of chemokines to target receptors is typically "one-to-many", with several chemokines binding more than one receptor, and several receptors binding more than one chemokine. Chemokines also bind with low affinity to endothelial cell surface glycosaminoglycans (GAGs), and this is

Downloaded from http://www.jbc.org/ by guest on April 22, 2018

necessary for chemokine function *in vivo* (5). The 19 chemokine receptors that activate chemotaxis are expressed in varying combinations on adaptive and innate immune cells, and activation by chemokines promotes their directional migration to sites of chemokine expression (6-8). The "one-to-many" interactions between chemokines and receptors, the expression of multiple receptor types on immune and inflammatory cells, and the expression of multiple chemokines at the site of injury or diseased tissues leads to the creation of a robust network that is not amenable to traditional therapeutics that monovalently target either chemokines or their receptors.

Natural selection in viruses, helminths and ticks has resulted in the convergent evolution of proteins that target the chemokine network by different mechanisms (reviewed in (9,10)). For instance, the viral proteins MC148 and vMIP-II bind and inhibit multiple chemokine receptors. Other viruses have evolved chemokine binding proteins (CKBPs) that bind multiple CC and CXC chemokines, and either disrupt GAG binding, or disrupt chemokine binding to the receptor, or both (11). Helminth CKBP also binds multiple CC and CXC chemokines but the mechanism of action is not clearly understood (12). Ticks, uniquely, have two classes of CKBPs, called evasins, with one class, typically containing eight conserved Cys residues ("8-Cys" tick CKBPs), that bind subsets of CC-chemokines, and another class containing six conserved Cys residues ("6-Cys" CKBPs) that bind CXC chemokines. Following the initial identification of class I tick CKBPs, exemplified by evasin 1 (EVA1_RHISA, abbreviated to EVA1) and evasin 4 (EVA4_RHISA, abbreviated to EVA4), and a class II CKBP, exemplified by evasin 3 (EVA3_RHISA (13), abbreviated to EVA3), we (14) and others (15) have identified several other examples of CC-CKBPs from diverse tick species. The structure of EVA1 in complex with CCL3 shows that it has 1:1 stoichiometry, with the N- and C-termini of EVA1 binding the N-terminus and N-loop of CCL3 (16). The selectivity of the EVA1 – CCL3 interaction resides in the 6 residues that immediately precede the double cysteine motif in CCL3. Binding results in a conformational change of the N-terminus of CCL3, and this, together with the binding of the N-loop, explains the inhibition of chemokine activity (16). *In silico* modelling and mutagenesis studies indicate that EVA4 also targets the CCL3 N-terminus (17). Both EVA1 and EVA4 have been shown to have anti-inflammatory efficacy in several pre-clinical disease models, suggesting that they may be potential therapeutics in inflammatory disease (13).

Using yeast surface display, we have isolated a novel CCL8 binding CKBP from the tick *Rhipicephalus pulchellus* called P672_RHIPU (abbreviated to P672). We show that P672 binds and neutralizes several CC chemokines, and that its ability to bind and neutralize chemokines is modulated by the location of a purification tag. We show that binding to CCL8 occurs with 1:1 stoichiometry, and disrupts CCL8 homodimer formation. Using molecular modelling we identify a CCL8 binding region in P672 that can be transplanted to EVA1, a protein that does not bind CCL8. These results show that tick CKBP function can be modulated in some cases by addition of a tag, and provide proof of concept that regions within tick CC-CKBPs with transportable properties can be identified and can be manipulated to create non-natural hybrid proteins with altered characteristics.

Results

Screening of a yeast surface display library

We used fluorescent activated cell sorting (FACS) to screen a yeast surface display library as described in detail previously(14). The plasmid library was constructed to express 352 putative tick CKBPs with either N-terminal (AGA2) or C-terminal (SAG1 or AGA2) surface display tags. The plasmid library was transformed as a pool into yeast, and cells labelled with biotinylated CCL8 and streptavidin-AF647. Labelled cells were sorted by two rounds of FACS (Fig. 1A, B). In each round, we used a sorting gate, determined by FACS analysis of the yeast cells with streptavidin-AF647 alone. The sorting gate was used to exclude yeast cells displaying background fluorescence generated by streptavidin-AF647 binding to yeast. Cells that were recovered in the

Downloaded from http://www.jbc.org/ by guest on April 22, 2018

first sort were re-grown, and were then sorted once again (Fig. 1C). Cells recovered in the second sort were next plated at low density, and individual yeast clones were picked and re-tested by labelling with biotinylated CCL8 and streptavidin – Alexa 647. The clones picked were compared to control yeast expressing the relevant surface display tag (Fig.1D). In these experiments, we found that only a proportion (30.8%) of the clonal yeast population would bind CCL8. Two independent clones recovered in this screen encoded a novel tick CKBP, P672 (accession JAA60789.1). Both clones were obtained with a N-terminal surface display tag.

Sequence analysis of P672

P672 has 104 amino acid residues with a predicted molecular weight of 11.7 kDa, and predicted pI of 4.45. Glycosylation site prediction indicates several N-glycosylations and a single O-glycosylation site. Protein sequence alignment with EVA1, EVA4 and other CC-CKBPs identified by yeast surface display shows that P672 retains the eight Cys residues that form disulfide bonds in EVA1. The arrangement of the Cys residues is consistent with motif C-x(14,17)-C-x(3)-C-x(11,16)-C-x(17,20)-C-x(4)-C-x(4)-C-x(8)-C that we have previously described (14) (Fig. 2A). Phylogenetic analysis of the protein sequence shows that P672 is most closely related to EVA4 (Fig. 2B), with which it shares 36% identity over an alignment length of 105 residues. It shares only 29% identity with EVA1, over an alignment length of 89 residues. There is no significant homology to EVA3. The Pro residue in EVA1 that immediately follows the first Cys, and contacts the disulfide bond in CCL3 (18), is replaced by a Tyr residue, as is the case for EVA4. The conservation plot (Fig. 2C) shows that the N and C-termini of CC-CKBPs are less well conserved than the central core region.

Expression and purification of P672

We expressed P672 as a secreted protein from mammalian cells essentially as described previously (14). We purified P672 with a C-terminal StrepII:His purification tag by nickel affinity followed by size exclusion chromatography. However, as P672 was obtained only in a N-terminal tagged orientation in the yeast surface display screen, we also used a N-terminal His:StrepII tag approach to purify the protein. The purified protein in each case migrated at a larger molecular weight than expected (Fig. 3, Fig. S1**)**. This is consistent with its predicted glycosylation, which was confirmed by digestion of the protein with the glycosidases PNGaseF and EndoF1. On digestion, the smeared band collapses to a single band close to the predicted molecular weight on SDS-PAGE (Fig. 3) together with a corresponding change in retention volume on size exclusion chromatography (Fig. S1A).

Tandem mass spectrometry identification of glycosylated sites in P672

Tandem mass spectrometry (MS/MS) analysis at the peptide level of P672 treated with PNGaseF and Endo F1 was performed, and we were able to achieve sequence coverage of 87%, excepting residues indicated in Fig. 2A. This identified several deamidated residues that had converted from Asn to Asp, corresponding to a mass shift of +0.98 Da, in N-X-S/T motifs (supplementary material Table S1). Deamidation of Asn is a characteristic feature of N-glycosylation cleavage by PNGaseF (19), and indicates that the Asn residues are N-glycosylated. Only partial deglycosylation by PNGaseF and Endo F1 was achieved as supported by the finding of several peptides in deamidated and glycosylated forms, carrying N-acetylglucosamine and/or N-acetylgalactosamine (HexNAc) moieties. The presence of HexNAc can be explained by the Endo F1 cleavage. The N-glycosylation sites identified by MS/MS are indicated in Fig 2A**.**

Binding of P672 to chemokines

We next explored the binding profile of glycosylated P672, with both the N- and C-terminally tagged forms to a chemokine panel using biolayer interferometry (20). CKBPs were immobilized on the sensor through their His tag, and initial screening assays performed at 300 nM chemokine concentration indicated that P672 bound only certain CC chemokines. No binding was detected to CXC, XC or CX3C chemokines (data not shown). Binding affinities (K_d) were subsequently determined through biolayer interferometry titration studies against these CC

Downloaded from http://www.jbc.org/ by guest on April 22, 2018

chemokines (Fig. 4). Notably, we observed different binding patterns when P672 was tagged at the C-terminus, specifically the loss of binding to CCL14, CCL15, CCL11, CCL7, CCL2, CCL13, CCL1 and CCL16 at 300 nM chemokine concentration. We also noted a marked variation in target residence time (calculated from the off-rate) with P672 tag positioning, e.g. for its binding to CCL8.

Neutralization of chemokines by P672

We next explored the ability of P672, in N- and C-terminally tagged versions, to inhibit chemokine function. We monitored their effects on the migration of THP-1 human monocyte cells in response to human CC chemokines in 96 well Boyden chamber assays (Fig. 5). We determined the effect of titrating in progressively increasing doses of P672 at the EC_{80} dose for each CC chemokine and found that N-terminally tagged P672 inhibits THP-1 cell migration in response to CC chemokines with IC_{50} <10 nM (Fig. 5A-C). The relative effects of tag position were determined by comparing the ability of the N- or C-terminally tagged forms of P672 to inhibit THP-1 cell migration (Fig. 5D). The C-terminal tag position had marked effects on the ability of P672 to inhibit CCL2 and CCL7 activated chemotaxis. Tag position had no significant effect on the ability of P672 to inhibit CCL3, CCL3L1, or CCL8 function. This is consistent with the binding data presented above, and indicates that tag position can affect not only the binding of P672 to chemokines but also its function in solution.

Characterization of P672 in complex with CCL8

To understand the mechanism of P672 binding to CCL8, we characterized individual proteins and the complex using native mass spectrometry. As glycosylation can affect native mass spectrometry unpredictably, we used partially deglycosylated P672 for these experiments. The affinity of partially deglycosylated N-terminally tagged P672 for CCL8 was 7.25E-8 M (Fig. S1B), indicating that native mass spectrometry of the P672-CCL8 complex would be feasible, and would allow us to elucidate the stoichiometry of the interaction.

Initially, CCL8 and P672 were characterized separately. CCL8 was bacterially expressed as a N-terminal His-SUMO fusion, which following SUMO cleavage produced a new N-terminus corresponding to glutamine (Q24). The presence of the glutamine N-terminal residue was confirmed using high resolution native tandem MS. The N-terminal glutamine of CCL8 can cyclise to form pyroglutamic acid, which is required for CCL8 biological activity (21). During electrospray ionization the N-terminal glutamine can also readily cyclise to form pyroglutamic acid and this change corresponded to the most intense peak observed and the identity and site of modification was supported by HCD (higher-energy collision dissociation) fragment ions (Fig. S2). Purified CCL8 was biologically active in a cell migration assay (data not shown). We found that CCL8 formed a homodimer under native mass spectrometric conditions with an average mass of 22566.6 ± 0.8 Da (Fig. 6A). In the case of P672 treated with PNGaseF and Endo F1, native MS spectra were more complex due to the presence of partial glycosylations, deamidations and sodium adducts (Fig. 6B). The average masses observed ranged from 14588 Da to 16628 Da depending on the modifications present. Moreover, mass differences of ~203 Da are observed, suggesting the presence of HexNAc moieties, supporting the results obtained by bottom-up proteomics (Fig. S3).

Native mass spectrometry of the CCL8:P672 complex (mixed in at a 1:1 ratio) showed peaks of average masses ranging from 25.9 to 27.9 kDa, which correspond well with that expected for a glycosylated and sodiated CCL8:P672 heterodimer (Fig. 6C, top panel). In order to demonstrate that this is the CCL8:P672 complex, the *m/z* 2956 was isolated with a 100 *m/z* isolation window and fragmented with HCD (higher energy collision dissociation) at 100 V. We observed that the complex clearly dissociates into CCL8 and a partially glycosylated P672 (Fig. 6C, bottom panel). To further explore complex formation, we performed native mass spectrometry of the P672:CCL8 complex with increasing amounts of CCL8 (Fig. S4). At a 1:1 and 2:1 ratios of CCL8:P672 we observed 3 peaks corresponding to 1:1 heterodimers. At a 3:1 ratio

Downloaded from http://www.jbc.org/ by guest on April 22, 2018

of CCL8:P672, the 1:1 heterodimeric complex continued to be observed along with monomeric and homodimeric CCL8 species. This confirms the 1:1 complex of P672 with CCL8 and indicates that CCL8 homodimers are disrupted by P672.

Homology modelling of P672 in complex with CCL8

The published structure of the EVA1:CCL3 complex (3FPU) also has 1:1 stoichiometry (16), and this template allowed the modelling of the P672:CCL8 complex, using the program MODELLER (22) (Fig. 7). The model suggested that the conserved Cys residues in P672 formed disulfide bonds in a manner similar to EVA1. We next used the Arpeggio (23) webserver to identify interchain interactions, and the binding surface on P672. The model suggested that key CCL8 interacting residues were present in the N-terminus of P672, i.e. residues E17-N44. The model does not provide any role for the extended N-terminus of P672 (i.e. residues V1-T16), which do not align to EVA1 (Fig. 2A). Truncation of residues V1-T16 in P672 resulted in a modest decrease in binding affinity to CCL8 (K_d = 30.4 nM) suggesting that these residues may contribute to binding (Fig. S5). The model also shows that part of the binding surface (residue N34) is adjacent to the C-terminal residue of P672 in the 3D structure (Fig. 7).

Characterisation of P672:EVA1 hybrid molecules

The homology model constructed above suggested that the N-terminal residues of P672 may represent a region that conferred binding to CCL8. To evaluate this hypothesis, we took advantage of the fact the EVA1 does not bind CCL8. Alignment of EVA1 with P672 (Fig. 2A) indicated that CCL8 binding residues predicted are proximal to the second conserved Cys in P672. We replaced the N-terminal 29 residues of EVA1 with the equivalent N-terminal 44 residues of P672. This construct maximized the predicted CCL8 binding interface. We also created other, more extended hybrid molecules, replacing longer regions of EVA1 with the equivalent residues of P672 (Fig. 8A). These proteins were tagged at the C-terminus with a StrepII:His tag so that changes (e.g. deletions) at the N-terminus of P672 could be made without creating steric effects. We also constructed an identically tagged version of EVA1. We expressed these proteins as described above (Fig. S6), and characterised them for binding to target chemokines by biolayer interferometry. We initially assessed all CKBPs for binding at 300 nM chemokine concentration, and then performed titration experiments to determine K_d (Fig 8B). EVA1 bound to the closely related chemokines CCL4L1, CCL4, CCL3L, CCL3, CCL18 and CCL14. No binding was detected to other CC chemokines, consistent with previously reported results (16). Binding to CCL3, CCL3L1 and CCL23 was lost in all the hybrids. All hybrid CKBPs bound CCL8 and CCL18. We next tested if the P672 (1_44): EVA1(29_94) hybrid would neutralize CCL8 function, and we found that it did so with a mean IC_{50} of 48 nM (Fig. 8C). As wild type EVA1 does not bind CCL8, these results indicate that the N-terminal 44 residues of P672, which represent 42% of the P672 protein, contains a CCL8-binding region that is transportable to another evasin.

Discussion

In this work, we have identified, using a yeast surface display approach, a novel evasin-like protein P672_RHIPU (P672) encoded in the salivary transcriptome of the tick *Rhipicephalus pulchellus*. In the yeast surface display experiment, we found that only a proportion of the clonal yeast population would bind CCL8. This finding is likely due, in part, to the fact that only a proportion of clonal yeast express surface display proteins (24), and is consistent with our previous studies (14). As we are using yeast surface display as a screening technique, rather than a quantitative measure of affinity, we explored the affinity of P672 for CCL8 using purified recombinant proteins.

Alignment to other CC chemokine binding evasins indicates that P672 is a "8-Cys" CKBP, with four disulfide bonds predicted in its structure. P672 is most closely related to EVA4, with which it shares 36% identity. In particular, these are the only two evasins identified to date that end immediately following the terminal disulfide forming Cys residue (ending on a

Downloaded from http://www.jbc.org/ by guest on April 22, 2018

tryptophan) and having a tyrosine residue immediately following the first disulfide forming Cys residue instead of proline. Notably this proline in EVA1 forms part of the binding surface and is the residue that targets the conserved disulfide bond in the target chemokine CCL3 (18). The significance of the substitution with tyrosine in P672 is yet unclear.

Like other evasins (14,16,25), P672 has several predicted N- and O-glycosylation sites, and this is consistent with its significantly higher observed molecular weight, and presence of several molecular weight species on size exclusion chromatography. PNGaseF treatment reduced the molecular weight, indicating that there is significant N-glycosylation. We investigated P672 glycosylation using mass spectrometry and found that N-glycosylation was indeed present and was heterogeneous. Our data indicate that deglycosylated P672 also binds CCL8, albeit with reduced affinity. The mechanism for this is unclear. Our mass spectrometry data indicate that residue N34 in P672, which is part of the predicted binding surface, is glycosylated, and upon deglycosylation, is either converted to D, or has a single HexNac sugar moiety attached. It is possible that these changes may affect affinity, and studies are in progress to elucidate the mechanism. Although the affinity was reduced it did not hinder us from studying the stoichiometry of the P672:CCL8 complex by native mass spectrometry.

We noted that P672 was obtained only in a single surface display tag orientation in the yeast surface display screen, with the tag being positioned at the N-terminus. This was unusual, as in previous screens where other evasins were identified we typically obtained clones with tags in both N- and C-terminal positions (14). This observation is consistent with the marked discrepancy in chemokine binding affinities, measured by biolayer interferometry, between N- and C-terminally tagged versions of P672. The reduction in binding affinity was consistent with the reduction in the ability of the protein to neutralize the target chemokine in solution. An important issue that we have not addressed here is the binding of untagged P672 to chemokines. The StrepII:His tag is necessary for rapid purification and, crucially, for binding to the biolayer interferometry biosensor, allowing comparable experiments for K_d determination. An exploration of the properties of untagged P672 is necessary in future work and will require development of strategies for P672 purification and quantifying binding affinities in the absence of a tag. Another issue that we have not addressed is the possibility that untagged or tagged P672 would bind non-chemokine proteins or molecules. This is potentially important as such binding may mediate off-target effects if used therapeutically, and investigation of such binding is necessary in future work.

Taken together these results indicate that the C-terminal tag causes steric interference in the binding of P672 to certain chemokines. The reduction in binding affinity seen with C-terminal tagging may be explained by the close proximity of residues in the chemokine binding surface of P672 with the C-terminal residue of P672, which could lead to steric hindrance.

P672 was identified in a screen performed with the chemokine CCL8, (also known as MCP-2), and in addition binds the closely related chemokines CCL2 (MCP-1) and CCL7 (MCP-3). These three chemokines target the common receptor CCR2, and CCL7 and CCL8 are thought to be partial agonists in comparison to CCL2 (26). CCR2 is a key regulator of monocyte and macrophage migration (27), with potential roles in diverse inflammatory disease including rheumatoid arthritis and inflammatory bowel disease (1). Notably, P672 binds also to a number of other CC chemokines. Some of these such as CCL3 and CCL3L1 have functions in monocyte recruitment, and P672 inhibits the function of these chemokines in monocyte THP-1 cell migration assays. P672 also binds chemokines such as CCL18, CCL14, CCL23, and CCL11 with <10 nM affinity. These chemokines are involved also in lymphocyte (CCL18 (28), CCL14 (29)), in monocyte (CCL14 (29), CCL23 (30)) and eosinophil (CCL11 (31), CCL14 (29)) migration. As several monocyte recruiting chemokines are bound, a potential role of P672 may be to block monocyte migration in the target

Downloaded from http://www.jbc.org/ by guest on April 22, 2018

hosts of the tick *Rhipicephalus pulchellus*. Interestingly, we observed no binding of P672 to CCL5 at chemokine concentrations below 300 nM. CCL5 is a CCR1, CCR3 and CCR5 ligand (32), and is a major chemoattractant for monocytes. The most likely explanation is that ticks such as *Rhipicephalus pulchellus* have other evasins such as P467_RHIPU (14) that can bind CCL5 and thus complement the action of P672.
Tick evasins appear to bind chemokines in a mutually exclusive manner, with "8-Cys" evasins binding exclusively to CC chemokines, and "6-Cys" evasins such as EVA3 binding exclusively to CXC chemokines. Furthermore, within each class, evasins bind only subsets of CC or CXC chemokines. This has been most clearly revealed by initial work showing that EVA4 would bind > 20 CC chemokines, whereas EVA1 bound only 4 CC chemokines (13). P672, like EVA1, binds only to CC chemokines, with some degree of overlap. For instance, both P672 and EVA1 are able to bind to CCL3, CCL3L1, and CCL18. EVA1 binds CCL4, which is not bound by P672. Conversely P672 binds CCL8, whereas EVA1 does not.

An interesting observation is that the IC_{50} of P672 for inhibiting CCL8-induced cell migration is close to the K_d of the CCL8:P672 interaction. In this context, CCL8 binds as an agonist to the chemokine receptors CCR1, CCR2, CCR3, and CCR5 (32), and these receptors are known to act synergistically to activate cell migration (33). Based on this, one explanation for our observation is that titration of CCL8 by P672 may ablate the synergistic effects at a cellular level that occur following binding of CCL8 to its receptors. This could have larger effects on cell migration than are predicted by the K_d. An alternative explanation is that affinity measured by BLI may be underestimated as it involves immobilization of the evasin, and this does not happen in the cell migration assay.

To begin to explore how binding specificity in the context of interactions between evasins and chemokines is created, we used native mass spectrometry. These studies showed that the stoichiometry of the P672:CCL8 complex is 1:1, the same as the previously reported EVA1:CCL3 structure. A homology model of the P672:CCL8 complex based on the EVA1:CCL3 structure, and a deletion study, suggested that the major CCL8 binding region is located in the N-terminal 44 residues of P672. Transferring this region, which represents 42% of the P672 protein, to EVA1 transported the CCL8 binding activity confirming that the determinants of CCL8 binding do indeed reside in the N-terminus. The reduced affinity of CCL8 binding by the hybrids suggests that either other residues outside the transported regions are needed for optimal binding to CCL8, or that the folding of the transported residues is not optimal in the context of the hybrid evasin. The loss of binding to other chemokines (CCL3, CCL3L1 and CCL23) observed in the hybrids also suggest that either other residues in P672 are needed for binding to these chemokines or that the folding of the transported residues is not optimal. The region identified as binding CCL8 represents approximately 42% of P672, and further experiments, beyond the scope of this work, are in progress to narrow down the binding region further. Taken together, these results suggest that regions within a tick CKBP that act to confer chemokine binding can be identified by creating hybrid evasins.
In conclusion, the identification of several novel evasins that bind distinctive subsets of CC chemokines provides the potential ability to match chemokine binding properties of an evasin to disease expression patterns of a chemokine, and thus generate biological tool compounds that target only disease-relevant chemokines. A key challenge is to identify functional regions within an evasin that could be used to engineer novel CKBPs with altered properties, including increased binding to certain chemokines, and reduced binding to others. Analogous approaches have been used, for instance to rationally engineer antibodies with desired properties (34). In this study, by identifying and functionally characterizing a novel tick evasin, we provide proof of concept that regions within evasins with transportable properties can be identified and can be manipulated to create non-natural hybrid proteins with altered characteristics. Further development of these approaches combined with structural approaches and judicious application of steric hindrance through tag location may allow

Downloaded from http://www.jbc.org/ by guest on April 22, 2018

us to systematically engineer novel evasins with desired chemokine binding activities.

Experimental procedures

Yeast surface display

Yeast surface display screening was performed as described previously (14). Briefly, EBY100 yeast transformed with putative evasin library plasmids were induced with galactose to drive expression of the surface displayed protein, labelled with biotinylated CCL8 (Almac) and streptavidin-AlexaFluor647, and then sorted using FACS, excluding cells non-specifically binding streptavidin-AF647 using a sorting gate (Fig. 1). Sorted cells were regrown, a second round of sorting performed, following which cells were plated at low dilution to recover individual clones. Individual yeast clones were re-tested to confirm CCL8 binding by FACS. Inserts from plasmids isolated from individual clones were then PCR amplified and sequenced to identify the cloned evasin.

Plasmids

The P672 N-terminal and C-terminal tagged mammalian expression plasmids were constructed in plasmid pHLSec (35) using PCR and infusion cloning as described (14). The purification tags were either N-terminal strep II - 8xHis protein purification tag (HHHHHHHHSAWSHPQFEKGGGGS), or C-terminal (TGGGGGSGGGGSGGASAWSHPQFEKLEH HHHHHHH). Following signal peptide cleavage an additional ETG sequence predicted by SignalP 3.0 (36) is expected at the N-terminus of each peptide. P672:EVA1 hybrids and EVA1 expression plasmids were made by PCR and infusion cloning into pHLSec, with the C-terminal purification tag. The EVA1 plasmid used here was based on GenBank sequence EZ406190.1, which encodes EVA1 but with the variation K92N. The CCL8 expression plasmid was constructed by PCR amplification of a SUMO-CCL8 cassette and ligation independent cloning into the vector pNIC-BIO3 (gift from Nicola Burgess Brown) (37) to create a 6xHIS-SUMO-CCL8 expression vector with a GSKGGYGLNDIFEAQKIEWHE C-terminal tag.

Protein sequence analysis

We used MUSCLE in Megalign Pro (DNAStar version 12.3.1, DNAStar Inc.), to construct the CKBP and chemokine sequence alignments and generate sequence-similarity based phylogenetic trees. These were exported to FigTree (version 1.4.2, http://tree.bio.ed.ac.uk/software/figtree/). The amino acid conservation was plotted using the EMBOSS (38) program plotcon (http://www.bioinformatics.nl/emboss-explorer/). Glycosylation sites were predicted using NetNGlyc1.0 (http://www.cbs.dtu.dk/services/NetNGlyc/) and NetOGlyc4.0 (http://www.cbs.dtu.dk/services/NetOGlyc/) (39). Molecular weight and isoelectric point (pI) of proteins were calculated at ExPASy (http://web.expasy.org/compute_pi/). We performed homology modelling using MODELLER (22), within PYMOD2.0 (40), using the EVA1: CCL3 structure 3FPU (16) as template. Disulfide bonds prediction was performed using the Protein Interaction Calculator (41) and inter-chain interactions using the Arpeggio server (23).

CKBP production

P672 in N- and C-terminally tagged versions were produced as described previously (14). Briefly, culture supernatants from transiently transfected HEK293F cells were purified using Nickel charged IMAC Sepharose 6 Fast Flow resin (GE Healthcare), followed by size exclusion chromatography. Fractions showing absorption at 280 nm were analyzed by electrophoresis and pooled for subsequent experiments.

Production of deglycosylated P672

The glycosylated protein precursor was prepared as above except that upon transfection of the cells kifunensine was added to a final concentration of 7.5µg/mL. Purified glycosylated protein was concentrated and the solution diluted 1:1 with 40mM HEPES, 300mM NaCl and 1mM TCEP. PNGaseF (NEB) and EndoF1 (gift from C. Siebold, STRUBI) was added to 2 mg of glycosylated P672 at a ratio of 1:1000 and incubated overnight at 37°C. Degylcosylated protein was then separated from glycosylase

Downloaded from http://www.jbc.org/ by guest on April 22, 2018

enzymes by size exclusion chromatography into 20mM HEPES, 150mM NaCl and 0.5mM TCEP. We analysed fractions showing absorption at 280 nm by electrophoresis on a 12% SDS-PAGE gel which was stained with colloidal Coomassie.

CCL8 production

We expressed human CCL8 (residues Q24 to P99) in *E.coli* RosettaGami™ 2 (DE3) cells (Novagen). Cells were grown at 37°C overnight in LB medium containing chloramphenicol (25 μg/mL), tetracycline (10 μg/mL) and kanamycin (50 μg/mL). This culture was then diluted 1 in 30 into terrific broth containing kanamycin (50 μg/mL) and grown at 37°C until an OD_{600} of 0.8 was reached when IPTG was added to a final concentration of 1 mM, and cultured overnight at 18°C. Cells were pelleted by centrifugation (4000 g) and the resulting pellet was frozen and stored at -80C. A 10g pellet was suspended in sonication buffer (20mM NaH_2PO_4, 500mM NaCl, 1mM PMSF, pH 7.4) and sonicated on ice to lyse the cells. The soluble and insoluble fractions were separated by centrifugation (31000 g) and the soluble fraction loaded by gravity flow through Nickel charged IMAC Sepharose 6 Fast Flow resin (GE Healthcare), equilibrated with binding buffer (20 mM NaH_2PO_4, 500 mM NaCl, pH 7.4), washed after binding with wash buffer (20 mM NaH_2PO_4, 1 M NaCl, 20 mM imidazole, pH 7.4) and eluted in 4mL elution buffer (20 mM NaH_2PO_4, 500 mM NaCl, 500 mM imidazole, pH 7.4) dropwise into 20mL cation exchange buffer (20 mM NaH_2PO_4, 100 mM NaCl, pH 7.4). SUMO protease (Ubl-specific protease from *Saccharomyces cerevisiae*, gift from Dr Ritika Sethi) was added (final concentration 50 μg/mL) to the diluted elution and left overnight at 30°C. The cleaved protein mixture was loaded on to a HiTrap Capto S 1mL cation exchange column (GE healthcare) pre-equilibrated in cation exchange buffer (20 mM NaH_2PO_4, 100 mM NaCl, pH 7.4) using an AKTA start. The column was then washed with 5% elution buffer (20 mM NaH_2PO_4, 1M NaCl, pH 7.4) and the protein eluted with a step elution of 50% elution buffer in 1mL fractions. The cleaved chemokine was purified to homogeneity using size exclusion chromatography (Sephadex 16/600, GE healthcare), pre-equilibrated in a final buffer consisting of 20mM HEPES, 500mM NaCl, pH 7.4.

Biolayer interferometry

Biolayer interferometry was performed on an OctetRed® system as described previously (14). Briefly, we performed cross-binding against a panel of human chemokines at 300 nM chemokine concentration. Chemokines excluded were CCL25, CCL26, and CXCL16, which non-specifically bound to the sensor, and CXCL17, CXCL4L1, and XCL2, which were not available. We evaluated binding kinetics with chemokine concentrations ranging from 300 nM to 0.4 nM, and using a non-interacting reference protein to allow for non-specific binding to the sensor. We used ForteBio Data Analysis 9 software to process the data and calculate association (k_{on}), dissociation (k_{off}), and affinity (K_d) constant. Data with poor curve fits ($R^2 < 0.9$) were excluded. The dissociation half-life or target residence time was calculated as described (14,42) from biolayer interferometry off-rates (k_{off}, s^{-1}, as $t_{1/2} = 0.693/(k_{off} \times 60)$).

THP-1 cell migration assays

THP-1 monocyte migration assays were performed as described previously (14). Briefly, effective concentration (EC) EC_{80} for each chemokine was determined using a 96-transwell migration plate (5 μM pore size, Corning), with chemokine doses (0-100 nM) in the bottom chamber and THP-1 cells in the top chamber. Cells were counted on a ATTUNE flow cytometer and data analysed in GraphPad Prism fitting an agonist response curve with 4 parameters. IC_{50} was determined using the above system. An EC_{80} dose of the chemokine and 0 – 100 nM doses of the evasin were added to the bottom chamber and incubated for 30 min at 37°C before beginning the assay. IC_{50} was calculated in GraphPad Prism fitting an inhibitor response curve with 4 parameters.

Determination of glycosylation sites

Aliquots of deglycosylated P672 were reduced with dithiothreitol, alkylated using iodoacetamide and digested with trypsin or neutrophil elastase. Peptide aliquots from tryptic digests (n=3) were analysed by LC-MS/MS using an Easy-nLC 1000

Downloaded from http://www.jbc.org/ by guest on April 22, 2018

coupled to an Orbitrap-LTQ-XL (Thermo Fisher Scientific). Peptides were desalted and concentrated by a C18 PepMap 100 trap (300µm x 5mm, 5µm particle size, 100 Å) for 5 minutes at a flow rate of 20 µl/min and separated by a C18 Acclaim PepMap RSLC column (75 µm x 250 mm, 2µm particle size, 100Å) using a linear gradient from 0 to 64% acetonitrile:H_2O with 0.1% formic acid during 25 min at a flow rate of 300 nL/min. For samples run in the Orbitrap-LTQ-XL, precursor ions were acquired at a mass resolution of 60,000 (m/z 400) and product ions were acquired in the ion trap. The 5 most intense precursor ions of charge ≥2 were selected for fragmentation by collision induced dissociation (35V) and dynamic exclusion settings allowed a precursor to be selected up to 3 times in a period of 30 s prior to be excluded for 60 s. The peptide aliquot (n=1) from an elastase digest was analyzed using a Q Exactive mass spectrometer coupled with a Dionex Ultimate 3000 UPLC as described previously (43). In brief, samples were desalted online (PepMap C18, 300µm x 5mm, 5 µm particle size) for 1 min at a flow rate of 20 µl/min and separated on a nEASY column (PepMap C18, 75 µm x 500 mm, 2 µm particle size) over 60 min using a gradient of 2%-35% acetonitrile in 5% DMSO/0.1% Formic acid at a flow rate of 250nL/min. Survey scans were acquired at a resolution of 70,000 @ 200m/z, and the 15 most abundant precursors of charge between 2 and 7 were selected for HCD fragmentation (35V) and dynamic exclusion parameters were set in order to select a precursor ion once prior to be excluded for 60 s. The mass spectrometry proteomics data have been deposited to the ProteomeXchange Consortium via the PRIDE (44) partner repository with the dataset identifier PXD008025 and 10.6019/PXD008025. Reviewer account details are: Username: reviewer94002@ebi.ac.uk, Password: oKO6TjrK

Native mass spectrometry

All samples were analysed under native conditions using a modified Q-Exactive mass spectrometer (Thermo Fisher Scientific) for high-mass range measurements. CCL8 was buffered exchanged into 200 mM ammonium acetate solution (pH = 6.5) and deglycosylated P672 was buffer exchanged into 50 mM ammonium bicarbonate buffer (pH = 6.5). The proteins were initially analysed separately using a capillary voltage of 1.2 KV and source temperature of 100°C. In the case of deglycosylated P672, 50 V of source induced dissociation (SID) was added to improve desolvation. CCL8 protein sequence was characterized from its monomers by increasing the source temperature to 200°C and adding 30 V of SID. The two major precursor ions of CCL8 monomer, *m/z* 2257 and *m/z* 2821, were selected with an isolation window of 5 m/z and fragmented using several acceleration voltages (80, 100, 150 and/or 180 V) of HCD. All precursor and fragment ions were acquired using a mass resolution of 60000, with averaging of 3 microscans and a signal-to-noise threshold of 3. The Xtract algorithm from Xcalibur 3.0 software (Thermo Fisher Scientific) was used to determine the decharged masses of the observed ions, which were then inserted into ProSight Lite (http://prosightlite.northwestern.edu) for identification of putative post-translational modifications within a precursor and product ion tolerance of 10 ppm. Aliquots of CCL8 and deglycosylated P672 were mixed in a 1:1 ratio to reach a final concentration of 2.5 µM and incubated for 1 h at 4°C. The mixture was analysed using the following parameters: capillary voltage of 1.2 KV, source temperature of 130°C and 60 V of SID. The most intense charge state was isolated with a 100 *m/z* isolation window and dissociated using 100 V of HCD. In this case, precursor and dissociated products were acquired using a mass resolution of 17500 and 60000, respectively. Moreover, 2:1 and 3:1 ratios were also evaluated. All measurements were done in triplicate.

Statistical analyses

GraphPad Prism was used to calculate summary statistics and tests of significance. The P value (probability of a type I error) reported was adjusted for multiple comparisons. The threshold (alpha) for a type I error was $P<0.05$.

Downloaded from http://www.jbc.org/ by guest on April 22, 2018

ACKNOWLEDGEMENTS
This research was funded by British Heart Foundation Chair Award to SB (CH/09/003), Oxford BHF Centre of Research Excellence (RE/13/1/30181), BHF Oxbridge Centre for Regenerative Medicine (AVMEBCA1), Radcliffe Department of Medicine University of Oxford, and Wellcome Trust Core Award (203141/Z/16/Z) to the Wellcome Trust Centre for Human Genetics. CVR is funded by MRC Grant No. MR/N020413/1**.** JE is funded by a studentship from the Oxford BHF Centre of Research Excellence, YA is supported by a studentship from the Saudi Arabian Cultural Bureau, and AK by a Royal Society Dorothy Hodgkin Fellowship.

CONFLICT OF INTEREST
The CKBP sequences and hybrid CKBP concept form part of the basis of a patent application. SB has received funding from Lab282 for development of tick CKBPs as therapeutics in partnership with Evotec AG.

AUTHOR CONTRIBUTIONS
JE, YA, GD, and KS designed, performed and interpreted yeast, protein interaction and cell-based experiments. SB conceived and designed the yeast surface display and hybrid CKBP approach, and performed bioinformatic and statistical analyses, plasmid library construction, peptide sequence analysis and homology modelling. LG-A, BK and JE performed glycosylation site determination analysis. LG-A and CVR performed native mass spectrometry studies and data interpretation. AK and SB supervised and interpreted experiments and all authors contributed to writing the manuscript.

REFERENCES
1. Garin, A., and Proudfoot, A. E. I. (2011) Chemokines as targets for therapy. *Experimental Cell Research* **317**, 602-612
2. Schall, T. J., and Proudfoot, A. E. (2011) Overcoming hurdles in developing successful drugs targeting chemokine receptors. *Nat Rev Immunol* **11**, 355-363
3. Zheng, Y., Han, G. W., Abagyan, R., Wu, B., Stevens, R. C., Cherezov, V., Kufareva, I., and Handel, T. M. (2017) Structure of CC Chemokine Receptor 5 with a Potent Chemokine Antagonist Reveals Mechanisms of Chemokine Recognition and Molecular Mimicry by HIV. *Immunity* **46**, 1005-1017 e1005
4. Kufareva, I., Gustavsson, M., Zheng, Y., Stephens, B. S., and Handel, T. M. (2017) What Do Structures Tell Us About Chemokine Receptor Function and Antagonism? *Annu Rev Biophys* **46**, 175-198
5. Kufareva, I., Salanga, C. L., and Handel, T. M. (2015) Chemokine and chemokine receptor structure and interactions: implications for therapeutic strategies. *Immunol Cell Biol* **93**, 372-383
6. Allen, S. J., Crown, S. E., and Handel, T. M. (2007) Chemokine:Receptor Structure, Interactions, and Antagonism. *Annu. Rev. Immunol.* **25**, 787-820
7. Fernandez, E. J., and Lolis, E. (2002) Structure, function, and inhibition of chemokines. *Annu. Rev. Pharmacol. Toxicol.* **42**, 469-499
8. Szpakowska, M., Fievez, V., Arumugan, K., van Nuland, N., Schmit, J.-C., and Chevigné, A. (2012) Function, diversity and therapeutic potential of the N-terminal domain of human chemokine receptors. *Biochemical Pharmacology* **84**, 1366-1380
9. Gonzalez-Motos, V., Kropp, K. A., and Viejo-Borbolla, A. (2016) Chemokine binding proteins: An immunomodulatory strategy going viral. *Cytokine Growth Factor Rev* **30**, 71-80
10. Proudfoot, A. E., Bonvin, P., and Power, C. A. (2015) Targeting chemokines: Pathogens can, why can't we? *Cytokine* **74**, 259-267
11. Kufareva, I. (2016) Chemokines and their receptors: insights from molecular modeling and crystallography. *Curr Opin Pharmacol* **30**, 27-37

Downloaded from http://www.jbc.org/ by guest on April 22, 2018

12. Smith, P., Fallon, R. E., Mangan, N. E., Walsh, C. M., Saraiva, M., Sayers, J. R., McKenzie, A. N. J., Alcami, A., and Fallon, P. G. (2005) Schistosoma mansoni secretes a chemokine binding protein with antiinflammatory activity. *J. Exp. Med.* **202**, 1319-1325
13. Bonvin, P., Power, C. A., and Proudfoot, A. E. (2016) Evasins: therapeutic potential of a new Family of Chemokine-Binding proteins from ticks. *Front Immunol* **7**, 1-7
14. Singh, K., Davies, G., Alenazi, Y., Eaton, J. R. O., Kawamura, A., and Bhattacharya, S. (2017) Yeast surface display identifies a family of evasins from ticks with novel polyvalent CC chemokine-binding activities. *Sci Rep* **7**, 4267
15. Hayward, J., Sanchez, J., Perry, A., Huang, C., Rodriguez Valle, M., Canals, M., Payne, R. J., and Stone, M. J. (2017) Ticks from diverse genera encode chemokine-inhibitory evasin proteins. *J Biol Chem* **292**, 15670-15680
16. Dias, J. M., Losberger, C., Déruaz, M., Power, C. A., Proudfoot, A. E. I., and Shaw, J. P. (2009) Structural Basis of Chemokine Sequestration by a Tick Chemokine Binding Protein: The Crystal Structure of the Complex between Evasin-1 and CCL3. *PLoS ONE* **4**, e8514
17. Bonvin, P., Dunn, S. M., Rousseau, F., Dyer, D. P., Shaw, J., Power, C. A., Handel, T. M., and Proudfoot, A. E. I. (2014) Identification of the Pharmacophore of the CC Chemokine-binding Proteins Evasin-1 and-4 Using Phage Display. *Journal of Biological Chemistry* **289**, 31846-31855
18. Lubman, O. Y., and Fremont, D. H. (2016) Parallel Evolution of Chemokine Binding by Structurally Related Herpesvirus Decoy Receptors. *Structure* **24**, 57-69
19. Yen, T. Y., Dutta, S. M., Litsakos-Cheung, C., Corona, A. A., Timpe, L. C., and Macher, B. A. (2013) Overcoming challenges and opening new opportunities in glycoproteomics. *Biomolecules* **3**, 270-286
20. Concepcion, J., Witte, K., Wartchow, C., Choo, S., Yao, D., Persson, H., Wei, J., Li, P., Heidecker, B., Ma, W., Varma, R., Zhao, L. S., Perillat, D., Carricato, G., Recknor, M., Du, K., Ho, H., Ellis, T., Gamez, J., Howes, M., Phi-Wilson, J., Lockard, S., Zuk, R., and Tan, H. (2009) Label-free detection of biomolecular interactions using BioLayer interferometry for kinetic characterization. *Comb Chem High Throughput Screen* **12**, 791-800
21. Van Coillie, E., Proost, P., Van Aelst, I., Struyf, S., Polfliet, M., De Meester, I., Harvey, D. J., Van Damme, J., and Opdenakker, G. (1998) Functional comparison of two human monocyte chemotactic protein-2 isoforms, role of the amino-terminal pyroglutamic acid and processing by CD26/dipeptidyl peptidase IV. *Biochemistry* **37**, 12672-12680
22. Webb, B., and Sali, A. (2014) Protein structure modeling with MODELLER. *Methods Mol Biol* **1137**, 1-15
23. Jubb, H. C., Higueruelo, A. P., Ochoa-Montano, B., Pitt, W. R., Ascher, D. B., and Blundell, T. L. (2017) Arpeggio: A Web Server for Calculating and Visualising Interatomic Interactions in Protein Structures. *J Mol Biol* **429**, 365-371
24. Chao, G., Lau, W. L., Hackel, B. J., Sazinsky, S. L., Lippow, S. M., and Wittrup, K. D. (2006) Isolating and engineering human antibodies using yeast surface display. *Nat Protoc* **1**, 755-768
25. Déruaz, M., Bonvin, P., Severin, I. C., Johnson, Z., Krohn, S., Power, C. A., and Proudfoot, A. E. I. (2013) Evasin-4, a tick-derived chemokine-binding protein with broad selectivity can be modified for use in preclinical disease models. *FEBS Journal* **280**, 4876-4887
26. Huma, Z. E., Sanchez, J., Lim, H. D., Bridgford, J. L., Huang, C., Parker, B. J., Pazhamalil, J. G., Porebski, B. T., Pfleger, K. D. G., Lane, J. R., Canals, M., and Stone, M. J. (2017) Key determinants of selective binding and activation by the monocyte chemoattractant proteins at the chemokine receptor CCR2. *Sci Signal* **10**
27. Bachelerie, F., Ben-Baruch, A., Burkhardt, A. M., Combadiere, C., Farber, J. M., Graham, G. J., Horuk, R., Sparre-Ulrich, A. H., Locati, M., Luster, A. D., Mantovani, A., Matsushima, K., Murphy, P. M., Nibbs, R., Nomiyama, H., Power, C. A., Proudfoot, A. E., Rosenkilde, M. M., Rot, A., Sozzani, S., Thelen, M., Yoshie, O., and Zlotnik, A. (2014) International Union of Basic and

Downloaded from http://www.jbc.org/ by guest on April 22, 2018

Clinical Pharmacology. LXXXIX. Update on the extended family of chemokine receptors and introducing a new nomenclature for atypical chemokine receptors. *Pharmacol Rev* **66**, 1-79
28. Krohn, S., Garin, A., Gabay, C., and Proudfoot, A. E. I. (2013) The Activity of CCL18 is Principally Mediated through Interaction with Glycosaminoglycans. *Front Immunol* **4**, 193
29. Detheux, M., Standker, L., Vakili, J., Munch, J., Forssmann, U., Adermann, K., Pohlmann, S., Vassart, G., Kirchhoff, F., Parmentier, M., and Forssmann, W. G. (2000) Natural proteolytic processing of hemofiltrate CC chemokine 1 generates a potent CC chemokine receptor (CCR)1 and CCR5 agonist with anti-HIV properties. *J Exp Med* **192**, 1501-1508
30. Berahovich, R. D., Miao, Z., Wang, Y., Premack, B., Howard, M. C., and Schall, T. J. (2005) Proteolytic activation of alternative CCR1 ligands in inflammation. *J Immunol* **174**, 7341-7351
31. Lampinen, M., Carlson, M., Hakansson, L. D., and Venge, P. (2004) Cytokine-regulated accumulation of eosinophils in inflammatory disease. *Allergy* **59**, 793-805
32. Harding, S. D., Sharman, J. L., Faccenda, E., Southan, C., Pawson, A. J., Ireland, S., Gray, A. J. G., Bruce, L., Alexander, S. P. H., Anderton, S., Bryant, C., Davenport, A. P., Doerig, C., Fabbro, D., Levi-Schaffer, F., Spedding, M., Davies, J. A., and Nc, I. (2017) The IUPHAR/BPS Guide to PHARMACOLOGY in 2018: updates and expansion to encompass the new guide to IMMUNOPHARMACOLOGY. *Nucleic Acids Res*
33. Gouwy, M., Schiraldi, M., Struyf, S., Van Damme, J., and Uguccioni, M. (2012) Possible mechanisms involved in chemokine synergy fine tuning the inflammatory response. *Immunol. Lett.* **145**, 10-14
34. Tiller, K. E., and Tessier, P. M. (2015) Advances in Antibody Design. *Annu Rev Biomed Eng* **17**, 191-216
35. Zhao, Y., Bishop, B., Clay, J. E., Lu, W., Jones, M., Daenke, S., Siebold, C., Stuart, D. I., Jones, E. Y., and Aricescu, A. R. (2011) Automation of large scale transient protein expression in mammalian cells. *J. Struct. Biol.* **175**, 209-215
36. Bendtsen, J. D., Nielsen, H., von Heijne, G., and Brunak, S. (2004) Improved prediction of signal peptides: SignalP 3.0. *J Mol Biol* **340**, 783-795
37. Keates, T., Cooper, C. D., Savitsky, P., Allerston, C. K., Phillips, C., Hammarstrom, M., Daga, N., Berridge, G., Mahajan, P., Burgess-Brown, N. A., Muller, S., Graslund, S., and Gileadi, O. (2012) Expressing the human proteome for affinity proteomics: optimising expression of soluble protein domains and in vivo biotinylation. *N Biotechnol* **29**, 515-525
38. Rice, P., Longden, I., and Bleasby, A. (2000) EMBOSS: the European Molecular Biology Open Software Suite. *Trends Genet* **16**, 276-277
39. Steentoft, C., Vakhrushev, S. Y., Joshi, H. J., Kong, Y., Vester-Christensen, M. B., Schjoldager, K. T., Lavrsen, K., Dabelsteen, S., Pedersen, N. B., Marcos-Silva, L., Gupta, R., Bennett, E. P., Mandel, U., Brunak, S., Wandall, H. H., Levery, S. B., and Clausen, H. (2013) Precision mapping of the human O-GalNAc glycoproteome through SimpleCell technology. *EMBO J* **32**, 1478-1488
40. Janson, G., Zhang, C., Prado, M. G., and Paiardini, A. (2017) PyMod 2.0: improvements in protein sequence-structure analysis and homology modeling within PyMOL. *Bioinformatics* **33**, 444-446
41. Tina, K. G., Bhadra, R., and Srinivasan, N. (2007) PIC: Protein Interactions Calculator. *Nucleic Acids Res* **35**, W473-476
42. Copeland, R. A., Pompliano, D. L., and Meek, T. D. (2006) Drug-target residence time and its implications for lead optimization. *Nat Rev Drug Discov* **5**, 730-739
43. Fischer, R., and Kessler, B. M. (2015) Gel-aided sample preparation (GASP)--a simplified method for gel-assisted proteomic sample generation from protein extracts and intact cells. *Proteomics* **15**, 1224-1229
44. Vizcaino, J. A., Csordas, A., del-Toro, N., Dianes, J. A., Griss, J., Lavidas, I., Mayer, G., Perez-Riverol, Y., Reisinger, F., Ternent, T., Xu, Q. W., Wang, R., and Hermjakob, H. (2016) 2016 update of the PRIDE database and its related tools. *Nucleic Acids Res* **44**, D447-456

Downloaded from http://www.jbc.org/ by guest on April 22, 2018

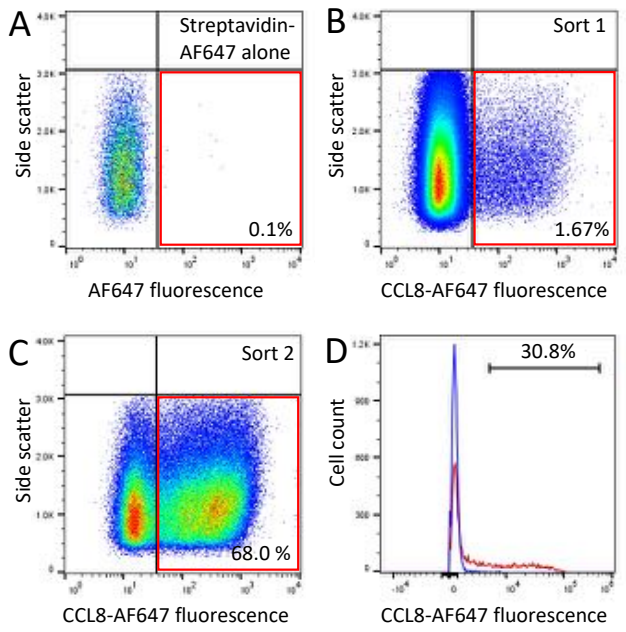


Figure 1. (A) Fluorescence profile of yeast surface display library expressing putative tick evasins incubated with streptavidin-AF647 alone. The red box indicates the sorting gate. (B) Yeast surface display library incubated with biotinylated CCL8 plus streptavidin-AF647. The sorting gate was identified from the negative control and was used to sort CCL8 binding yeast from the library. (C) Second round sorting of CCL8-binding yeast identified above. The proportions of cells within the sorting gate are indicated as a percentage. (D) Binding of P672 to CCL8. Yeast expressing P672 are shown in red, and control yeast bearing empty vector surface display plasmid are shown in blue. Y-axis shows cell count, and X-axis the fluorescence intensity on a $\log_{10}$-scale. The proportion of cells exceeding background is indicated as a percentage.

Downloaded from http://www.jbc.org/ by guest on April 22, 2018

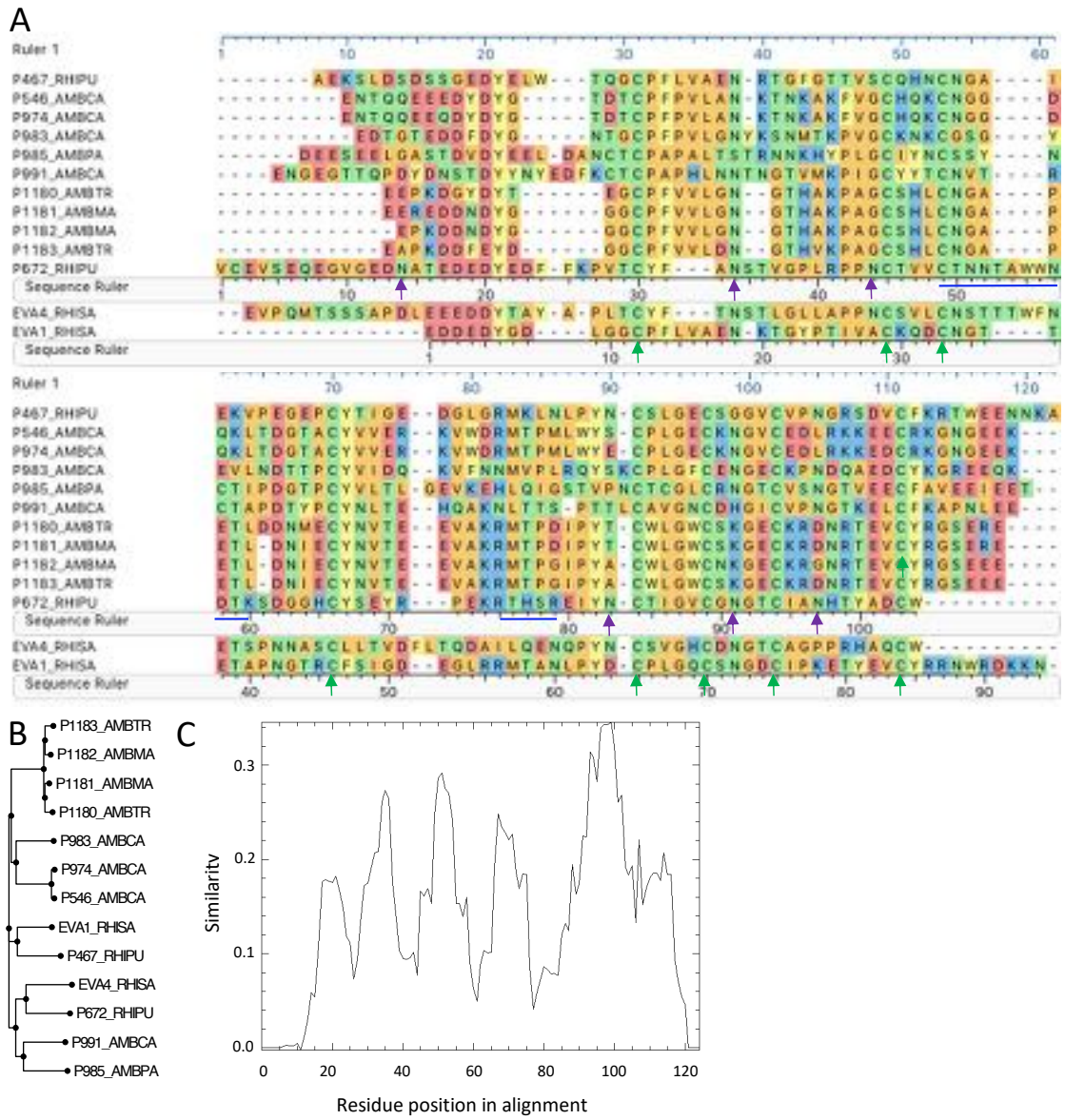


Figure 2. (A) Sequence alignment of P672 with CC-binding evasins. Peptide sequence prefix indicates the identity, and suffixes indicate the tick species as follows: RHISA and RHIPU – *Rhipicephalus sanguineus* and *pulchellus* respectively, and AMBPA, AMBCA, AMBMA, AMBTR - *Amblyomma parvum, cajennense, maculatum and triste*) respectively. Amino acid residues are colour coded by physicochemical properties. Yellow: aromatic (F, W, Y); Red: acidic (D, E); Blue: basic (R, H, K); Orange: Nonpolar aliphatic (A, G, I, L, M, P, V); Green: polar neutral (C, N, Q, T). Green arrows indicate disulfide bond positions in EVA1. Magenta arrows indicate the six N-glycosylated residues identified in P672 by mass spectrometry. The blue lines indicate the regions of P672 not covered by elastase and tryptic digest bottom-up mass spectrometry. Sequence rulers of P672, EVA1 and the alignment (ruler 1) are indicated. (B) Phylogenetic tree of CC-binding evasins. P672 is related most closely to EVA4, with which it shares 36% identity over 105 residues. (C) Conservation plot of evasins identified by yeast surface display. The plot was generated from the sequence alignment using the EMBOSS program plotcon with a window size of 10 residues. Y-axis shows similarity score and X-axis shows the residue position in the alignment.

Downloaded from http://www.jbc.org/ by guest on April 22, 2018

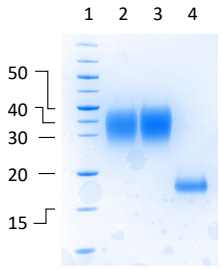


Figure 3. SDS-PAGE gel stained with colloidal Coomassie blue showing molecular weight markers (kDa, lane 1), N-terminally tagged P672 protein (lane 2), C-terminally tagged P672 protein (lane 3) and N-terminally tagged P672 protein (lane 4), partially deglycosylated using PNGaseF and EndoF1. All proteins were purified using nickel affinity followed by size exclusion chromatography.

Downloaded from http://www.jbc.org/ by guest on April 22, 2018

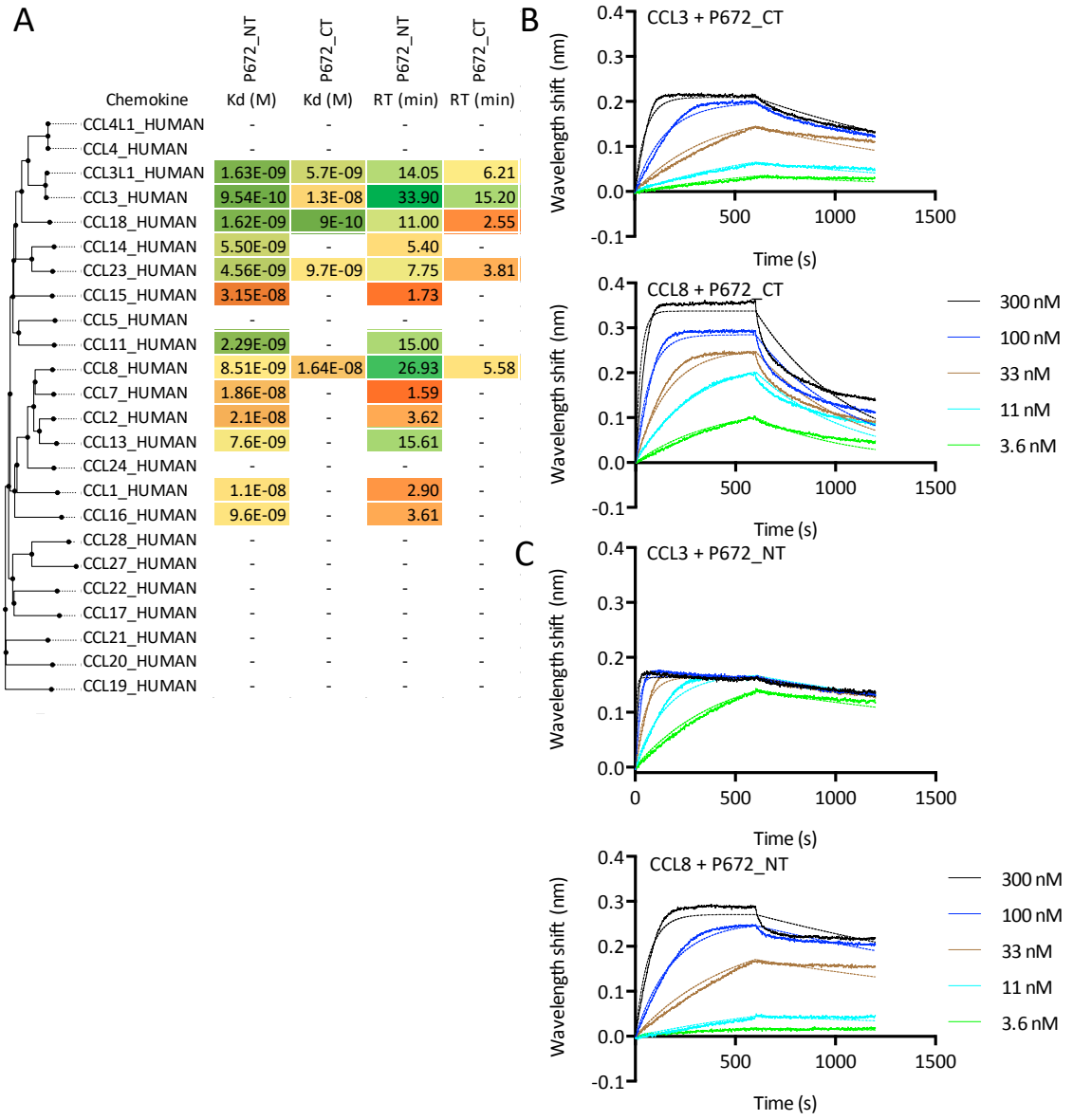


Figure 4. (A) Binding affinities (K_d, M) and target residence times (RT, minutes) of immobilized P672 (either N or C-terminally tagged as indicated) to human CC-chemokines using biolayer interferometry. High affinity binding and longer residence times are indicated as shades of green, medium affinity as yellow, and low affinity as shades of orange. Chemokines are arranged by sequence-similarity based phylogeny. A dash (-) indicates that binding was not detected at 300 nM chemokine concentration. (B) Biolayer interferometry sensorgrams showing C-terminally tagged P672 binding to different doses of chemokines CCL3 (top panel) and CCL8 (bottom panel). Plots display wavelength shift (Y-axis, nm) versus time (X-axis, seconds). Solid lines indicate collected data, dashed lines indicate fitted data. (C) Biolayer interferometry sensorgrams showing N-terminally tagged P672 binding to different doses of chemokines CCL3 (top panel) and CCL8 (bottom panel). Plots display wavelength shift (Y-axis, nm) versus time (X-axis, seconds). Solid lines indicate collected data, dashed lines indicate fitted data.

Downloaded from http://www.jbc.org/ by guest on April 22, 2018

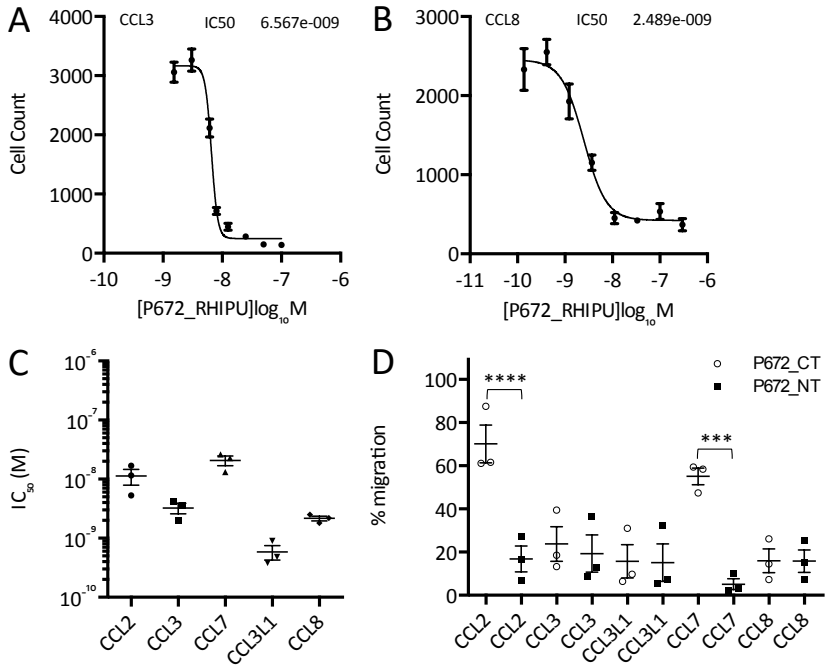


Figure 5. (A, B) Neutralization of CCL3 (A) and CCL8 (B) induced THP-1 cell migration by N-terminally tagged P672. Y-axis shows cell count of THP-1 cells migrating through to the bottom chamber in response to a EC_{80} dose of the indicated chemokines. Data (three technical replicates) are shown as mean ± s.e.m. X-axis shows P672 concentration (Log_{10} Molar). IC_{50} indicated was estimated by fitting an agonist response curve with 4 parameters as described (14). (C) Summary of N-terminally tagged P672 IC_{50} data (M, mean, s.e.m. of three biological replicates analysed as above) for chemokines that induce THP-1 cell migration. The EC_{80} dose of the indicated chemokines were as follows: CCL2 (0.52nM), CCL3 (3.55nM), CCL7 (7.18nM), CCL3L1 (0.52nM), CCL8 (5.75nM). (D) Percentage of migration inhibition by a fixed concentration (100 nM) of P672_CT (C-terminally tagged, open circles) or P672_NT (N-terminally tagged, filled squares). The experiment was performed at an EC_{80} concentration of the chemokines indicated. Data (three technical and three biological replicates) were normalised to chemokine alone control to account for day to day variation. Data were analyzed with one-way ANOVA and corrected for multiple comparisons with the Sidak method. *** indicates $p<0.001$, and ****$p<0.0001$.

Downloaded from http://www.jbc.org/ by guest on April 22, 2018

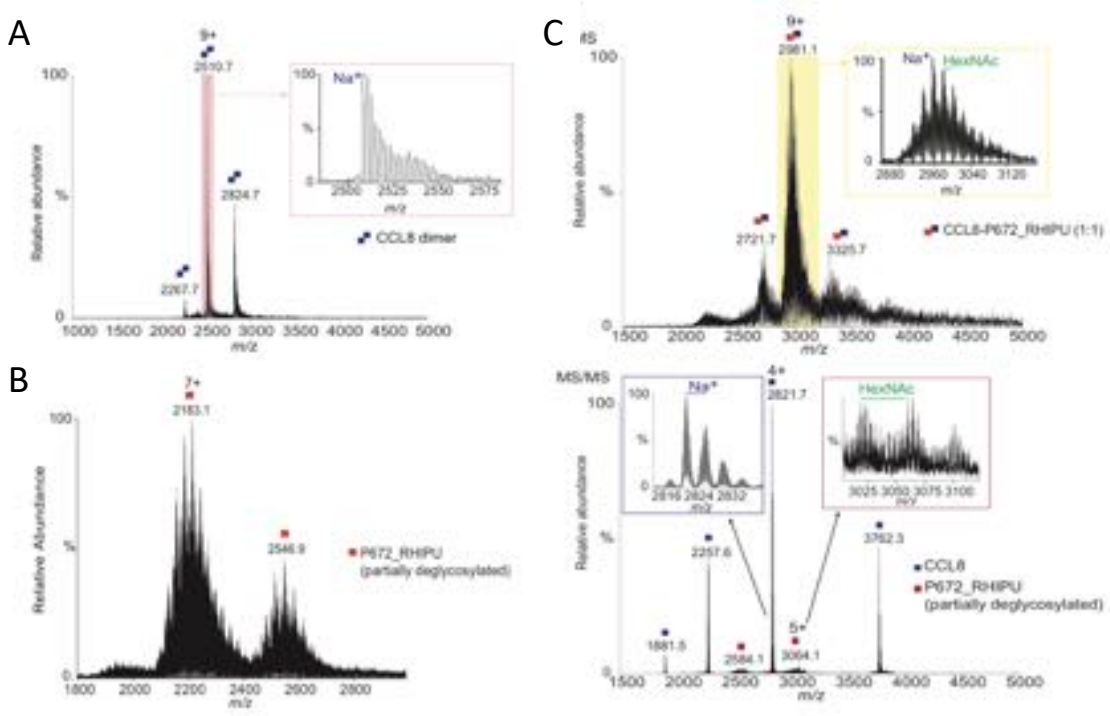


Figure 6. (A) Native mass spectrometry (MS) of CCL8 homodimer. Inset shows sodium adducts of the homodimer. (B) Native MS of partially deglycosylated N-terminally tagged P672. (C) *Top panel and inset.* Native MS of P672:CCL8 complex. CCL8 and P672 were mixed in a 1:1 ratio (at a final concentration of 2.5 uM) and incubated for 1 hour at 4°C. Peaks corresponding with a glycosylated and sodiated CCL8 - P672 heterodimer (lowest intensity average mass observed is 25915.3 ±1.4 Da) are indicated (inset). *Bottom panel:* HCD fragmentation at 100 V of the *m/z* 2956 isolated using a 100 *m/z* isolation window. Peaks corresponding to sodiated CCL8 (top left inset) and a partially glycosylated P672 (top right inset) are indicated. In all sections of this figure, peaks are indicated as CCL8 (blue squares) or P672 (red squares). Monomers are indicated as a single square, and homo or heterodimers as double squares. Y-axis indicates relative abundance, X-axis indicates *m/z* (mass/charge) ratio.

Downloaded from http://www.jbc.org/ by guest on April 22, 2018

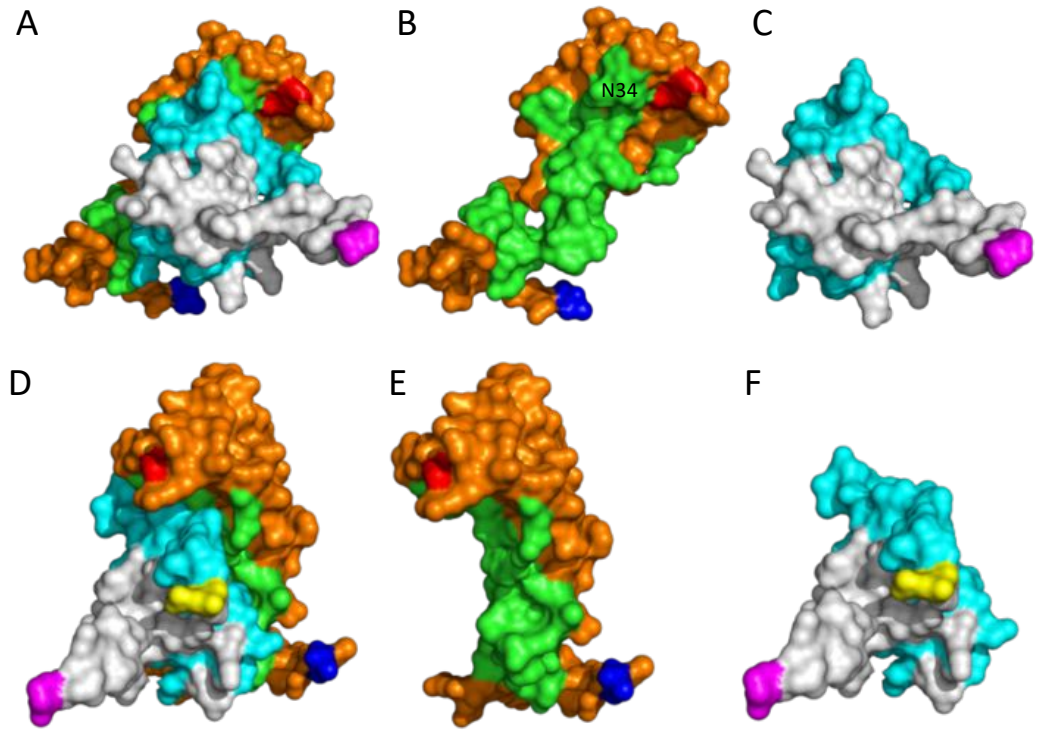


Figure 7 3D structural model of P672 (orange and green) and CCL8 (grey and cyan), modelled as a 1:1 complex using the EVA1: CCL3 structure (3FPU) as template using MODELLER with default parameters after alignment with the MUSCLE algorithm. The residues forming the binding surfaces predicted using Arpeggio (23) are indicated in green (P672), and cyan (CCL8). The N-terminus residue of P672 (V1) is indicated in blue and the C-terminus residue (W104) in red. The N- and C-termini of CCL8 are indicated in yellow and magenta respectively. (A, D) P672:CCL8 complex shown in two orientations. (B, E) P672 alone shown in two orientations. The position of residue N34, which is in close proximity to the C-terminal W104, is indicated. (C, F) CCL8 alone shown in two orientations.

Downloaded from http://www.jbc.org/ by guest on April 22, 2018

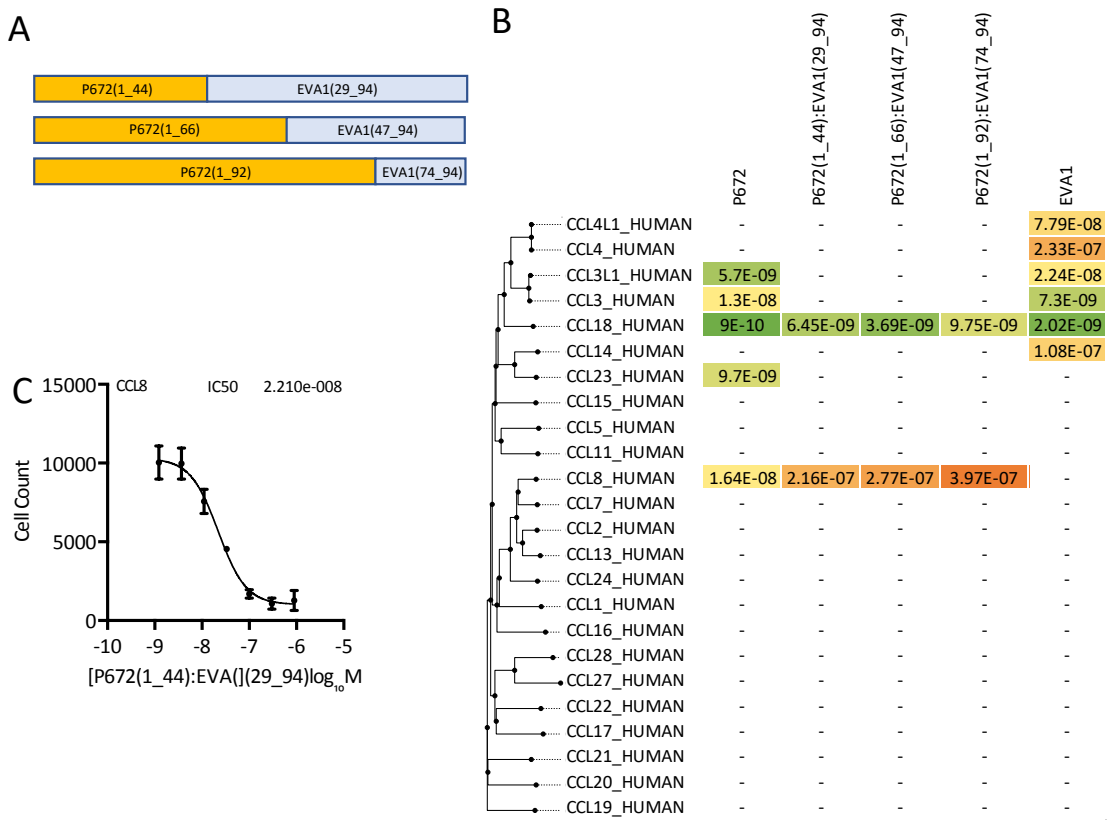


Figure 8. (A) Constructions of hybrid evasins are indicated in the diagram. (B) Binding affinities (K_d, M) of immobilized P672, P672_EVA1 hybrids and EVA1 to human CC-chemokines using biolayer interferometry. High affinity binding is indicated as shades of green, medium affinity as yellow, and low affinity as shades of orange. Chemokines are arranged by sequence-similarity based phylogeny. A dash (-) indicates that binding was not detected at 300 nM chemokine concentration. (C) Neutralization of CCL8 induced THP-1 monocyte cell migration by P672(1_44):EVA1(29_94). Y-axis shows cell count migrating through to the bottom chamber in response to an EC_{80} dose of CCL8. Data (3 technical replicates, 3 biological replicates) are shown as mean ± s.e.m. X-axis shows P672(1_44):EVA1(29_94) concentration (Log_{10} Molar). IC_{50} was estimated by fitting an agonist response curve with 4 parameters as described (14).

Downloaded from http://www.jbc.org/ by guest on April 22, 2018

The N-terminal domain of a tick evasin is critical for chemokine binding and neutralization and confers specific binding activity to other evasins

James R.O. Eaton, Yara Alenazi, Kamayani Singh, Graham Davies, Lucia Geis-Asteggiante, Benedikt Kessler, Carol V Robinson, Akane Kawamura and Shoumo Bhattacharya

J. Biol. Chem. published online February 27, 2018

Access the most updated version of this article at doi: 10.1074/jbc.RA117.000487

Alerts:
- When this article is cited
- When a correction for this article is posted

Click here to choose from all of JBC's e-mail alerts

Downloaded from http://www.jbc.org/ by guest on April 22, 2018

SCIENTIFIC REPORTS

OPEN

Yeast surface display identifies a family of evasins from ticks with novel polyvalent CC chemokine-binding activities

Received: 18 April 2017
Accepted: 31 May 2017
Published online: 27 June 2017

Kamayani Singh[1], Graham Davies[1], Yara Alenazi[1], James R. O. Eaton[1,2], Akane Kawamura[1,2] & Shoumo Bhattacharya[1]

Chemokines function via G-protein coupled receptors in a robust network to recruit immune cells to sites of inflammation. Due to the complexity of this network, targeting single chemokines or receptors has not been successful in inflammatory disease. Dog tick saliva contains polyvalent CC-chemokine binding peptides termed evasins 1 and 4, that efficiently disrupt the chemokine network in models of inflammatory disease. Here we develop yeast surface display as a tool for functionally identifying evasins, and use it to identify 10 novel polyvalent CC-chemokine binding evasin-like peptides from salivary transcriptomes of eight tick species in *Rhipicephalus* and *Amblyomma* genera. These evasins have unique binding profiles compared to evasins 1 and 4, targeting CCL2 and CCL13 in addition to other CC-chemokines. Evasin binding leads to neutralisation of chemokine function including that of complex chemokine mixtures, suggesting therapeutic efficacy in inflammatory disease. We propose that yeast surface display is a powerful approach to mine potential therapeutics from inter-species protein interactions that have arisen during evolution of parasitism in ticks.

Chemokines are secreted small extracellular proteins that are major drivers of inflammation in diverse diseases[1]. The 46 human chemokines fall into four groups - CC, CXC, XC and CX3C - defined by the spacing between N-terminal cysteine residues[2]. Structural features of chemokines include a flexible N-terminus, an invariant pair of disulphide bonded cysteine residues, a N-loop, a three-stranded β-sheet with loops designated 30S (between β1-β2) and 40S (between β2-β3), and a C-terminal helix. Chemokines function to recruit inflammatory and immune cells, including monocytes, neutrophils, eosinophils, dendritic cells, and T and B lymphocytes, to sites of inflammation and injury[3–5]. They bind to a family of G-protein coupled chemokine receptors (GPCRs) on these cells through two chemokine receptor sites (CRS1 and CRS2). The chemokine globular core binds to the extracellular N-terminus (CRS1) of the receptor via the proximal N-terminus and N-loop/40S loop grooves, whereas the chemokine distal N-terminus binds to CRS2 in the GPCR pocket, and is essential for activating signaling and chemotaxis[6]. In addition, chemokines bind with low affinity to glycosaminoglycans (GAGs) on the surface of endothelial cells, and this binding is necessary for chemokine function *in vivo*.

The chemokine system functions as a robust network. Properties of this network that engender robustness are the expression of multiple chemokine receptors on inflammatory cells[7], expression of several chemokines in diseased tissues[8], polyvalent chemokine-receptor interactions - with chemokines typically targeting more than one receptor, and receptors typically being activated by more than one chemokine[2], synergistic and cooperative interactions between chemokines and chemokine receptors[9], and feed-forward loops wherein inflammatory cells recruited to diseased tissue themselves secrete chemokines amplifying the network response[10]. The robustness of the chemokine network is clearly demonstrated by the observation that targeting individual chemokines or receptors has failed as a strategy to develop effective therapeutics for inflammatory disorders[7,8,11].

A number of pathogens have evolved distinct peptides to target the chemokine network. These peptides have one common feature, namely, that they are typically polyvalent and target multiple chemokine network nodes

[1]RDM Division of Cardiovascular Medicine and Wellcome Trust Centre for Human Genetics, University of Oxford, Roosevelt Drive, Oxford, OX3 7BN, United Kingdom. [2]Dept of Chemistry, University of Oxford, Mansfield Road, Oxford, OX1 3TA, United Kingdom. Kamayani Singh and Graham Davies contributed equally to this work. Correspondence and requests for materials should be addressed to S.B. (email: sbhattac@well.ox.ac.uk)

(reviewed in ref. 11). Viral peptides such as MC148 and vMIP-II are homologous to chemokines, and bind and inhibit multiple chemokine receptors. Other viral proteins (CKBPs, chemokine binding proteins[12]) such as herpesvirus R17 and M3, papova virus CBP, and poxvirus CrmD and vCCI bind multiple chemokines typically via either the proximal N-terminus or via the N-loop/40s loop groove, preventing binding to CRS1[6]. A characteristic of CKBPs is that they target the invariant disulfide in all chemokines[13].

Tick saliva contains proteins that suppress chemokine-driven inflammation by binding and neutralizing multiple chemokines simultaneously[14,15], helping them to suck blood for several weeks without eliciting inflammation[16]. Two related polyvalent CC-chemokine binding proteins, evasins 1 and 4, and one unrelated polyvalent CXC-binding protein, evasin 3, have been cloned from the brown dog tick *Rhiphicephalus sanguineus*[15,17]. The structure of evasin 1 in complex with the chemokine CCL3 shows that it has 4 intra-chain disulfide bonds, and targets the N-terminus of CCL3 in addition to the invariant disulfide[13,18,19]. *In silico* and mutagenesis studies indicate that evasin 4 also targets the N-terminus of CCL3[19]. Evasin 3 shows no sequence homology to evasins 1 or 4, and has a novel structural fold[15].

Certain properties of evasins suggest that they may be potential therapeutics in inflammatory disease. Like other CKBPs, the ability of evasins to disrupt the chemokine network by binding multiple chemokines provides significant advantages over monoclonal antibodies that target single chemokines and have been unsuccessful as therapeutics for inflammation. The preferential binding to discrete subsets of chemokines could provide a method to target the disease-relevant chemokine network without unnecessarily targeting all chemokines. Evasins are highly glycosylated proteins, and as glycosylation is a well-recognized immune evasion strategy[20], this predicts reduced immunogenicity[21]. Evasins 1 and 4 inhibit inflammation in a diverse range of pre-clinical animal models, including pancreatitis, joint inflammation, lung inflammation and fibrosis, post-myocardial infarction injury, psoriasis, and graft-versus-host disease (reviewed in ref. 21). Evasins administered subcutaneously have systemic anti-chemokine effects and do not appear to be significantly immunogenic in mice. This makes it likely that they have the potential, like other naturally occurring peptides such as coversin, a tick salivary peptide that targets complement, to be translated for clinical therapy[22].

Bioinformatic analysis of salivary transcriptomes from species of ticks that are important human disease vectors indicates that they likely contain novel evasins[23,24]. We speculated that such novel tick evasins may have distinct but selective chemokine binding characteristics that would make them valuable tool compounds and potential therapeutics for a broad range of inflammatory diseases. Here, we describe the development of yeast surface display for tick evasins, and the identification of a novel family of polyvalent CC chemokine-binding evasin peptides from tick species using this technology.

Results

Yeast surface display of evasins. To determine if functional evasins could be displayed on yeast surface, evasins 1, 3 and 4 were expressed with yeast surface display tags AGA2 at the N- or C-terminus[25,26], or SAG1 at the C-terminus[27], under the control of a galactose inducible promoter (Fig. 1A). We used different yeast surface display methods as it was unclear if the nature or position of the tag would affect evasin structure or function as in the case of antibodies[26]. To minimize steric hindrance and loss of evasin function we inserted a $(Gly_4S)_3$ linker between evasins and surface display tags. Following galactose induction, yeast cells were labelled with a target biotinylated chemokine, followed by fluorescent streptavidin conjugate and analysed by flow cytometry. Yeast expressing evasins showed increased fluorescence compared to similarly treated controls (Fig. 1B,C). For evasins 1 and 4 the C-terminal fusions performed equivalently to the N-terminal fusion (Fig. 1B,C). For evasin 3 we noted that the N-terminal AGA2 tag performed significantly better (Fig. 1B). Consistent with observations from other yeast display methods[28], we noted that a proportion of yeast do not display the protein. We assayed this using antibodies to epitope tags and found that ~60–80% of yeast express the display tag (see Supplementary Fig. S1). These results indicated that functionally active evasins with different structural folds can be expressed on yeast cell surface, and provided proof of concept that yeast surface display could be used to functionally characterize evasins. They also indicated that the location and nature of the display tag can affect evasin function.

Identification of putative evasins by searching transcriptome datasets. Publicly available salivary transcriptome datasets from Prostriate (*Ixodes ricinus*) and Metastriate (*Amblyomma cajennense, A. maculatum, A. triste, A. parvum, A. americanum, Rhiphicephalus pulchellus, R. sanguineus*) ticks were initially searched with the sequences of evasins 1,3 and 4, and then with the sequences of functional novel evasins (P467_RHIPU and P546_AMBCA, identified below), using three iterations of psiBLAST. We identified 352 distantly related putative evasins from the eight tick species.

Creation and screening of a yeast surface display mini-library. To establish if yeast surface display could be used to identify novel functional evasins from a pool of putative evasins, we initially created a mini-library encoding 24 putative mature evasin peptides. These were fused to surface display tags at either the N-terminus (to AGA2) or at the C-terminus (to SAG1 or AGA2). Pooled libraries were transformed into yeast, cells labelled with biotinylated CCL5 followed by streptavidin-AF647 and then sorted by FACS to identify and recover a population of positive cells, using a gate determined by omitting the chemokine (Fig. 2A). Positive cells recovered in the first round were re-grown, and a second round of FACS was performed as above to further enrich the positive cell pool. This pool was plated at low density to enable picking of individual yeast clones. We initially selected for CCL5 binding evasins in these experiments as it is an important monocyte recruiting chemokine in cardiovascular disease[29]. Library plasmids from individual clones were rescued, sequenced to identify the peptide, and re-transformed to EBY100 yeast for re-testing by FACS (Fig. 2B,C). Four different clones were obtained, and we performed detailed retesting of one clone, P467_RHIPU, which was obtained in both N and C-terminally tagged orientations, against a panel of chemokines to examine its binding profile. This analysis

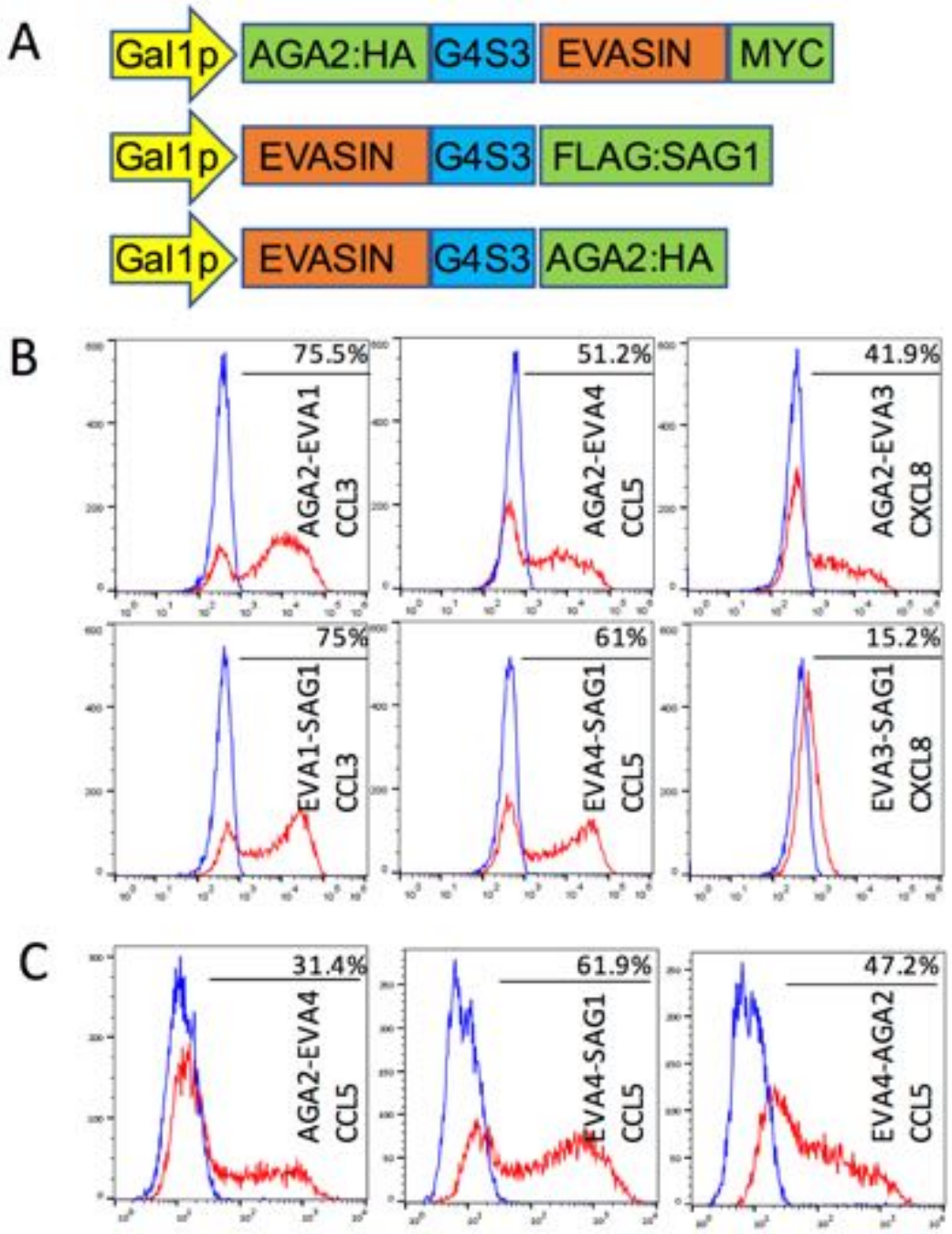


Figure 1. Yeast surface display of evasins. (**A**) Arrangement of evasin expression constructs (not to scale). Evasin fusion peptides were either tagged at the N-terminus with a AGA2 peptide (top), or at the C-terminus with SAG1 (middle) or AGA2 peptides (bottom). The position of antibody epitope tags (HA, MYC, FLAG), and the $(Gly_4Ser)_3$ linker (G4S3) is also indicated. Evasin fusion expression was driven by a Gal1p promoter. (**B**) Fluorescence profiles (red curves) of yeast displaying evasin 1 (left), evasin 4 (middle) and evasin 3 (right) panels incubated with indicated biotinylated chemokines and streptavidin-AF647(red curves). Data show a representative experiment of three biological repeats. Surface display tags were placed at the evasin N-terminus (AGA2, top panels) or at the evasin C-terminus (SAG1, bottom panels). Y-axis shows cell count (side scatter), and x-axis the fluorescence intensity on a log-scale. The blue curve is the profile of yeast containing a negative control surface display vector plasmid treated as above, and is used to determine background. The percentages of cells exceeding background levels in evasin displaying yeast are indicated. (**C**) Fluorescence profiles (red curves) of yeast displaying evasin 4 incubated with biotinylated CCL5 and streptavidin-AF647 (red curves). Data show a representative experiment of three biological repeats. Surface display tags were placed at the evasin N-terminus (AGA2, left panel) or at the evasin C-terminus (SAG1, AGA2, middle and right panels respectively). y-axis shows cell count, and x-axis the fluorescence intensity on a log-scale. The blue curve is the profile of yeast containing a negative control surface display vector plasmid treated as above, and is used to determine background. The percentages of cells exceeding background levels in evasin 4 displaying yeast are indicated.

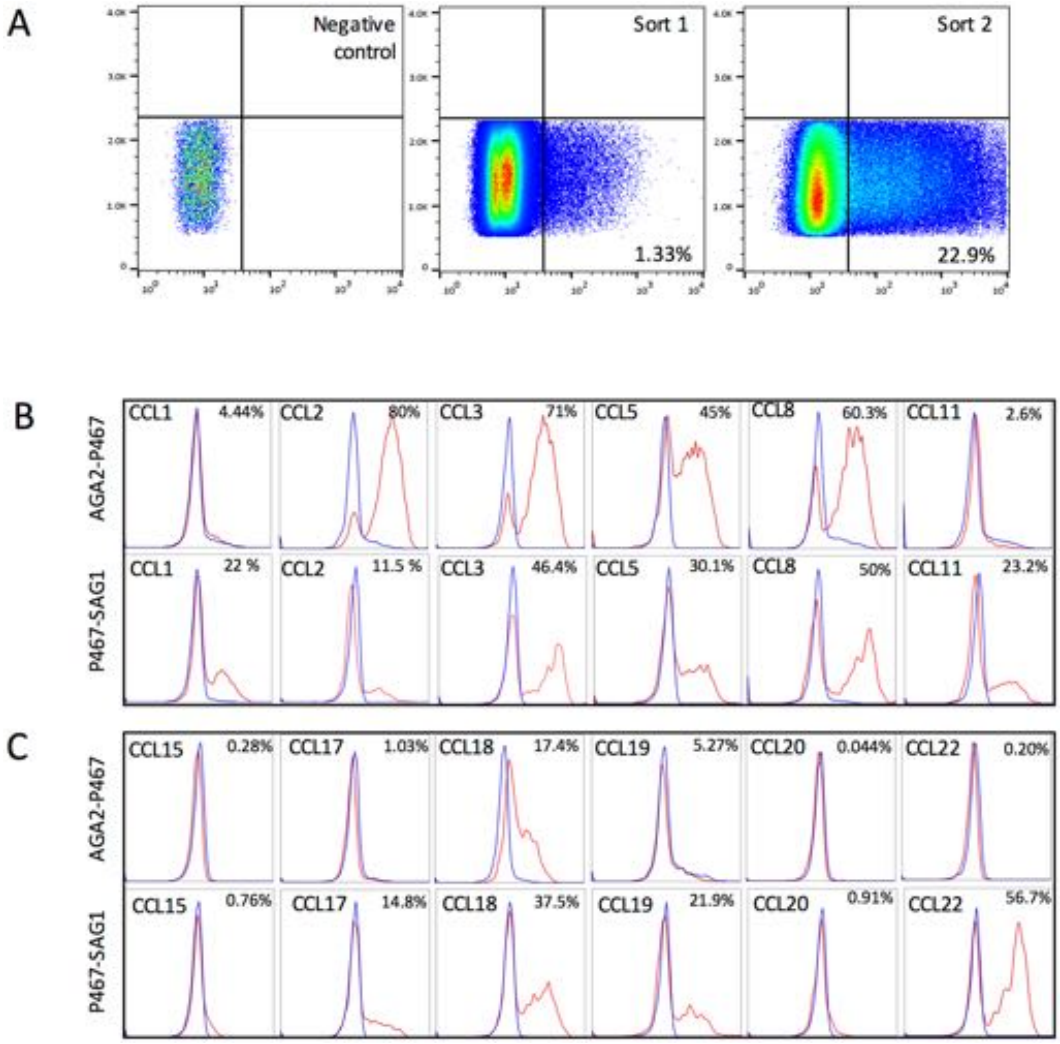


Figure 2. FACS screening of mini-library and retesting of recovered clones. (**A**) Fluorescence profiles of yeast surface display library incubated with streptavidin -AF647 alone (negative control), and incubated with biotinylated CCL5 plus streptavidin -AF647 (middle panel). The sorting gate was identified from the negative control, and was used to sort CCL5 binding yeast from the library. Yeast were sorted a second time similarly (right panel). Y-axis shows cell count and x-axis the fluorescence intensity on a log-scale. The proportions of cells within the sorting gate are indicated as a percentage. (**B,C**) Binding of P467_RHIPU to a panel of chemokines. Yeast surface display fluorescence profiles showing the binding of P467_RHIPU (N-terminal AGA2 fusion, top panels), and C-terminal SAG1 fusion) bottom panels, to a panel of CC chemokines as indicated in the figure. Yeast expressing P467_RHIPU are shown in red, and control yeast bearing empty vector surface display plasmid are shown in blue. Y-axis shows cell count, and x-axis the fluorescence intensity on a log-scale. The proportion of cells exceeding background are indicated as a percentage. The peptide sequence prefix indicates the identity, and suffix RHIPU indicates the species *Rhipicephalus pulchellus*.

showed that it clearly bound to CCL5, which it was initially selected for, as well as CCL2, CCL3, CCL8, CCL18 in the N-terminal AGA2 fusion. In the C-terminal SAG1 fusion, it revealed additional binding to CCL1, CCL11, CCL17, CCL19 and CCL22 (Fig. 2B,C). These results indicated that novel evasin clones could indeed be functionally recovered from a library of putative evasins using yeast surface display, and that a variety of chemokines could be used in such screens. They also confirmed that the nature and location of the surface display tag affected the chemokine-binding function of an evasin unpredictably, and that P467_RHIPU likely has two binding sites, as N and C-terminally tagged constructs bound different chemokines.

Creation and screening of a yeast surface display maxi-library. We next constructed a maxi-library containing sequences encoding the mature peptides of 352 putative evasins identified by searching transcriptome databases. These were fused at the N-terminus to AGA2 or at the C-terminus to SAG1 or AGA2, and a pooled maxi-library created as above. We screened the maxi-library as described above using 13 of the 26 known human CC–chemokines that were commercially available as biotinylated versions. These were CCL1, CCL2, CCL3, CCL4, CCL5, CCL8, CCL11, CCL15, CCL17, CCL18, CCL20, CCL22 and CCL25. We performed screens

Evasin	Accession	Clone Tag	Chemokine screen	Length	MW	pI	N-Glyc	O-Glyc
P991_AMBCA	JAC19654.1	N11C30	CCL2, CCL4, CCL5, CCL8, CCL17, CCL18, CCL19, CCL22	108	11.9	4.6	13, 33, 36, 50, 64, 72, 94	6, 7, 74
P985_AMBPA	JAC24842.1	N1C3	CCL5	108	11.7	4	21, 45, 50, 79, 87, 93	10, 23
P546_AMBCA	JAC18992.1	N1C7	CCL1, CCL3, CCL5, CCL22	97	11.1	5.2	24	3
P974_AMBCA	JAC18993.1	N6C35	CCL1, CCL3, CCL4, CCL8, CCL17, CCL18, CCL22	97	11.1	5.2	24	None predicted
P983_AMBCA		N3C11	CCL2, CCL3, CCL8	98	11	4.6	27, 46	None predicted
P1181_AMBMA	JAC19634.1	N1C2	CCL3, CCL4	90	10.1	4.7	20, 47, 78	None predicted
P1182_AMBMA	AEO33551.1	N4C12	CCL2, CCL3, CCL4, CCL8, CCL18	89	9.7	4.9	19, 46, 77	None predicted
P1183_AMBTR	JAC29608.1	N2C6	CCL2	90	10	4.6	20, 47, 78	None predicted
P1180_AMBTR	JAC29349.1	N6C31	CCL2, CCL3, CCL4, CCL8, CCL18	91	10.2	4.7	19, 46, 77	None predicted
P467_RHIPU	JAA60786.1	N6C5	CCL1, CCL2, CCL3, CCL5	106	11.5	4.6	28, 73	None predicted

Table 1. Evasin clones recovered in human CC chemokine screens. The position of the surface display tag (clone tag) is described as NXCY, where X is the number of clones recovered with the tag at the N-terminus, and Y the number of clones recovered with the tag at the C-terminus. Abbreviations: MW – molecular weight (KDa), N-Glyc – predicted N-glycosylation sites, O-Glyc - predicted O-glycosylation sites. Length refers to number of amino acid residue.

with each biotinylated chemokine individually, and recovered 26 novel CC chemokine binding evasins. To date we have expressed, purified and characterized 10 of the 26 CC-chemokine binding evasins identified by yeast surface display and report them here (Table 1). Clones were obtained in either orientation, with a predominance of C-terminally tagged clones.

Sequence analysis of novel evasin peptides. Peptide lengths varied between 89 to 108 residues, molecular weights between 9.7 to 12 kDa, and pI between 4–5.2 (Table 1). Glycosylation site prediction indicates that all 10 evasins have between one to seven predicted N-glycosylation sites, and only three evasins have one or more predicted O-glycosylation sites (Table 1). Sequence alignment with CC-chemokine binding evasins 1 and 4 showed that all novel CC-chemokine binding evasins retained the Cys residues predicted to form disulfide bonds in evasin 1, and the Pro13 residue in evasin 1 that targets the disulfide bond in CCL3 (Fig. 3A). The arrangement of Cys residues is C-x(14,17) -C-x(3)-C-x(11,16)-C-x(17,20)-C-x(4)-C-x(4)-C-x(8)-C, with numbers in parentheses indicating spacing between Cys residues. Other residues in the novel evasins were poorly conserved with evasins 1 and 4, with overall identity ranging from 24 to 53% (Fig. 3B). Three residues in evasin 1 (F14, N88 and W89) are important for binding CCL3[19]. While F14 is conserved in 10 of 12 sequences, N88 and W89 are poorly conserved. Residues E16 and Y19 in evasin 4 are important for CCL3 binding. While Y19 is conserved (eight of 12 sequences), E16 is poorly conserved. The glycosylated residue in evasin 1 (N19) is highly conserved in nine of the other evasin sequences, which are also predicted to be glycosylated. A group of novel evasins, P1180 – P1183 show very high sequence identity (86–92%), and cluster together on a phylogenetic tree constructed from protein sequence similarity. P546 and P974 have 97% sequence identity, and also cluster together.

Expression and purification of novel evasins. To further characterise the novel evasins biochemically and functionally, we expressed them as secreted proteins in mammalian cells fused to a StrepII:His tag. We used mammalian cells as these have previously been used to produce biologically active evasins suitable for use *in vitro* and *in vivo*[30]. We used a plasmid vector designed for secretion[31], and isolated expressed proteins from the tissue culture supernatant by nickel affinity followed by size exclusion chromatography (see Supplementary Fig. S2) to remove contaminating higher and lower molecular weight proteins observed after nickel affinity purification (see Fig. 3C top panel). Analysis of column chromatography fractions indicated that each evasin typically eluted in several fractions depending on molecular weight, and migrated at a larger molecular weight than expected (Fig. 3C, bottom panel), even accounting for the molecular weight of the affinity tag and linker, which was 3.4 kDa. This is consistent with the glycosylation predicted above, and is consistent with that observed with evasins 1 and 4 expressed in mammalian cells[18,30].

Binding of novel evasins to human chemokines *in vitro*. We assayed the binding of all 10 evasins using biolayer interferometry[32] against a panel of human chemokines. In these assays evasins were bound to the probe through the C-terminal His tag. An initial screening assay was performed at 300 nM chemokine concentration to identify chemokines that bound to the evasin (Fig. 4A, and see Supplementary Table S1). While all novel evasins bound to CC chemokines as expected from the yeast-display results, none of the 10 evasins bound CXC, CX3C or XC chemokines at a chemokine concentration of 300 nM. For determining binding affinities, we used serial dilutions of chemokines that bound respective evasins in the cross-binding screen (Fig. 4B). Binding affinities (K_d) for all 10 CC-chemokine binding evasins against 24 CC-chemokines are shown in Fig. 5A. The

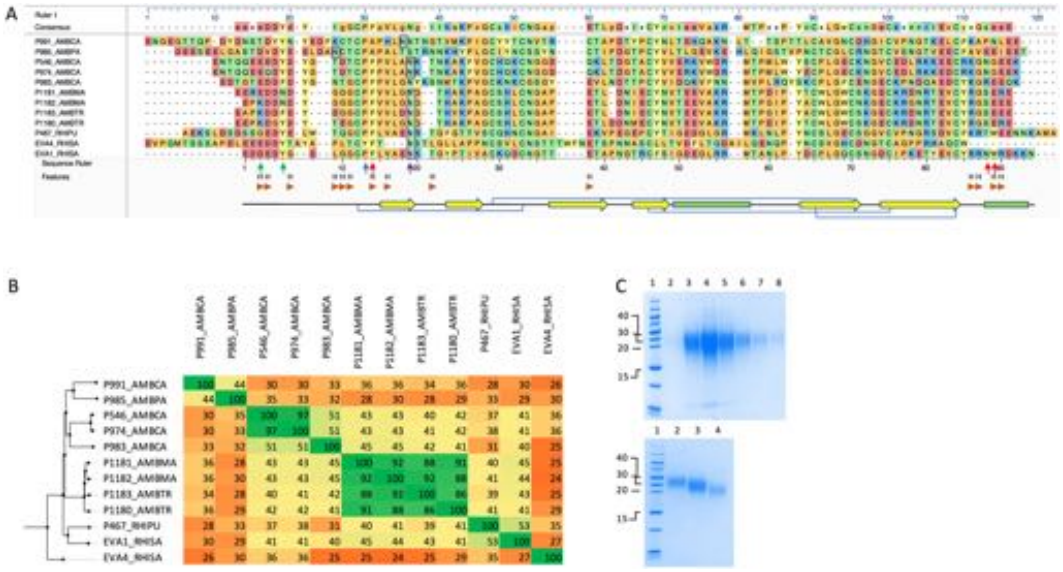


Figure 3. Analysis of CC-chemokine binding evasin sequences. (**A**) CLUSTAL-W alignment of CC-chemokine binding evasins with evasins 1 and 4 (EVA1, EVA4). Peptide sequence prefix indicates the identity, and suffix indicate the tick species as follows: RHISA and RHIPU – *Rhipicephalus sanguineus* and *pulchellus* respectively, and AMBPA, AMBCA, AMBMA, AMBTR - *Amblyomma parvum, cajennense, maculatum, triste*) respectively. Amino acid residues are color coded by physicochemical properties, and consensus sequence presented above the alignment. Evasin 1 H-bonds to CCL3 are shown as "H". Evasin 1 structural motifs are indicated as yellow arrows (beta-sheet), green bars (alpha-helix), and blue connectors (disulfide bonds), and were taken from the analysis of the evasin 1:CCL3 structure 3FPU provided in PDBSum[18]. The blue arrow indicates the P13 residue in evasin 1 that targets the disulfide bond in CCL3[13]. Red arrows indicate F14, N88 and W89 residues in evasin 1 that make contact with CCL3. Green arrows indicate E16 and Y19 residues of evasin 4. The purple arrow indicates N19 in evasin 1, which is glycosylated. The conserved glycosylation sites at the N-terminus predicted using NetNGlyc are boxed in purple. (**B**) Sequence conservation between CC-chemokine binding evasins and EVA1 and EVA4 peptides. Percent identities between sequences are shown and were calculated by performing BLASTP with default parameters, and are color coded with green indicating high sequence conservation, yellow indicating medium, and orange indicating low conservation. CC-chemokine binding evasins are arranged according to the sequence-similarity based phylogenetic tree shown on the left of the figure. (**C**) Expression and purification of P991_AMBCA. Colloidal Coomassie stained gels of proteins fractionated by SDS-PAGE. Top panel: Elutions from nickel affinity column, lanes 3–8. Molecular weight ladder (kDa) lane 1. His-tagged P991_AMBCA has a predicted MW including tag of 15.7 kDa. Bottom panel: Fractions collected from size exclusion column chromatography of the pooled material obtained from the nickel affinity column.

number of chemokines bound, and the binding affinities vary significantly depending on the evasin. The binding profiles of novel evasins cannot be predicted by sequence similarity, with the exception of the very closely related group consisting of P1180, P1181, P1182 and P1183. A unifying feature that distinguishes these evasins from the binding profile reported for evasins 1 and 4 is their ability to bind CCL2 and CCL13. Importantly we observed a wide variation in chemokine off rates as seen in Fig. 4B. This variation in off rate translated into large variations in the dissociative half-life (Fig. 5B) that are not predicted by sequence similarity. For instance, for P991_AMBCA, the dissociation half-lives for the closely related chemokines CCL2, CCL13 and CCL7 were 4.78, 163 and 144 minutes respectively.

Binding of P991_AMBCA to mouse chemokines *in vitro*. Our studies suggested that P991_AMBCA appears to be the evasin most suitable for development as a broad-spectrum CC-chemokine inhibitor (Fig. 5A), and we therefore characterized it in further detail. A significant consideration in the development of tool compounds and therapeutics is their ability to target not only human proteins but also those in animal models. Mouse – the most commonly used model for inflammatory human disease - has diverged from humans ~75 million years in the past and has a significantly divergent set of chemokines[33]. We therefore screened the novel evasins for binding to a panel of mouse CC-chemokines at 300 nM (see Supplementary Table S2) and found that several chemokines bind. We therefore characterized the binding of P991_AMBCA to mouse CC-chemokines using biolayer interferometry as described above (Fig. 6). Arranging P991_AMBCA binding data to a protein sequence-similarity based phylogenetic tree of mouse and human CC-chemokines shows that there is excellent correlation of evasin binding between mouse and related human chemokines. Thus P991_AMBCA appears to be suitable for mouse studies as a biological probe.

Inhibition of chemokine function by P991_AMBCA. We next determined if P991_AMBCA would inhibit chemokine function. For this we monitored its effects on the migration of THP-1 human monocyte cells

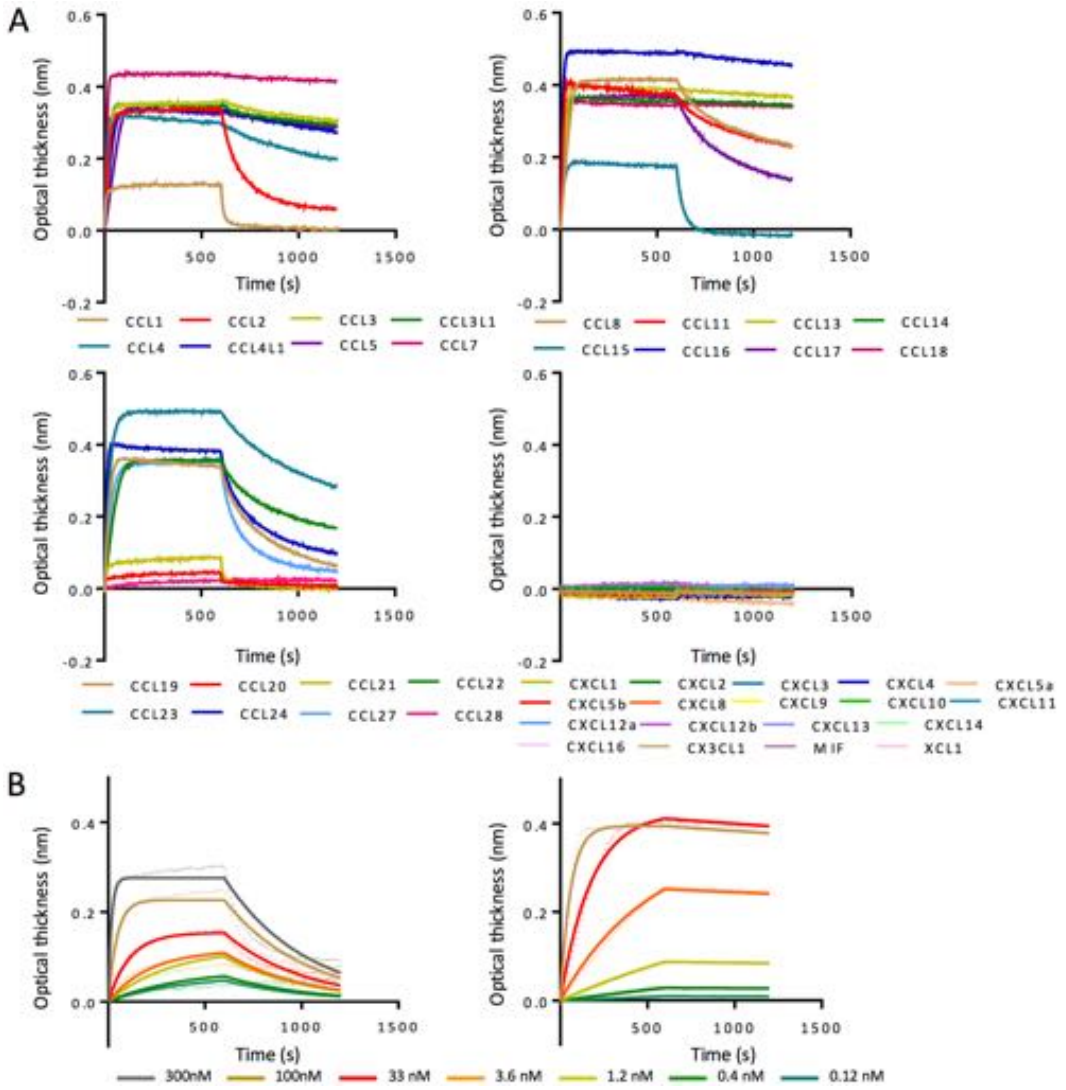


Figure 4. Characterization of P991_AMBCA by biolayer interferometry. (**A**) P991_AMBCA cross binding. Biolayer interferometry sensorgrams showing P991_AMBCA binding to different chemokines at 300 nM. Plots display optical thickness (y-axis, nm) versus time (x-axis, seconds). (**B**) P991_AMBCA binding to indicated chemokines. Biolayer interferometry sensorgrams showing P991_AMBCA binding to different doses (ranging from 300 nM to 0.4 nM) of chemokines CCL2 (left panel), and CCL13 (right panel). Plots display optical thickness (y-axis, nm) versus time (x-axis, seconds).

in response to human chemokines in 96 well Boyden chamber assays. In initial experiments, we determined the EC_{80} of several chemokines, and found that these cells responded to low nM doses of CCL2, CCL3, CCL3L1, CCL5, CCL7 and CCL8 (see Supplementary Table S3). We next determined the effect of titrating in progressively increasing doses of evasins to determine IC_{50} (Fig. 7A,B). These results showed that P991_AMBCA inhibits the chemokine-induced migration of THP-1 cells with IC_{50} in the low nM range. Since migration under these conditions does not depend on GAG binding, it suggests that P991_AMBCA directly inhibits binding of chemokine to their receptors on THP-1 cells.

Inhibition of a complex chemokine mixture by P991_AMBCA. The expression of multiple chemokines in disease tissue and chemokine receptor synergism is a source of network robustness. The orphan disease giant cell myocarditis is characterized by the expression of chemokines CCL5, CCL13, CCL18, CCL20 and CXCL9[34,35], and pathologically by the infiltration of the heart with monocytes and macrophages[36,37]. Of these, CCL5[38], CCL13[39] and CCL20[40] are known monocyte chemoattractants, CCL18 is an agonist of the receptor CCR8[41] which is expressed on monocytes and macrophages[42], and CXC and CC chemokines are known to synergize in monocyte chemotaxis[43], suggesting that all five chemokines could play a role in disease pathogenesis. We found using a THP-1 monocyte cell-migration assay that in low doses (20 nM), CCL5 caused a small degree of THP-1 cell migration in comparison to baseline (NIL, absence of chemokine), but that the other chemokines individually did not (Fig. 7C). When added in combination these five chemokines caused a substantial increase

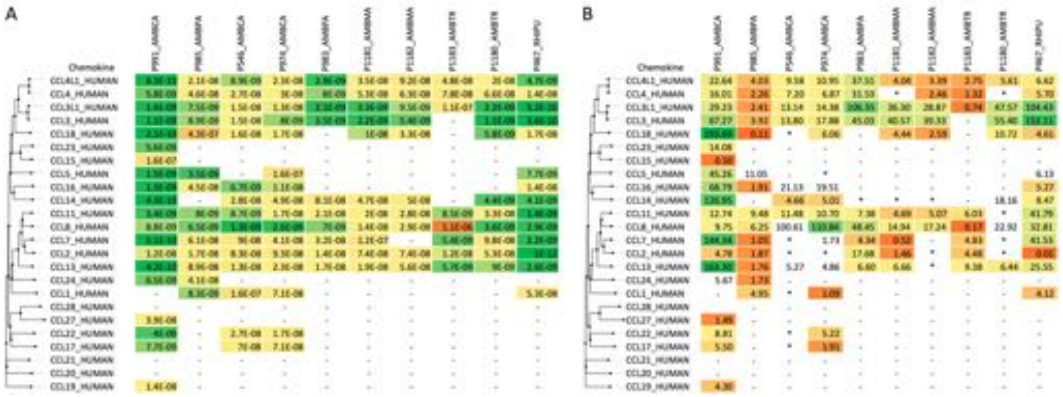


Figure 5. Binding of novel evasins to human CC chemokines. (**A**) Binding affinities (K_d, moles/litre) of novel evasins to human CC-chemokines using biolayer interferometry. Higher affinity binding is indicated as shades of green, medium affinity as yellow, and lower affinity as shades of orange. Evasins and chemokines are arranged by sequence-similarity based phylogeny. - Indicates that binding was not detected at 300 nM chemokine concentration. (**B**) Dissociative half-life times ($t_{1/2}$, minutes) of novel evasins with human CC-chemokines, calculated from biolayer interferometry off-rates ($t_{1/2} = 0.693/(k_{off} \times 60)$[60]. - Indicates that binding was not detected at 300 nM chemokine concentration. *Indicates that k_{off} data were not available (as a steady-state fit was performed, see methods) and the dissociative half-life time could not be calculated. Evasins and chemokines are arranged by sequence-similarity based phylogeny. Longer half-lives are indicated as shades of green, medium as yellow, and shorter half-lives as shades of orange.

in THP-1 migration over baseline, indicating a synergistic effect. We found that P991_AMBCA completely blocked the migration of THP-1 cells produced by the chemokine combination. These results indicated that P991_AMBCA, which targets three of the five chemokines (CCL5, CCL13, CCL18), is capable of overcoming the combinatorial and synergistic effects of these chemokines on THP-1 monocyte migration.

Discussion

Mitochondrial phylogenetic studies indicate that ticks arose ~300 milion years (myr) ago and likely parasitized amphibians, and later reptiles, birds and mammals[44]. Metastriate hard ticks such as *Rhiphicephalus* and *Amblyomma* first appear in the late Jurassic (~134 myr), concomitant with the appearance of placental mammals[44]. Bioinformatic analyses of transcriptome data indicate that Metastriate ticks have evolved divergent evasin-like molecules[23,24]. Such novel peptides could be valuable tool compounds and therapeutics.

We developed a peptide display approach to rapidly select chemokine binders from putative evasins identified in tick salivary transcriptomes. Peptide display technologies have in common the ability to physically link peptide sequences with the encoding DNA, and are powerful ways to select a variety of molecular shapes based on protein interactions. Approaches that have been used include yeast surface display – used to select antibody fragments[25], monobodies[45], knottins[46], tick salivary antigens[47], and tick gut peptides interacting with *B. burgdorferi* proteins[48], mammalian cell surface display used for single chain antibodies[49], bacterial surface display used for nanobodies[50], cyclotides[51] and anticalins[52], phage display used for antibodies[53], monobodies[54] and evasins[19], and mRNA display – used for cyclic peptides[55]. A major advantage of yeast surface display for eukaryotic secreted proteins is that unlike mammalian cell surface display, large stably transfected yeast libraries can easily be made, and as protein disulfide isomerases and chaperones are present in the secretory pathway of yeast[25], they do not need to be artificially introduced as in phage or bacterial display[19]. We therefore explored if evasins could be rapidly identified and functionally characterised using yeast surface display.

Our initial studies showed that evasins of two unrelated structural classes can be displayed on yeast surface in either N- or C-terminally tagged orientations. The display orientation affected the ability of the evasin to recognize the target chemokine, confirming previous studies[56]. These experiments provided proof-of-concept that surface displayed evasins can be identified using flow sorting with a fluorescent chemokine probe. We created a library consisting of 24 members, screened it with the chemokine CCL5, as it is important in the pathogenesis of cardiovascular disease, and successfully recovered novel evasins. These yeast display studies confirmed that the nature and location of the surface display tag affected the chemokine-binding function of an evasin unpredictably, and support the use of display tags in different orientations when constructing such libraries. Moreover, they mean that a clone need not be recovered in either orientation in a screen as the display tag may interfere with binding.

Comparison of the chemokine binding pattern of C-terminally tagged P467_RHIPU in yeast with that of C-terminally tagged purified protein showed that they were similar, with both showing binding to CCL1, CCL2, CCL3, CCL5, CCL8, CCL11 and CCL18. However, there were some discrepancies, with the purified protein not binding CCL17, CCL19 and CCL22. We do not understand the mechanisms of the discrepancy, but they possibly arise from underlying differences in the assays and in the C-terminal tag used. Our unpublished data (J.R.O.E., A.K., S.B.) also indicate that altering the position of the purification tag in mammalian expressed proteins affects binding specificity, and indeed this phenomenon could potentially be used to engineer the desired chemokine binding properties of an evasin. By extending our screening studies with other chemokines, and our library to

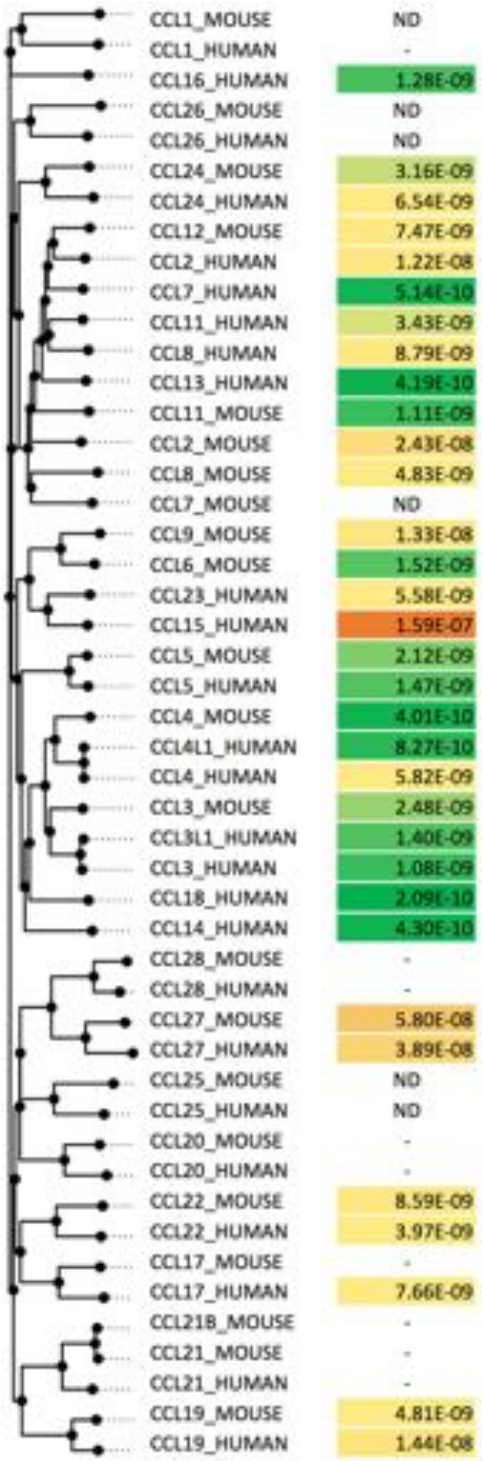


Figure 6. Binding of P991_AMBCA to mouse CC chemokines. Binding affinities (K_d, moles/litre) of P991_AMBCA to mouse CC-chemokines using biolayer interferometry. ND indicates not done. - Indicates that binding was not detected at 300 nM chemokine concentration. Human and mouse CC-chemokines are arranged by sequence-similarity based phylogeny. Human chemokine binding to P991_AMBCA is as shown in Fig. 5, and shown here for comparison to mouse binding data. Higher affinity binding is indicated as shades of green, medium affinity as yellow, and lower affinity as shades of orange.

>350 members, we successfully identified a total of 26 CC-chemokine binding evasins of which we have characterised 10 in detail here. These studies suggest that many putative evasins identified by bioinformatics may not have high enough affinity for chemokines used in the screens performed to date in order for them to be selected by yeast surface display, but may bind other chemokines or have functions other than chemokine binding.

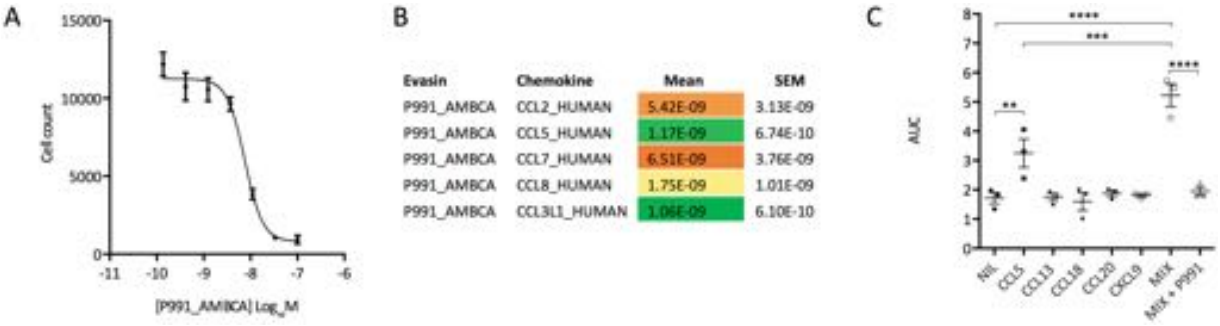


Figure 7. Functional neutralization of chemokine activity. (**A**) Neutralization of CCL2 induced THP-1 cell migration by P991_AMBCA. Y-axis shows cell count of THP-1 cells migrating through to the bottom chamber in response to EC_{80} dose of CCL2. Data (3 technical replicates) are shown as mean ± s.e.m. X-axis shows P991_AMBCA concentration (Log_{10} Molar). (**B**) Summary of P991_AMBCA IC_{50} data (moles/litre, mean, s.e.m. of 3 biological replicates analyzed as above) for chemokines that induce THP-1 cell migration. Lower IC_{50} is indicated as shades of green, medium as yellow, and high as shades of orange. (**C**) Neutralization of a complex chemokine mixture by P991_AMBCA. Y-axis shows AUC (area under progress curve) in response to indicated treatments shown on the x-axis. NIL indicates baseline migration without any chemokine. Results (mean ± s.e.m., and individual data points) of 3 independent biological replicate experiments are shown, and were analyzed with one-way ANOVA with Sidak's multiple comparisons test and P values adjusted for multiple comparisons. *Indicates $P < 0.05$, **Indicates $P < 0.01$, ***$P < 0.001$, ****$P < 0.0001$.

Analysis of the novel CC-chemokine binding evasins showed that they resemble evasin 1 in retaining Cys residues that are necessary for intra-chain disulfide bond formation, and conserve the Pro residue that targets the invariant disulfide in chemokines. The novel evasins are however remarkably dissimilar to evasin 1 or 4 in primary structure. Conservation of the Cys residues suggests that these CC-chemokine binding evasins have a common disulfide bonded structure that arose in a common ancestor. The lack of conservation of other key residues suggest that these novel evasins evolved different pharmacophores to bind target chemokines.

Like evasins 1 and 4, the novel evasins have multiple predicted glycosylation sites[18,30], and consistent with this, migrate at a significantly higher apparent molecular weight. The striking conservation of the N-terminal glycosylation site corresponding to N19 in evasin 1 suggests that there is evolutionary pressure maintaining glycosylation at this site. As glycosylation is not essential for chemokine recognition by an evasin[18], a possible explanation is that such glycosylation reduces access to neutralizing antibodies by creating a "glycan-shield"[57,58], and likely explains the lack of detectable antibody response following evasin therapy[59].

Binding assays performed using purified proteins showed that the novel evasins bound to a range of CC chemokines with high affinity. Remarkably, the off-rates and consequently the dissociative half-lives of the interactions showed wide variations even with closely related chemokines and closely related evasins. The large dissociative half-lives, in excess of a 100 minutes observed in 5 of 10 evasins, with k_{off} similar to that of antibody-antigen interactions, suggests that for these interactions there is a change in conformation leading to greater steric complementarity between evasin and chemokine after binding, and resulting in a very slowly dissociating complex. Indeed, conformational changes in both partners has been observed in the interaction between evasin 1 and CCL3[18]. Advantages of a long residence time for a pharmacological agent include prolonged action, complete physiological inhibition requiring endogenous synthesis of target for recovery, and reduced off-target effects[60,61]. Notably, chemokine interaction with cell surface glycosaminoglycans (GAGs) is known to promote chemokine stability, is essential for chemokine function *in vivo*[62], and can result in conformational changes in chemokine structure and oligomerization[63]. While the ability of an evasin to bind GAG-bound chemokines is not known, it is conceivable that the prolonged residence time of certain evasins may be an evolutionary adaptation to neutralizing GAG-bound chemokines.

The remarkable differences in dissociative half-lives between similar chemokines (e.g. the binding of P991_AMBCA to CCL2 and CCL13), suggest that different evasin-chemokine binding mechanisms must exist. For instance, the ability to block eosinophil chemotaxis by CCL13 could be very relevant to the role that eosinophils play in parasitic infestation[64]. This is also suggested by the different combinations of chemokines that are bound by individual evasins, and also by the ability of certain evasins to target a very large number of structurally distinct chemokines. These mechanisms can be understood by structural analyses of chemokine – evasin complexes, and we have initiated such studies. Our studies, and those previously reported with evasins 1 and 4, also indicate that binding by an evasin predicts its ability to neutralize the chemotactic function of a target chemokine. In the case for evasins 1 and 4, binding occurs to the N-terminus of CCL3[18,19], which prevents access to the CRS2 domain of the receptor. It is possible that the novel evasins reported here also function in a similar manner, and needs further exploration.

A key novel feature of this group of evasins, absent in evasins 1 and 4, is their ability to bind and neutralize CCL2 and CCL13, in addition to other CC-chemokines. Further structural studies are needed to understand the mechanism used in targeting these two chemokines that makes them distinct from evasins 1 and 4. The ability to target CCL2 - a monocyte recruiting chemokine expressed in the tumour microenvironment[65], myocarditis[66], myocardial infarction[67] and stroke[68] - in addition to other chemokines makes these evasins potentially useful in disrupting the

chemokine network in these diseases. Similarly, CCL13 is expressed in myocarditis[35], myocardial infarction[69] and idiopathic lung fibrosis[70], making these new evasins useful tool compounds and potential therapeutics in these and other chemokine-driven inflammatory disease. Our data also indicate that certain evasins such as P991_AMBCA can bind related chemokines from species such as mouse and human that diverged ~75 million years ago. This is not unsurprising as ticks such as *Amblyomma cajennense* parasitize not only humans, but also dogs, cattle, birds, and capybaras[24]. The ability to bind related targets across different species is relevant in the development of new therapeutics in pre-clinical animal models that then have to be translated into human disease.

Key features of the chemokine network that have evolved to make it robust to attack by pathogens but frustrate the development of novel therapeutics are the multiplicity of chemokines typically expressed in disease, the polyvalent nature of chemokine - receptor interactions, and expression of several chemokine receptors on a single cell type that can act synergistically. Our studies using a small group of five chemokines that are expressed in giant cell myocarditis show that they can indeed act synergistically on the recruitment of monocytes, and also that a single evasin that targets three of these five chemokines can abolish monocyte recruitment by the chemokine combination. Future studies to determine the *in vivo* concentration of an evasin necessary to neutralize myocarditis chemokines are necessary to extend our *in vitro* data.

In conclusion, we have developed yeast surface display as an approach to rapidly identify proteins from tick saliva that bind and neutralize members of the mammalian chemokine network. These proteins could be developed as potential therapeutics to target diverse inflammatory diseases that are driven by chemokines. More broadly, the explosion of transcriptome sequence information from diverse biological resources requires efficient proteomic approaches for identification and functional characterisation of inter-species protein interactions. Our studies provide evidence that yeast surface display could be used to systematically identify such protein interactions, and rapidly mine potential therapeutics from organisms that have, as evolutionary adaptations, developed peptide arsenals in "endless forms most beautiful"[71].

Methods

Bioinformatics. Tick transcriptome datasets were accessed at NCBI (http://blast.ncbi.nlm.nih.gov/, non-redundant and transcriptome shotgun assembly databases), and searched using three iterations of psiBLAST[72], using the mature peptide sequences of evasins 1 and 4, in order to detect biologically relevant but weak protein similarities. Peptides with e-value $<$ 1E-5, possessing a signal peptide defined by SignalP 3.0[73], and mature peptide length $<$ 200 amino acid residues were classed as putative evasins.

Plasmids. Yeast expression shuttle plasmids and plasmid libraries were assembled from constituent idempotent parts (promoter, signal peptide, cDNA, surface display tags, epitope tags, terminator, replication origins, antibiotic and/or auxotrophic selection markers) that we have developed as part of a synthetic biology toolkit for use in GoldenGate cloning[74]. Constituent parts were generated using PCR or gene synthesis (GeneWiz, South Plainfield, NJ, USA), cloned into plasmids, and sequenced to confirm lack of mutations. Evasin part overhangs were designed so that they were compatible with either N- or C-terminal surface display tags. Plasmid assembly was performed using the single pot GoldenGate/GoldenBraid cloning method[74] that we modified to incorporate a negative selection *ccdb* gene cassette (Invitrogen) for improved cloning efficiency, enabling library construction. Yeast expression shuttle plasmids contained a yeast GAL1 promoter, synthetic AMYG_RHIOR signal peptide, 2-micron replication origin and ADH1 terminator, and TRP auxotrophic marker. Surface display tags were AGA2_YEAST (from pCTCon2[25]) or SAG1_YEAST (residues 332–650[27]), and were separated from the evasin cDNA using a linker encoding (GGGGS)x3. Yeast shuttle plasmids and libraries were created in three configurations, with N-terminal AGA2_YEAST, C-terminal AGA2_YEAST, and C-terminal SAG1_YEAST surface display tags. Each plasmid library was made to achieve $>$10-fold overrepresentation of the evasin library inserts. Mammalian expression plasmids were created in the vector pHLSec[31] (kind gift from Radu Aricescu) by Infusion cloning (Clontech) following the manufacturers recommendations. Evasin expression plasmids contained a C-terminal G4S linker and strep II-8xHis protein purification tag (GGGGGSGGGGSGGASAWSHPQFEKLEHHHHHHHH)[75] and N-terminal ETG sequence from plasmid pHLSec.

Yeast surface display. Yeast surface display was performed essentially as described[28]. EBY100 yeast (Invitrogen) were transformed with shuttle plasmids. For library screens, we achieved $>$10 fold overrepresentation of each unique evasin. Yeast cells were induced with galactose, 5E5 cells labelled in 1 ml PBS with biotinylated chemokines (Almac, 20 uM, 2.75 μl) and streptavidin-Alexa647 (2mg/ml, Invitrogen, 1.25 μl), incubated for 30 minutes on ice in the dark, spun at 8000 rpm for 5 minutes in a benchtop microcentrifuge, the pellet resuspended in 200 μl PBS, and sorted using a MoFlo FACS system with a gate defined by a negative control that omitted the chemokine. Cells recovered were re-grown and sorted a second time. For initial experiments, shuttle plasmids were isolated from individual sorted yeast colonies using a DNA prep kit (The Epigenetics Company), rescued into electrocompetent DH5α cells by electroporation, plasmid DNA miniprepped, and evasin insert identified by capillary sequencing followed by BLAST searching of a local database. Subsequently, we adopted a more efficient method wherein we directly amplified the insert using PCR typically from 24 independent colonies, and sequenced them prior to plasmid rescue. Rescued plasmids were re-transformed to yeast to confirm chemokine binding by FACS analyses as above but using a 96-well ATTUNE NXT system (Life Technologies). FACS data was analysed using FlowJo v10.02.

Evasin peptide sequence analysis. Peptide sequence alignments were performed using Clustal-W in Megalign Pro (DNAStar version 12.3.1, DNAStar Inc.), and a sequence-similarity based phylogenetic tree exported to FigTree (version 1.4.2, http://tree.bio.ed.ac.uk/software/figtree/). Glycosylation site prediction was

performed using NetNGlyc1.0 (http://www.cbs.dtu.dk/services/NetNGlyc/) and NetOGlyc4.0 (http://www.cbs.dtu.dk/services/NetOGlyc/)[76]. Peptide molecular weight and isoelectric point (pI) were calculated at ExPASy (http://web.expasy.org/compute_pi/). Chemokine sequence alignments and sequence-similarity based phylogenetic trees were constructed using MUSCLE in Megalign Pro.

Cell lines. HEK293F cells were a gift from Nicola Burgess-Brown (University of Oxford), and THP-1 cells were from Sigma. Cell lines were confirmed mycoplasma free by a kit (MycoAlert™, Lonza) and by DAPI staining and authenticated functionally by protein production for HEK293F, and chemokine – induced migration for THP-1.

Evasin protein production. HEK293F cells were transiently transfected using polyethylineimine (Sigma) and cultured in Freestyle™ 293 expression medium (ThermoFisher) at 37 °C, 8% CO_2, with shaking for 5 days. Proteins were purified from filtered supernatants by gravity flow through Nickel charged IMAC Sepharose 6 Fast Flow resin (GE Healthcare), equilibrated with binding buffer (20 mM NaPO4, 500 mM NaCl, pH 7.4), washed after binding with wash buffer (20 mM NaPO4, 1 M NaCl, 20 mM imidazole, pH 7.4) and eluted in elution buffer (20 mM NaPO4, 500 mM NaCl, 500 mM imidazole, pH 7.4). Elutions were concentrated using an Amicon Ultra-15 Centrifugal Filter Unit with Ultracel-3 membrane (Millipore), and purified by size exclusion chromatography on an AKTA Start system using HiLoad 16/600 Superdex 75 (GE Healthcare), in SEC buffer (phosphate buffer saline (Sigma), with 150mM NaCl). Fractions showing absorption at 280 nm were analyzed by electrophoresis on a 12% SDS-PAGE gel, and stained with colloidal Coomassie.

Biolayer interferometry cross-binding screen. Biolayer interferometry was performed on an OctetRed® system at 30 °C using the dip and read Ni-NTA biosensors (ForteBio). The assay buffer used was 10 mM Na_2HPO_4, 1.8 mM KH_2PO_4, 2.7 mM KCl, 500 mM NaCl, 0.1% BSA, 0.002% TWEEN-20, pH 7.4. Assay buffer was used to establish the response baseline (180 seconds). The temperature condition was recommended by the manufacturer and buffers optimized to minimize non-specific binding of chemokines to the sensor (J.R.O.E., A.K. & S.B., unpublished data). Purified His-tagged evasin was immobilized on the Ni-NTA sensor using 1 μM evasin in assay buffer (500 seconds). After washing the sensor with assay buffer (60 seconds), the sensor was then subjected to 300 nM chemokine in assay buffer (600 seconds) to record the association phase. The cross-binding screen was performed as a single experiment against all human chemokines with the exception of CCL25, CCL26, and CXCL16, where the chemokine non-specifically bound to the sensor, and CXCL17, CXCL4L1, and XCL2, which were not available from Peprotech. Assay buffer was then reapplied (600 seconds) to measure the dissociation. The sensor was then exposed to 10 mM glycine, pH 1.7 for five seconds and assay buffer for five seconds three times to strip the sensors of nickel and protein. The sensor was regenerated by placing the sensor into 10 mM $NiCl_2$ for 60 seconds and then reused. Reference experiments were performed by placing a sensor with evasin alone loaded into buffer to account for baseline drift which was then subtracted. Data was processed in ForteBio Data Analysis 9 software. A similar protocol was used for mouse chemokines.

Biolayer Interferometry K_d and k_{off} determination experiments. Measurements were carried as above. Each experiment was performed once, with a range of chemokine dilutions from 300 nM to 0.4 nM. Briefly, after washing the sensor with assay buffer for 60 seconds, the sensors were then subjected to a serial dilution of chemokine in assay buffer for 600 seconds to record the association phase. Assay buffer was then reapplied to measure the dissociation for 600 seconds. To account for non-specific binding to the sensor, a non-interacting reference protein of sequence DGGQRNAICRLPPDEGICRASIPRFYFNPAEGKCSFFIYGGCEGNENNFETIE ECEKTCGEPERPSDFEGADFETGCAPKPQRGFCKGFLDHWFFNVTSGECEAFLYSGCGGNDNNYESKEEC EIACKLTGGASAWSHPQFEKLEHHHHHHHH was loaded on to the sensor and any binding observed subtracted. This protein was shown to display no binding to any of the chemokines tested and was produced in house as above. Data was processed in ForteBio Data Analysis 9 software. Association (k_{on}), dissociation (k_{off}), and affinity (K_d) constants were determined by using the 1:1 binding-model, and global fitting, followed by 'R_{max} unlinked by sensor' to allow independent fitting of R_{max} (maximal signal response upon saturating binding of the partner to the immobilized protein). For certain chemokine-evasin interactions where a curve fit was not possible, a steady state analysis was performed using ForteBio Data Analysis 9 software to obtain the K_d, from the equilibrium response, and here k_{off} and k_{on} were not calculated. Data with poor curve fits ($R^2 < 0.9$) were excluded. Dissociation half-life (minutes) was calculated as 0.693/ ($k_{off} \times 60$) from the off-rate (k_{off}, s^{-1}) obtained from biolayer interferometry analysis[60].

Cell migration assays. Effective concentrations (EC) EC_{80} and EC_{50} for each chemokine was determined in three technical and three biological replicates essentially as described[77], using a 96 well transwell migration plate (5 μM pore size, Corning). Chemokines (0–100 nM (Peprotech), in 150 μl RPMI-1640 + L-glu (2mM) + 0.5% heat treated fetal bovine serum, all from Sigma) were placed in the bottom chamber. Cells (THP-1, 3E5, in 50 μl RPMI-1640 + L-glu (2 mM) + 0.5% heat treated fetal bovine serum)) were placed in the top chamber, and incubated at 37 °C, 5% CO_2 for 4 hours. The migration plate was shaken at 850 r.p.m. for 10 minutes, and media from bottom plate transferred to a V-bottomed 96 well plate. Cells were counted on a ATTUNE flow cytometer using a FSC versus SSC dot plot, and data analysed in GraphPad Prism fitting an agonist response curve with 4 parameters.

IC_{50} for each evasin was determined in three technical and three biological replicates essentially as described[77] using the above system. Chemokine (EC_{80} dose) and evasin (0–100 nM doses) were added to the bottom chamber and incubated for 30 min at 37 °C before beginning the cell migration assay. Data (3 technical replicates for each IC_{50} determination) were analysed in GraphPad Prism fitting an inhibitor response curve with 4 parameters. The mean IC_{50} from 3 biological replicates was then calculated. For studies where we investigated neutralization of a complex chemokine mixture we used an Incucyte ZOOM® chemotaxis system and recorded progress curves over 24 hours following the manufacturer's instructions, and calculated the area under the progress curve.

Statistical analyses. Summary statistics were calculated in GraphPad Prism. Tests of significance were calculated using ordinary one-way ANOVA, assuming Gaussian distribution and equal variance, in GraphPad Prism, with Sidak's multiple comparisons test (Fig. 7C). For each case the P value (probability of a type I error) reported was adjusted for multiple comparisons. The threshold (alpha) for a type I error was $P < 0.05$. For all cell based experiments sample sizes were $n = 3$ technical and $n = 3$ biological replicates, and were not powered to detect a pre-specified effect size. Investigators were not blinded to group allocation.

Data availability. The authors declare that data supporting this manuscript are available either within the manuscript or as Supplementary Information.

References

1. Garin, A. & Proudfoot, A. E. I. Chemokines as targets for therapy. *Experimental Cell Research* **317**, 602–612 (2011).
2. Schall, T. J. & Proudfoot, A. E. Overcoming hurdles in developing successful drugs targeting chemokine receptors. *Nat Rev Immunol* **11**, 355–363 (2011).
3. Allen, S. J., Crown, S. E. & Handel, T. M. Chemokine:Receptor Structure, Interactions, and Antagonism. *Annu. Rev. Immunol.* **25**, 787–820 (2007).
4. Fernandez, E. J. & Lolis, E. Structure, function, and inhibition of chemokines. *Annu. Rev. Pharmacol. Toxicol.* **42**, 469–499 (2002).
5. Szpakowska, M. *et al*. Function, diversity and therapeutic potential of the N-terminal domain of human chemokine receptors. *Biochemical Pharmacology* **84**, 1366–1380 (2012).
6. Kufareva, I. Chemokines and their receptors: insights from molecular modeling and crystallography. *Curr Opin Pharmacol* **30**, 27–37 (2016).
7. Horuk, R. Chemokine receptor antagonists: overcoming developmental hurdles. *Nature Reviews Drug Discovery* **8**, 23–33 (2009).
8. Szekanecz, Z. & Koch, A. E. Successes and failures of chemokine-pathway targeting in rheumatoid arthritis. *Nat Rev Rheumatol* **12**, 5–13 (2016).
9. Proudfoot, A. E. & Uguccioni, M. Modulation of Chemokine Responses: Synergy and Cooperativity. *Front Immunol* **7**, 183 (2016).
10. Brandes, M., Klauschen, F., Kuchen, S. & Germain, R. N. A systems analysis identifies a feedforward inflammatory circuit leading to lethal influenza infection. *Cell* **154**, 197–212 (2013).
11. Proudfoot, A. E., Bonvin, P. & Power, C. A. Targeting chemokines: Pathogens can, why can't we? *Cytokine* **74**, 259–267 (2015).
12. Gonzalez-Motos, V., Kropp, K. A. & Viejo-Borbolla, A. Chemokine binding proteins: An immunomodulatory strategy going viral. *Cytokine & growth factor reviews* **30**, 71–80 (2016).
13. Lubman, O. Y. & Fremont, D. H. Parallel Evolution of Chemokine Binding by Structurally Related Herpesvirus Decoy Receptors. *Structure* **24**, 57–69 (2016).
14. Hajnická, V. *et al*. Anti-interleukin-8 activity of tick salivary gland extracts. *Parasite Immunol.* **23**, 483–489 (2001).
15. Deruaz, M. *et al*. Ticks produce highly selective chemokine binding proteins with antiinflammatory activity. *Journal of Experimental Medicine* **205**, 2019–2031 (2008).
16. Kazimírová, M. & Štibrániová, I. Tick salivary compounds: their role in modulation of host defences and pathogen transmission. *Front Cell Infect Microbiol* **3**, 1–19 (2013).
17. Frauenschuh, A. *et al*. Molecular cloning and characterization of a highly selective chemokine-binding protein from the tick Rhipicephalus sanguineus. *J. Biol. Chem.* **282**, 27250–27258 (2007).
18. Dias, J. M. *et al*. Structural Basis of Chemokine Sequestration by a Tick Chemokine Binding Protein: The Crystal Structure of the Complex between Evasin-1 and CCL3. *PLoS ONE* **4**, e8514 (2009).
19. Bonvin, P. *et al*. Identification of the Pharmacophore of the CC Chemokine-binding Proteins Evasin-1 and-4 Using Phage Display. *Journal of Biological Chemistry* **289**, 31846–31855 (2014).
20. Schmolke, M. & Garcia-Sastre, A. Evasion of innate and adaptive immune responses by influenza A virus. *Cell Microbiol* **12**, 873–880 (2010).
21. Bonvin, P., Power, C. A. & Proudfoot, A. E. Evasins: therapeutic potential of a new Family of Chemokine-Binding proteins from ticks. *Front Immunol* **7**, 1–7 (2016).
22. Weston-Davies, W. H. *et al*. Clinical and Immunological Characterisation of Coversin, a Novel Small Protein Inhibitor of Complement C5 with Potential As a Therapeutic Agent in PNH and Other Complement Mediated Disorders. *Blood* **124**, 4280 (2014).
23. Karim, S. & Ribeiro, J. M. An Insight into the Sialome of the Lone Star Tick, Amblyomma americanum, with a Glimpse on Its Time Dependent Gene Expression. *PLoS One* **10**, e0131292 (2015).
24. Garcia, G. R. *et al*. The sialotranscriptome of Amblyomma triste, Amblyomma parvum and Amblyomma cajennense ticks, uncovered by 454-based RNA-seq. *Parasit Vectors* **7**, 430 (2014).
25. Boder, E. T. & Wittrup, K. D. Yeast surface display for screening combinatorial polypeptide libraries. *Nat Biotechnol* **15**, 553–557 (1997).
26. Wang, Z., Mathias, A., Stavrou, S. & Neville, D. M. A new yeast display vector permitting free scFv amino termini can augment ligand binding affinities. *Protein Engineering Design and Selection* **18**, 337–343 (2005).
27. Chen, J., Zhou, J., Sanders, C. K., Nolan, J. P. & Cai, H. A surface display yeast two-hybrid screening system for high-throughput protein interactome mapping. *Analytical Biochemistry* **390**, 29–37 (2009).
28. Chao, G. *et al*. Isolating and engineering human antibodies using yeast surface display. *Nat Protoc* **1**, 755–768 (2006).
29. Dusi, V., Ghidoni, A., Ravera, A., De Ferrari, G. M. & Calvillo, L. Chemokines and Heart Disease: A Network Connecting Cardiovascular Biology to Immune and Autonomic Nervous Systems. *Mediators Inflamm* **2016**, 5902947 (2016).
30. Déruaz, M. *et al*. Evasin-4, a tick-derived chemokine-binding protein with broad selectivity can be modified for use in preclinical disease models. *FEBS Journal* **280**, 4876–4887 (2013).
31. Zhao, Y. *et al*. Automation of large scale transient protein expression in mammalian cells. *J. Struct. Biol.* **175**, 209–215 (2011).
32. Concepcion, J. *et al*. Label-free detection of biomolecular interactions using BioLayer interferometry for kinetic characterization. *Comb Chem High Throughput Screen* **12**, 791–800 (2009).
33. Nomiyama, H., Osada, N. & Yoshie, O. The evolution of mammalian chemokine genes. *Cytokine Growth Factor Rev.* **21**, 253–262 (2010).
34. Lassner, D. *et al*. Improved diagnosis of idiopathic giant cell myocarditis and cardiac sarcoidosis by myocardial gene expression profiling. *Eur Heart J* **35**, 2186–2195 (2014).
35. Kittleson, M. M. *et al*. Gene expression in giant cell myocarditis: Altered expression of immune response genes. *International journal of cardiology* **102**, 333–340 (2005).
36. Caforio, A. L. *et al*. Current state of knowledge on aetiology, diagnosis, management, and therapy of myocarditis: a position statement of the European Society of Cardiology Working Group on Myocardial and Pericardial Diseases. *Eur Heart J* **34**, 2636–2648, 2648a–2648d (2013).
37. Basso, C., Calabrese, F., Angelini, A., Carturan, E. & Thiene, G. Classification and histological, immunohistochemical, and molecular diagnosis of inflammatory myocardial disease. *Heart Fail Rev* **18**, 673–681 (2013).

38. Dutta, P. & Nahrendorf, M. Regulation and consequences of monocytosis. *Immunol Rev* **262**, 167–178 (2014).
39. Mendez-Enriquez, E. & Garcia-Zepeda, E. A. The multiple faces of CCL13 in immunity and inflammation. *Inflammopharmacology* **21**, 397–406 (2013).
40. Lee, A. Y. & Korner, H. CCR6 and CCL20: emerging players in the pathogenesis of rheumatoid arthritis. *Immunol Cell Biol* **92**, 354–358 (2014).
41. Islam, S. A., Ling, M. F., Leung, J., Shreffler, W. G. & Luster, A. D. Identification of human CCR8 as a CCL18 receptor. *J Exp Med* **210**, 1889–1898 (2013).
42. Bachelerie, F. *et al*. An atypical addition to the chemokine receptor nomenclature: IUPHAR Review 15. *British journal of pharmacology* **172**, 3945–3949 (2015).
43. Gouwy, M. *et al*. Synergy between Coproduced CC and CXC Chemokines in Monocyte Chemotaxis through Receptor-Mediated Events. *Mol. Pharmacol.* **74**, 485–495 (2008).
44. Jeyaprakash, A. & Hoy, M. A. First divergence time estimate of spiders, scorpions, mites and ticks (subphylum: Chelicerata) inferred from mitochondrial phylogeny. *Exp. Appl. Acarol.* **47**, 1–18 (2009).
45. Lipovsek, D. *et al*. Evolution of an interloop disulfide bond in high-affinity antibody mimics based on fibronectin type III domain and selected by yeast surface display: molecular convergence with single-domain camelid and shark antibodies. *Journal of molecular biology* **368**, 1024–1041 (2007).
46. Silverman, A. P., Levin, A. M., Lahti, J. L. & Cochran, J. R. Engineered Cystine-Knot Peptides that Bind αvβ3 Integrin with Antibody-Like Affinities. *Journal of molecular biology* **385**, 1064–1075 (2009).
47. Schuijt, T. J. *et al*. Identification and characterization of Ixodes scapularis antigens that elicit tick immunity using yeast surface display. *PLoS One* **6**, e15926 (2011).
48. Narasimhan, S. *et al*. A tick gut protein with fibronectin III domains aids Borrelia burgdorferi congregation to the gut during transmission. *PLoS Pathog* **10**, e1004278 (2014).
49. Ho, M., Nagata, S. & Pastan, I. Isolation of anti-CD22 Fv with high affinity by Fv display on human cells. *Proc. Natl. Acad. Sci. USA* **103**, 9637–9642 (2006).
50. Fleetwood, F. *et al*. Surface display of a single-domain antibody library on Gram-positive bacteria. *Cell Mol Life Sci* **70**, 1081–1093 (2013).
51. Daugherty, P. S. Protein engineering with bacterial display. *Current Opinion in Structural Biology* **17**, 474–480 (2007).
52. Binder, U., Matschiner, G., Theobald, I. & Skerra, A. High-throughput Sorting of an Anticalin Library via EspP-mediated Functional Display on the Escherichia coli Cell Surface. *Journal of molecular biology* **400**, 783–802 (2010).
53. Finlay, W. J., Bloom, L. & Cunningham, O. Phage display: a powerful technology for the generation of high specificity affinity reagents from alternative immune sources. *Methods Mol Biol* **681**, 87–101 (2011).
54. Koide, A., Bailey, C. W., Huang, X. & Koide, S. The fibronectin type III domain as a scaffold for novel binding proteins. *Journal of molecular biology* **284**, 1141–1151 (1998).
55. Passioura, T., Katoh, T., Goto, Y. & Suga, H. Selection-Based Discovery of Druglike Macrocyclic Peptides. *Annu. Rev. Biochem.* (2014).
56. Pepper, L. R., Cho, Y. K., Boder, E. T. & Shusta, E. V. A decade of yeast surface display technology: where are we now? *Comb Chem High Throughput Screen* **11**, 127–134 (2008).
57. Sommerstein, R. *et al*. Arenavirus Glycan Shield Promotes Neutralizing Antibody Evasion and Protracted Infection. *PLoS Pathog* **11**, e1005276 (2015).
58. Wei, X. *et al*. Antibody neutralization and escape by HIV-1. *Nature* **422**, 307–312 (2003).
59. Russo, R. C. *et al*. Therapeutic Effects of Evasin-1, a Chemokine Binding Protein, in Bleomycin-Induced Pulmonary Fibrosis. *Am J Respir Cell Mol Biol* **45**, 72–80 (2011).
60. Copeland, R. A., Pompliano, D. L. & Meek, T. D. Drug-target residence time and its implications for lead optimization. *Nature reviews. Drug discovery* **5**, 730–739 (2006).
61. Copeland, R. A. The drug-target residence time model: a 10-year retrospective. *Nature reviews. Drug discovery* **15**, 87–95 (2016).
62. Kufareva, I., Salanga, C. L. & Handel, T. M. Chemokine and chemokine receptor structure and interactions: implications for therapeutic strategies. *Immunol Cell Biol* **93**, 372–383 (2015).
63. Liang, W. G. *et al*. Structural basis for oligomerization and glycosaminoglycan binding of CCL5 and CCL3. *Proceedings of the National Academy of Sciences of the United States of America* **113**, 5000–5005 (2016).
64. Ravin, K. A. & Loy, M. The Eosinophil in Infection. *Clin Rev Allergy Immunol* **50**, 214–227 (2016).
65. Yoshimura, T. The production of monocyte chemoattractant protein-1 (MCP-1)/CCL2 in tumor microenvironments. *Cytokine* (2017).
66. Escher, F. *et al*. Fractalkine in human inflammatory cardiomyopathy. *Heart* **97**, 733–739 (2011).
67. de Lemos, J. A. *et al*. Serial measurement of monocyte chemoattractant protein-1 after acute coronary syndromes: results from the A to Z trial. *Journal of the American College of Cardiology* **50**, 2117–2124 (2007).
68. Mirabelli-Badenier, M. *et al*. CC and CXC chemokines are pivotal mediators of cerebral injury in ischaemic stroke. *Thrombosis and haemostasis* **105**, 409–420 (2011).
69. Orn, S. *et al*. The chemokine network in relation to infarct size and left ventricular remodeling following acute myocardial infarction. *Am J Cardiol* **104**, 1179–1183 (2009).
70. DePianto, D. J. *et al*. Heterogeneous gene expression signatures correspond to distinct lung pathologies and biomarkers of disease severity in idiopathic pulmonary fibrosis. *Thorax* **70**, 48–56 (2015).
71. Darwin, C. On the Origin of Species by Means of Natural Selection, or the Preservation of Favoured Races in the Struggle for Life, Edn. 1st. (John Murray, London, 1859).
72. Altschul, S. F. *et al*. Gapped BLAST and PSI-BLAST: a new generation of protein database search programs. *Nucleic Acids Res* **25**, 3389–3402 (1997).
73. Bendtsen, J. D., Nielsen, H., von Heijne, G. & Brunak, S. Improved prediction of signal peptides: SignalP 3.0. *Journal of molecular biology* **340**, 783–795 (2004).
74. Sarrion-Perdigones, A. *et al*. GoldenBraid: an iterative cloning system for standardized assembly of reusable genetic modules. *PLoS ONE* **6**, e21622 (2011).
75. Schmidt, T. G. & Skerra, A. The Strep-tag system for one-step purification and high-affinity detection or capturing of proteins. *Nat Protoc* **2**, 1528–1535 (2007).
76. Steentoft, C. *et al*. Precision mapping of the human O-GalNAc glycoproteome through SimpleCell technology. *The EMBO journal* **32**, 1478–1488 (2013).
77. Proudfoot, A. E. I. *et al*. Glycosaminoglycan binding and oligomerization are essential for the *in vivo* activity of certain chemokines. *Proc. Natl. Acad. Sci. USA.* **100**, 1885–1890 (2003).

Acknowledgements

This research was funded by British Heart Foundation Chair Award to S.B. (CH/09/003); Oxford BHF Centre of Research Excellence (RE/13/1/30181), BHF Oxbridge Centre for Regenerative Medicine (AVMEBCA1), Radcliffe Department of Medicine University of Oxford, and Wellcome Trust Core Award to the Wellcome Trust Centre

for Human Genetics. J.R.O.E. is supported by a studentship from the Oxford BHF Centre of Research Excellence, Y.A. by a studentship from the Saudi Arabian Cultural Bureau, and A.K. by a Royal Society Dorothy Hodgkin Fellowship. We thank Pat Nuttall and Manjunatha Kini for comments on the manuscript. S.B. has received funding from LAB282 for development of evasins as therapeutics in partnership with Evotec AG.

Author Contributions

K.S., G.D., Y.A., and J.R.O.E. designed, performed and interpreted yeast, protein interaction and cell-based experiments. S.B. conceived and designed the yeast surface display approach, and performed bioinformatic and statistical analyses, plasmid library construction, and evasin peptide sequence analysis. A.K. and S.B. supervised and interpreted experiments and all authors contributed to writing the manuscript.

Additional Information

Supplementary information accompanies this paper at doi:10.1038/s41598-017-04378-1

Competing Interests: Novel evasin sequences described in the ms. form part of the basis of a patent application PCT/GB2017/050563. SB has received funding from Lab282 for development of evasins as therapeutics in partnership with Evotec AG.

Publisher's note: Springer Nature remains neutral with regard to jurisdictional claims in published maps and institutional affiliations.

Open Access This article is licensed under a Creative Commons Attribution 4.0 International License, which permits use, sharing, adaptation, distribution and reproduction in any medium or format, as long as you give appropriate credit to the original author(s) and the source, provide a link to the Creative Commons license, and indicate if changes were made. The images or other third party material in this article are included in the article's Creative Commons license, unless indicated otherwise in a credit line to the material. If material is not included in the article's Creative Commons license and your intended use is not permitted by statutory regulation or exceeds the permitted use, you will need to obtain permission directly from the copyright holder. To view a copy of this license, visit http://creativecommons.org/licenses/by/4.0/.

© The Author(s) 2017